



**UNIVERSITÉ  
DE LORRAINE**

**BIBLIOTHÈQUES  
UNIVERSITAIRES**

## AVERTISSEMENT

Ce document est le fruit d'un long travail approuvé par le jury de soutenance et mis à disposition de l'ensemble de la communauté universitaire élargie.

Il est soumis à la propriété intellectuelle de l'auteur. Ceci implique une obligation de citation et de référencement lors de l'utilisation de ce document.

D'autre part, toute contrefaçon, plagiat, reproduction illicite encourt une poursuite pénale.

Contact bibliothèque : [ddoc-theses-contact@univ-lorraine.fr](mailto:ddoc-theses-contact@univ-lorraine.fr)  
*(Cette adresse ne permet pas de contacter les auteurs)*

## LIENS

Code de la Propriété Intellectuelle. articles L 122. 4

Code de la Propriété Intellectuelle. articles L 335.2- L 335.10

[http://www.cfcopies.com/V2/leg/leg\\_droi.php](http://www.cfcopies.com/V2/leg/leg_droi.php)

<http://www.culture.gouv.fr/culture/infos-pratiques/droits/protection.htm>



UNIVERSITÉ  
DE LORRAINE



---

# Stratigraphic correlation uncertainty: On the impact of the sediment transport direction in computer-assisted multi-well correlation

## PhD THESIS

presented and defended on April 12th, 2022 for the degree of

**Doctor of the Université de Lorraine**

**Geosciences Specialization**

by

**Paul BAVILLE**

---

### Composition of the jury

<i>President of the jury</i>	Pr. Jean BORGOMANO	Aix-Marseille Université, France
<i>Reporters</i>	Pr. Andrea MOSCARIELLO	Université de Genève, Switzerland
	Dr. Cécile ROBIN	Université de Rennes 1, France
<i>Examiners</i>	Pr. Jean BORGOMANO	Aix-Marseille Université, France
	Dr. Sophie LELEU	Université de Bordeaux, France
<i>Director</i>	Pr. Guillaume CAUMON	Université de Lorraine, France
<i>Co-directors</i>	Dr. Cédric CARPENTIER	Université de Lorraine, France
	Dr. Marcus APEL	Equinor ASA, Norway
<i>Guests</i>	Dr. Silvan HOTH	Equinor ASA, Norway
	Dr. Dirk KNAUST	Equinor ASA, Norway

---

**GeoResources - UMR 7359**  
Université de Lorraine – CNRS  
École Nationale Supérieure de Géologie  
2 rue du Doyen Marcel Roubault - BP 10162  
54505 Vandœuvre-lès-Nancy, FRANCE



---

**Incertitude des corrélations stratigraphiques :  
À propos de l'impact de la direction de transport des  
sédiments sur les corrélations multi-puits assistées  
par ordinateur**

**THÈSE DE DOCTORAT**

présentée et défendue le 12 Avril 2022 pour l'obtention du diplôme de

**Docteur de l'Université de Lorraine**

**Spécialité Géosciences**

par

**Paul BAVILLE**

---

**Composition du jury**

<i>Président du jury</i>	Pr. Jean BORGOMANO	Aix-Marseille Université, France
<i>Rapporteurs</i>	Pr. Andrea MOSCARIELLO	Université de Genève, Switzerland
	Dr. Cécile ROBIN	Université de Rennes 1, France
<i>Examineurs</i>	Pr. Jean BORGOMANO	Aix-Marseille Université, France
	Dr. Sophie LELEU	Université de Bordeaux, France
<i>Directeur</i>	Pr. Guillaume CAUMON	Université de Lorraine, France
<i>Co-directeurs</i>	Dr. Cédric CARPENTIER	Université de Lorraine, France
	Dr. Marcus APEL	Equinor ASA, Norway
<i>Invités</i>	Dr. Silvan HOTH	Equinor ASA, Norway
	Dr. Dirk KNAUST	Equinor ASA, Norway

---

**GeoRessources - UMR 7359**  
Université de Lorraine – CNRS  
École Nationale Supérieure de Géologie  
2 rue du Doyen Marcel Roubault - BP 10162  
54505 Vandœuvre-lès-Nancy, FRANCE



*Je dédie cette thèse à Claire, mon amie, mon amour, mon âme-sœur ...*



*“Two years he walks the Earth. No phone, no pool, no pets, no cigarettes. Ultimate freedom. An extremist. An aesthetic voyager whose home is the road. Escaped from Atlanta. Thou shalt not return, 'cause “the West is the best”. And now after two rambling years comes the final and greatest adventure. The climactic battle to kill the false being within and victoriously conclude the spiritual pilgrimage. Ten days and nights of freight trains and hitchhiking bring him to the Great White North. No longer to be poisoned by civilization he flees, and walks alone upon the land to become lost in the wild.”*

Alexander Supertramp (May 1992)

*“Happiness only real when shared.”*

Christopher Johnson McCandless (Aug 1992)



## Corréler le temps

*“Allez viens, Paul, corréler le temps  
Je t’emmène voir des sédiments  
Et je voudrais que tu te rappelles  
La strati est séquentielle et pas  
Artificielle*

*Tes corrélations seront belles, mon grand  
Les diagraphies, c’est excitant  
Et je voudrais que tu te rappelles  
La strati est séquentielle vraiment  
Exceptionnelle*

*Je voudrais gérer plein d’échelles, souvent  
De la biostrat, des sédiments  
Et je voudrais que tu te rappelles  
La strati est séquentielle aussi  
Un peu cruelle*

*Je voudrais que ça soit multi-well, mais pourtant  
Que ça ne calcule pas trop longtemps  
Et je voudrais que tu te rappelles  
Les strates sont éternelles mais  
Parfois rebelles*

*Je voudrais que tu les corrèles, sachant  
Qu’il y a des gaps de temps en temps  
Et je voudrais que tu te rappelles  
La strati est séquentielle et pas  
Artificielle”*

Guillaume Caumon (2022)

Sur l’air de *J’t’emmène au vent*, Louise Attaque (1997)



# Remerciements stratigraphiques

Dans ce drôle de chapitre, je vais essayer de mentionner toutes les personnes qui ont compté au cours de ma vie et plus particulièrement au cours de cette thèse et de les remercier de tout le support qu'ils m'ont apporté.

À l'instar de ce manuscrit, je vais essayer de catégoriser ces remerciements en différentes catégories stratigraphiques.

## Remerciements biostratigraphiques

Tout d'abord, je voudrais sincèrement remercier mes parents *Laurent* et *Florence*, et mes frères et sœurs *Manon*, *Alice* et *Romain*, qui m'ont toujours accompagné et soutenu depuis que je suis né. Merci aussi *Valentina* de t'être ajoutée à cette petite famille proche. Merci beaucoup à vous six.

Je voudrais aussi rendre hommage à tous mes arrière-grands-parents et mon arrière-grand-tante que j'ai eu la joie de connaître et qui à leur façon ont pu exercer une influence sur l'homme que je suis devenu. Je rends aussi hommage à mes grands-parents *Bon-Papa*, *Bonne-Maman*, et *Mam* et je les remercie d'avoir toujours été là pour moi ... et puis *Papou* que j'ai pu imaginer à travers les souvenirs de chacun.

J'aimerais aussi remercier *Caroline* et *Thomas* qui ont toujours accepté de s'occuper de moi et m'ont créé des souvenirs inoubliables comme les quelques matchs de foot, les concerts incroyables et bien sûr le séjour en Guadeloupe.

Enfin, je voudrais remercier ceux qui ne sont pas de la famille du sang, mais de celle du cœur. Merci beaucoup à vous les *Chatain*, les *Soulard*, les *Humbert*, les *Crécy* et les *Bonneau*. Enfin merci *Jean*, *Sylvie* et *Léa* de m'avoir accueilli dans votre famille avec *Lucas*.

La meilleure pour le fin évidemment, je tiens profondément à te remercier *Claire*. Tu as toujours été et tu seras pour toujours le bout de famille le plus cher à mes yeux. Je t'aime de tout mon cœur, merci d'être là, et surtout merci d'être toi !

---

## Remerciements chronostratigraphiques

Après ma famille, je voudrais mentionner et remercier mes camarades et mes professeurs que j'ai eu la chance de rencontrer tout au long de mon cursus scolaire.

Je voudrais intuitivement remercier les premières personnes avec lesquelles j'ai tissé des liens d'amitié dès la maternelle. Merci *Clément*, *Laurène*, *Clémence* et *Julie* pour les beaux souvenirs qui sont une solide base de l'idée que je me faisais et que je me fais toujours de l'amitié. Merci aussi à *Julien* et *Clémence* qui nous ont ensuite accompagnés *Clément* et moi jusqu'à la fin de l'école primaire.

Après les camarades d'école primaire, je voudrais remercier mes camarades de la classe d'Allemand Euro du collège Emile Zola avec qui j'ai partagé tant de beaux souvenirs, merci entre autres à *Louis*, *Yann*, *Anthony* et *Paul*. Voici ensuite le lycée Paul Langevin et une bonne bande d'Anormaux qui en plus des amis du collège m'a accompagné jusqu'au Baccalauréat et même après. Merci *Lucie*, *Marion*, *Chloé*, *Alexane*, *Claire*, *Stéph*, *Héloïse*, *Antoine*, *Léo*, *Mathieu* et *Théo*.

Après le lycée, voici la prépa au Lycée Chaptal qui n'aurait pas pu être mieux sans vous *Amaury*, *Arthur* et *Jérémy*, toujours à l'affut de bons bails et de bons plans pour passer du bon temps ensemble. Merci pour tous les bons moments qu'on a passés et qu'on continuera de passer ensemble.

La plus importante des étapes de ma formation est sûrement celle qui a eu lieu au sein des murs de Géol à Nancy. J'ai toujours autant de plaisir à revoir tous les copains que j'ai pu côtoyer pendant ces trois années. Pour commencer, le noyau dur de la Cycliste, merci *Yoann*, *Martin*, *Valentin*, *Thomas*, *Romain* et les deux *Quentins* pour tous les bons moments qu'on a passés ensemble. Merci aussi à mes deux colocs de la Pom' Potes, *Maëlle* et *Omblin*, qui m'ont supporté (et que j'ai supportées) pendant toute une année. Merci aux copains de la G202 en Géol Num' grâce auxquels la dernière année a été super, merci *Quentin*, *Thomas*, *Lucile*, *Jérémie*, *Hugo* et *Zoé*. Merci aussi à *Loeiza*, *Louise*, *Claire*, les deux *Clémences*, *Augustin*, *Baptiste*, le reste de la *Pucelle* et puis les membres du *PVT*, du *Mirador* et des *4E* pour tous les bons moments passés ensemble. Enfin merci à mes colocs du Duplex, merci *Grégré*, *Cléclé*, *Piépié* et *Tiennetienne* pour tous les bons moments qu'on a passés et qu'on continue aussi de passer ensemble depuis avec *Elodie* et *Héloïse*. Merci aussi à tous les autres copains de la promo 100 et des promos que j'ai côtoyés pendant mes trois années à Géol grâce à qui elles ont pu être si folles et mémorables. Merci entre autres à *Coco*, *Damien*, *Jules*, *Julien*, *Anna*, *Lauranne*, *Emma*, *Rémi*, *Solana* et bien sûr encore toi *Claire*.

Je voudrais enfin remercier les personnes avec lesquelles je n'ai pas partagé les bancs d'écoles mais qui m'ont donné la soif de savoir et l'envie de suivre la direction de la recherche. Je remercie donc beaucoup de tous mes professeurs et

---

ce depuis l'école primaire dont j'ai de très clairs souvenirs. Merci *Christelle* et *Gabrielle* d'avoir attisé la flamme de la connaissance à l'école des Cottages puis à l'école Vaillant-Jaurès. Merci ensuite à l'ensemble des enseignants du collège Emile Zola puis du lycée Paul Langevin. Je voudrais remercier plus particulièrement mes professeurs d'Allemand de m'avoir donné le goût de cette langue, et mes professeurs de matières scientifiques (SVT, Maths et Physique/Chimie) qui m'ont donné la soif des sciences. Je voudrais aussi remercier mes professeurs de prépa à Chaptal qui m'ont appris la rigueur et grâce auxquels j'ai pu réussir avec succès les concours d'entrée aux Grandes Ecoles. Enfin, je voudrais remercier tous les professeurs qui m'ont appris la géologie et les géosciences en règle générale.

## Remerciements lithostratigraphiques

J'en ai fini de rendre hommage à ma famille et à mes amis, il me reste donc à rendre hommage et à remercier les personnes qui m'ont accompagné pendant ces trois ans de thèse au Laboratoire GeoRessources.

Tout d'abord, un petit clin d'œil à tous les élèves auxquels j'ai eu le plaisir d'enseigner (en tous cas j'ai essayé) la programmation et les géostatistiques et que j'ai pu encadrer en projet de recherche ... notamment *Amandine* qui m'a supporté en géostat' (ah non) mais surtout en tant qu'encadrant de projet 2A.

Je voudrais ensuite remercier tous les copains thésards de GeoRessources avec qui j'ai pu interagir et passer de bons moments, notamment pendant les fameux bars doctorant du mardi soir. Merci *Lucas*, *Sylvain*, *Laurie*, *Martin*, *Thomas*, *Célestine*, *Chloé*, *Bastien*, *Pierric* et *Caroline*. Merci aussi à tous les membres de GeoRessources, et plus particulièrement à *Anne-Sylvie*, *Judith* et *Yann*. Je voudrais te remercier *Jeanne* d'avoir participé à cette formation sur le "savoir-communiquer" durant laquelle je t'ai rencontrée et grâce à laquelle je te compte aujourd'hui parmi mes plus proches amies.

Je voudrais aussi et surtout remercier tous les membres de l'équipe RING que j'ai eu la chance et le privilège de croiser et de côtoyer durant ma 3A et puis pendant ma thèse. Coucou les vieux thésards / docteurs, coucou *Modeste*, *Pierre* et *Margaux*, coucou les deux *Nicos*, coucou *Coco*, *Yves* et *Melchior*. J'aimerais bien raconter une petite anecdote à propos de chacun d'entre vous, mais j'en ai trop et puis ça serait trop long de toutes manières. Coucou les copains italiens qui se sont incrustés quelques mois, ciao *Gloria* e *Mattia* : "En bianco per mi e na spuma per el bocia". Coucou aussi les bébés thésards, coucou *Zoé* et *Capu*, coucou *Enrico* et *Fabrice*, coucou *Marius*, *Paul*, *Augustin* et *Julien*. Vous c'est pareil, j'aurais aimé raconter une anecdote avec chacun d'entre vous, mais c'est pareil, ça prendrait trop de temps ... et puis vous n'êtes pas (encore) docteurs.

---

Enfin coucou les membres permanents de l'équipe et leurs petites familles, coucou *François, Julie, Arthur et Thomas*, coucou *Pauline et Benoît*, coucou *Paul et Léo*, coucou *Christine et Denis*, coucou *Marie, Jérémie, Christophe, Maryse, Armelle, Mustapha*, et puis coucou *Julien Charreau*. Merci à tous de m'avoir supporté moi et mes blagues bien souvent excellentes et parfois un peu moins bonnes ...

Coucou *Guillaume*, tu as cru que je t'avais oublié ... non non, je ne t'oublierai jamais, et je voudrais encore une fois te remercier pour tout ce que tu m'as permis de faire au sein de cette équipe depuis mon Master jusqu'à maintenant. Merci d'avoir cru en moi et de m'avoir toujours soutenu et supporté quand j'allais moins bien, mais surtout quand j'allais bien. Je te serai toujours reconnaissant et je te remercie une dernière fois dans ce manuscrit d'avoir accepté de diriger cette thèse avec moi, merci encore !

En parlant de cette thèse, merci aussi à *Cédric* de l'avoir co-encadrée et d'avoir apporté tant de connaissances et de réflexions sur les aspects plus géologiques et sédimentaires de ce travail de thèse. Ich möchte mich auch bei *Marcus, Silvan und Dirk* für ihre Hilfe während dieser Doktorarbeit bedanken, tausendmal vielen Dank. Et puis je voulais aussi encore une fois remercier mon jury de thèse d'avoir accepté de rapporter et d'examiner ces travaux. Merci à *Jean* d'avoir aussi accepté d'être le président de ce jury et merci à *Cécile, Sophie et Andrea* pour leurs retours et commentaires des plus intéressants et pertinents tout au long de la discussion qui a suivi la soutenance de thèse.

## Remerciements musicostratigraphiques

Je voudrais remercier une dernière catégorie de personnes, ce sont toutes les personnes qui ont partagé ma passion pour le chant, les messes et les opéras à la *Maîtrise des Hauts-de-Seine*, puis le chant un peu plus contemporain a capella au sein du chœur *Sine Nomine* à Nancy. Merci en particulier à *Mehdi, Julien, Matthieu, Juliette* et *Xavier* de m'avoir supporté pendant toutes ces années à la maîtrise ("Y a pas de soucis Alix ...") et puis en dehors depuis que je suis allé m'enterrer à Nancy.

Et puis maintenant que les remerciements sérieux sont faits, on va pouvoir un peu déconner ! Je voudrais grandement remercier tous les chanteurs et musiciens qui m'ont accompagné durant ses trois années de thèse. Voici une liste non exhaustive des artistes que je n'ai cessés d'écouter pendant ces trois ans : *Louise Attaque, Georges Brassens, Bon Entendeur, Les Cowboys Fringants, Debout sur le Zinc, Les Fatals Picards, Leïla Huissoud, Oldelaf, Renaud, Renan Luce, Angelina Wismes, Daniel Balavoine, Calogero, Claude Nougaro, Léo Ferret, Jean Ferrat, Georges Moustaki, Jacques Brel, Eddie Vedder* et puis beaucoup d'autres.

---

## Remerciements radiostratigraphiques

Je voudrais aussi remercier la bande de *Par Jupiter* sur France Inter qui m'a bien fait rire pendant cette thèse, je me suis farci l'intégral des *Moment Meurice* de *Guillaume Meurice* et des *Actualizik* de *Thomas VDB*. Et puis merci à *Fabrice Drouelle* pour ses fabuleuses *Affaires sensibles* qui ont aussi rythmé mes soirées sur la route, ou en fin de thèse lors de la rédaction du manuscrit.

## Remerciements cinématostratigraphiques

Extrait du film **Caumonix et Bavillix : Mission Corrélation**

*C'est une bonne corrélation, ça maître ? Vous savez, moi je ne crois pas qu'il y ait de bonne ou de mauvaise corrélation. Moi si je devais résumer la stratigraphie aujourd'hui, je dirais que c'est d'abord des rencontres. Des grains qui se tendent la main, qui se déposent, qui s'érodent, et se déposent un peu plus loin. Et c'est assez curieux de se dire que les rencontres de ces grains forment une strate... Et quand on a le goût de la strate bien faite, bien datée, et bien parfois, on ne trouve pas la bestiole en face, c'est-à-dire, le fossile qui vous aide à bien dater. Alors du coup on ne sait pas vraiment si la corrélation va bien. Mais je dis quand même merci à la mer, je kiffe la mer qui a transporté tous ces grains de sable ! Et finalement, quand beaucoup de gens aujourd'hui me disent "Mais comment fais-tu pour savoir vraiment comment corréler ?", et bien je leur réponds très simplement, je leur dis que c'est le goût du caillou, ce goût donc qui m'a poussé à entreprendre cette corrélation deltaïque, et en fait, qui sait... peut-être simplement à me mettre au service de la distalité et du dip, du dip des strates !*

Guillaume Caumonix (-34 av. 2056)





# Contents

Extended Abstract	xxi
Introduction	1
<b>I WELL CORRELATION</b>	<b>13</b>
<b>1 Stratigraphic well correlation</b>	<b>15</b>
1.1 Subsurface stratigraphic data . . . . .	17
1.1.1 Direct observations . . . . .	20
1.1.2 Geophysical measurements . . . . .	21
1.1.3 Depositional information . . . . .	22
1.2 Sequence Stratigraphy . . . . .	23
1.2.1 Accommodation rate & Sedimentation rate . . . . .	25
1.2.2 Sequence Stratigraphy: Nomenclature & Definitions . . . . .	28
1.2.2.1 Stratigraphic surfaces . . . . .	29
1.2.2.2 Stratigraphic system tracts . . . . .	29
1.2.2.3 Prograding parasequences / Clinofolds . . . . .	31
1.2.2.4 Stratigraphic conformity . . . . .	32
1.2.3 Lithostratigraphy <i>versus</i> chronostratigraphy . . . . .	33
1.3 Stratigraphic well correlation . . . . .	35
1.3.1 From stratigraphic data to well markers . . . . .	35
1.3.2 Principles of chronostratigraphic well correlation . . . . .	37
1.3.3 Uncertainties in stratigraphic well correlation . . . . .	39
<b>2 Computer-assisted well correlation</b>	<b>43</b>
2.1 Computer-assisted well correlation algorithms . . . . .	45
2.1.1 Frequency space approaches and multi-scale analysis . . . . .	45
2.1.2 Well-log cross-correlation . . . . .	46
2.1.3 Well-log section correlation . . . . .	47
2.1.4 Dynamic well correlation algorithms . . . . .	47
2.2 Dynamic Time Warping algorithm . . . . .	48
2.2.1 Well-to-well correlation . . . . .	49
2.2.2 Multi-well correlation . . . . .	51

---

<b>II</b>	<b>PRINCIPLES OF CORRELATION</b>	<b>57</b>
<b>3</b>	<b>Sedimentary facies vs Well distality</b>	<b>59</b>
3.1	Principle of correlation . . . . .	61
3.2	Correlation likelihood computation . . . . .	64
3.2.1	Correlation cost computation . . . . .	64
3.2.1.1	Contribution of the sedimentary facies . . . . .	65
3.2.1.2	Contribution of the relative well distality . . . . .	67
3.2.1.3	Correlation cost . . . . .	69
3.2.2	Transition cost computation . . . . .	71
3.3	First results: Synthetic data set . . . . .	72
3.3.1	Sedimentary margin transverse cross-section . . . . .	72
3.3.2	Sedimentary margin longitudinal cross-section . . . . .	74
3.3.3	Sedimentary bay-head delta transverse cross-section . . . . .	75
3.4	Discussion . . . . .	76
3.4.1	Order of wells and correlation path . . . . .	76
3.4.2	Number of propagated realizations . . . . .	77
3.4.3	Principal sediment transport direction . . . . .	78
3.4.4	Well position within the depositional system . . . . .	79
3.4.5	Laterally equivalent sedimentary facies . . . . .	80
<b>4</b>	<b>Depositional profile vs Dip data</b>	<b>85</b>
4.1	From well markers to depositional surfaces . . . . .	88
4.1.1	Sedimentary facies and vertical/lateral extension . . . . .	88
4.1.2	Depositional strike orientation and dip angle . . . . .	90
4.1.3	Depositional profile interpolation . . . . .	91
4.1.3.1	Depositional curve interpolation . . . . .	91
4.1.3.2	Depositional surface interpolation . . . . .	93
4.1.3.3	From well marker to correlation lines . . . . .	94
4.2	From sediment source to depositional surfaces . . . . .	95
4.2.1	Two-dimensional analytical model . . . . .	96
4.2.2	Three-dimensional analytical model . . . . .	97
4.3	Correlation likelihood computation . . . . .	101
4.3.1	Theoretical depositional profile translation . . . . .	101
4.3.2	Absolute integral computation . . . . .	104
4.3.3	Correlation cost computation . . . . .	107
4.4	First results: Synthetic data set . . . . .	109
4.5	Discussion . . . . .	110
4.5.1	Impact of the theoretical depositional profile. . . . .	110
4.5.2	Impact of the correlation cost computation. . . . .	111
4.5.3	Impact of the order of correlation. . . . .	112

<b>III</b>	<b>APPLICATIONS</b>	<b>117</b>
<b>5</b>	<b>Middle Jurassic Hugin Formation: Paleogeographic context</b>	<b>119</b>
5.1	Zone of interest: Gudrun-Sigrun Field area . . . . .	123
5.1.1	Sedimentary facies interpretation . . . . .	123
5.1.2	Biostratigraphic interpretation . . . . .	125
5.1.3	Relative well distality interpretation . . . . .	126
5.2	Application of the distality rule of correlation . . . . .	130
5.2.1	Scenario A: One single bay-head delta . . . . .	131
5.2.2	Scenario B: Several independent bay-head deltas . . . . .	131
5.2.2.1	Southeast bay-head delta . . . . .	132
5.2.2.2	Northwest bay-head delta . . . . .	133
5.2.2.3	Bay-head deltas and lagoonal environments . . . . .	135
<b>6</b>	<b>Middle Jurassic Hugin Formation: Subsurface modeling</b>	<b>139</b>
6.1	Zone of interest: Sigrun Field area . . . . .	141
6.2	Application of the distality rule of correlation . . . . .	142
6.2.1	Lithostratigraphic subsurface model simulation . . . . .	144
6.2.2	Chronostratigraphic subsurface model simulation . . . . .	146
6.2.3	Impact of the sedimentary facies clustering . . . . .	150
6.3	Discussion . . . . .	156
6.3.1	Principal sediment transport direction . . . . .	156
6.3.2	Size of the system with respect to well spacing . . . . .	157
6.3.3	Sedimentary facies clustering . . . . .	158
6.3.4	Minor changes in the correlation cost . . . . .	159
6.3.5	Additional principles of correlation . . . . .	159
	<b>Conclusion</b>	<b>163</b>
	<b>Bibliography</b>	<b>167</b>
	<b>APPENDIXES</b>	<b>191</b>
<b>A</b>	<b>Middle Jurassic Hugin Formation: Sedimentary facies</b>	<b>191</b>
A.1	Lagoonal depositional environments . . . . .	193
A.2	Bay-head delta depositional environments . . . . .	196
A.3	Fluvial depositional environments . . . . .	200



# List of Figures

1	The four successive steps of the geometrical interpolation approach of geomodel building: (A) stratigraphic well correlation, (B) stratigraphic unit geometry interpolation/extrapolation, (C) stratigraphic unit conformity, and (D) subsurface property estimation/simulation. Redrawn from <a href="#">Edwards (2017)</a> . . . . .	4
2	(A) Every topologically possible well-marker association. (B) Integration of prior knowledge on depositional context (e.g., sediment transport direction) to quantify the likelihood of each well-marker association (e.g., <a href="#">Baville et al., 2022</a> ; <a href="#">Lallier et al., 2016</a> ). (C) Integration of the depositional geometry (e.g., dipmeter data) to quantify the likelihood of of each well-marker association (e.g., <a href="#">Baville et al., 2021a</a> ). . . . .	5
1.1	Illustration of the vertical and lateral resolutions of seismic imaging (background) and subvertical wells (well path: gray lines, and well logs: black lines). These data correspond to the Malampaya gas reservoir interior reflectors located offshore western Palawan island, Philippines. Modified from <a href="#">Fournier and Borgomano (2007)</a> ; <a href="#">Grötsch and Mercadier (1999)</a> ; <a href="#">Lallier et al. (2012)</a> . . . . .	18
1.2	Proportion of the zone of interest corresponding to the type of data as a function of the scale of measurements. Well data (well logs and core samples) capture geobodies which have a thickness under the seismic resolution ( <a href="#">Ringrose and Bentley, 2016</a> ) but correspond to less than $10^{-5}\%$ of the zone of interest. Red boxes correspond to vertical dimensions, green boxes correspond to horizontal dimensions, and blue boxes correspond to vertical and horizontal dimensions. Modified from <a href="#">Howell et al. (2014)</a> ; <a href="#">Raguanel (2019)</a> . . . . .	19
1.3	Examples of several data acquired along a vertical well: (left) core photographs, gamma ray, log porosity, facies interpretation, T-R sequence interpretation, biozone interpretation (right). Data courtesy of <a href="#">Equinor ASA</a> . . . . .	20

## LIST OF FIGURES

---

- 1.4 Diagrammatic representation of cyclicities of stratigraphic units. Each stratigraphic order corresponds approximately to a frequency time-window. Stratigraphic units (second to fifth order) may occur at more than one frequency. Inspired from [Catuneanu et al. \(2011\)](#) and [Mitchum and Van Wagoner \(1991\)](#). . . . . 23
- 1.5 Successive transgressive and regressive parasequences corresponding to intervals observed at different scale of depth and time ([Posamentier and Vail, 1988b](#); [van Wagoner et al., 1990](#)). Inspired by [Kedzierski et al. \(2008\)](#). (A) Depth cross-section and (B) time cross-section (Wheeler diagram; [Wheeler \(1958\)](#)). Redraw from [Baville et al. \(2022\)](#). . . . . 24
- 1.6 Relationship between the rate of eustatic change, the rate of subsidence, and the rate of relative sea-level change. In this example, the subsidence is constant. It means that if the eustatic level rises, or the amplitude of the eustatic fall is lower than the subsidence, the accommodation stays positive. At the opposite, if the amplitude of the eustatic fall is higher than the subsidence rate, the accommodation becomes negative. Modified from [Edwards \(2017\)](#); [Kedzierski \(2007\)](#); [Posamentier and Vail \(1988a\)](#). . . . . 26
- 1.7 Impact of the ratio  $A/S$  (accommodation rate / sedimentation rate) on the coastline migration (illustrated by bold arrows), and on the stratigraphic unit geometries. (A-C) positive accommodation rate, (D) null accommodation rate, and (E) negative accommodation rate. Modified from [Edwards \(2017\)](#); [Homewood et al. \(2000\)](#); [Kedzierski \(2007\)](#). . . . . 27
- 1.8 Evolution of stratigraphic sequence definitions since [Sloss et al. \(1949\)](#) have defined the concept of “Sequence Stratigraphy”. Chronologically, the concept of genetic sequences ([Frazier, 1974](#); [Galloway, 1989b](#)), the concept of depositional sequence I ([Mitchum et al., 1977b](#)), the concept of T-R sequence ([Embry and Johannessen, 1992](#); [Johnson and Murphy, 1984](#)), the concept of depositional sequence II ([Haq et al., 1987](#); [Posamentier et al., 1988](#)), the concept of depositional sequence III ([Christie-Blick, 1991](#); [van Wagoner et al., 1988, 1990](#)), and the concept of depositional sequence IV ([Helland-Hansen and Gjelberg, 1994](#); [Hunt and Tucker, 1992](#)). Modified from [Catuneanu \(2006\)](#). . . . . 29

1.9	Definition of stratigraphic surfaces and system tracks considering the Genetic Sequence (Frazier, 1974; Galloway, 1989b) and the T-R Sequence (Embry and Johannessen, 1992; Johnson and Murphy, 1984) concepts. Triangles represent the sediment grain-size according to the depositional conditions. HNR: Highstand Normal Regression; LNR: Lowstand Normal Regression; T: Transgression; FR: Forced Regression; MFS: Maximum Flooding Surface; MRS: Maximum regressive Surface; RSL: Relative Sea-Level. Inspired from Catuneanu et al. (2010). . . . .	30
1.10	Geometry of clinoforms along a shoreline with redistribution by wave action or tidal currents (laterally to the river mouth). (A) Dip direction cross-section. (B) Strike direction cross-section. Modified from Baville et al. (2022). . . . .	32
1.11	Geometry of clinoforms in the axis of the deltaic system (vertical scale exaggerated). (A) Dip direction cross-section. (B) Strike direction cross-section. Modified from Baville et al. (2022); Gani and Bhattacharya (2005). . . . .	32
1.12	(A-D) Different stratigraphic sequence conformities: conformable, erosional unconformity (top) and angular unconformity (base). (E) An example of conformity interpretation along well path: (1) erosional unconformity or pure progradation, (2) conformable, and (3) angular unconformity. Bold lines are stratigraphic sequence interface, and fine lines are substratigraphic lines. Modified from Edwards (2017). . . . .	33
1.13	An example of lithology interpretation along two wells and their (A) lithostratigraphic and (B) chronostratigraphic geological layer interpolation and extrapolation from the same data set. Modified from Ainsworth et al. (1999); Baville et al. (2022). . . . .	34
1.14	Illustration of the two types of well data and their associated well markers: (A) well logs (gamma ray and porosity) and regularly sampled well markers and (B) well regions (lithology and biozones) and irregularly sampled well markers. . . . .	36
1.15	(A) Every topologically possible well-marker associations. Two examples of topologically inconsistent correlation sets: (B) two well-marker associations intersect, and (C) all the well marker are not associated. . . . .	37
2.1	Illustration of the two-dimensional version of the Dynamic Time Warping algorithm at step $[i, j]$ with two wells containing $I$ and $J$ markers. . . . .	50

LIST OF FIGURES

---

2.2 Illustration of the three-dimensional version of the Dynamic Time Warping algorithm at step  $[i, j, k]$  with three wells containing  $I$ ,  $J$  and  $K$  markers. Cells correspond to triplets of well markers (correlation cost  $c$ ), and arrows correspond to transitions between two triplets (transition cost  $t$ ). . . . . 52

2.3 Illustration of the three-dimensional version of the Dynamic Time Warping algorithm at step  $[i, j, k]$  with three wells containing  $I$ ,  $J$  and  $K$  markers. Cells correspond to triplets of well markers (correlation cost  $c$ ), and arrows correspond to transitions between two triplets (transition cost  $t$ ). . . . . 53

2.4 Illustration of three possible the stratigraphic column propagations during the well correlation computation.  $LSC^{i:j}$  is the local stratigraphic column between wells  $i$  and  $j$ ;  $GSC^{i:j}$  is the global stratigraphic column between wells  $i$  and  $j$ .  $U_n^{i:j}$  is to the stratigraphic unit  $n$  interpreted between wells  $i$  and  $j$ .  $G^{i:j}$  is a stratigraphic gap interpreted between wells  $i$  and  $j$ .  $\cup$  is the union of two units or gaps. Redrawn from [Edwards et al. \(2018\)](#). . . . . 55

3.1 Three-dimensional illustration of a simplified sedimentary basin margin geometry along the depositional strike direction (AA') and the principal sediment transport direction (BB'). Parasequence boundaries (black bold lines) are isochronous lines separating clinoforms. Modified from [Baville et al. \(2022\)](#). . . . . 62

3.2 Well-marker correlation likelihood based on facies association within a sedimentary basin along (A) the depositional strike direction and (B) the principal sediment transport direction. Facies association likelihood is represented by a dashed or full green or red line. Modified from [Baville et al. \(2022\)](#). . . . . 63

3.3 (A) Sedimentary facies  $f$  interpreted along a typical paleogeographic depositional profile and encoded from the most deep ( $f = 1$ ) to the most shallow ( $f = 15$ ). (B-C-D)  $\Delta f_{ab}^\lambda(i, j)$  is the relative facies variation  $\Delta f_{ab}(i, j)$  composed by the discretization function  $\lambda$  which characterizes possible relationship between several values of facies variations (Equation (3.4)). . . . . 66

3.4 (A) Well distality  $d$  interpreted along a typical paleogeographic depositional profile and encoded from the most distal ( $d = 1$ ) to the most proximal ( $d = 15$ ). (B-C-D)  $\Delta d_{ab}^\alpha(i, j)$  is the distality variation  $\Delta d_{ab}(i, j)$  weighted by the scaling coefficient  $\alpha$  which represents how the lateral size of the depositional system is deemed to scale with the inter-well distance (Equation (3.10)). . . . . 68

- 
- 3.5 (A) Sedimentary facies interpretations given (B) facies variations (Equation (3.7)) and (C) distality variation ( $\alpha = 1$ , Equation (3.11)) used to compute (D) the correlation cost  $c[i, j]$  (Equation (3.15)) of each possible marker correlation  $[i, j]$ .  $f^\lambda(i, j)$  and  $d^\alpha(i, j)$  are normalized parameters given by Equations (3.4) and (3.10). The gray level corresponds to the correlation cost value  $c[i, j]$ . Modified from [Baville et al. \(2022\)](#). . . . . 71
- 3.6 Best scenarios generated by applying the proposed cost function on a sedimentary basin margin transversal cross-section. (A) Wells are added to the correlation process from the left to the right, and (B) from the right to the left. Green lines are correlation lines, and the *cost* correspond to the cumulative correlation cost (combination of both correlation costs  $c$  and transition costs  $t$ ). Blue lines are manual interpretations of lower-order parasequence boundaries. Modified from ([Baville et al., 2022](#)). . . . . 73
- 3.7 Best scenarios generated by applying the proposed cost function on a sedimentary basin margin or deltaic longitudinal cross-section. (A) Wells are added to the correlation process from the left to the right, and (B) from the right to the left. Green lines are correlation lines that occur in the both scenarios, whereas red lines are correlation lines which occur in only one of the two scenarios. The *cost* corresponds to the cumulative correlation cost (combination of both correlation costs  $c$  and transition costs  $t$ ). Blue lines are manual interpretations of the lower-order parasequence boundaries. Modified from ([Baville et al., 2022](#)). . . . . 74
- 3.8 Best scenarios generated by applying the proposed cost function on a sedimentary deltaic transversal cross-section. (A) Wells are added to the correlation process from the left to the right, and (B) from the right to the left. Green lines are correlation lines that occur in all the scenarios, whereas red lines are correlation lines which do not occur in all the scenarios. The *cost* correspond to the cumulative correlation cost (combination of both correlation costs  $c$  and transition costs  $t$ ). Blue lines are manual interpretations of the lower-order parasequence boundaries. Modified from ([Baville et al., 2022](#)). . . . . 75

3.9	Best scenarios generated by applying the proposed cost function on a sedimentary deltaic transversal cross-section. (A) the fifty best correlation sets, and (B) the five hundred best correlation sets, are kept at each step of the process to propagate the uncertainties. Green lines are correlation lines that occur in all the scenarios, whereas red lines are correlation lines which do not occur in all the scenarios. The <i>cost</i> correspond to the cumulative correlation cost (combination of both correlation costs $c$ and transition costs $t$ ). Blue lines are manual interpretations of the lower-order parasequence boundaries. . . . .	77
3.10	Best scenarios generated by applying the proposed cost function on the same data set but but modifying the principal sediment transport direction. (A) Wells are located along the depositional strike direction ( <i>i.e.</i> , the distality is the same), and (B) wells are located along the depositional dip direction ( <i>i.e.</i> , the distality is different). . . . .	79
3.11	Best scenarios generated by applying the proposed cost function on the same data set but but modifying the scaling coefficient: (A) $\alpha = 1$ and (B) $\alpha = 1/2$ . . . . .	80
3.12	Best scenarios generated by applying the proposed cost function on the same data (A) without considering different laterally equivalent facies and (B) considering two groups of laterally equivalent facies. . . . .	81
4.1	Generalized intra-parasequence bedding geometry and facies architecture of a prograding delta. (A) Dip section shows the seaward-dipping bedset boundaries (clinoforms), which follow time lines and are bidirectional in (B) strike section. Vertical and horizontal red arrows represent the vertical and lateral facies extension. Note that the drawings are not to scale. Inspired by <a href="#">Gani and Bhattacharya (2005)</a> . . . . .	89
4.2	Three-dimensional Bézier cubic curve interpolations. $\mathbf{p}_{30}$ and $\mathbf{p}_{03}$ are corner points, defined by spatial extensions $r_{30}$ and $r_{03}$ , and normal vectors $\mathbf{n}_{30}$ and $\mathbf{n}_{03}$ . $\mathbf{p}_{21}$ and $\mathbf{p}_{12}$ are the control points constraining the inclination and the stiffness of the interpolation computed from corner points. (A) Initial position of corner and control points, and (B) final position of control points. . . . .	92
4.3	Three-dimensional Bézier cubic curve interpolations. $\mathbf{p}_{300}$ , $\mathbf{p}_{030}$ and $\mathbf{p}_{003}$ are corner points, defined by spatial extensions $r_{300}$ , $r_{030}$ and $r_{003}$ , and normal vectors $\mathbf{n}_{300}$ , $\mathbf{n}_{030}$ and $\mathbf{n}_{003}$ . All other $\mathbf{p}_{ijk}$ are the control points constraining the inclination and the stiffness of the interpolation computed from corner points. (A) Initial position of corner and control points, and (B) final position of control points. . . . .	94

4.4 several examples of marker-to-marker Bézier cubic correlation line interpolation. Black dots are well markers. Dashed blue circles represent the lateral and vertical extension range around well markers (depending on the facies) and blue dots are the Bézier control point positions (for each pair of well markers) constrained by facies lateral extension. Red lines are dipmeter data at each well marker (apparent dip angle) and red dots are control point positions updated using apparent dip measurements at well markers. Black lines are Bézier cubic curve interpolations between well markers constrained by facies interpretations and dipmeter data. . . . . 95

4.5 (A) Line drawings from seismic profiles, (B) seismic line interpolations, of a siliciclastic continental submarine slope of the Antarctic Peninsula Pacific margin (Rebesco and Camerlenghi, 1997). (C) Planar morphology described by a linear function (Equation (4.10)). (D) Concave curvature described by an exponential function (Equation (4.11)). (E) Sigmoidal morphology described by a Gaussian distribution (Equation (4.12)). See text for description of parameters. Modified from Adams and Schlager (2000). . . . . 97

4.6 (A) Depositional depth  $z_p$  and (B) depositional *dip* divided in three zones: (1) the lateral zone described by Equations (4.14) and (4.15), (2) the radial zone described by Equations (4.17) and (4.19), and (3) the flat zone described by Equation (4.20). . . . . 98

4.7 A theoretical depositional profile generated from a sediment source (black point) being described by a deltaic extension ( $\delta_{x_p} = 50$  m,  $\delta_{y_p} = 100$  m,  $\delta_{z_p} = 20$  m). (A) The depositional depth (Equations (4.14), (4.17) and (4.20)). (B) The depositional dip (Equations (4.15), (4.19) and (4.20)). (C) The azimuth (degree) computed from the position of the sediment source. (D) The facies repartition on the depositional profile depending on the depositional depth. . . . . 100

4.8 (A) A theoretical depositional profile generated from a sediment source (black point) being described by a delta spatial extension ( $\delta_{x_p} = 50$  m,  $\delta_{y_p} = 100$  m,  $\delta_{z_p} = 20$  m). (B) A well marker interpreted along a well, described by a strike direction  $\theta$ , a dip angle  $\phi$  (dip direction  $\theta^*$ ), and a sedimentary facies. (C) Depositional depth  $z_p$  and depositional *dip* ranges corresponding to the sedimentary facies interpreted at the marker position. . . . . 104

4.9 Correlation lines and correlation surfaces discretization for the absolute integral computation. (A) Absolute area between two lines (gray surface) and (B) the line discretization based on the vertical projected barycentric coordinates. (C) Absolute volume between two surfaces (gray volume) and (D) the surface discretization based on the vertical projected barycentric coordinates. . . . . 106

4.10 Likelihood computation of candidate isochronous lines obtained by Bézier interpolation. (A) A paleogeographic depositional profile on which the facies are drawn is translated within the model to define the paleogeographic depositional profile for each well marker  $i$  and  $j$  to be compared to Bézier cubic interpolations. (B-C) The two markers are located on two different theoretical depositional profiles, the likelihood is the sum of the absolute integral between the Bézier cubic interpolation and the two paleogeographic depositional profiles. . . . . 108

4.11 Multi-well correlation using (A) triangular surface interpolated between three markers, and (B) piece-wise triangular surface interpolated between five markers. . . . . 109

4.12 (A) Nine wells drilling six successive paleogeographic depositional profiles generated using Equations (4.14), (4.17) and (4.20) with a deltaic extension (100 m, 500 m, 20 m) and a principal sediment transport direction  $\theta = N135$ . (B) Paleogeographic depositional lines along the principal sediment transport direction and well markers corresponding to each paleogeographic depositional profile. (C) Every possible well marker correlation corresponding to a three-dimensional Bézier cubic interpolation. (D) The most likely correlation set ( $cost = 152706.88 \text{ m}^2$ ) generated using the proposed correlation cost function. . . . . 110

4.13 (A) Paleogeographic depositional lines along the principal sediment transport direction  $\theta = N135$  and well markers corresponding to each paleogeographic depositional profile generated with a deltaic extension (100 m, 500 m, 20 m). (B) The most likely correlation set. (C) Five realizations having the second highest likelihood (red lines highlight the difference between the five realizations). (D) The correlation having the third highest likelihood. . . . . 112

4.14 (A) Paleogeographic depositional lines along the principal sediment transport direction  $\theta = N135$  and well markers corresponding to each paleogeographic depositional profile generated with a deltaic extension (100 m, 500 m, 20 m). (B) The most likely correlation set and its cost according to the path of correlation. (C) Well marker correlations belonging to the hundred most likely correlation sets computed using the proposed method correlating wells from Northwest to Southeast. (D) Well marker correlations belonging to the hundred most likely correlation sets computed using the proposed method correlating wells from Southeast to Northwest. . . . . 113

5.1	Well section: the Middle Jurassic Hugin Formation in the Gudrun-Sigrun Field area (map based on <a href="http://www.npd.no">http://www.npd.no</a> ). Facies correspond to twelve depositional environments interpreted along wells and described in Section 5.1.1 and Appendix A. Biozones correspond to the six depositional time-periods interpreted from Early Bathonian to Late Callovian along the wells (Section 5.1.2). Note the poor chronostratigraphic resolution and lack of interpreted biozones in the three western wells due to lack of data. . . . .	122
5.2	(A) Map view of the Gudrun-Sigrun Field area (Block 15/3), and spatial location of the seven wells drilled into the Middle Jurassic Hugin Formation. Gray areas are oil, gas and condensate reservoirs. Map based on <a href="http://www.npd.no">http://www.npd.no</a> . (B) Middle Jurassic Hugin Formation regional depositional system, a siliciclastic bay-head delta within a lagoonal environment. Modified from (Baville et al., 2022). . . . .	123
5.3	Twelve sedimentary facies interpreted by Knaust and Hoth (2021) from core samples of the Middle Jurassic Hugin Formation in the Gudrun-Sigrun Field area. Sedimentary facies are described in Appendix A. Redrawn from (Baville et al., 2022). . . . .	124
5.4	Middle Jurassic Hugin Formation paleogeographic depositional system interpretation of Knaust et al. (2019): a single bay-head delta prograding into a lagoonal depositional environment. (left) Plan view and (right) block diagram of the five wells in the Gudrun-Sigrun Field area ( <a href="http://www.npd.no">http://www.npd.no</a> ). Gray arrows represent the sediment transport directions, derived from dipmeter logs and borehole images, corresponding to the depositional system. . . . .	127
5.5	Middle Jurassic Hugin Formation paleogeographic depositional system interpretation of Knaust and Hoth (2021): (Bathonian) a bay-head delta interpreted in well 09 prograding into a lagoonal depositional environment interpreted in wells 04 and 11, and (Callovian) several independent bay-head deltas in both sides of well 09. (left) wells 09 and 11 along which are interpreted the Bathonian and Callovian paleogeographic depositional systems, and (right) block diagrams of wells in the Gudrun-Sigrun Field area. . . . .	129
5.6	Computer-assisted chronostratigraphic correlation computed between wells 04, 05 and 11 using the distality rule of correlation defined in Chapter 3. The relative well distalities correspond to the scenario B (Figure 5.5 and Equations (5.4) and (5.6)). Bathonian: wells 04 and 11 are distal ( $d_{04} = d_{11} = 1$ ). Callovian: well 04 (and $d = 5$ Callovian) is more proximal than well 11 ( $d = 3$ ), and well 05 ( $d = 5$ ) is a bit more off-axis of the system. Red correlation lines are inconsistent with respect to the biozones. . . . .	133

## LIST OF FIGURES

---

- 5.7 Computer-assisted chronostratigraphic correlation computed between wells 01, 03 and 07 using the distality rule of correlation defined in Chapter 3. The relative well distalities correspond to the scenario B (Figure 5.5 and Equations (5.4) and (5.6)). Bathonian: No information given by biostratigraphic interpretation. Callovian: Wells 01 and 07 correspond to delta and have approximately the same relative distality ( $d_{01} = d_{07} = 3$ ) and there is no biostratigraphic interpretation along the well 03, but it mainly corresponds to deltaic depositional environments ( $d_0 =$ ). . . . . 134
- 5.8 Computer-assisted chronostratigraphic correlation computed between wells 07, 09 and 11 using the distality rule of correlation defined in Chapter 3. The relative well distalities correspond to the scenario B (Figure 5.5 and Equations (5.4) and (5.6)). Bathonian: well 11 ( $d_{11} = 1$ ) is more distal than well 09 ( $d_{09} = 5$ ). Callovian: wells 07 and 11 have approximately the same distality ( $d_{07} = 3$  and  $d_{11} = 4$ ) and are more proximal than well 09 ( $d_{09} = 1$ ). Red correlation lines are inconsistent with respect to the biozones. . . 136
- 6.1 (A) Map view and (B) block diagram of the Sigrun Field area (Block 15/3), and spatial location of wells 04 and 11 in the Callovian Hugin Formation (Maps based on <http://www.npd.no>). (C) Stratigraphic correlation between wells 04 and 11 generated by the distality rule of correlation defined in Chapter 3 (Section 5.2.2.3). 141
- 6.2 Eight sedimentary facies interpreted by [Knaust and Hoth \(2021\)](#) from core samples of the Early Callovian Hugin Formation in the Sigrun Field area. Sedimentary facies are described in Appendix A. Redrawn from ([Baville et al., 2022](#)). . . . . 142
- 6.3 Sedimentary facies, parasequence and biostratigraphic interpretation of Wells 04 and 11 in the lower part of the Hugin Formation in the Sigrun Field area. Redrawn from [Baville et al. \(2022\)](#). . . . 143
- 6.4 (A) Correlation panel. Black lines correspond to the best correlation set computed by Equation (3.16) (*i.e.*, lithostratigraphic well correlation). Red bands highlight well-marker correlations which are inconsistent with the distality interpreted in both wells. (B) Correlation cost matrix. The black line corresponds to the correlation path of the best correlation set minimizing the facies variation  $\Delta f$ . Cells are colored by the correlation cost computed by Equation (3.16). Modified from ([Baville et al., 2022](#)). . . . . 145

6.5 (A) Correlation panel. Black lines (respectively dashed red lines) correspond to the best correlation set computed by Equation (3.17) (respectively using Equation (3.16)). Green bands highlight well-marker correlations which were inconsistent using the variation minimization and which are consistent using the distality rule of correlation. (B) Correlation cost matrix. Black line (respectively dashed red line) corresponds to the correlation path of the best correlation computed by the distality rule of correlation (respectively the variation minimization). Cells are colored by the correlation cost computed by Equation (3.17). Modified from (Baville et al., 2022). . . . . 147

6.6 (A) Correlation panel. Black lines correspond to identical well-marker correlations among the four best correlation sets computed by Equation (3.17) *i.e.*, the four correlation sets with the four lowest cumulative costs computed by Equation (2.1). Colored correlation lines are the different well-marker correlations in the four best correlation sets. (B) Correlation cost matrix. The four lines correspond to the four most likely scenarios. Note that the transition costs  $t$  associated to the edges or corners of the cost matrix are not visible in this display. Modified from (Baville et al., 2022). 149

6.7 (A) Correlation panel. Black lines (respectively dashed red lines) correspond to the best correlation set computed by Equation (3.17) with the facies association A (respectively without facies association). Purple bands highlight the main difference between the correlation sets generated with the facies association A, and without the facies association. (B) Correlation cost matrix. Black line (respectively dashed red line) corresponds to the correlation path of the best correlation set computed with the facies association A (respectively without facies association). Modified from (Baville et al., 2022). . . . . 152

6.8 (A) Correlation panel. Black lines (respectively dashed red lines) correspond to the best correlation set computed by Equation (3.17) with the facies association B (respectively without facies association). Purple bands highlight the main difference between the correlation sets generated with the facies association B, and without the facies association. (B) Correlation cost matrix. Black line (respectively dashed red line) corresponds to the correlation path of the best correlation set computed with the facies association B (respectively without facies association). Modified from (Baville et al., 2022). . . . . 153

## LIST OF FIGURES

---

6.9	(A) Correlation panel. Black lines (respectively dashed red lines) correspond to the best correlation set computed by Equation (3.17) with the facies association C (respectively without facies association). Purple bands highlight the main difference between the correlation sets generated with the facies association C, and without the facies association. (B) Correlation cost matrix. Black line (respectively dashed red line) corresponds to the correlation path of the best correlation set computed with the facies association C (respectively without facies association). Modified from (Baville et al., 2022). . . . .	154
6.10	Correlation cost matrix summarizing the best correlation sets generated by the distality rule of correlation using the eight initial facies and the three facies associations A, B and C. Modified from (Baville et al., 2022). . . . .	156
6.11	Correlation cost matrix corresponding to chronostratigraphic correlation given by Equation (3.15) (facies versus distality). This case is intermediate between Equations (3.11) and (3.13) with $\alpha = 2/7$ . The black line corresponds to the most likely correlation set and the dashed red line corresponds to the most likely correlation set computed with $\alpha = 1$ (Figure 6.6). Modified from (Baville et al., 2022). . . . .	158
A.1	Location of the area of interest and the seven studied wells (A) within the Norwegian North Sea, (B) within the South Viking Graben together with other fields, and (C) within the Gudrun Field area (Block 15/3). Map based on <a href="http://www.npd.no">http://www.npd.no</a> . . . . .	193
A.2	Relative grain size of the laminated mudstone, depositional environment corresponding to restricted lagoon, and lithofacies core photograph. Modified from Baville et al. (2022). . . . .	194
A.3	Relative grain size of the sandy-bioclastic mudstone, depositional environment corresponding to open lagoon, and lithofacies core photograph. Modified from Baville et al. (2022). . . . .	195
A.4	(Relative grain size of the oyster shell bed, depositional environment corresponding to patch reef, and lithofacies core photograph. Modified from Baville et al. (2022). . . . .	196
A.5	Relative grain size of the muddy disturbed siltstone, depositional environment corresponding to prodelta, and lithofacies core photograph. Modified from Baville et al. (2022). . . . .	197
A.6	Relative grain size of the heterolithic sandstone, depositional environment corresponding to lower delta front, and lithofacies core photograph. Modified from Baville et al. (2022). . . . .	197

---

A.7	Relative grain size of the bioturbated sandstone, depositional environment corresponding to upper delta front, and lithofacies core photograph. Modified from <a href="#">Baville et al. (2022)</a> . . . . .	198
A.8	Relative grain size of the cross-bedded sandstone, depositional environment corresponding to mouth bar, and lithofacies core photograph. Modified from <a href="#">Baville et al. (2022)</a> . . . . .	199
A.9	Relative grain size of the cross-bedded sandstone, depositional environment corresponding to distributary channel, and lithofacies core photograph. Modified from <a href="#">Baville et al. (2022)</a> . . . . .	199
A.10	Relative grain size of the coal, depositional environment corresponding to swamp, and lithofacies core photograph. Modified from <a href="#">Baville et al. (2022)</a> . . . . .	200
A.11	Relative grain size of the silty mudstone, depositional environment corresponding to marsh, and lithofacies core photograph. Modified from <a href="#">Baville et al. (2022)</a> . . . . .	201
A.12	Relative grain size of the current-ripple cross-laminated sandstone, depositional environment corresponding to fluvial overbank, and lithofacies core photograph. Modified from <a href="#">Baville et al. (2022)</a> . . . . .	201
A.13	Relative grain size of the laminated mudstone, depositional environment corresponding to restricted lagoons, and lithofacies core photograph. Modified from <a href="#">Baville et al. (2022)</a> . . . . .	202



# List of Tables

5.1	Sedimentary facies indexing for correlation cost computation and coloring for correlation panel interpretation. . . . .	125
5.2	Biozone indexing and coloring for correlation panel interpretation (ages based on the <a href="#">International Chronostratigraphic Chart - May 2021</a> ). . . . .	126
6.1	Sedimentary indexing and coloring corresponding to the three sedimentary facies clusters. . . . .	150



# Extended Abstract

Subsurface modeling is a way to predict the structure and the connectivity of stratigraphic units by honoring subsurface observations. These observations are commonly sampled along wells at a large and sparse horizontal scale (kilometer-scale) but at a fine vertical scale (meter-scale). There are several types of well data:

- **Well logs** correspond to quasi-continuous (regular sampling) physical / geophysical measurements along the well path (e.g., gamma ray, sonic, neutron porosity) (e.g., [Serra and Serra, 2003](#)).
- **Well cores** correspond to vertical pieces of subsurface extracted during the drilling. These subsurface samples are generally analyzed in laboratory to generate additional physical / geophysical measurements, to give information about the structure and the nature of the subsurface.
- ⇒ **Well sections** correspond to intervals within which the reservoir properties (interpreted from wells logs and core samples) are homogeneous and characteristic of the depositional condition. These intervals are labeled (e.g., biozones, structural zones, sedimentary facies), and defined by their top and bottom depths along the well path.

Well markers are interpreted along the well path. They can also be associated in order to generate a consistent set of well-marker associations called well correlations.

Stratigraphic well correlations may be achieved manually by experts based on well - log and core sample - interpretations (e.g., [Bourquin et al., 1998](#); [Knaust and Hoth, 2021](#); [Shiers et al., 2017](#)). The resulting scenario is a correlation set. A geologist generally proposes the “best correlation set” or sometimes more (two to five) scenarios on a careful data analysis and prior experience, reflecting some interpretation uncertainties. Increasing the number of interpreters may help to gain confidence about a particular interpretation, or conversely to produce more scenarios ([Bond et al., 2007](#); [Borgomano et al., 2008](#)).

Ideally, a quantification of correlation uncertainties would call for generating every topologically possible scenario (Figure 2.A) and evaluating its likelihood. However, the very large number of topologically possible scenarios makes their manual validation almost impossible (Lallier et al., 2016). To overcome this limitation, numerical methods to provide automatically multiple stratigraphic scenarios have been proposed (e.g., Baviile et al., 2022; Edwards et al., 2018; Lallier et al., 2016; Pels et al., 1996).

Similar to the work of Edwards (2017); Lallier (2012); Smith and Waterman (1980), the algorithm used in this PhD work to simulate a large number of well stratigraphic correlation scenarios and rank them by their likelihood is the Dynamic Time Warping algorithm (Needleman and Wunsch, 1970; Sakoe and Chiba, 1978).

The Dynamic Time Warping algorithm uses a conceptual multi-dimensional correlation cost matrix whose axis correspond to the input wells. Using a correlation cost function, each well-marker association is defined by a correlation cost  $c$ , and each transition between two well-marker associations are defined by a transition cost  $t$ .

Finally the sum of all the costs along a correlation path (within the cost matrix) gives the cumulative correlation cost of the correlation set, and the Dynamic Time Warping algorithm returns the best or the  $n$ -best correlation sets thanks to the correlation cost function.

Scenarios are consistent with the input data and with some explicitly defined correlation rules which enable to discern the most likely solutions. Therefore, correlation rules must be carefully chosen to produce solutions which are geologically acceptable.

## Principles of correlation and applications

This PhD work introduces two principles of correlation, which tend to reproduce the chronostratigraphy and the depositional processes at the parasequence scale :

### Principle 1: Sedimentary facies *versus* Well distality

The purpose of this first proposed correlation cost function is to generate stratigraphic well correlations based on the principle stating that “*a marker (described by facies and distality taken at the center of an interval having a constant facies and a constant distality) cannot be associated with another marker described by a depositionally deeper facies at a more proximal position, or a depositionally shallower facies at a more distal position*” (Baviile et al., 2022).

This method requires sedimentary facies interpretations along well paths, and the distality of all wells computed from the well position along a distal-to-proximal transect, to compute a correlation cost for each possible well-marker correlation. This method has been applied on the Middle Jurassic Hugin Formation in the Gudrun-Sigrun Field area in order to evaluate the consistency of the paleogeographic interpretation with respect to biostratigraphic data (Chapter 5).

It has also been applied to model the stratigraphic layering of the Early Callovian Hugin Formation in the Sigrun Field area (Chapter 6). In both applications, the distality rule of correlation leads to promising outcomes which are consistent with respect to biostratigraphic interpretations.

## **Principle 2: Depositional profile versus Dip data**

The purpose of this second proposed correlation cost function method is to generate stratigraphic well correlation based on the principle stating that “*the lower the difference between a chronostratigraphic interpolation (in between markers) and a conceptual depositional profile, the higher the likelihood of the marker association*” (Baville et al., 2021a).

This method requires dipmeter data and depositional facies interpretations along wells to interpolate stratigraphic horizons, and a theoretical depositional profile defined by a principal sediment transport direction and a deltaic vertical and lateral extension, to compute a correlation cost for each possible well-marker correlation.

The proposed method has only been tested on a synthetic data set, and the first results are promising but may be biased by the construction of the synthetic data set. This method must be improved by being applied on more complex synthetic data set and the main goal of this method is to be applied on a real data set to generate a chronostratigraphic models from sparse well data and evaluate the uncertainties on these models.

These two principles of computer-assisted well correlation are first benchmarked with analytical solutions and applied on synthetic cases in two different purposes :

### **Application 1: Depositional consistency**

The uncertainties on the depositional system are high : well correlation simulations are used to compare the proposed depositional context with additional subsurface data such as biostratigraphic interpretations. In this case, well correlations are simulated using specific correlation rules adapted from the proposed depositional context (e.g., Baville et al., 2019, 2021b).

## Application 2: Stratigraphic subsurface prediction

The uncertainties on the depositional system are low : well correlation simulations are used to predict the subsurface structure. In this other case, the geometry and the connectivity of the stratigraphic units are simulated from well data and prior knowledge on sedimentary rock depositional processes and depositional systems (e.g., [Baville et al., 2021a, 2022](#)).

The methods are applied on a siliciclastic coastal deltaic system targeting the Middle Jurassic Hugin Formation in the Gudrun-Sigrun Field area, North Sea.

## Conclusions and Perspectives

This work enables to define two specific principles of correlation defined by a few parameters. They can be used to generate automatically well correlations within coastal deltaic systems.

The results obtained on the synthetic data sets based on the correlation principles enable to validate the correlation cost functions implemented during this PhD work. Finally, the results obtained by applying these correlation rules to real data sets are promising and allow to generate stratigraphic models of the subsurface using automatic stratigraphic well correlations.

The Dynamic Time Warping algorithm also enables to combine different correlation principles, by combining correlation costs. Thus new correlation principles could be added and combined with the two correlation principles proposed in this PhD work. For example, the correlation cost could be weighted by the lateral variation of facies in stratigraphic units. Another example would be to take into account structural fault interpretations between and along wells to constrain the geometric interpolation of stratigraphic horizons between wells.

Furthermore, the Dynamic Time Warping algorithm can be used in a deterministic way, but also in a stochastic way. The stochastic version of the algorithm ensures the reproducibility of the results and allows the assessment and the quantification of uncertainties on well correlations, and thus on the characterization of coastal deltaic sedimentary systems.

Finally, the evaluation and quantification of uncertainties in stratigraphic correlation models can be integrated and propagated in the general workflow of static and dynamic reservoir modeling. Indeed, several stratigraphic correlation models could lead to different geological models and thus to different reservoir properties simulations (porosity, facies, etc.) and flow simulations within these different models. Thus the quantification of uncertainties on reservoir models could take into account the step of stratigraphic well correlation.





# Résumé étendu

La modélisation du sous-sol est un moyen de prédire la structure et la connectivité des unités stratigraphiques en honorant les observations de subsurface. Ces observations sont généralement échantillonnées le long de puits de manière éparse à une large échelle horizontale (échelle kilométrique) mais à une fine échelle verticale (échelle métrique). Il existe plusieurs types de données de puits :

- **Les diagraphies de puits** correspondent à des mesures physiques / géophysiques quasi-continues (échantillonnage régulier) le long de la trajectoire du puits (e.g., porosité gamma, sonique, porosité neutron) (e.g., [Serra and Serra, 2003](#)).
- **Les carottes de puits** correspondent à des échantillons du sous-sol extraits lors du forage. Ces échantillons de subsurface sont généralement analysés en laboratoire afin de générer des mesures physiques / géophysiques supplémentaires, pour donner des informations sur la structure et la nature du sous-sol.
- ⇒ **Les sections de puits** correspondent à des intervalles au sein desquels les propriétés réservoir (interprétées à partir des diagraphies de puits et des carottes) sont homogènes et caractéristiques des conditions de dépôt. Ces intervalles sont labellisés (e.g., biozones, zones structurales, faciès sédimentaires) et définis par leurs profondeurs supérieure et inférieure le long de la trajectoire du puits.

Les marqueurs de puits sont interprétés le long de la trajectoire du puits. Ils peuvent être aussi associés afin de générer un ensemble cohérent d'associations de marqueurs appelé corrélations de puits.

Les corrélations stratigraphiques des puits peuvent être réalisées manuellement par des experts sur la base d'interprétations des diagraphies et des carottes de puits (e.g., [Bourquin et al., 1998](#); [Knaust and Hoth, 2021](#); [Shiers et al., 2017](#)). Le scénario résultant est un ensemble de corrélations. Un géologue propose généralement le “meilleur ensemble de corrélations” ou parfois plusieurs (deux à cinq)

scénarios sur la base d'une analyse minutieuse des données et de sa propre expérience, en tenant compte de certaines incertitudes d'interprétation. Augmenter le nombre d'interprètes peut aider à gagner en confiance sur une interprétation particulière, ou inversement à produire plus de scénarios (Bond et al., 2007; Borgomano et al., 2008).

Idéalement, une quantification des incertitudes de corrélation nécessiterait de générer chaque scénario topologiquement possible et d'évaluer sa vraisemblance. Cependant, le très grand nombre de scénarios topologiquement possibles rend leur validation manuelle presque impossible (Lallier et al., 2016). Pour surmonter cette limitation, des méthodes numériques permettant de fournir automatiquement de multiples scénarios stratigraphiques ont été proposées (e.g., Baviile et al., 2022; Edwards et al., 2018; Lallier et al., 2016; Pels et al., 1996).

À l'instar des travaux de Edwards (2017); Lallier (2012); Smith and Waterman (1980), l'algorithme utilisé dans ces travaux de thèse pour simuler un grand nombre de scénarios de corrélations stratigraphiques de puits et les classer en fonction de leur vraisemblance est l'algorithme de Déformation Temporelle Dynamique (Needleman and Wunsch, 1970; Sakoe and Chiba, 1978).

L'algorithme de Déformation Temporelle Dynamique utilise une matrice de coûts de corrélation conceptuelle multi-dimensionnelle dont les axes correspondent aux différents puits. En utilisant une fonction de coût de corrélation, chaque association de marqueurs de puits est définie par un coût de corrélation  $c$ , et chaque transition entre deux associations de marqueurs de puits est définie par un coût de transition  $t$ .

Enfin, la somme de tous les coûts le long d'un chemin de corrélation (dans la matrice de coûts) donne le coût de corrélation cumulé de l'ensemble de corrélation, et l'algorithme de Déformation Temporelle Dynamique retourne le meilleur ou les  $n$  meilleurs ensembles de corrélation en fonction de la fonction de coût de corrélation.

Les scénarios sont cohérents avec les données d'entrée et avec certaines règles de corrélation explicitement définies qui permettent de discerner les solutions les plus probables. Par conséquent, les règles de corrélation doivent être choisies avec soin pour produire des solutions qui soient géologiquement acceptables.

## Principes de corrélation et applications

Ce travail de thèse introduit deux fonction de coût de corrélation automatiques, fondées sur deux principes de corrélation, qui tendent à reproduire le plus possible la chronostratigraphie et les processus de dépôt à l'échelle de la paraséquence.

## Principe 1 : Faciès sédimentaires *versus* Distalité relative

L'objectif de cette première fonction de coût de corrélation proposée est de générer des corrélations de puits stratigraphiques basées sur le principe selon lequel “*un marqueur de puits (décrit par un faciès et une distalité pris au centre d'un intervalle ayant un faciès constant et une distalité constante) ne peut pas être associé à un autre marqueur de puits décrit par un faciès plus profond d'un point de vue du dépôt à une position plus proximale, ou un faciès moins profond d'un point de vue du dépôt à une position plus distale*” (Baville et al., 2022).

Cette méthode nécessite des interprétations de faciès sédimentaires le long des trajectoires de puits, et la distalité de tous les puits calculée à partir de la position du puits le long de la direction entre le pôle distal et le pôle proximal, afin de calculer un coût de corrélation entre chaque association de marqueurs.

Cette méthode a été appliquée à la Formation Hugin du Jurassique moyen dans la champ Gudrun-Sigrun situé en Mer du Nord afin d'évaluer la cohérence de l'interprétation paléogéographique par rapport aux données biostratigraphiques. Elle a également été appliquée pour modéliser la stratigraphie de la Formation Hugin du Callovien Inférieur dans le champ Sigrun. Dans les deux applications, la règle de corrélation de la distalité conduit à des résultats prometteurs qui sont cohérents par rapport aux interprétations biostratigraphiques.

## Principe 2 : Profil de dépôt *versus* Données de pendage

L'objectif de cette deuxième méthode de fonction de coût de corrélation proposée est de générer une corrélation stratigraphique des puits basée sur le principe selon lequel “*plus la différence entre une interpolation chronostratigraphique (entre les marqueurs de puits) et un profil de dépôt conceptuel est faible, plus la vraisemblance de l'association des marqueurs de puits est élevée*” (Baville et al., 2021a).

Cette méthode nécessite des données de pendage et des interprétations de faciès de dépôt le long des puits pour interpoler la géométrie des horizons stratigraphiques, et un profil de dépôt théorique défini par une direction principale de transport de sédiments et une extension verticale et latérale du delta, afin de calculer un coût de corrélation entre chaque association de marqueurs.

La méthode proposée n'a été testée que sur un jeu de données synthétique, et les premiers résultats sont prometteurs mais peuvent être biaisés par la construction du jeu de données synthétique. Cette méthode doit être améliorée en l'appliquant à des jeux de données synthétiques plus complexes et l'objectif principal de cette méthode est d'être appliquée sur un jeu de données réel pour générer des modèles chronostratigraphiques à partir de données de puits éparses et évaluer les incertitudes sur ces modèles.

Ces deux principes de corrélation stratigraphique de puits assistée par ordinateur sont d'abord comparés à des solutions analytiques et appliqués à des cas synthétiques dans deux buts différents :

### **Application 1 : Cohérence du système de dépôt**

Les incertitudes sur le système de dépôt sont élevées : les simulations de corrélation de puits sont utilisées pour comparer le système de dépôt proposé avec des données de subsurface supplémentaires telles que les interprétations biostratigraphiques. Dans ce cas, les corrélations de puits sont simulées en utilisant des règles de corrélation spécifiques adaptées au contexte de dépôt proposé (e.g., [Baville et al., 2019, 2021b](#)).

### **Application 2 : Prédiction stratigraphique du sous-sol**

Les incertitudes sur le système de dépôt sont faibles : des simulations de corrélation de puits sont utilisées pour prédire la structure du sous-sol. Dans cet autre cas, la géométrie et la connectivité des unités stratigraphiques sont simulées à partir des données de puits et des connaissances préalables sur les processus de dépôt des roches sédimentaires et les systèmes de dépôt. (e.g., [Baville et al., 2021a, 2022](#)).

Les méthodes sont ensuite appliquées sur un jeu de donnée d'un système deltaïque côtier silicoclastique daté du Jurassique Moyen correspondant à la Formation de Hugin dans la région de Gudrun-Sigrun en Mer du Nord.

## **Conclusions et perspectives**

Ce travail permet de définir deux principes spécifiques de corrélation stratigraphique de puits, définis par quelques paramètres. Ils peuvent être utilisés pour générer automatiquement des corrélations de puits dans les systèmes deltaïques côtiers.

Les résultats obtenus sur les jeux de données synthétiques à partir des principes de corrélation ont permis de valider les fonctions de coût de corrélation implémentées durant ces travaux. Enfin les résultats obtenus en appliquant ces règles de corrélations à des jeux de données réels sont prometteurs et permettent de générer des modèles stratigraphiques du sous-sol à partir de corrélations de puits automatiques.

L'algorithme de Déformation Temporelle Dynamique permet aussi de combiner les différents principes de corrélation, en combinant les coûts de corrélation. Ainsi de nouveaux principes de corrélation pourraient être ajoutés et combinés aux deux principes de corrélation proposés dans ces travaux. Par exemple, le coût

de corrélation pourrait être pondéré par la variation latérale de faciès dans les unités stratigraphiques. Un autre exemple serait de prendre en compte les interprétations de failles structurales entre et le long des puits pour contraindre l'interpolation géométrique des horizons stratigraphiques entre les puits.

De plus, l'algorithme de Déformation Temporelle Dynamique peut être utilisé de manière déterministe, mais aussi de manière stochastique. La version stochastique de l'algorithme assure la reproductibilité des résultats et permet l'évaluation et la quantification des incertitudes sur les corrélations de puits, et donc sur la caractérisation des systèmes sédimentaires deltaïques côtiers.

Enfin, l'évaluation et la quantification des incertitudes des modèles de corrélations stratigraphiques peuvent être intégrées et propagées dans le processus général de modélisation statique et dynamique des réservoirs. En effet, plusieurs modèles de corrélation stratigraphiques pourraient mener à différents modèles géologiques et donc à différents résultats de simulation de propriétés réservoir (e.g., porosité, faciès, etc.) et de simulations d'écoulements au sein de ces différents modèles. Ainsi la quantification d'incertitudes sur les modèles réservoirs pourrait prendre en compte l'étape de corrélation stratigraphique de puits.



# Introduction

It is impossible to see what lies underground, or to get a full view at a fine scale of the subsurface. However, geologists have defined concepts (e.g., stratigraphy by [Steno \(1669\)](#)), have postulated principles, and have made assumptions about the subsurface structures and sedimentary rock depositional processes. These hypotheses enable the conception of multi-dimensional numerical subsurface models in space and time, also called geomodels, of a zone of interest.

These geomodels are usually built from sparse data or low resolution data, and are usually used as the support of numerical simulations such as static properties simulations (e.g., [Journel, 1974](#); [Matheron, 1963, 1969](#)) or dynamic physical process simulations (e.g., [Durlafsky, 2005](#); [Eaton, 2006](#); [King and Mansfield, 1999](#)).

## How geologically true are these geomodels?

The answer to this question is not easy because a model is by definition geologically inaccurate and imprecise. Indeed, geomodel building is constrained by geological principles which are based on observations and interpretations. The geological likelihood of these geomodels is therefore evaluated with respect to these principles.

The consistency of principles may be evaluated without taking into account the quality of a model, but based on prior knowledge about the depositional context. The previous question now becomes:

## How consistent are the principles used to model the subsurface?

[Steno \(1669\)](#) has proposed the concept of **stratigraphy** defined by [Rey \(1983\)](#) as “*the study of the arrangement in space and time of geological formations and the events they materialize, in order to reconstruct the history of the Earth and its various states at different moments in time*”.

The stratigraphy enables the understanding of the subsurface organization of geobodies in space and time through field data descriptions and interpretations

(Steno, 1669). In the case of sedimentary subsurface basins, the understanding of their structure and the prediction of available resources within these areas is a key element in several applied fields of the Geosciences:

- A first application is the study of the underground to help the prediction and the management of natural risks (earthquakes, landslides, *etc.*) (e.g., Chung and Fabbri, 1999; Chéneau and Risser, 2019; Scheidegger, 1973; Scholz et al., 1973).
- Another application is the exploitation of subsurface raw materials (hydrocarbons, groundwater, ores, *etc.*), which are crucial for the energy transition. The good understanding of the subsurface structure and the position of the targeted resources enables the generation of fine-scale multi-dimensional models (e.g., three-dimensional space + time). The subsurface structure has a strong impact on the understanding and the production of these resources (e.g., Baville et al., 2019; Fredman et al., 2007; Vincent et al., 1999).

Geomodels are built to numerically represent the subsurface (e.g., to visualize stratigraphic units, to compute their volumes and their inter-connectivity, to test multiple resource recovery scenarios, *etc.*). They are useful, for example, to test multiple facies distributions (Homewood et al., 1992) and to assess their impact on subsurface flow simulations (e.g., Cavero et al., 2016; Jackson et al., 2009; Lallier, 2012).

A first approach to generate stratigraphic models is the use of direct modeling methods. These methods are based on physical laws constraining sediment transport and sedimentation, and iteratively compute deposited sediments at each time step (e.g., Burgess et al., 2012; Granjeon, 1997; Kendall et al., 1991; Lawrence et al., 1990; Tetzlaff and Harbaugh, 1989). However, these methods make it difficult to match observation data (well data, outcrops, seismic data, *etc.*), and the tuning of settings controlling sediment transport and deposition is limited.

Another approach to build geomodels is the use of the geometric interpolation methods (e.g., Frank et al., 2007; Mallet, 1992, 2002; Tertois, 2007). The geometry of the subsurface units is interpolated between observation data (well data, outcrops, seismic data, *etc.*).

Both approaches are used to generate stratigraphic models of the subsurface. However, stratigraphic units may be thinner than the seismic resolution, making their interpretation from the seismic data difficult (e.g., Baville et al., 2022; Knaust and Hoth, 2021). The interpretation of stratigraphic units, which are thinner than the seismic resolution, may thus be performed at small vertical meter-scale and large horizontal kilometer-scale from well data:

- **Well logs** correspond to quasi-continuous (regular sampling) physical / geophysical measurements along the well path (e.g., gamma ray, sonic, neutron porosity) (e.g., [Serra and Serra, 2003](#)).
  - **Well cores** correspond to vertical pieces of subsurface extracted during the drilling. These subsurface samples are generally analyzed in laboratory to generate additional physical / geophysical measurements, to give information about the structure and the nature of the subsurface.
- ⇒ **Well sections** correspond to intervals within which the reservoir properties (interpreted from well logs and cores) are homogeneous and characteristic of the depositional condition. These intervals are labeled (e.g., biozones, structural zones, sedimentary facies) and defined by their top and bottom depths along the well path.

In this PhD work, well data are used as input data to build and constrain models. The generation of geomodels from well data using geometrical methods may be separated into four successive steps (Figure 1):

- **Stratigraphic well correlation** (Figure 1.A). Well markers corresponding to stratigraphic heterogeneities interpreted along well paths from well data (e.g., stratigraphic unit interface, structural fault, *etc.*), are associated according to correlation rules (e.g., [Baville et al., 2021a, 2022](#); [Edwards, 2017](#); [Lallier, 2012](#)). Their associations return correlation lines (between two wells) and surfaces (between more than two wells), whose corners correspond to well markers.
- **Stratigraphic unit interpolation** (Figure 1.B). Correlation lines / surfaces represent stratigraphic unit interfaces and their geometries can be interpolated / extrapolated from well markers, e.g., using dipmeter data (e.g., [Baville et al., 2021a](#); [Mallet, 2002](#)).
- **Stratigraphic unit conformity** (Figure 1.C). The conformity, which have been interpreted from well data, and the substratigraphic sedimentation structures are represented within each stratigraphic unit (e.g., [Allen, 1963](#)).
- **Subsurface property prediction** (Figure 1.D). Stratigraphic units are populated by reservoir properties (sedimentary facies, porosity, permeability, *etc.*) using geostatistical estimations or simulations (e.g., [Journel, 1974](#); [Matheron, 1963, 1969](#)).

Stratigraphic well correlations may be achieved manually by experts based on well - log and core sample - interpretations (e.g., [Bourquin et al., 1998](#); [Knaust and Hoth, 2021](#); [Shiers et al., 2017](#)). The resulting scenario is a correlation set.

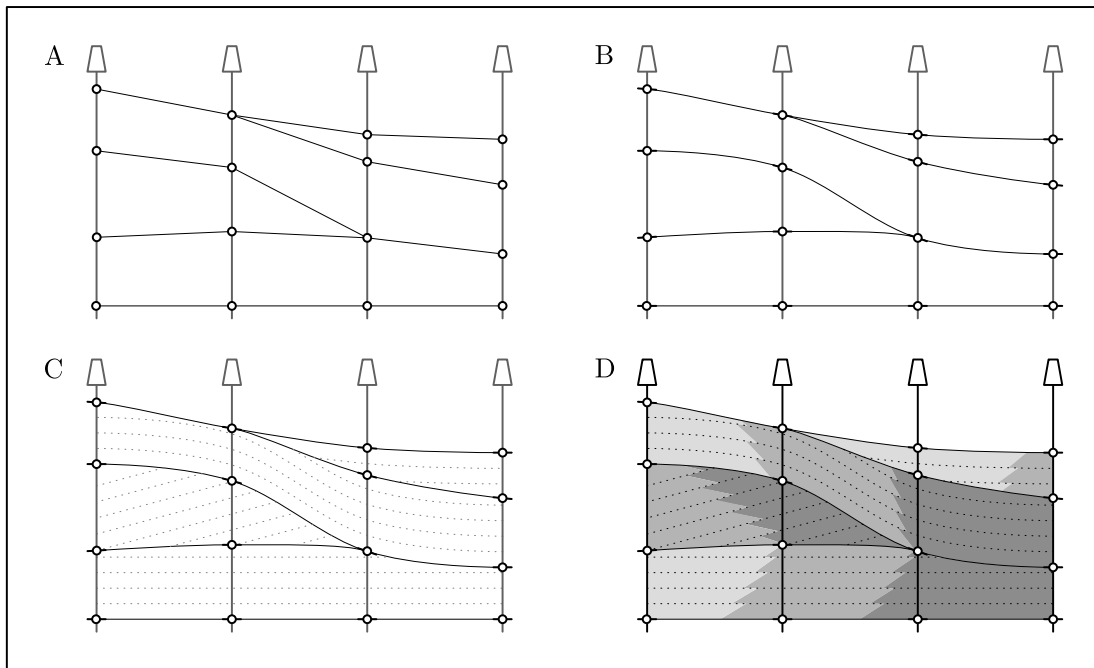


*Figure 1: The four successive steps of the geometrical interpolation approach of geomodel building: (A) stratigraphic well correlation, (B) stratigraphic unit geometry interpolation/extrapolation, (C) stratigraphic unit conformity, and (D) subsurface property estimation/simulation. Redrawn from [Edwards \(2017\)](#).*

A geologist generally proposes the “best correlation set” or sometimes more (two to five) scenarios on a careful data analysis and prior experience, reflecting some interpretation uncertainties. Increasing the number of interpreters may help to gain confidence about a particular interpretation, or conversely to produce more scenarios ([Bond et al., 2007](#); [Borgomano et al., 2008](#)).

Ideally, a quantification of correlation uncertainties would call for generating every topologically possible scenario (Figure 2.A) and evaluating its likelihood. However, the very large number of topologically possible scenarios makes their manual validation almost impossible ([Lallier et al., 2016](#)).

To overcome this limitation, numerical methods to provide automatically multiple stratigraphic scenarios have been proposed (e.g., [Edwards et al., 2018](#); [Lallier et al., 2016](#); [Pels et al., 1996](#)). Scenarios are consistent with the input data and with some explicitly defined correlation rules which enable to discern the most likely solutions. Therefore, correlation rules must be carefully chosen to produce solutions which are geologically acceptable (Figure 1.B-C).

This PhD work proposes two new principles of correlation based on chronostratigraphic concepts, and two correlation rules that can be integrated in automated well correlation simulation processes:

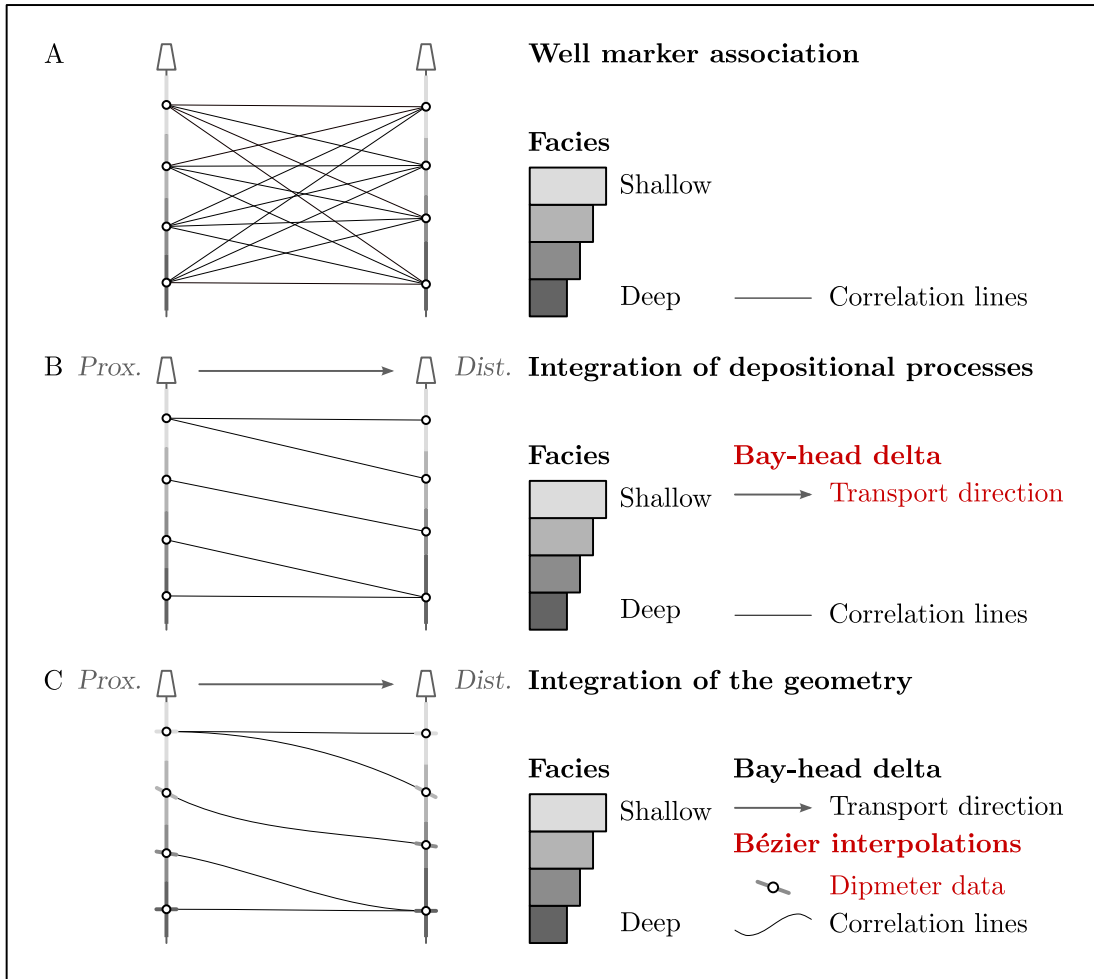


Figure 2: (A) Every topologically possible well-marker association. (B) Integration of prior knowledge on depositional context (e.g., sediment transport direction) to quantify the likelihood of each well-marker association (e.g., [Baville et al., 2022](#); [Lallier et al., 2016](#)). (C) Integration of the depositional geometry (e.g., dipmeter data) to quantify the likelihood of each well-marker association (e.g., [Baville et al., 2021a](#)).

- **Sedimentary facies versus well distality.** “A well marker (described by a facies and a well distality taken at the center of an interval having a constant facies and a constant well distality) cannot be associated with another well marker described by a depositionally deeper facies at a more proximal well position, or a depositionally shallower facies at a more distal well position” ([Baville et al., 2021b, 2022](#)). Well-marker associations which go against this principle of correlation are excluded and cannot be simulated.
- **Depositional profile versus dipmeter data:** “The lower the difference between a chronostratigraphic interpolation (in between well markers) and a conceptual depositional profile, the higher the likelihood of the well marker association” ([Baville et al., 2021a](#)).

These two principles of correlation enable the generation of multiple correlation sets computed from the same input data set. All these generated scenarios may be ranked according to their likelihood, which is given by the principles of correlation. However, it is important to note that these principles of correlation are chosen according to the prior knowledge of the depositional system. Therefore, the uncertainties on the prior knowledge must be taken into account within the subsurface modeling process.

The main purpose of this PhD work is to generate computer-assisted stratigraphic well correlations. These well correlations may be used in two different ways:

- **Depositional system consistency.** The uncertainties on the depositional system are high: well correlation simulations are used to compare the proposed depositional context with additional subsurface data such as biostratigraphic interpretations. In this case, well correlations are simulated using specific correlation rules adapted from the proposed depositional context (e.g., [Baville et al., 2019, 2021b](#)).
- **Stratigraphic subsurface prediction.** The uncertainties on the depositional system are low: well correlation simulations are used to predict the subsurface structure. In this other case, the geometry and the connectivity of the stratigraphic units are simulated from well data and prior knowledge on sedimentary rock depositional processes and depositional systems (e.g., [Baville et al., 2021a, 2022](#)).

## Structure of the manuscript

Part I provides an overview of the concepts of chronostratigraphy and introduces the main principles of stratigraphic well correlation (Chapter 1). It presents different approaches to automatically compute and stochastically simulate well correlations in order to assess the uncertainties (Chapter 2).

Part II presents the two principles of correlation based on sedimentary rock depositional processes by taking into account the relative well position within the depositional system (Chapter 3), and by reproducing the geometry of the depositional profile from dipmeter data (Chapter 4).

Part III reports on the application of the rule of correlation proposed in Chapter 3 on a data set provided by [Equinor ASA](#) targeting the Middle Jurassic Hugin Formation in the Gudrun-Sigrun Field area (Block 15/3), Norwegian North Sea (Appendix A). Chapter 5 compares the simulated stratigraphic well correlations based on two different paleogeographic depositional environment interpretations

with biostratigraphic data. Chapter 6 proposes to predict the depositional paleogeography from stratigraphic well correlation simulations based on a consistent depositional context with respect to biostratigraphy.

## General context of the PhD

This PhD work was carried out for nearly three years (January 2019 - April 2022) in the RING Team (<https://www.ring-team.org>) within the GeoResources laboratory (CNRS / Université de Lorraine) in Vandœuvre-lès-Nancy, France. This PhD work has been supervised by Guillaume Caumon (Université de Lorraine), Cédric Carpentier (Université de Lorraine) and Marcus Apel (Equinor ASA).

### RING Consortium



This PhD work has been co-funded by the RING Consortium (Research for Integrative Numerical Geology) managed by ASGA (Association Scientifique pour la Géologie et ses Applications). RING is currently funded by a worldwide consortium of universities and companies comprising both international and national oil companies and service providers.

This PhD position co-funded by the RING Consortium has led to the publication of scientific proceedings, to the realization of technical trainings, and to poster or oral presentations for industrial sponsors of the RING Consortium during annual meetings.

### Equinor ASA



This PhD work has also been co-funded by Equinor ASA. This collaboration with Equinor enabled three missions to Stavanger, Norway, to study core and logging data directly on site. The application of correlation rules on the digitized data could also be directly compared to on-site data.

The data set used to calibrate the correlation rules developed during this PhD is a Middle Jurassic data set from the Norwegian North Sea (Part III), and the publication of all results obtained on it have been authorized by Equinor ASA.

Moreover, a presentation of the possible application of this PhD work on real data set have been presented at the *NPS Reservoir Characterization 2019*.

## **RING Team**

The purpose of the RING Team is to develop numerical technologies to model the subsurface by integrating the uncertainty assessment during the modeling process. The purpose of this PhD is to generate stratigraphic model of the subsurface by simulating well correlations.

The principal contribution of this PhD work is the development of numerical rules of correlation to constrain computer-assisted stratigraphic well correlation. The two correlation rules developed during this PhD have been implemented in *WeCo*, a C++ and Python library which simulates several sets of possible correlations between multiple wells (<https://www.ring-team.org/technologies/WeCo>).

The scientific contributions of this PhD work have been presented in international conferences such as the *81st EAGE ACE* and the *AAPG 2020 ACE*. One of the two correlation rules developed during this PhD has been published in the peer-reviewed scientific journal *Marine & Petroleum Geology*.

Finally, being part of the RING Team has allowed me to teach numerical approaches in geosciences, and to co-supervise students' laboratory projects at the ENSG (Ecole Nationale Supérieure de Géologie de Nancy).

## Scientific publications

Notations: <sup>(r)</sup>peer-reviewed article, <sup>(a)</sup>proceeding article, <sup>(e)</sup>extended abstract, <sup>(o)</sup>oral presentation, <sup>(p)</sup>poster presentation, <sup>(w)</sup>online webinar, \* presenter.

### Peer-reviewed article

- <sup>(r)</sup> **P. Baville**<sup>\*</sup>, M. Apel, D. Knaust, S. Hoth, C. Antoine, C. Carpentier, and G. Caumon (2022). Computer-assisted stochastic multi-well correlation: Sedimentary facies versus Well distality. In: *Marine and Petroleum Geology*. doi:[10.1016/j.marpetgeo.2021.105371](https://doi.org/10.1016/j.marpetgeo.2021.105371).

### International conferences

- <sup>(o)</sup> **P. Baville**<sup>\*</sup>, M. Apel, C. Carpentier, G. Caumon, S. Hoth, D. Knaust, and C. Antoine (2020). Assisted chronostratigraphic multi-well correlation using the Dynamic Time Warping algorithm. In: *AAPG 2020 Annual Convention and Exhibition*. American Association of Petroleum Geologists.
- <sup>(o,e)</sup> **P. Baville**<sup>\*</sup>, J. Peisker, and G. Caumon (2019). From well logs to stratigraphic layering: Automation, uncertainties and impact on reservoir behavior. In: *81st EAGE Conference and Exhibition 2019*. European Association of Geoscientists and Engineers. doi:[10.3997/2214-4609.201901293](https://doi.org/10.3997/2214-4609.201901293).

### Annual RING Meeting

- <sup>(o,a)</sup> **P. Baville**<sup>\*</sup>, M. Apel, D. Knaust, S. Hoth, C. Antoine, C. Carpentier, and G. Caumon (2021). Computer-assisted stochastic multi-well correlation: Surface simulation versus Depositional profile. In: *2021 RING Meeting*. ASGA.
- <sup>(p,a)</sup> **P. Baville**<sup>\*</sup>, M. Apel, D. Knaust, S. Hoth, and G. Caumon (2021). Application of the Distality rule of WeCo on the  *Gudrun-Sigrun Field* Middle Jurassic data set, North Sea. In: *2021 RING Meeting*. ASGA.
- <sup>(o,a)</sup> **P. Baville**<sup>\*</sup>, G. Caumon, C. Carpentier, M. Apel, S. Hoth, and D. Knaust (2020). Computer-assisted multi-well stochastic correlations: Chronostratigraphic surface simulation using Bézier cubic interpolations. In: *2020 RING Meeting*. ASGA.
- <sup>(o,a)</sup> **P. Baville**<sup>\*</sup>, G. Caumon, M. Apel, D. Knaust, S. Hoth, C. Carpentier, and C. Antoine (2019). Stochastic well correlation based on facies and sequence interpretations using the hierarchical algorithm WeCo. In: *2019 RING Meeting*. ASGA.

## RING Webinars

- <sup>(w)</sup> **P. Bavi**le\* (2021). Computer-assisted stochastic well correlation: Well distality *versus* Sedimentary facies. RING Consortium. [url: Online RING Webinar](#).

## Other contributions result from parallel works

- <sup>(p,a)</sup> G. Caumon\*, C. Antoine, **P. Bavi**le, S. Hoth, and J. Charreau (2021). Magnetostratigraphic data and assisted well correlation: Some thoughts and first results, Triassic North Sea. In: *2021 RING Meeting*. ASGA.
- <sup>(o,a)</sup> J. Herrero\*, **P. Bavi**le, and G. Caumon (2021). GeosteeRING: A Bayesian methodology for real-time updating of well trajectory in depositional space. In: *2021 RING Meeting*. ASGA.
- <sup>(o,a)</sup> Y. Perrier\*, **P. Bavi**le, and G. Caumon (2021). Stochastic simulation of stratigraphic sequences from well log data using Continuous Wavelet Transforms. In: *2021 RING Meeting*. ASGA.
- <sup>(o)</sup> G. Caumon\*, C. Antoine, **P. Bavi**le, M. Apel, S. Hoth, and D. Knaust (2021). Assisted Stratigraphic Correlation for integrating seismic images, wells and geology: achievements and challenges. In: *Decision based integrated reservoir modeling*. Workshop AAPG.
- <sup>(o)</sup> G. Caumon\*, C. Antoine, S. Hoth, **P. Bavi**le, J. Charreau, and D. Knaust (2021). Using magnetostratigraphic data in assisted well correlation to reduce uncertainty: Some thoughts and first results. In: *Stratigraphic and Reservoir Challenges with Triassic Plays in the North Sea Central Graben*. Workshop AAPG.
- <sup>(o)</sup> D. Knaust\*, M. Apel\*, S. Hoth, and **P. Bavi**le (2019). The Middle Jurassic *Hugin Formation* in Block 15/3 of the South Viking Graben, North Sea, Norway. *Reservoir Characterization 2019*. Norwegian Petroleum Society.

## Algorithmic contributions

**B3D** (Bézier 3D interpolations) is a Python/C++ stand-alone algorithm which interpolates Bézier curves and patches between well markers to represent depositional profiles. © RING Consortium.

**WeCo** (Well Correlation) is a Python/C++ stand-alone algorithm which simulates stochastic multi-well correlations using a graph-based version of the Dynamic Time Warping algorithm. © RING Consortium.

## Academic contributions

### Teaching

Year	Lecture	Description	Level
2021/22	Geostatistics	<i>Geostatistical kriging and simulation</i> <i>Categorical approaches</i>	ENSG - M1 (18h)
2020/21	Geostatistics	<i>Spatial data analysis</i> <i>Spatial variability characterization</i> <i>Geostatistical kriging and simulation</i> <i>Categorical approaches</i>	ENSG - M1 (36h)
2019/20	Geostatistics	<i>Spatial variability characterization</i> <i>Geostatistical kriging and simulation</i>	ENSG - M1 (18h)
2019/20	Algorithmic	<i>Python object-oriented programing</i> <i>Multi-module project development</i>	ENSG - M1 (32h)
2018/19	Reservoir modeling	<i>Seismic interpretation</i> <i>Static and dynamic reservoir modeling</i>	ENSG - M1 (18h)

### Supervision

Year	Student	Project	Level
2020/21	J. Herrero	<i>GeosteeRING: A Bayesian methodology for real-time updating of well trajectory in depositional space</i>	ENSG - M2
2020/21	Y. Perrier	<i>Stochastic simulation of stratigraphic sequences from well log data using Continuous Wavelet Transforms</i>	ENSG - M2
2020/21	B. Thebault	<i>Erosion line simulation from stratigraphic multi-well correlations</i>	ENSG - M1
2019/20	G. Peyssard	<i>Directional drill trajectory correction according to a prior stratigraphic model</i>	ENSG - M2
2019/20	K. Souhy	<i>Integration of hard depositional age interpretation in time-to-depth correlation stochastic simulations</i>	ENSG - M2
2019/20	Q. Capillon	<i>Dipmeter data simulation from 4-directional resistivity logs using the Dynamic Time Warping algorithm</i>	ENSG - M1
2019/20	A. Fratani	<i>Integration of a minimal thickness constraint on stratigraphic sequence stochastic simulations for wells' interpretation</i>	ENSG - M1



Part I

**WELL CORRELATION**



# Chapter 1

## Stratigraphic well correlation

### Contents

---

<b>1.1</b>	<b>Subsurface stratigraphic data</b>	<b>17</b>
1.1.1	Direct observations	20
1.1.2	Geophysical measurements	21
1.1.3	Depositional information	22
<b>1.2</b>	<b>Sequence Stratigraphy</b>	<b>23</b>
1.2.1	Accommodation rate & Sedimentation rate	25
1.2.2	Sequence Stratigraphy: Nomenclature & Definitions	28
1.2.2.1	Stratigraphic surfaces	29
1.2.2.2	Stratigraphic system tracts	29
1.2.2.3	Prograding parasequences / Clinofolds	31
1.2.2.4	Stratigraphic conformity	32
1.2.3	Lithostratigraphy versus chronostratigraphy	33
<b>1.3</b>	<b>Stratigraphic well correlation</b>	<b>35</b>
1.3.1	From stratigraphic data to well markers	35
1.3.2	Principles of chronostratigraphic well correlation	37
1.3.3	Uncertainties in stratigraphic well correlation	39

---

This chapter first presents the acquisition and interpretation of one-dimensional well data (Section 1.1). It then presents the mechanisms and concepts of Sequence Stratigraphy (Section 1.2) that are used to interpret well data as well markers (Section 1.3.1). Finally, it presents the methods used to correlate these well markers (Sections 1.3.2 and 1.3.3).

*N.B.: This chapter contains paragraphs which are modified or partially/entirely taken from [Baville et al. \(2022\)](#).*

## Introduction

Subsurface modeling is a very challenging task: it enables to foresee the structure of geological units where human are not able to go. Moreover, the geological likelihood of these subsurface geomodels is directly linked to the geological concepts used to build them. As introduced previously, a very challenging question to answer is:

### **How consistent are the principles used to model the subsurface?**

Subsurface stratigraphic description depends on the paradigm used to define geological structures and objects. The simplest way to define the subsurface stratigraphy is to assume the three principles formulated by [Steno \(1669\)](#):

- **Principle of superposition:** “*Strata have been deposited above older strata than themselves*”.
- **Principle of lateral continuity:** “*Strata have continuously been laterally deposited in space*”.
- **Principle of original horizontality:** “*Strata have been deposited horizontally or sub-horizontally*”. However, this last principle is questioned since the layers are not necessarily deposited horizontally but they can be deposited on sedimentary slopes (e.g., [Dade et al., 1994](#)).

Moreover, in cases these three configurations are not strictly observed, [Steno \(1669\)](#) postulated that post-deposition events may have had an impact on the sedimentary deposits and that their structures should have been modified.

[Hutton \(1788\)](#) has been the first to formalize that the structure of current, or recent, sedimentary deposits is highly similar to the structure of sediments that have been deposited in the past. [Hutton \(1788\)](#) has then been the first to consider that events which have structured the past deposits are identical to the events which are currently structuring the sedimentary deposits.

This assumption, also supported by [Lyell \(1830\)](#), went therefore against the explanations given in the Bible explaining that the past sedimentary deposits are the results of the Flood, and has finally been defined as the **principle of uniformitarianism** by [Whewell \(1837\)](#) ([Bushman, 1983](#)).

The concept of stratigraphy has led to the concept of **stratigraphic column**. A stratigraphic column corresponds to the superposition of each stratigraphic

unit with respect to their depositional ages. However, it is not always complete because of lack of information and hiatus, and may be updated if intermediate stratigraphic units are discovered within the depositional system.

[Gressly \(1838\)](#) proposed the concept of **facies**, which describes the petrographical and paleontological characteristics of a stratigraphic unit ([Cross and Homewood, 1997](#)). [Gressly \(1838\)](#) also observed that these characteristics may laterally vary according to changes of depositional environments. Moreover, the same facies may be observed in different depositional units since facies are not just linked to specific stratigraphic units, but to specific depositional conditions.

Based on the concept of facies proposed by [Gressly \(1838\)](#), [Walther \(1894\)](#) has specified that the succession of facies in the stratigraphic column is logical. The **Walther's law of the correlation of facies** states that “*the various deposits of the same facies-area and similarly the sum of the rocks of different facies-areas are formed beside each other in space, though in a cross-section we see them lying on top of each other. As with biotypes, it is a basic statement of far reaching significance that only those facies and facies-areas can be superimposed primarily which can be observed beside each other at the present time*” ([Middleton, 1973](#)).

The purpose of this chapter is to review different ways to laterally correlate these stratigraphic units observations along vertical wells or sections (Section 1.3). The association of stratigraphic units is called **stratigraphic correlation**, and can be achieved using different stratigraphic concepts constrained by stratigraphic properties and prior knowledge about depositional environments (e.g., [Baville et al., 2022](#); [Edwards et al., 2018](#); [Gani and Bhattacharya, 2005](#); [Lallier, 2012](#); [Lallier et al., 2016](#); [Miall, 1991](#); [Vail et al., 1987](#); [van Wagoner et al., 1990](#); [Wheeler and Hale, 2014](#)).

The prior uncertainties on these stratigraphic properties (Section 1.1) and the prior uncertainties on the depositional environment (Section 1.2) must be taken into account in the choice of geological concept of correlation in order to generate the most likely stratigraphic correlations.

## 1.1 Subsurface stratigraphic data

The stratigraphic study of a zone of interest is based on the different data acquired within this zone. These data may correspond to different scales of observation and different resolutions of measurements (Figure 1.1):

- Seismic imaging (seismic reflection) uses the acoustic waves, whose echos propagate in the subsurface and are recorded and processed to build a multi-

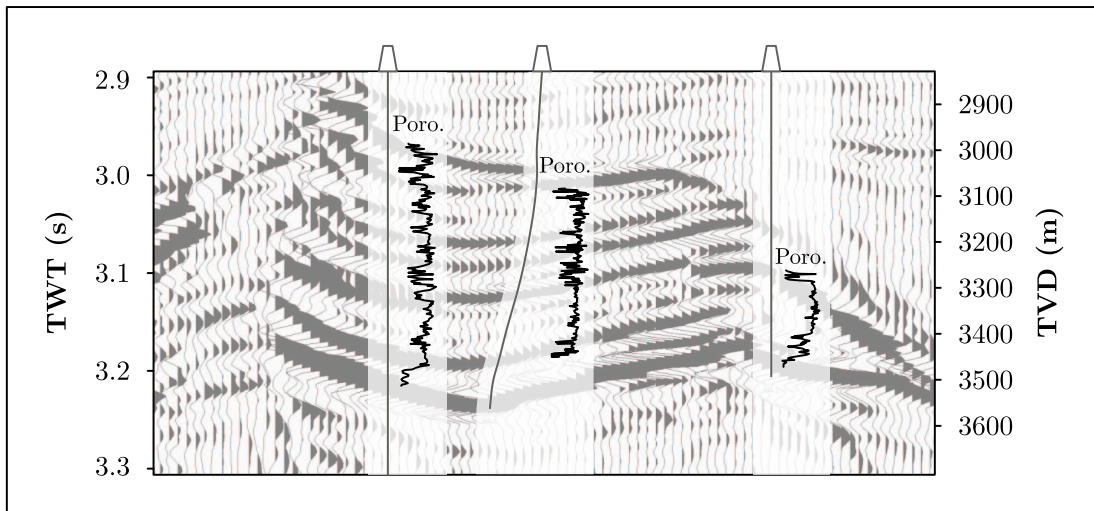


Figure 1.1: Illustration of the vertical and lateral resolutions of seismic imaging (background) and subvertical wells (well path: gray lines, and well logs: black lines). These data correspond to the Malampaya gas reservoir interior reflectors located offshore western Palawan island, Philippines. Modified from [Fournier and Borgomano \(2007\)](#); [Grötsch and Mercadier \(1999\)](#); [Lallier et al. \(2012\)](#).

dimensional model of subsurface heterogeneities ([Yilmaz, 2001](#)). **Seismic data** have low vertical resolution (approximately 10 m) but sample the subsurface at high lateral resolution (decametric scale).

- Geological wells (subvertical wells) are drilled in the subsurface after which reservoir properties (e.g., neutron porosity in Figure 1.1) may be acquired *in situ* ([Serra and Serra, 2003](#)), and core samples may be extracted to be analyzed in laboratory. **Well data** are sparse vertical one-dimensional data (approximately kilometeric lateral spacing) with a high vertical resolution (approximately 1/2 feet).

Moreover, Figure 1.2 illustrates that the coverage of the zone of interest depends on the type of subsurface data:

- Seismic imaging often cover the zone of interest, but the lateral and vertical resolution limit the interpretation of stratigraphic units, whose thickness or width are lower than the seismic resolution (e.g., [Baville et al., 2022](#); [Knaust and Hoth, 2021](#)).
- Well data have a very high vertical resolution and enable to interpret stratigraphic units whose thickness is lower than the seismic resolution. However, the lateral behavior of these stratigraphic units cannot be captured by subvertical wells which are sparsely sampled within the zone of interest ([Knaust and Hoth, 2021](#); [Nagy and Bjørlykke, 2015](#)) but can be used to match facies and petrophysical properties to seismic profile (Figure 1.1).

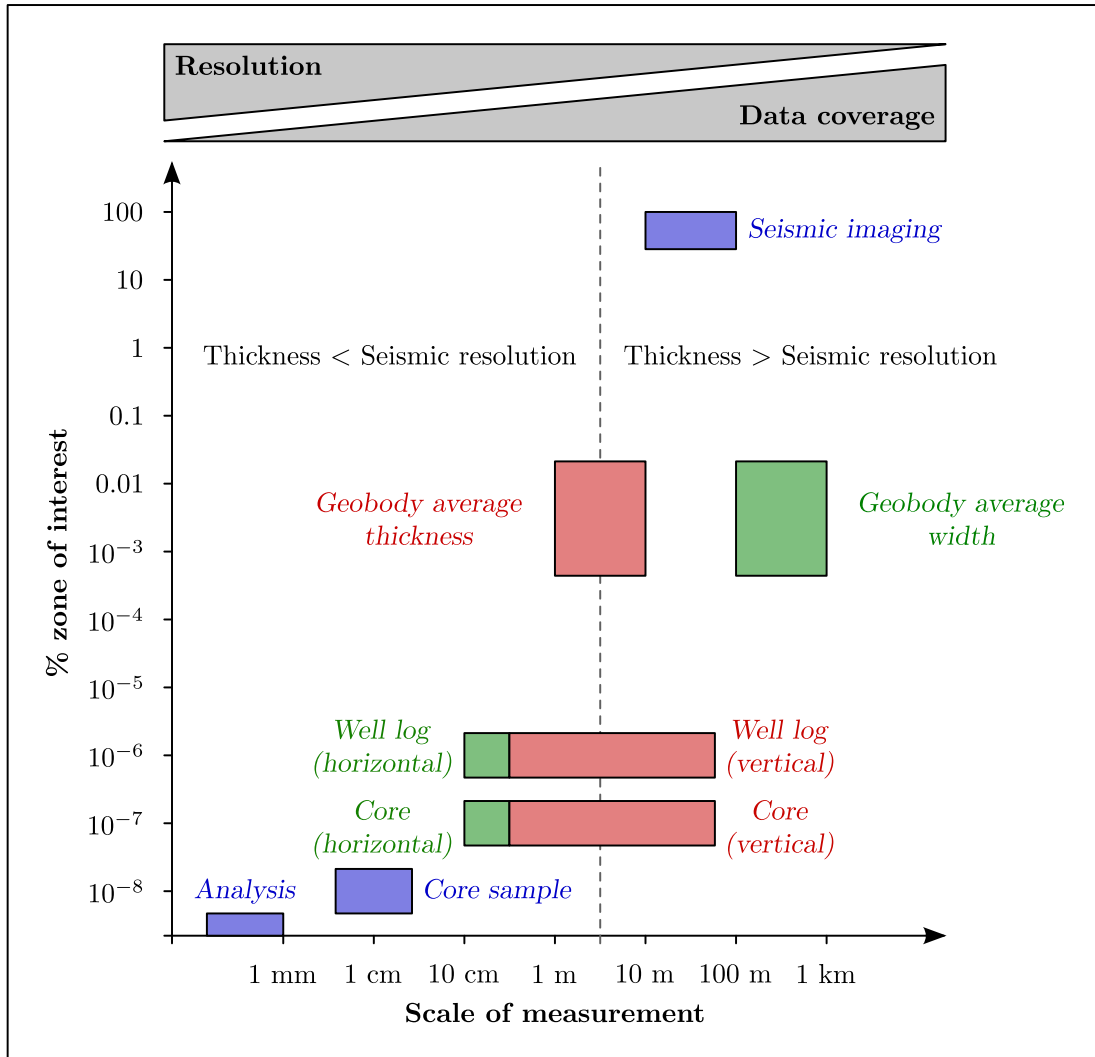


Figure 1.2: Proportion of the zone of interest corresponding to the type of data as a function of the scale of measurements. Well data (well logs and core samples) capture geobodies which have a thickness under the seismic resolution (Ringrose and Bentley, 2016) but correspond to less than  $10^{-5}\%$  of the zone of interest. Red boxes correspond to vertical dimensions, green boxes correspond to horizontal dimensions, and blue boxes correspond to vertical and horizontal dimensions. Modified from Howell et al. (2014); Ragueneil (2019).

- Moreover, petrographical and micropaleontological analyses may be performed in laboratory at a very small scale from core samples.

The purpose of this PhD work is to predict or to reproduce the subsurface stratigraphic unit structures corresponding to fourth to fifth order stratigraphic units (see Section 1.2 and Figure 1.4 for more details on multi-scale Sequence Stratigraphy). Unlike well data, seismic data do not enable the interpretation of fourth to fifth order stratigraphic units whose size is generally under the seismic resolution (Ringrose and Bentley, 2016).

Vertically, well data intercept fourth to fifth order sequences (Figure 1.3). These stratigraphic observations may be manually interpreted (e.g., Bourquin et al., 1998; Serra and Serra, 2003) or automatically simulated (e.g., Baviile et al., 2019; Pan et al., 2008; Perrier et al., 2021; Ruiz and Le Nir, 1999).

Laterally, vertical wells are sparsely sampled and the fourth to fifth order sequences should be correlated to predict or reproduce the subsurface stratigraphic architecture by interpolating their boundaries between wells. These correlation may be manually interpreted (e.g., Bourquin et al., 1998; Knaust and Hoth, 2021) or automatically simulated (e.g., Borgomano et al., 2008; Edwards, 2017; Lallier, 2012).

Usually, the outer limits of the studied stratigraphic units are given by stratigraphic markers. For example, first to third order stratigraphic unit interfaces may be interpreted directly on seismic images (e.g., Hoth et al., 2018; Knaust and Hoth, 2021), so they constrain higher-order correlations.

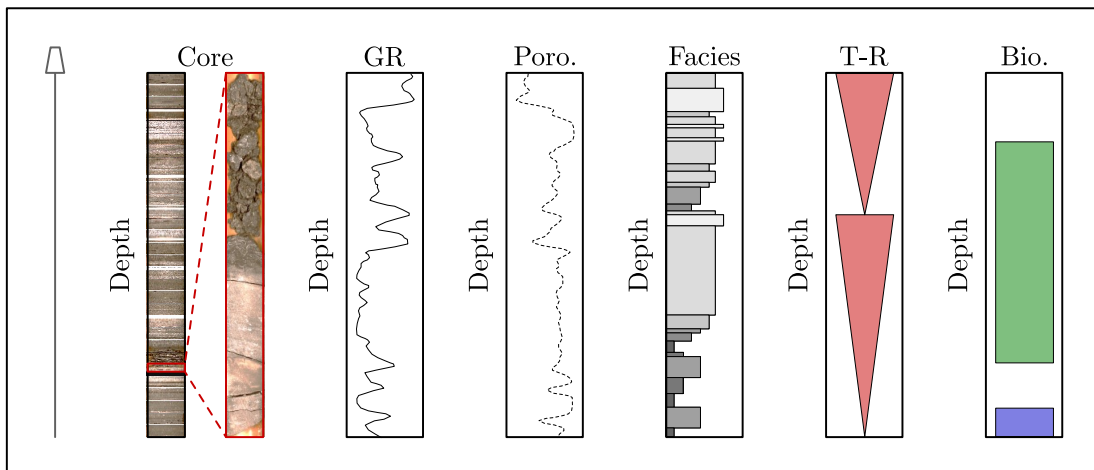


Figure 1.3: Examples of several data acquired along a vertical well: (left) core photographs, gamma ray, log porosity, facies interpretation, T-R sequence interpretation, biozone interpretation (right). Data courtesy of Equinor ASA.

### 1.1.1 Direct observations

The first type of data are **direct observations**. These observations correspond to the description of units (lithology, facies, etc.), and the description of the relationships between units (connectivity, conformity, etc.).

These direct observations may be directly made on the field (landscapes, outcrops, photographs, rock samples) or on subsurface **core samples**, which are extracted during the drilling (core photographs in Figure 1.3):

- Outcrops and core samples enable the global observation and the study of rocks. The study of rocks may lead to information such as their mineralogical or petrophysical composition, their depositional environment, their alteration, *etc.*. However, outcrops may provide information on geometries that cannot be obtained from core samples.

The global observation of outcrops and top views may lead to the understanding of the stratigraphic structure of deposits (*e.g.*, apparent orientation and inclination), and the connectivity between the different units.

However, outcrops and landscapes are limited to the topography and their accessibility, and give information which are not always easy to vertically interpret.

- Vertical wells enable to punctually sample the subsurface (*e.g.*, true strike and true dip, unit successions, *etc.*) along kilometeric scale well paths. Along these vertical wells, core samples may be extracted allowing direct observations at a very high resolution.

Microscopic core sample analyses may be done in laboratory to determine the composition of rocks, and potentially their depositional age thanks to biostratigraphic elements (sedimentary facies interpretation from core photographs and biozone interpretations in Figure 1.3).

As illustrated in Figure 1.2, direct observations are observed at different scales from outcrops and landscapes (metric scale to kilometeric scale) and from core samples (millimetric scale to metric scale).

### 1.1.2 Geophysical measurements

The second type of data are **geophysical measurements**. These measurements correspond to reservoir properties which cannot be directly determined from outcrops or core samples without a measurement device:

- Seismic imaging are multi-dimensional geophysical measurements (Yilmaz, 2001), which are acquired at the scale of the zone of interest, *i.e.*, usually at a kilometeric scale (Figures 1.1 and 1.2).

However, as discussed previously, seismic data are able to intercept first to third order stratigraphic sequence interfaces but not to capture fourth to fifth order stratigraphic sequences (Ringrose and Bentley, 2016).

- Along well paths, geophysical measurements may be acquired after the drilling (Serra and Serra, 2003). These measurements are called **well logs** and give local information about the subsurface geophysics (e.g., gamma ray and neutron porosity as illustrated in Figure 1.3).

Well logs enable a vertical sampling at the centimetric scale, but may be analyzed at several scales (Baville et al., 2019; Pan et al., 2008; Perrier et al., 2021; Serra and Serra, 2003).

- Core samples may also be analyzed in laboratory to measure additional geophysical properties. These properties may be similar to those obtained by well logging.

Moreover, geophysical properties measured in laboratory may be done including the time dimension, which is not enabled during the drilling, in order to get more information about the subsurface (e.g., the capillarity by monitoring the water through the connected porosity as a function of time).

### 1.1.3 Depositional information

Direct observations and geophysical measurements may be combined to interpret a lot of additional subsurface data along wells and within the zone of interest.

In this PhD work, the principal **depositional information** that are interpreted from seismic imaging, well logs, core samples and regional syntheses are:

- The general depositional environment (e.g., siliciclastic coastal sedimentary margin, siliciclastic coastal bay-head deltas) may be interpreted from seismic data and from well log and core sample interpretations (e.g., Knaust and Hoth, 2021; Serra and Serra, 2003).
- The stratigraphic unit interpretations, *i.e.*, T-R sequences (Figure 1.3), are interpreted from well logs (gamma ray and porosity) and core sample interpretation (facies successions) (e.g., Baville et al., 2019; Knaust and Hoth, 2021; Perrier et al., 2021).
- The principal sediment transport directions within a sedimentary basin may be interpreted from dipmeter data (strike and dip data) measured in the different interpreted sedimentary facies (e.g., Knaust and Hoth, 2021).
- The proximal pole (most internal depositional conditions) and the distal pole (most external depositional condition) of a sedimentary basin are based on stratigraphic surfaces interpretation (maximum flooding and maximum regressive surfaces) and on sedimentary facies and well logs interpretations.

Moreover, these depositional information about the zone of interest (e.g., the depositional environment, the vertical stratigraphic unit succession) are not directly obtained from seismic imaging, well log and core sample but are the result of several loops between data and the interpretations (e.g., [Knaust et al., 2019](#)).

## 1.2 Sequence Stratigraphy

**Sequence Stratigraphy** provides several concepts and methods to analyze, characterize and predict stratigraphic and sedimentary architectures in the subsurface. Sedimentary strata may be subdivided into several stratigraphic units based on genetic considerations ([Sloss et al., 1949](#)).

The succession of these stratigraphic units is called a **stratigraphic sequence**, and is defined as “*relatively conformable successions of genetically related strata bounded by unconformities or their correlative conformities*” by [Mitchum et al. \(1977a\)](#) ([Miall, 1997](#); [Sloss, 1988](#); [van Wagoner et al., 1988](#)).

Stratigraphic subsurface corresponds to multi-frequency recording with the interlocking of different orders according to the duration of the stratigraphic sequences. Low order stratigraphic sequences are observed at a low time / space resolution, and may be subdivided into several stratigraphic subsequences observed at higher time / space resolutions as illustrated in Figure 1.4 ([Guillocheau, 1991](#); [Haq et al., 1988](#); [Mitchum and Van Wagoner, 1991](#); [Vail et al., 1977](#)).

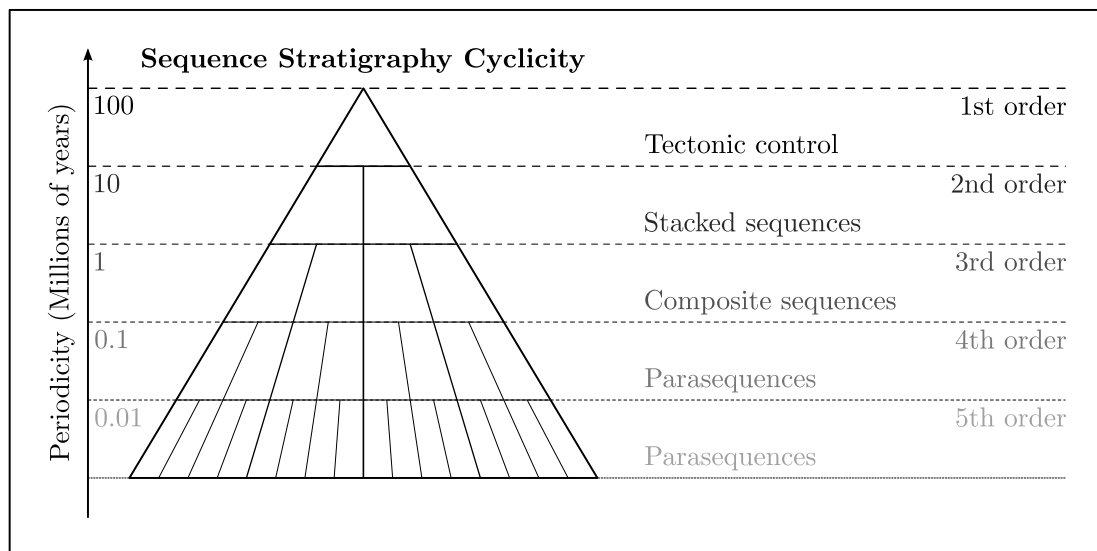


*Figure 1.4: Diagrammatic representation of cyclicities of stratigraphic units. Each stratigraphic order corresponds approximately to a frequency time-window. Stratigraphic units (second to fifth order) may occur at more than one frequency. Inspired from [Catuneanu et al. \(2011\)](#) and [Mitchum and Van Wagoner \(1991\)](#).*

As illustrated in Figure 1.4, stratigraphic sequences are defined according to their duration. The lowest order (second order) corresponds to stratigraphic units presenting a cyclicity of approximately ten millions of years (supercycles), and are called stacked sequences (Mitchum and Van Wagoner, 1991). The following order (third order) corresponds to stratigraphic units presenting a cyclicity of approximately one million of years (fundamental cycles), and are called composite sequences (Mitchum and Van Wagoner, 1991). The highest orders (fourth, fifth, and sometimes sixth orders) correspond to stratigraphic units presenting a cyclicity lower than one million years (paracycles), and are called parasequences (Mitchum and Van Wagoner, 1991).

Fourth to fifth order stratigraphic units (*i.e.*, parasequences) belong to composite sequences (third order), whose stratigraphic boundaries are usually observable or interpretable at the seismic resolution. Then parasequences are usually not observable at the seismic imaging resolution.

Figure 1.5 illustrates the multi-scale behavior of stratigraphic sequences. Within a stratigraphic sequence at a fixed order, stratigraphic sequences may be interpreted at higher orders. These higher-order stratigraphic sequences are bounded by time lines. This multi-scale interpretation may lead to several stratigraphic sequences subdividing lower-order stratigraphic sequences at different scales of depth and time (Posamentier *et al.*, 1992).

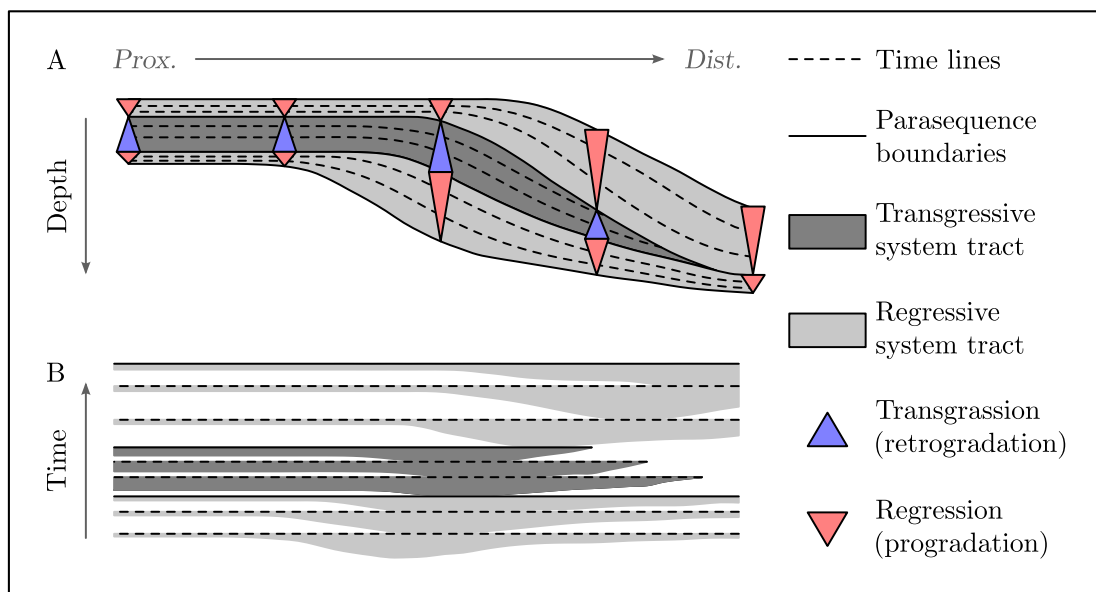


*Figure 1.5: Successive transgressive and regressive parasequences corresponding to intervals observed at different scale of depth and time (Posamentier and Vail, 1988b; van Wagoner *et al.*, 1990). Inspired by Kedzierski *et al.* (2008). (A) Depth cross-section and (B) time cross-section (Wheeler diagram; Wheeler (1958)). Re-draw from Baviile *et al.* (2022).*

Wheeler (1958) proposed combined diagrams, which show the same stratigraphic section using two different representations: (1) a stratigraphic section as a function of depth (Figure 1.5.A), and (2) a stratigraphic section as a function of geological age (Figure 1.5.B) (Amosu and Sun, 2017; Driscoll and Karner, 1999; Holbrook and Bhattacharya, 2012; Mallet, 2004; Qayyum et al., 2017).

### 1.2.1 Accommodation rate & Sedimentation rate

The objective of Sequence Stratigraphy is to relate stratigraphic units to cycles. These cycles are given by cyclicity of accommodation and sedimentation rate, which are controlled by four main parameters including global (eustatic) sea-level changes, climate, sediment supply, and basement subsidence or uplift (Catuneanu et al., 2011; Galloway, 1989a; Johnson and Murphy, 1984; Posamentier and Vail, 1988a; Ruiz and Le Nir, 1999).

Figure 1.6 illustrates the relationship between the rate of relative sea-level change, the rate of subsidence (tectonics), and the rate of eustatic changes (Posamentier and Vail, 1988a). The rate of relative sea-level change, corresponds to the rate of variation of available space for sediment deposition (Homewood et al., 2000; Kedzierski et al., 2007; Posamentier and Vail, 1988a).

This rate is calculated as the time derivative of the accommodation, which corresponds to the space (full or empty) available for potential sedimentation (Jervey, 1988). The accommodation may be considered as a proxy for the relative sea-level (Homewood et al., 2000; Robin, 1995). The rate of relative sea-level change is also called accommodation rate  $A$ .

The sediment flow describes the sediment supply and the production of sediments. In siliciclastic depositional systems, the sediment flow only corresponds to the amount of sediment which arrives in the basin. However, the preservation of the sediments is highly sensitive to the erosion, to the reuse of sediments already deposited, and to the sediment compaction which may modify the thickness and hence the volume of preserved sediments (Kedzierski, 2007). The sedimentation rate  $S$  is calculated as the time derivative of the sediment flow, and describes variation in the thickness of the not-compacted sediment (Kedzierski, 2007).

The accommodation is not directly related to the sediment flow, because it only refers to the space available for the sediment. The ratio  $A/S$ , which compares the accommodation rate  $A$  and the sedimentation rate  $S$ , controls the filling or not of the potential depositional space, and have an impact on the architecture of the stratigraphic units (Borgomano et al., 2020; Homewood et al., 2000; Kedzierski, 2007; Muto and Steel, 1997).

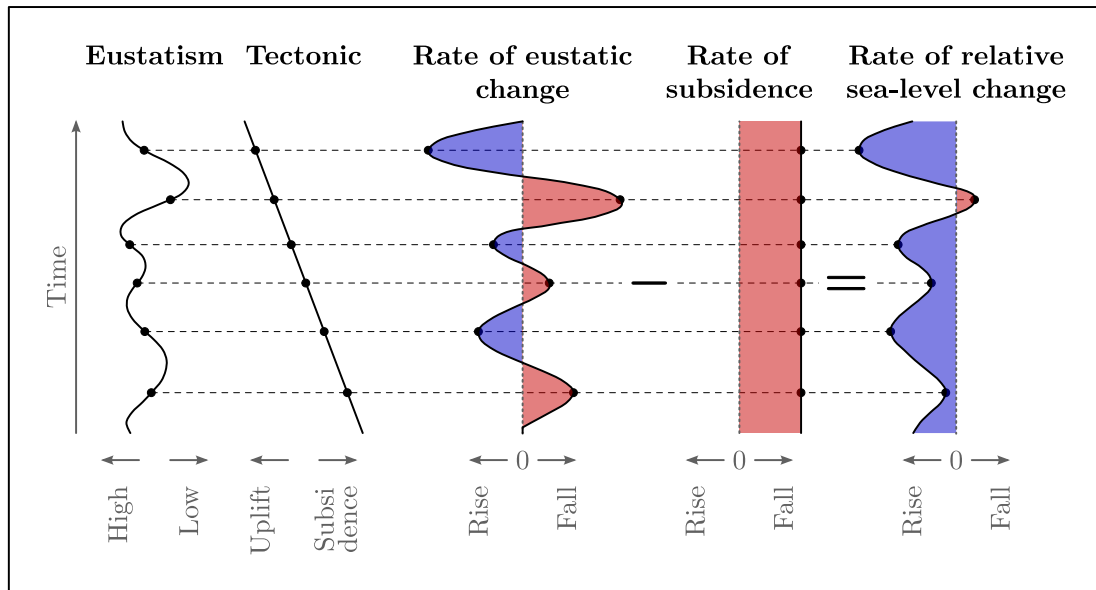
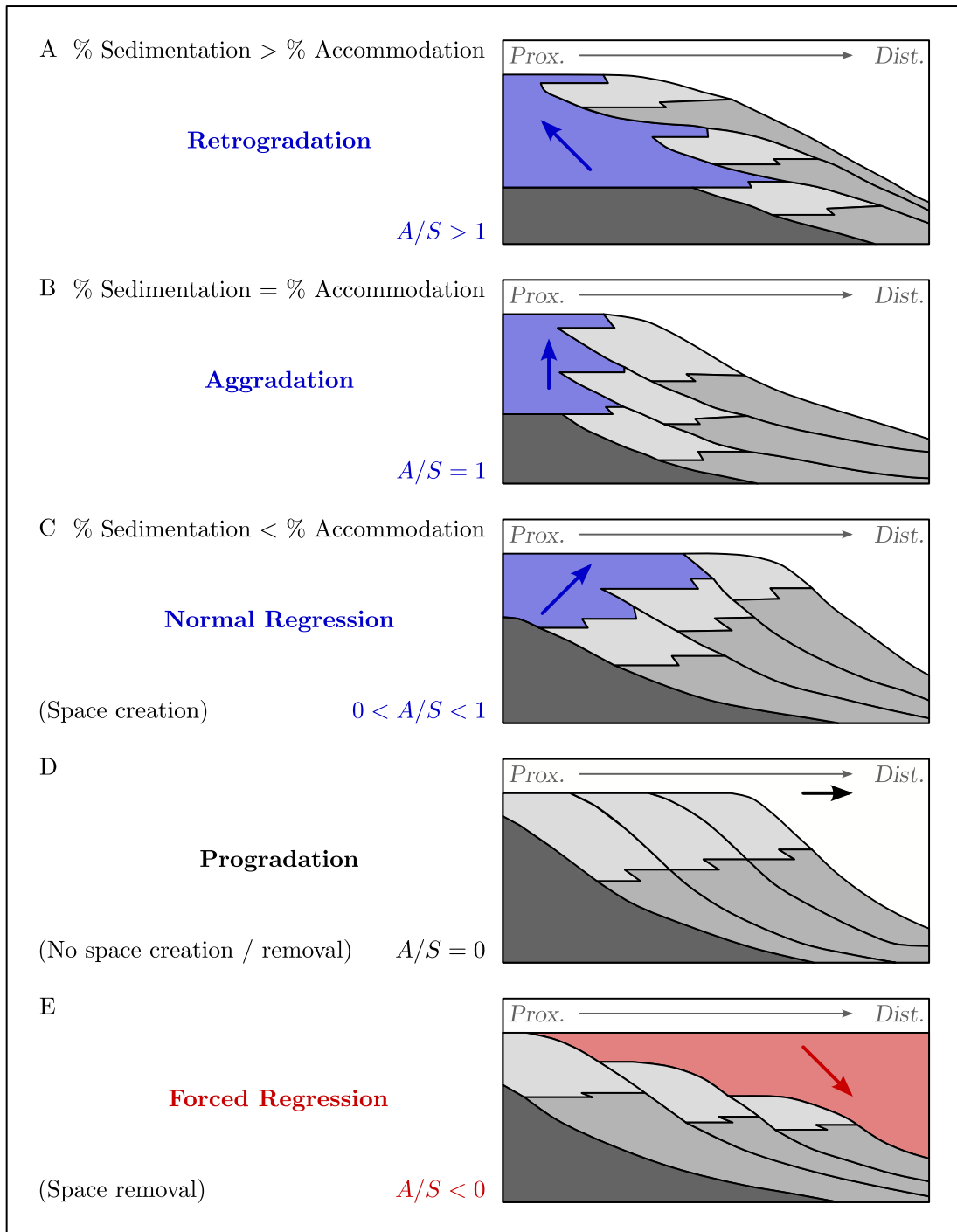


Figure 1.6: Relationship between the rate of eustatic change, the rate of subsidence, and the rate of relative sea-level change. In this example, the subsidence is constant. It means that if the eustatic level rises, or the amplitude of the eustatic fall is lower than the subsidence, the accommodation stays positive. At the opposite, if the amplitude of the eustatic fall is higher than the subsidence rate, the accommodation becomes negative. Modified from [Edwards \(2017\)](#); [Kedzierski \(2007\)](#); [Posamentier and Vail \(1988a\)](#).

Figure 1.7 illustrates the five possible configurations given by the ratio  $A/S$ , assuming that the sedimentation rate is strictly positive:

- $A/S > 1$ : **retrogradation**. The accommodation rate is positive and larger than the sedimentation rate (creation of depositional space). The result is a backstepping of the coastline to the proximal pole (Figure 1.7.A).
- $A/S = 1$ : **aggradation**. The accommodation rate is positive and equal to the sedimentation rate (creation of depositional space). The result is a rise of the coastline at the same position within the basin (Figure 1.7.B).
- $0 < A/S < 1$ : **normal regression**. The accommodation rate is positive but lower than the sedimentation rate (creation of depositional space). The result is a migration of the coastline to the distal pole (Figure 1.7.C). Normal regression corresponds to simultaneous progradation and aggradation ([Catuneanu, 2006](#)).
- $A/S = 0$ : **progradation**. The accommodation rate is null (no creation or removal of depositional space). The impact is a horizontal move of the coastline towards the distal pole (Figure 1.7.D).



**Figure 1.7:** Impact of the ratio  $A/S$  (accommodation rate / sedimentation rate) on the coastline migration (illustrated by bold arrows), and on the stratigraphic unit geometries. (A-C) positive accommodation rate, (D) null accommodation rate, and (E) negative accommodation rate. Modified from [Edwards \(2017\)](#); [Homewood et al. \(2000\)](#); [Kedzierski \(2007\)](#).

- $A/S < 0$ : **forced regression**. The accommodation rate is negative (removal of depositional space). The impact is a topographic fall of the coastline towards the distal pole (Figure 1.7.E).

Considering these five configurations, there are two main behaviors of the coastline that may be highlighted:

- The coastline retreats towards the proximal pole of the depositional system (Figure 1.7.A). The cause of this migration is a rise of the water depth. This depositional event is called **transgression** (e.g., [Catuneanu, 2006](#)).
- The coastline migrates towards the distal pole of the depositional system (Figure 1.7.C-E). The cause of this migration is a fall of the water depth. This depositional event is called **regression** (e.g., [Catuneanu, 2006](#)).

All the configurations given by the ratio  $A/S$  lead to different geometries of the deposited stratigraphic units, and may be associated to a depositional event (transgression or regression). According to the depositional event, their geometries, and their induced connectivity, stratigraphic sequences may be defined following different nomenclatures ([Catuneanu, 2006](#); [Catuneanu et al., 2011](#)).

## 1.2.2 Sequence Stratigraphy: Nomenclature & Definitions

Sequence Stratigraphy has been accepted for decades to describe the subsurface stratigraphy. The ratio  $A/S$  has enabled to characterize the geometry of the deposited stratigraphic units but many terminologies have been proposed to identify various stages and objects associated with stratigraphic sequences based on their signature and chronological significance ([Catuneanu, 2006](#); [Catuneanu et al., 2011](#)).

Initially, a stratigraphic sequence is a succession of a regression (fall of the relative sea-level) and a transgression (rise of the relative sea-level) ([Catuneanu, 2002, 2006](#); [Catuneanu et al., 2011](#)). However, the definition of the stratigraphic sequence boundaries and the terminology of the system tracts in between may vary from a model to another (Figure 1.8).

The purpose of this PhD work is not to use a sophisticated definition of stratigraphic sequences to model the subsurface. The objective of this chapter is then to propose a simple definition of stratigraphic sequences from all existing models (Figure 1.8) to easily determine the position of core samples and well markers within these stratigraphic sequences.

Among all these definitions and variations of Sequence Stratigraphy, this PhD work uses a mixture of **Genetic Sequences** ([Frazier, 1974](#); [Galloway, 1989b](#)) and **T-R sequences** ([Embry and Johannessen, 1992](#); [Johnson and Murphy, 1984](#)) to define the main stratigraphic surfaces and the sedimentary system tracts between these characteristic stratigraphic surfaces (Figure 1.9).

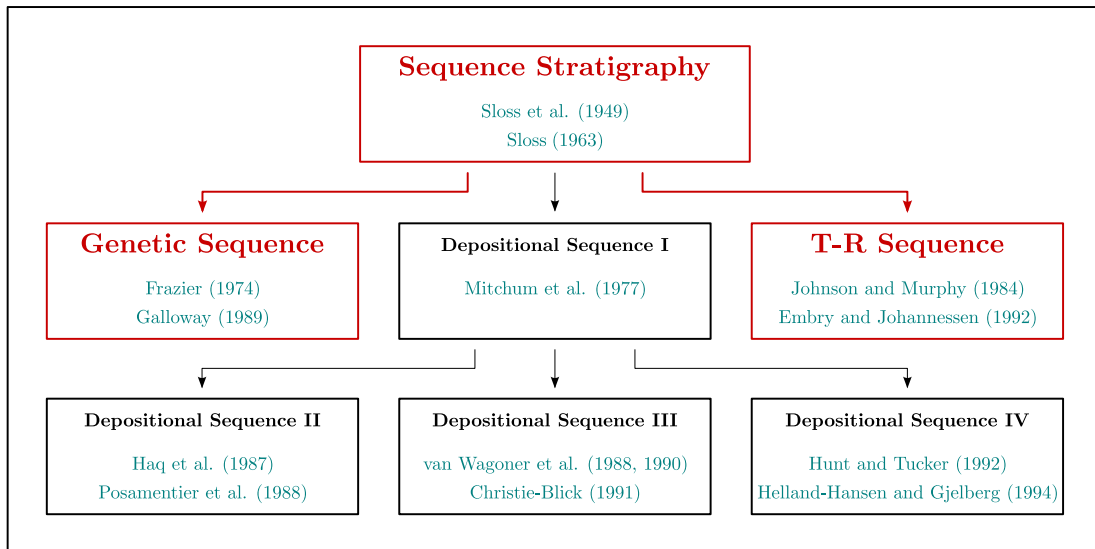


Figure 1.8: Evolution of stratigraphic sequence definitions since Sloss et al. (1949) have defined the concept of “Sequence Stratigraphy”. Chronologically, the concept of genetic sequences (Frazier, 1974; Galloway, 1989b), the concept of depositional sequence I (Mitchum et al., 1977b), the concept of T-R sequence (Embry and Johannessen, 1992; Johnson and Murphy, 1984), the concept of depositional sequence II (Haq et al., 1987; Posamentier et al., 1988), the concept of depositional sequence III (Christie-Blick, 1991; van Wagoner et al., 1988, 1990), and the concept of depositional sequence IV (Helland-Hansen and Gjelberg, 1994; Hunt and Tucker, 1992). Modified from Catuneanu (2006).

### 1.2.2.1 Stratigraphic surfaces

- Genetic sequences (Frazier, 1974; Galloway, 1989b) are bounded by **maximum flooding surfaces** (Figure 1.9). The maximum flooding surface is identified as the surface, within each stratigraphic sequence, which corresponds to the maximum landward backstepping of the shoreline.
- T-R sequences (Embry and Johannessen, 1992; Johnson and Murphy, 1984) are bounded by **maximum regressive surfaces** (Figure 1.9). The maximum regressive surface is identified as the surface, within each stratigraphic sequence, which corresponds to the maximum of basinward progradation of the shoreline.

### 1.2.2.2 Stratigraphic system tracts

- The **lowstand system tract** (*Genetic sequences*) is formed at the beginning of the sea-level rise, when the sedimentation rate  $S$  is larger than the accommodation rate  $A$  and corresponds to a lowstand normal regression (progradation + aggradation), i.e.,  $0 < A/S < 1$  (Figure 1.7.C).

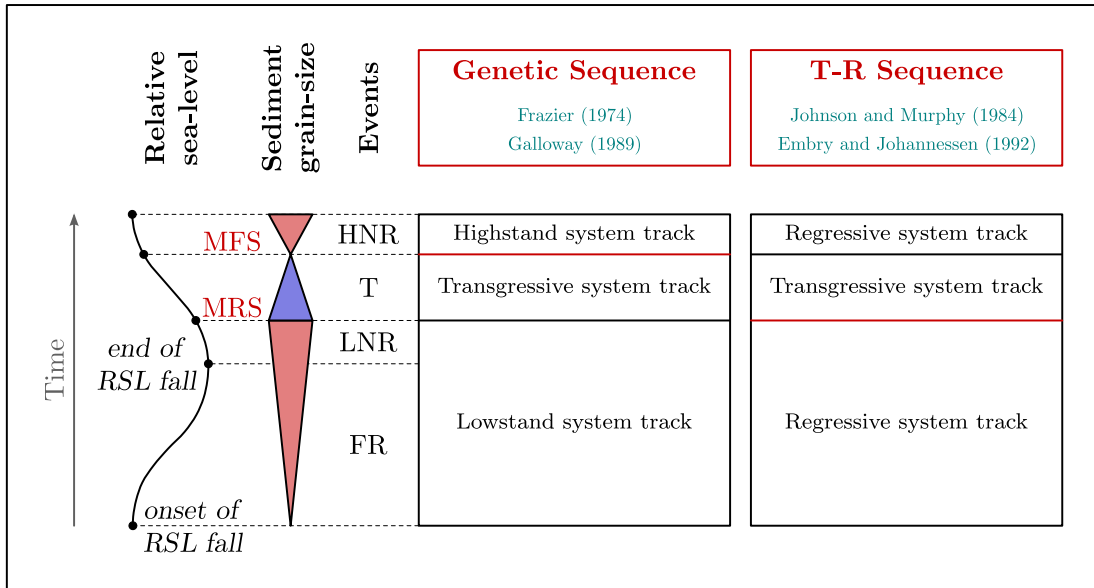


Figure 1.9: Definition of stratigraphic surfaces and system tracks considering the Genetic Sequence (Frazier, 1974; Galloway, 1989b) and the T-R Sequence (Embry and Johannessen, 1992; Johnson and Murphy, 1984) concepts. Triangles represent the sediment grain-size according to the depositional conditions. HNR: Highstand Normal Regression; LNR: Lowstand Normal Regression; T: Transgression; FR: Forced Regression; MFS: Maximum Flooding Surface; MRS: Maximum regressive Surface; RSL: Relative Sea-Level. Inspired from Catuneanu et al. (2010).

This system tract stops just below the maximum regressive surface and includes, in marine settings, coarsening-upward (prograding) deposits. However, these marine deposits are not always preserved due the erosion by the transgression occurring just above the maximum regressive surface.

- The **transgressive system tract** (*Genetic sequences* and *T-R sequences*) corresponds to a rapid rise of the sea-level (positive accommodation rate  $A$ ) which is not compensated by the sedimentation rate  $S$  and corresponds to a transgression (retrogradation), i.e.,  $A/S > 1$  (Figure 1.7.A).

It is globally characterized by a fining-upward trend in marine and alluvial deposits (not a systematic rule), and is bounded at the bottom by the maximum regressive surface, and at the top by the maximum flooding surface.

- The **highstand system tract** (*Genetic sequences*) is formed after the maximum flooding when the sedimentation rate  $S$  becomes larger than the accommodation rate  $A$  and corresponds to a highstand normal regression (progradation + aggradation), i.e.,  $0 < A/S < 1$  (Figure 1.7.C).

This system tract starts just above the maximum flooding surface and includes, in marine settings, coarsening-upward (prograding) deposits.

- The **regressive system tract** (*T-R sequences*) regroups all regressive deposits corresponding to the lowstand system track and highstand system tract.

This system track starts just above the maximum flooding surface and stops just below the maximum regressive surface. It generally corresponds to coarsening-upward deposits.

### 1.2.2.3 Prograding parasequences / Clinofolds

Prograding system tracts (Figure 1.7.C-E) may be subdivided in prograding sub-stratigraphic units, *i.e.*, prograding parasequences. Rich (1951) has defined these prograding parasequences as **clinofolds** (Patrino and Helland-Hansen, 2018; Patrino et al., 2015; Steel and Olsen, 2002).

Prograding sedimentary depositional systems are defined by the **principal sediment transport direction**, also called **dip direction** in this manuscript, and the direction orthogonal to the dip direction is called the **strike direction** in this manuscript.

However, there are two types of sedimentary depositional systems corresponding to two types of dip and strike directions:

- The dip direction is unidirectional and generally orthogonal to the coastline (*i.e.*, sedimentary margin).

In this configuration, clinofolds have a sigmoidal geometry along the dip direction (Figure 1.10.A), and have a monoclinical geometry along the strike direction (Figure 1.10.B).

- The dip direction stays unidirectional on the continental part until a punctual coastal position (sediment source), from which the dip direction becomes radial (*i.e.*, sedimentary delta).

In this other configuration, clinofolds have a sigmoidal geometry on the deltaic part along the dip direction (Figure 1.11.A), and a bell-shaped geometry along the strike direction (Figure 1.11.B).

The main difference between these two types is the fact of having a point source of sediment entry (*e.g.*, bay-head delta) and its redistribution or not by the dynamics of the basin (Figures 1.10 and 1.11).

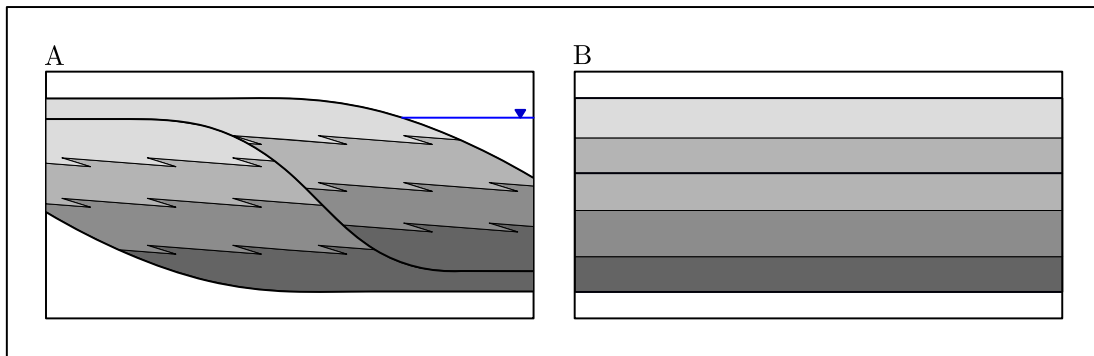


Figure 1.10: Geometry of clinoforms along a shoreline with redistribution by wave action or tidal currents (laterally to the river mouth). (A) Dip direction cross-section. (B) Strike direction cross-section. Modified from [Baville et al. \(2022\)](#).

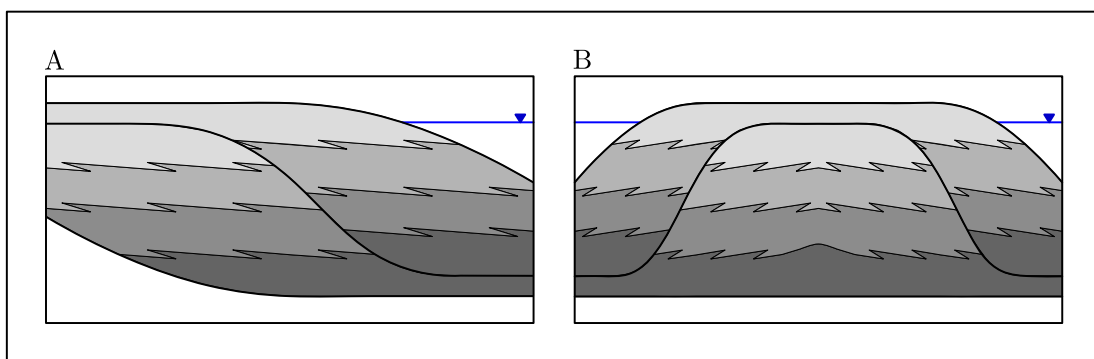


Figure 1.11: Geometry of clinoforms in the axis of the deltaic system (vertical scale exaggerated). (A) Dip direction cross-section. (B) Strike direction cross-section. Modified from [Baville et al. \(2022\)](#); [Gani and Bhattacharya \(2005\)](#).

#### 1.2.2.4 Stratigraphic conformity

At each stratigraphic order (Figure 1.4), the **conformity** of the stratigraphic units corresponds to the way structures, within a stratigraphic sequence, behave at the interface of the other stratigraphic sequences surrounding them (Figure 1.12) ([Christie-Blick, 1991](#); [Mitchum et al., 1977a](#)).

[Allen \(1963\)](#) presents the possible conformities that can be observed at stratigraphic sequence interfaces and has described their geometries in four configurations (Figure 1.12.A-D):

- Both top and base of the stratigraphic sequence are conformable, *i.e.*, substratigraphic lines are parallel to the stratigraphic sequence interfaces (Figure 1.12.A).
- The top is not conformable (erosional unconformity) and the base is conformable, *i.e.*, substratigraphic lines may intersect the top interface, and are

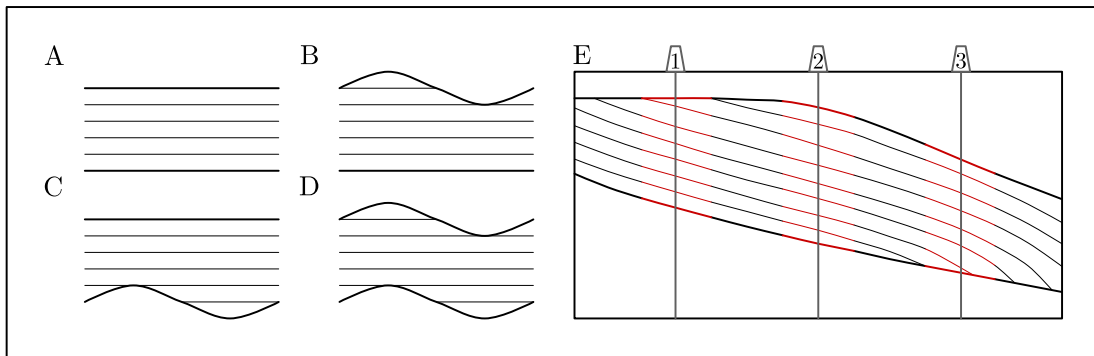


**Figure 1.12:** (A-D) Different stratigraphic sequence conformities: conformable, erosional unconformity (top) and angular unconformity (base). (E) An example of conformity interpretation along well path: (1) erosional unconformity or pure progradation, (2) conformable, and (3) angular unconformity. Bold lines are stratigraphic sequence interface, and fine lines are substratigraphic lines. Modified from [Edwards \(2017\)](#).

parallel to the base interface (Figure 1.12.B). It can also be due to toplaps during a pure progradation ( $A/S = 0$ ) without erosion (Figure 1.12.E).

- The top is conformable and the base is not conformable (angular unconformity), *i.e.*, substratigraphic lines are parallel to the top interface, and may intersect the base interface (Figure 1.12.C).
- Both top and base of the stratigraphic sequence are not conformable, *i.e.*, substratigraphic lines may intersect the stratigraphic sequence boundaries (Figure 1.12.D).

However, the conformity observed at stratigraphic sequence interfaces may vary according to the lateral position (*e.g.*, from one well to another) within a single stratigraphic sequence, as illustrated in Figure 1.12.E ([Edwards, 2017](#)).

The conformity of the stratigraphic units gives information about the depositional processes and about post-depositional events.

### 1.2.3 Lithostratigraphy versus chronostratigraphy

Stratigraphic units are bounded by stratigraphic surfaces which correspond to global depositional conditions, *e.g.*, maximum flooding surfaces correspond to the most distal depositional condition at a location along the profile (*e.g.*, [Embry and Johannessen, 1992](#); [Galloway, 1989b](#)). Stratigraphic sequence boundaries may be interpreted as time lines (**absolute chronostratigraphy**) from biostratigraphic data and other dating methods which usually intercepts first to third order stratigraphic sequences (*e.g.*, [Knaust and Hoth, 2021](#); [van Gorsel, 1988](#)).

The problem is now to recover strata from fourth to fifth order stratigraphic sections and vertical wells within lower order absolute chronostratigraphic sequences. This recovering can be performed using two different principles of Sequence Stratigraphy (Figure 1.13):

- **Lithostratigraphy** aims to associate strata by comparing their composition or rock type. Well markers are correlated if they are similar (or, even better, identical) to generate sedimentary units containing the same facies (characteristics). However, this method does not consider possible lateral shifts of facies along a proximal-to-distal direction in the basin, so it cannot correlate sequences which are too far away.
- **Relative chronostratigraphy** (referred to as **chronostratigraphy** in this manuscript) aims to associate strata by comparing their geological age, *i.e.*, when they are deemed to correspond to the same depositional time-window. This generates layers bounded by isochronous horizons, which may have lateral facies variations depending on depositional environments tending to produce realistic facies connectivity. Chronostratigraphy consider lateral shifts of facies to be possible along time lines.

These two principles of Sequence Stratigraphy may lead to very distinct subsurface models with direct implication for paleogeography and reservoir connectivity.

The difference between lithostratigraphy and chronostratigraphy is illustrated with an example in Figure 1.13. In this example, the lithology is interpreted along two wells of the depositional system. Stratigraphic units are interpolated between the two wells following the concept of lithostratigraphy (Figure 1.13.A), and following the concept of chronostratigraphy (Figure 1.13.B).

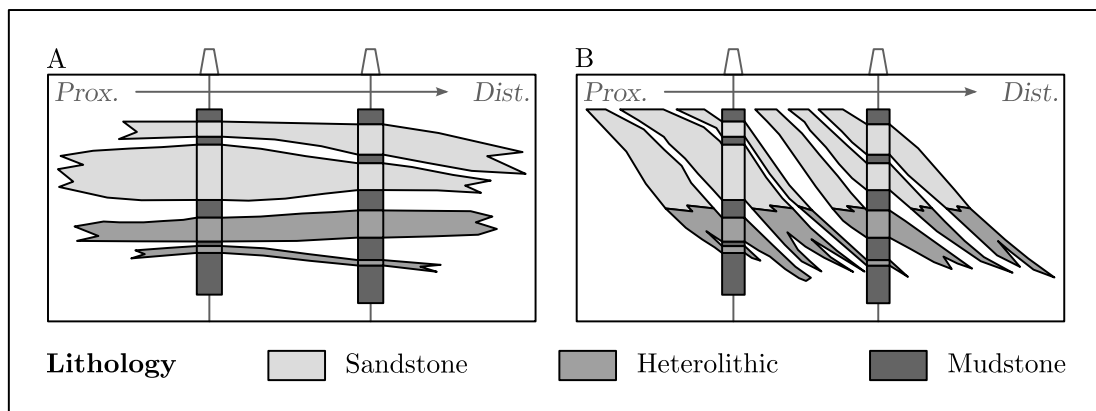


Figure 1.13: An example of lithology interpretation along two wells and their (A) lithostratigraphic and (B) chronostratigraphic geological layer interpolation and extrapolation from the same data set. Modified from [Ainsworth et al. \(1999\)](#); [Baville et al. \(2022\)](#).

Chronostratigraphy takes into account the depositional environments, which are not the same at each position of the depositional system. It means that the facies, which describes the petrophysical and paleontological properties within a stratigraphic unit (Cross and Homewood, 1997; Gressly, 1838), may vary along the depositional profile. For example, a stratigraphic sequence may be characterized by a marine facies on the distal part of the system and a continental facies on the proximal part of the depositional system.

The objective of chronostratigraphy is to identify the chronostratigraphic surfaces, *i.e.*, stratigraphic surfaces along which deposits are considered to have the same depositional age. From these chronostratigraphic surfaces, and from the conformity of adjacent units observed at these surface, the chronostratigraphy may identify chronostratigraphic system tracts, and chronostratigraphic sequences at different orders.

## 1.3 Stratigraphic well correlation

The purpose of this PhD work is to predict or to reproduce the subsurface stratigraphic unit structures corresponding to fourth to fifth order chronostratigraphic units (Section 1.2) from subsurface stratigraphic data (Section 1.1) which are able to interpret fourth to fifth order stratigraphic sequences.

### 1.3.1 From stratigraphic data to well markers

The three-dimensional subsurface modeling is based on geological principles and need conditioning data as input. The direct observations, geophysical measurements, and depositional information about the subsurface are the conditioning data which constrain the building of geomodels.

Seismic data are usually preliminary used to define the zone of interest at the coarsest scale, *i.e.*, first to third stratigraphic sequences are vertically and laterally interpreted in seismic data and from outcrop and landscape observations.

Fourth to fifth seismic units (Ringrose and Bentley, 2016), are vertically sampled along wells and should be laterally correlated from one well to the other.

The lateral correlation of stratigraphic observations along vertical wells is called **stratigraphic well correlation**. The stratigraphic well correlation is, first of all, based on facies interpretations and on stratigraphy concepts (Section 1.2). Several properties can be interpreted or measured during and after drilling, and these properties are sampled along the well path in **well markers**.

These well markers are defined by their position along the well path and the value of the property. There are two types of properties which lead to two types of well markers (Figure 1.14):

- **Well logs** correspond to quasi-continuous (regular sampling) geophysical measurements along the well path (e.g., gamma ray, sonic, neutron porosity). If the well data is a well log, the well markers are points and are regularly sampled along the well path (Figure 1.14.A).
- **Well sections** correspond to piecewise constant reservoir properties (e.g., petrophysical property, petrography, facies, and depositional environment) and are defined by their top and bottom depths along the well path (e.g., coarsening-up intervals, biozones, structural zones, sedimentary facies). If the well data is a well section, the well markers are intervals and are irregularly distributed along well paths (Figure 1.14.B).

Moreover, measurement gaps may exist and may lead to discontinuous well logs and to disjoint well sections.

The purpose of the stratigraphic well correlation is to associate well markers from one well with well markers from other wells. In this manuscript, the set of well-marker associations is called a **correlation set**.

Figure 1.15.A illustrates all the topologically possible well-marker associations. Every complete set of non-crossing well-marker associations correspond to a correlation set. Indeed, a correlation set cannot be composed of two correlation lines (i.e., well-marker associations) which cross (e.g., red correlation lines in Figure 1.15.B), and all well markers must be associated to another well marker. Additionally, top and bottom markers, which are high-order stratigraphic markers, are considered as correlated well markers (e.g., red well markers in Figure 1.15.C).

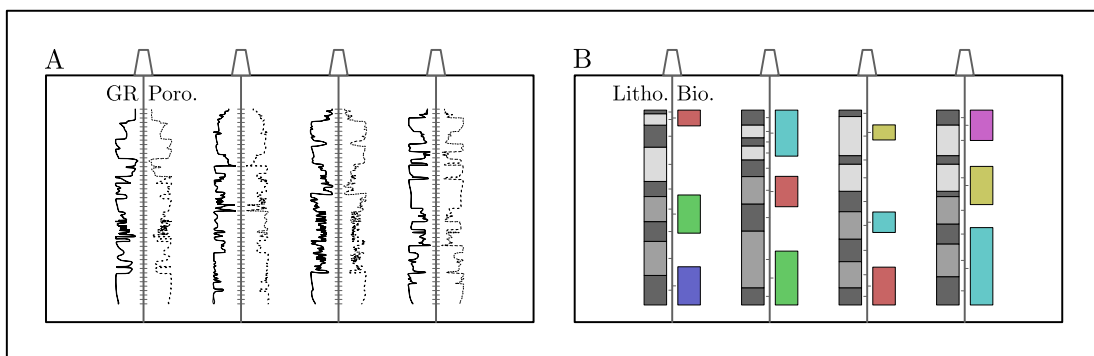


Figure 1.14: Illustration of the two types of well data and their associated well markers: (A) well logs (gamma ray and porosity) and regularly sampled well markers and (B) well regions (lithology and biozones) and irregularly sampled well markers.

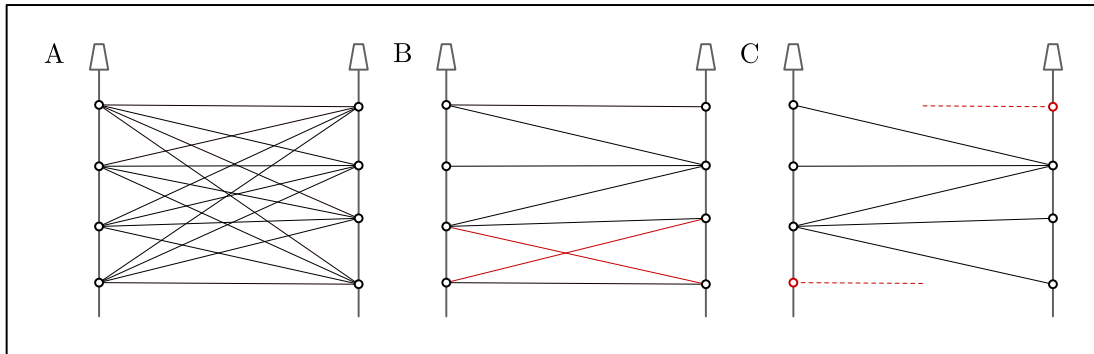


Figure 1.15: (A) Every topologically possible well-marker associations. Two examples of topologically inconsistent correlation sets: (B) two well-marker associations intersect, and (C) all the well marker are not associated.

### 1.3.2 Principles of chronostratigraphic well correlation

There are a lot of possibilities of well-marker associations (Figure 1.15.A) (Lallier et al., 2016). The use of one or several principles of correlation may enable to sort well-marker associations by their likelihoods with respect to the principles of correlation.

However, the principle of correlation used to associate well markers should be consistent with the depositional system. Finally, the choice of the principle of correlation may vary according the type of well data.

#### Walther's law of the correlation of facies

Chronostratigraphic correlation consists of correlating markers according to their depositional age, *i.e.*, markers are correlated if they correspond to the same depositional age or period (Figure 1.13.B). However the high number of various depositional environments and sedimentary facies which may be deposited at the same time and the complexity of depositional systems make it difficult to return likely chronostratigraphic well correlations.

Considering the Walther's law of the correlation of facies, *i.e.*, lithofacies may vary along the dip direction on the same depositional profile, Collins and Doveton (1993) propose to constrain the correlation of lithofacies using vertical and lateral lithofacies succession probabilities.

Moreover, along the strike direction, sedimentary facies may not vary within a chronostratigraphic unit (*e.g.*, Figure 1.10 and Chapter 3). In this configuration, use of the concept of lithostratigraphy may be a good way to correlate sedimentary facies (*e.g.*, Bavielle et al., 2022).

## Stratigraphic sequence well correlation

Sequence Stratigraphy may be used to interpret T-R sequences along well paths (Section 1.1). [Edwards \(2017\)](#) has essentially used the principle of Sequence Stratigraphy to constrain the correlation of transgressive and regressive sequences (well regions). Assuming that variations of subsidence are mild laterally, transgressive (respectively regressive) sequences cannot be correlated with regressive (respectively transgressive) sequences.

[Edwards \(2017\)](#) has also proposed to minimize the lateral thickness variation and the lateral dip variation along correlation lines. However, stratigraphic units usually correspond to sigmoidal geobodies (Figures 1.7, 1.10 and 1.11), which means that the thickness and the dip value may laterally vary within a T-R sequence.

## Stratigraphic model-based well correlation

[Lallier et al. \(2016\)](#) propose to use paleobathymetry and depositional slope to constrain the carbonate facies correlation. Correlation lines correspond to depositional lines and the lower the facies variation between well markers and the theoretical depositional profile, the most likely the correlation line.

Chapter 4 presents an adaptation of this principle of correlation to the siliciclastic depositional systems by adding dipmeter data to the correlation and being driven by the following principle: “*the lower the difference between a chronostratigraphic interpolation (in between markers) and a conceptual depositional profile, the higher the likelihood of the marker association*” ([Baville et al., 2021a](#)).

## Biostratigraphic well correlation

The analysis of the biological elements (e.g., fossils, pollens) in the cores can lead to biostratigraphic interpretations, also called **biozones** (e.g., [Hay and Southam, 1978](#); [Melo and Loboziak, 2000](#); [Nøhr-Hansen et al., 2017](#); [van Gorsel, 1988](#)). Core data may then be analyzed to determine, more or less approximately, their period of deposition.

These biostratigraphic interpretations are subject to uncertainty, but essentially identify well sections whose depositional age is known. Within these biozones, well markers are labeled and cannot be associated with well markers in a different biozone. On the other hand, markers within unidentified areas are not attached to a biozone and can be associated with labeled or unlabeled well markers.

Thus well correlations, constrained by biostratigraphic data, follow only one rule that constrains correlation lines to not completely intersect an area between two identified biozones (e.g., [Knaust and Hoth, 2021](#)).

## Chemostratigraphic well correlation

Chemostratigraphy is used on chemical fingerprints recorded in sediments and sedimentary rocks. It is based on stable isotope signatures fixed in sedimentary matter which are good proxies for depositional period (e.g., [Rodrigues, 2005](#); [Weissert et al., 2008](#)).

Chemostratigraphy involves the geochemical characterization and correlation of strata by using major and trace elements. It is generally used in chronostratigraphic correlation with poor biostratigraphic control (e.g., [Pearce et al., 1999](#)).

## Magnetostratigraphic well correlation

[Lallier et al. \(2013\)](#); [Man \(2008, 2011\)](#) propose a time-to-depth correlation of magnetostratigraphic data acquired along the well paths to the geomagnetic polarity time scale, which includes almost all the magnetic inversions as a function of time. Magnetostratigraphic logs are successions of positive and negative sections. The basic constraint is to correlate positive (respectively negative) zones in a signal with positive (respectively negative) zones in the other signals. [Lallier et al. \(2013\)](#) also constrain the correlation by the sedimentation rate which is computed from the thickness of sections along the well, and the duration of sections in the geomagnetic polarity time scale.

### 1.3.3 Uncertainties in stratigraphic well correlation

As shown previously, input data are subject to uncertainties (e.g., geophysical measurement uncertainties directly linked to the measurement device). The stratigraphic correlation process introduces additional uncertainties which compound with data prior uncertainties. These additional uncertainties on stratigraphic well correlations are mainly due to the dissemination of one-dimensional borehole data and to the fact that fourth to fifth order cycles are below the seismic resolution and cannot be visually correlated (e.g., [Ringrose and Bentley, 2016](#)). There is therefore a multitude of possible correlations (Figure 1.15.A).

Following the example of stratigraphic interpretations, manual stratigraphic well correlations are highly sensitive to the expert (e.g., [Baville et al., 2019](#); [Dewan,](#)

1983; Koehrer et al., 2011). This sensitivity leads to uncertainties which are difficult to assess on manual well correlations. Indeed, the geologist generate the “best” well correlation (or the several best correlations) according to his understanding of the zone of interest: the higher the number of interpreters, the higher the number of stratigraphic interpretations (Bond et al., 2007; Borgomano et al., 2008; Dewan, 1983). Moreover, loops between well data stratigraphic interpretations and well correlation are necessary to build the most consistent stratigraphic well correlation.

Finally, stratigraphic well correlations are highly sensitive to the structural interpretations and structural uncertainties. Structural faults may lead to local repetitions of stratigraphic units (normal faults) or to lack of stratigraphic units (inverse faults) according to their nature. Additionally, tectonic events such as folding or bedrock tilting can lead to modeling inconsistencies (*e.g.*, depositional dip *versus* apparent dip) and must be corrected or taken into consideration when interpreting and correlating subsurface data. In this PhD work, stratigraphic well correlations are preferentially provided within unfaulted areas in order to avoid these situations.

## Conclusion

Sequence Stratigraphy is a way to interpret and model the subsurface which may reproduce the paleogeographic depositional conditions. Stratigraphic interpretations may be performed at several scales (Figure 1.4) and are interpreted and combined in order to generate subsurface models (manual interpretation or computer-assisted generation) at these different scales. For example, first to third stratigraphic units may be interpreted on seismic data and on well data at large scale, whereas fourth to fifth stratigraphic units are interpreted from well data below the seismic resolution.

In addition to the multi-scale approach, the subsurface stratigraphic well correlation is directly based on several principles of correlation (Chapters 3 and 4). Additionally, the same input data set may lead to different subsurface geomodels according to the principle of correlation (Figure 1.13) (*e.g.*, Ainsworth et al., 1999; Baviile et al., 2022).

Moreover, manual well correlation are highly sensible to the expert which generate the best correlation according to his field of expertise and his knowledge about the depositional system. Moreover, from the same input data set, the higher the number of interpreters, the higher the number of well correlation (Borgomano et al., 2008; Dewan, 1983). The high sensitivity of the well correlation to the geologist reflects the uncertainties which are difficult to quantify. Therefore,

Chapter 2 introduces the computer-assisted well correlation which enable the automatic stratigraphic well correlations (e.g., [Borgomano et al., 2008](#); [Lallier, 2012](#); [Waterman and Raymond, 1987](#)), and which enable the uncertainties assessment by generating a high number of possible well correlations and classifying them according to their likelihood with respect to the principle of correlation (e.g., [Edwards et al., 2018](#); [Pels et al., 1996](#)).



# Chapter 2

## Computer-assisted well correlation

### Contents

---

<b>2.1</b>	<b>Computer-assisted well correlation algorithms . . . .</b>	<b>45</b>
2.1.1	Frequency space approaches and multi-scale analysis .	45
2.1.2	Well-log cross-correlation . . . . .	46
2.1.3	Well-log section correlation . . . . .	47
2.1.4	Dynamic well correlation algorithms . . . . .	47
<b>2.2</b>	<b>Dynamic Time Warping algorithm . . . . .</b>	<b>48</b>
2.2.1	Well-to-well correlation . . . . .	49
2.2.2	Multi-well correlation . . . . .	51

---

This chapter first presents the different approaches to automatically compute and stochastically simulate stratigraphic well correlations to assess the uncertainties (Section 2.1). This chapter presents then the Dynamic Time Warping algorithm. The Dynamic Time Warping algorithm is the algorithm used in this PhD work to automatically compute stratigraphic well correlations based on the computation of well-marker correlation costs and correlation-to-correlation transition costs (Section 2.2).

*N.B.: This chapter contains paragraphs which are modified or partially/entirely taken from [Baville et al. \(2022\)](#).*

## Introduction

Stratigraphic well correlation is a challenging way to model stratigraphic layers in the subsurface from sparse well data (Nagy and Bjørlykke, 2015). As discussed in Chapter 1, stratigraphic well correlations enable the interpolation of the stratigraphic units between well markers, and give information about the connectivity between these units.

Subsurface data measurement errors are a first source of uncertainties and their interpretations based on geological concepts are a second source of uncertainties. Moreover, the stratigraphic correlation of these subsurface data is a third source of uncertainties, *i.e.*, several likely stratigraphic well correlations may be generated from one input data set (Borgomano et al., 2008; Koehrer et al., 2011).

As discussed in Chapter 1, well marker correlations are sensitive to the interpreter and the concept of interpretation (Baville et al., 2019; Borgomano et al., 2008; Koehrer et al., 2011). The assessment of these well correlation uncertainties may be achieved by stochastically computing a high number of realizations, exactly like in other stochastic modeling methods which generate realizations of the subsurface parameters (*e.g.*, Caumon, 2010; Colombera et al., 2012; Eide et al., 1996; Haldorsen and Damsleth, 1990; Massonnat, 1997; Wellmann and Caumon, 2018).

Manual stratigraphic well correlation is not a quick step of the subsurface modeling workflow (Doveton, 1994). Indeed, manual stratigraphic well correlation needs loops between well data interpretations and their correlation following a stratigraphic concept (*e.g.*, Knaust et al., 2019). Moreover, the number of possible well correlations is very sensitive to the number of stratigraphic units to correlate, and to the number of wells, and the identification of the most likely realization is not an easy computational task (Edwards et al., 2018; Lallier et al., 2016).

In addition, the quality of well data interpretations, based on complex transport and depositional processes (*e.g.*, Vermaas et al., 2016) or on the geological knowledge of the interpreter (Bond et al., 2007), may have an impact on the generated well correlations (*e.g.*, Baville et al., 2019).

In the 1990's, the growth of computational and numerical technologies leads to the development of new software packages especially dedicated to geosciences. These software packages allow geologists to numerically generate subsurface geological models and to visualize these models in three dimensions (*e.g.*, Mallet, 1992).

The purpose of this chapter is to presents and briefly describe the different approaches to automatically compute and stochastically simulate stratigraphic well correlations to assess the uncertainties (Section 2.1). Among these approaches,

this PhD work uses the Dynamic Time Warping algorithm to automatically compute stratigraphic well correlations based on the computation of well-marker correlation costs and correlation-to-correlation transition costs (Section 2.2).

## 2.1 Computer-assisted well correlation algorithms

Several algorithms have been developed to generate automatically stratigraphic well correlations. The use of these algorithms is a way to discriminate the most likely scenarios in stratigraphic well correlations (Baville et al., 2019). Indeed, computer-assisted well correlations are no further based on manual interpretation but on automatic associations based on numerical rules (e.g., Edwards, 2017; Lallier, 2012).

Some algorithms enable to generate deterministic stratigraphic well correlations (e.g., Wheeler and Hale, 2014). However, improvements of these algorithms have led to the generation of stochastic well correlation scenarios (Lallier et al., 2013). This stochasticity has enabled geologists to generate not one but several well correlation scenarios from the same input data set in order to assess the uncertainties. It is also possible to evaluate their differences, and to rank them by their likelihood (e.g., Baville et al., 2019; Lallier, 2012; Lallier et al., 2016; Pels et al., 1996).

### 2.1.1 Frequency space approaches and multi-scale analysis

Preston and Henderson (1964) first proposed to correlate sedimentary formations from resistivity logs processed using Fourier analysis. The one-dimensional Fourier analysis consists of the decomposition of a one-dimensional signal into trigonometric functions (Fourier, 1822). These trigonometric functions are characterized by their frequencies, which lead to a spectrum containing the frequencies of all the trigonometric function decomposing the initial signal. Fourier analysis has been used in computer-assisted well correlation until the 1980's (e.g., Martinson et al., 1982).

Mann and Dowell (1978) also proposed to correlate electrical well logs using spectral analysis. The multi-scale approach enables to transform signals and to correlate sections at different scales.

Clark and Thompson (1979) propose to use the least squares method to correlate well logs from cubic splines. This method enables to deform the one-dimensional regularly sampled well logs (compression and stretching) to correlate them.

These methods of multi-scale well-log analyses and correlations are only applied on well logs, *i.e.*, the generated correlation correspond to lithostratigraphic correlations. Indeed, the purpose of these methods is to associate similar sections of well logs. Moreover, these methods are not able to generate hiatuses, which may correspond to erosional or non deposition surfaces during the correlation process.

### 2.1.2 Well-log cross-correlation

The cross-correlation is a statistical approach which enables the computation of the similarity between two one-dimensional signals which generally have different sizes by moving one series relative to the other. At the opposite of Fourier analyses, cross-correlation takes into account the spatial variations of the signals.

Holgate (1960) proposes to align core data and well logs from the same well and find a linear relation in between to evaluate the information of the cores (porosity) from the logs (sonic). Moran et al. (1962) also propose to correlate microresistivity logs during dip measurements in the same well using cross-correlation.

The cross-correlation algorithm has also been applied to the well-to-well correlation (Matuszak, 1972). The principal purpose of the application of the cross-correlation is the comparison of stratigraphic unit successions based on well logs (*e.g.*, Davis, 1973; Dean and Anderson, 1974; Harbaugh and Merriam, 1968; Merriam, 1971; Sackin, 1965).

The above methods only work on well logs treated as continuous signals, whereas geological interpretations may be categorical variables (*e.g.*, facies, T-R sequences, biozones). In these configurations, the cross-correlation approaches has been modified to be applied to categorical data (Sackin and Merriam, 1969).

As cross-correlation calls for moving windows of fixed size, Neidell (1969) proposes to improve the cross-correlation by using the covariance between two signals to create the “ambiguity function” (a stretching function). Southam and Hay (1978) propose to combine the cross-correlation and Fourier analysis in order to optimize stretches and compressions of stratigraphic units which are punctually correlated by their horizons. Despite these improvements, hiatuses are not managed.

Cross-correlation have been the most used algorithm to correlate wells until the 1980’s (Waterman and Raymond, 1987). However, these methods of well-log cross-correlations are only applied on well logs, *i.e.*, the generated correlation correspond to lithostratigraphic correlations. Indeed, the purpose of these methods is to associate similar sections of well logs. Moreover, the stretching / compression approaches do not take into account the sedimentation rate, and by extension are not able to generate hiatuses.

### 2.1.3 Well-log section correlation

Testerman (1962) proposes a variant of the cross-correlation method, that takes as input not whole signals and a fixed cross-correlation window size, but sections of variable length of these signals. These sections are constructed to minimize the variation of the analyzed property within these sections. Then the algorithm computes the difference between the average value of the property within the sections and associates two sections if the variation of the average values is similar to the variation of the property within these sections.

Kemp (1982) has proposed an algorithm to correlate well-log intervals. However, this algorithm do not subdivide well logs themselves and takes only well-log intervals already subdivided by a geologist as input parameters. Moreover, the purpose of this algorithm is not to find the best correlation set, but only to correlate intervals two-by-two without taking account to the rest.

The main difference between these two approach and the other presented earlier states in the simulation of hiatuses. Indeed, if an interval is correlated with no other interval in the other wells, a stratigraphic hiatus is directly simulated. However, these methods ask for the user to subdivide the well logs in intervals, and are only applied on well logs, *i.e.*, the generated correlation correspond to lithostratigraphic correlations. Indeed, the purpose of these methods is to associate similar sections of well logs.

### 2.1.4 Dynamic well correlation algorithms

The concept of dynamic correlation is based on the principle of optimality formulated by Bellman and Kalaba (1957). The principle of optimality consists of decomposing a problem into subproblems, solving these subproblems, storing the results, and finally solving the initial problem from these intermediate results (Dreyfus, 2002).

Gordon (1980); Gordon and Reyment (1979) propose an adaptation of the slotting method (Delcoigne and Hansen, 1975) to the well-log correlation. The purpose of this method is to embed the logs to form a single sequence. This amounts to consider that each element has no temporal equivalent on the other sequence, that it has been eroded or that it has not been deposited, *i.e.*, the correlation is a series of hiatuses. Thompson and Clark (1990) propose an improvement to this approach by enabling to constrain the thickness of the embed well-log parts.

Again, these methods of dynamic well-log correlations applied on well logs correspond to lithostratigraphic correlations. As discussed in Chapter 1, the lithos-

stratigraphic well correlation does not take into account the lateral variation of facies along a depositional profile (Walther's Law of the Correlation of Facies), whereas chronostratigraphic well correlation aims to associate well markers according to their depositional ages.

Cross-correlation has been presented to be applied on well logs but, it also can be applied on categorical data to generate outcomes which are consistent with the concept of sequence stratigraphy (Sackin and Merriam, 1969). However, well cross-correlation algorithms are not able to simulate or to reproduce hiatuses during the correlation process, whereas hiatuses correspond to the main part of sedimentary recordings (Ager, 1981, 1993; Miall, 2016).

The Levenshtein distance corresponds to the minimum number of modifications required to move from one sequence of elements to another, *i.e.*, insertions, deletions, substitutions (Levenshtein, 1966). Several algorithms of Dynamic Time Warping are based on the Levenshtein distance. These algorithms are efficient to compare two sequences and correlate them computing a correlation cost using rules of correlations.

Dynamic Time Warping algorithms are used for different purposes, such as bioinformatics (*e.g.*, Higgins and Sharp, 1988; Needleman and Wunsch, 1970), speech recognition (*e.g.*, Myers and Rabiner, 1981; Sakoe and Chiba, 1978), and subsurface modeling (*e.g.*, Edwards et al., 2018; Hale, 2013; Lallier et al., 2013; Waterman and Raymond, 1987).

The Dynamic Time Warping algorithm enables the correlation of two sequences of elements which may be regularly sampled, such as well logs and seismograms (*e.g.*, Hale, 2013), but also two sequences of elements which may be irregularly sampled, such as geological interpretations (*e.g.*, Lallier et al., 2016; Smith and Waterman, 1980). Furthermore, the number of elements in the two sequences may be different and the Dynamic Time Warping algorithm may generate correlations with stratigraphic hiatuses.

In this PhD work, the two correlation rules described in Chapters 3 and 4 define correlation costs which are used to compute all possible marker combinations aggregated by the Dynamic Time Warping algorithm.

## 2.2 Dynamic Time Warping algorithm

The correlation of  $n$  series by computing a  $n$ -dimensional correlation matrix and by evaluating of the maximum match has been first proposed by Needleman and Wunsch (1970) for the comparison of similarities in amino acid sequences. The

Dynamic Time Warping algorithm has been first developed by [Sakoe and Chiba \(1978\)](#) for speech recognition in order to associate two time series as likely as possible. The main idea was to minimize the squared difference between each association corresponding to the best correlation.

The Dynamic Time Warping algorithm has been first adapted to the stratigraphic well correlation by [Smith and Waterman \(1980\)](#), in order to associate the most likely lithologies interpreted along two vertical wells.

### 2.2.1 Well-to-well correlation

In the case of stratigraphic well correlation, the purpose of the Dynamic Time Warping algorithm is to return the best correlation sets from two vertical wells. A correlation set is a set of well marker associations.

A correlation set is admissible only if there are no correlation lines which intersect, and is conformable if each well marker on one well is correlated to other well markers on the other well ([Figure 1.15](#)). Moreover, the two well markers at the top (and the two well markers at the bottom) of the two correlated wells are automatically correlated together.

The Dynamic Time Warping algorithm uses a conceptual two-dimensional correlation cost matrix whose axis correspond to the two input wells, *i.e.*, lines correspond to well markers in the first well and column correspond to well markers in the other well ([Figure 2.1](#)). Moreover, vertical (respectively horizontal) transitions represent hiatuses simulated in the well corresponding to the horizontal axis (respectively vertical axis).

Within the conceptual correlation cost matrix, a correlation set corresponds to a correlation path, *i.e.*, a succession of transitions (arrows) between well marker associations (cells). In order to be conformable, the correlation path must respect three rules:

- The correlation path must start at the top left corner.
- The correlation can only go right, bottom or bottom right.
- The correlation path must finish at the bottom right corner.

Each well-marker association is defined by a correlation cost  $c$ . Each transition between two well-marker associations are defined by a transition cost  $t$ . Finally the sum of all the costs along a correlation path gives the cumulative correlation cost of the correlation set.

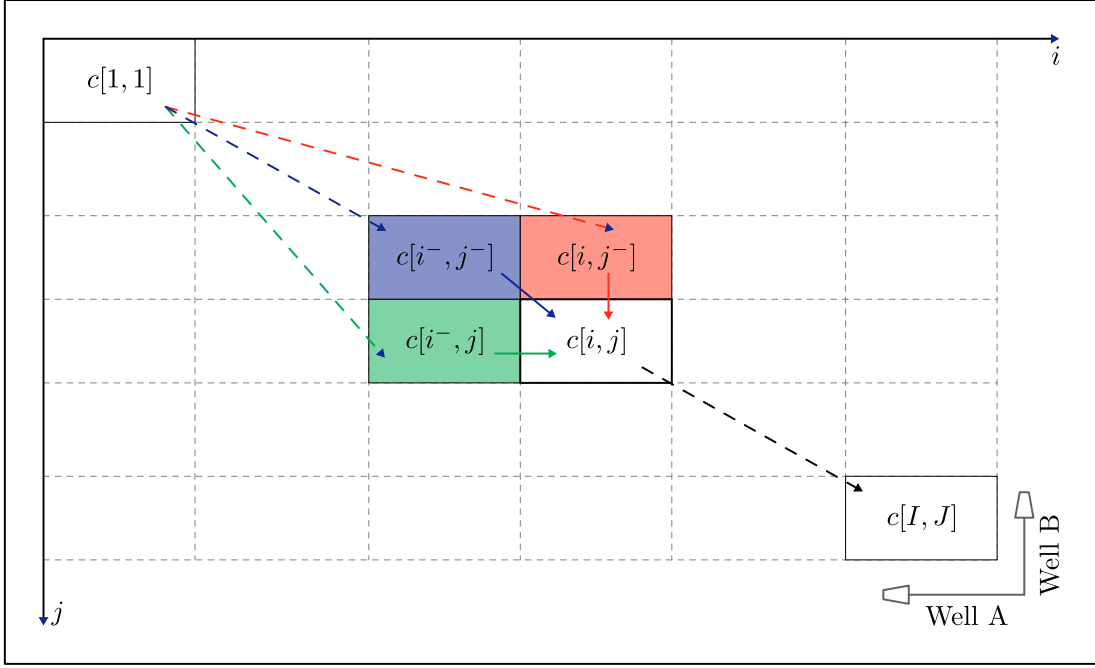


Figure 2.1: Illustration of the two-dimensional version of the Dynamic Time Warping algorithm at step  $[i, j]$  with two wells containing  $I$  and  $J$  markers.

The purpose of Dynamic Time Warping algorithm is to minimize the cumulative correlation cost and to return the correlation path having the minimum correlation cost among all the possible correlation sets using

$$C_{ab}[i, j] = c_{ab}[i, j] + \min \begin{pmatrix} t_{ab}[i, j^-][i, j] + C_{ab}[i, j^-] \\ t_{ab}[i^-, j^-][i, j] + C_{ab}[i^-, j^-] \\ t_{ab}[i^-, j][i, j] + C_{ab}[i^-, j] \end{pmatrix}. \quad (2.1)$$

Equation (2.1) is deterministic and return the correlation path having the lowest cumulative among all the possible correlation sets. However, the Dynamic Time Warping algorithm may be adapted to return the  $n$ -best correlation sets corresponding to the  $n$ -lowest cumulative correlation costs (e.g., [Caumon and Antoine, 2019](#); [Pels et al., 1996](#)).

To assess uncertainties on the correlation generation, [Lallier et al. \(2016\)](#) also propose a stochastic version of the two-dimensional Dynamic Time Warping algorithm given by

$$C_{ab}[i, j] = \min \begin{pmatrix} 1 / \alpha_1 & \text{if } p \in \left[ 0, \frac{\alpha_1}{\alpha_1 + \alpha_2 + \alpha_3} \right] \\ 1 / \alpha_2 & \text{if } p \in \left[ \frac{\alpha_1}{\alpha_1 + \alpha_2 + \alpha_3}, \frac{\alpha_1 + \alpha_2}{\alpha_1 + \alpha_2 + \alpha_3} \right] \\ 1 / \alpha_3 & \text{if } p \in \left[ \frac{\alpha_1 + \alpha_2}{\alpha_1 + \alpha_2 + \alpha_3}, 1 \right] \end{pmatrix}. \quad (2.2)$$

where  $p$  is a random value simulated from a uniform distribution  $U[0, 1]$ , and  $\alpha_1$ ,  $\alpha_2$  and  $\alpha_3$  correspond respectively to the likelihood of making a vertical, an oblique, or a horizontal transition and are given by

$$\alpha_1 = \frac{1}{(c_{ab}[i, j] + t_{ab}[i, j^-][i, j] + C_{ab}[i, j^-])}, \quad (2.3)$$

$$\alpha_2 = \frac{1}{(c_{ab}[i, j] + t_{ab}[i^-, j^-][i, j] + C_{ab}[i^-, j^-])}, \quad (2.4)$$

and

$$\alpha_3 = \frac{1}{(c_{ab}[i, j] + t_{ab}[i^-, j][i, j] + C_{ab}[i^-, j])}. \quad (2.5)$$

### 2.2.2 Multi-well correlation

The two-dimensional equation of the Dynamic Time Warping algorithm enable the correlation of only two wells. However, subsurface modeling is generally based on more than two wells.

#### Simultaneous multi-well correlation

The two-dimensional version of the Dynamic Time Warping algorithm may be adapted to an  $n$ -dimensional version in order to simultaneously correlate  $n$  wells (Brown, 1997). In the  $n$ -dimensional version of the algorithm, the conceptual correlation cost matrix becomes a  $n$ -dimensional matrix whose cells correspond to the correlation between  $n$  well markers.

For example, the three-dimensional version of the Dynamic Time Warping algorithm is based on a three-dimensional conceptual correlation cost matrix whose cells correspond to triplets of well markers, and each well-marker association is preceded by seven triplets of well markers (Figure 2.2). The correlation path must start from the cell corresponding to the triplet of top well markers, and finish in the cell corresponding to the triplet of bottom well markers. Moreover, within the conceptual correlation cost matrix, the correlation path has only seven possible directions at each step in order to generate admissible correlation sets (Figure 2.2).

A correlation cost  $c$  can be computed for each triplet of well markers, and a transition cost  $t$  can be computed for each succession of triplets. Finally the cor-

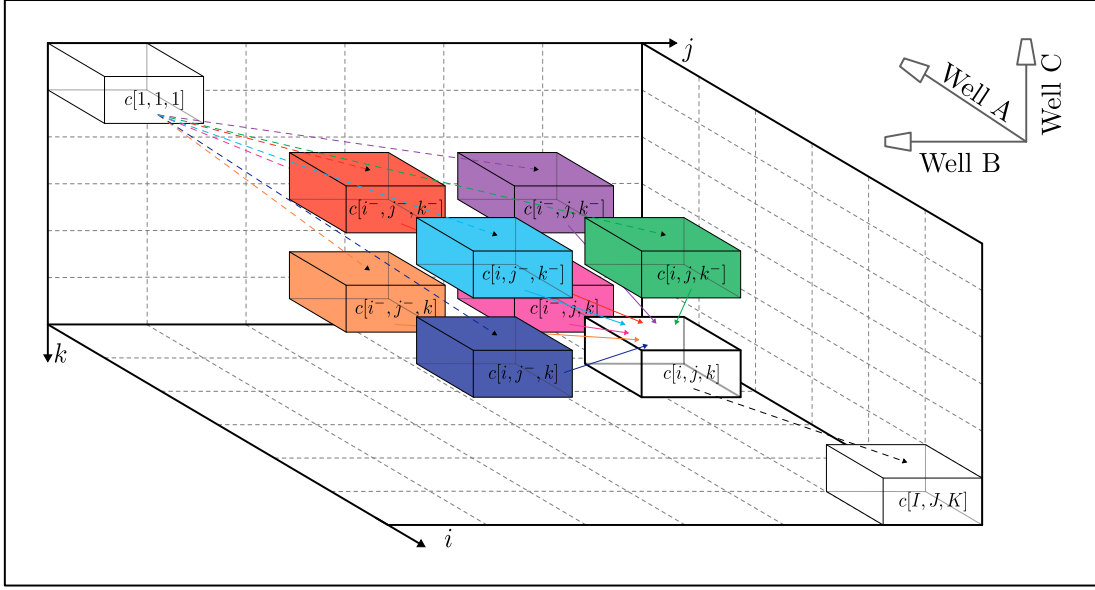


Figure 2.2: Illustration of the three-dimensional version of the Dynamic Time Warping algorithm at step  $[i, j, k]$  with three wells containing  $I$ ,  $J$  and  $K$  markers. Cells correspond to triplets of well markers (correlation cost  $c$ ), and arrows correspond to transitions between two triplets (transition cost  $t$ ).

relation set having the lowest cumulative cost among all the possible correlation sets is given by

$$C_{abc}[i, j, k] = c_{abc}[i, j, k] + \min \begin{pmatrix} t_{abc}[i, j, k^-][i, j, k] + C_{abc}[i, j, k^-] \\ t_{abc}[i^-, j, k^-][i, j, k] + C_{abc}[i^-, j, k^-] \\ t_{abc}[i, j^-, k^-][i, j, k] + C_{abc}[i, j^-, k^-] \\ t_{abc}[i^-, j^-, k^-][i, j, k] + C_{abc}[i^-, j^-, k^-] \\ t_{abc}[i^-, j, k][i, j, k] + C_{abc}[i^-, j, k] \\ t_{abc}[i^-, j^-, k][i, j, k] + C_{abc}[i^-, j^-, k] \\ t_{abc}[i, j^-, k][i, j, k] + C_{abc}[i, j^-, k] \end{pmatrix}. \quad (2.6)$$

However, the higher the number of wells, the higher the dimension of the system, and the higher the computational time. Indeed, the  $n$ -dimensional version of the Dynamic Time Warping algorithm is not efficient and the computational time ( $O(n^d)$  with  $n$  the number of wells and  $d$  the number of markers per well) make its application prohibitive (Fuellen, 1997).

### Iterative multi-well correlation

Another way to automatically generate multi-well correlations is to keep the two-dimensional version of the Dynamic Time Warping algorithm, but to add iteratively wells to the multi-well correlation process (Figure 2.3).

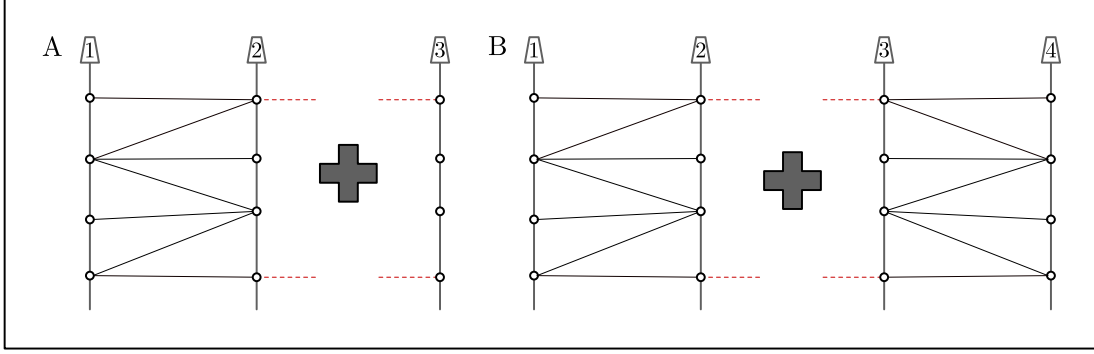


*Figure 2.3: Illustration of the three-dimensional version of the Dynamic Time Warping algorithm at step  $[i, j, k]$  with three wells containing  $I$ ,  $J$  and  $K$  markers. Cells correspond to triplets of well markers (correlation cost  $c$ ), and arrows correspond to transitions between two triplets (transition cost  $t$ ).*

Figure 2.3 illustrates two possible configurations for the iterative addition of wells to the multi-well correlation process:

- Figure 2.3.A illustrates the linear configuration. A lonely well (Well 3) is added to the group of correlated wells. The addition is linear, and the automated correlation is computed between one well of the group of wells (Well 2) and the lonely well (Well 3).
- Figure 2.3.B illustrates the pyramidal configuration. In this configuration, to group of wells are gathered through one well-to-well correlation. The addition is pyramidal because the automated correlation is computed between one well of the first group of wells (Well 2) and one well of the other group of wells (Well 3).

In both configurations, the Dynamic Time Warping algorithm computes the lowest cumulative correlation set between the two wells cost using Equation (2.1). [Lallier et al. \(2016\)](#) also proposed to redraw randomly correlation set between two successive wells along the correlation edge and to update the model until the convergence of the model, *i.e.*, a stable minimum correlation cost. However, this approach do not always converge and the order of correlation may have an impact on the outcomes.

During the correlation process, the existing well marker correlation on both sides of the current correlation may be included in the correlation cost computation by modifying Equation (2.1) to

$$C_{ab}[i, j] = c_{ab}[i, j] + \min \left( \begin{array}{l} t_{ab}[i, j^-][i, j] + C_{ab}[i, j^-] \\ t_{ab}[i^-, j^-][i, j] + C_{ab}[i^-, j^-] \\ t_{ab}[i^-, j][i, j] + C_{ab}[i^-, j] \end{array} \right) + C_a[i] + C_b[j], \quad (2.7)$$

where  $C_a[i]$  (respectively  $C_b[j]$ ) is the aggregated correlation cost computed at the previous steps corresponding to the association of the well marker  $i$  (respectively the well marker  $j$ ) in the well  $a$  (respectively in the well  $b$ ) with the other well markers in its group of wells:

- In the linear configuration (Figure 2.3.A),  $C_a[i]$  corresponds to the sum of all correlation costs  $c$  linked to the well marker  $i$ , and  $C_b[j]$  is null because the well marker  $j$  is not correlated to any other well marker.
- In the pyramidal configuration (Figure 2.3.B),  $C_a[i]$  corresponds to the sum of all correlation costs  $c$  linked to the well marker  $i$ , and  $C_b[j]$  corresponds to the sum of all correlation costs  $c$  linked to the well marker  $j$ .

The iterative multi-well correlation enable to solve the problem of computational time, which is too high with simultaneous multi-well correlation algorithms (Brown, 1997). However, the iterative multi-well correlation is efficient if there is no loop in the correlation path, *i.e.*, each well is considered at most twice, excepted for the two extreme wells which are considered once during the process. Indeed, loops in the correlation path may lead to the correlation of two different well markers from one single well, *i.e.*, loops may lead to inconsistent correlation sets (Lallier et al., 2016; Wheeler, 2015).

Edwards et al. (2018) proposed to propagate a stratigraphic column during the multi-well correlation process. The purpose of this stratigraphic column is to keep a memory of all the well markers which belong to the same correlation line (Figure 2.4). Using the stratigraphic column, it is possible to compute a stratigraphic model during the correlation process and to assess uncertainties on this stratigraphic model by simulating stochastic well correlation.

Moreover, keeping in memory every well marker corresponding to the same correlation line, *i.e.*, the same stratigraphic unit in the stratigraphic column, enable the computation of correlation costs based on more than two well markers (Antoine and Caumon, 2018, 2020; Caumon and Antoine, 2019). The other advantage of maintaining the stratigraphic column during the correlation computation is for gaps which correspond to erosion or non deposition (baselap).

## Conclusion

For decades, algorithms have been developed to generate stratigraphic well correlations. The first approach was able to correlate wells following the concept of

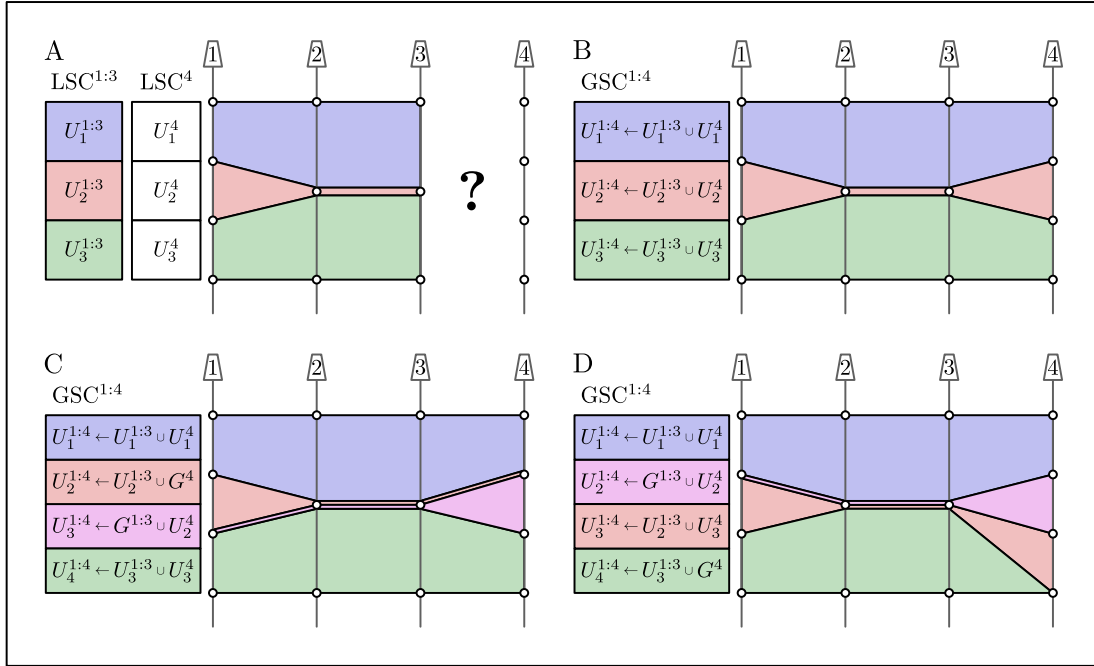


Figure 2.4: Illustration of three possible the stratigraphic column propagations during the well correlation computation.  $LSC^{i:j}$  is the local stratigraphic column between wells  $i$  and  $j$ ;  $GSC^{i:j}$  is the global stratigraphic column between wells  $i$  and  $j$ .  $U_n^{i:j}$  is to the stratigraphic unit  $n$  interpreted between wells  $i$  and  $j$ .  $G^{i:j}$  is a stratigraphic gap interpreted between wells  $i$  and  $j$ .  $\cup$  is the union of two units or gaps. Redrawn from [Edwards et al. \(2018\)](#).

lithostratigraphy by correlating well logs. However, lithostratigraphic well correlation do not take into account the possible variation of subsurface properties along a depositional profile, leading to inconsistent stratigraphic models.

Other approach have been developed to take into account this possible variation of properties along depositional profile, i.e., along correlation lines. Dynamic Time Warping algorithms have been adapted to stratigraphic well correlation to constrain the well marker associations by correlation costs consistent with depositional principles. Moreover, the Dynamic Time Warping algorithm can be applied on well log and is able to automatically stretch or squeeze.

These computer-assisted well correlations have a potential to reduce the interpretation bias and to assess uncertainties in stratigraphic modeling. In this PhD work, two principles of correlation have been developed (Chapters 3 and 4) to compute correlation and transition costs which are aggregated by the Dynamic Time Warping algorithm, and to assess uncertainties on stratigraphic subsurface models.



## Part II

# PRINCIPLES OF CORRELATION



# Chapter 3

## Sedimentary facies vs Well distality

### Contents

---

<b>3.1</b>	<b>Principle of correlation . . . . .</b>	<b>61</b>
<b>3.2</b>	<b>Correlation likelihood computation . . . . .</b>	<b>64</b>
3.2.1	Correlation cost computation . . . . .	64
3.2.1.1	Contribution of the sedimentary facies . . . . .	65
3.2.1.2	Contribution of the relative well distality . . . . .	67
3.2.1.3	Correlation cost . . . . .	69
3.2.2	Transition cost computation . . . . .	71
<b>3.3</b>	<b>First results: Synthetic data set . . . . .</b>	<b>72</b>
3.3.1	Sedimentary margin transverse cross-section . . . . .	72
3.3.2	Sedimentary margin longitudinal cross-section . . . . .	74
3.3.3	Sedimentary bay-head delta transverse cross-section . . . . .	75
<b>3.4</b>	<b>Discussion . . . . .</b>	<b>76</b>
3.4.1	Order of wells and correlation path . . . . .	76
3.4.2	Number of propagated realizations . . . . .	77
3.4.3	Principal sediment transport direction . . . . .	78
3.4.4	Well position within the depositional system . . . . .	79
3.4.5	Laterally equivalent sedimentary facies . . . . .	80

---

This chapter presents the distality rule of correlation. It defines the principle of correlation (Section 3.1), describes the computation of the correlation likelihood (Section 3.2), presents the first results obtained on a synthetic data set (Section 3.3), and discusses the impact of each parameter (Section 3.4).

*N.B.: This chapter contains paragraphs which are modified or partially/entirely taken from [Baville et al. \(2022\)](#).*

## **Abstract**

*Computer-assisted stratigraphic correlation can help to produce several scenarios reflecting interpretation uncertainties. The first method proposed in this work translates some sedimentary concepts into a correlation cost for each possible stratigraphic correlation lines. All these correlation costs are used to populate a cost matrix in order to apply the Dynamic Time Warping algorithm and to compute the  $n$ -best correlation sets having the  $n$ -least cumulative costs. The proposed cost function reflects prior knowledge about sediment transport direction, and it is illustrated on simple synthetic data sets. Well markers are described by two parameters: (1) the sedimentary facies corresponding to a depositional environment, and (2) the relative distality of the well computed from its position along the sediment transport direction. The main principle of correlation used in this method assumes that “a well marker (described by a facies index  $f$  and a distality value  $d$ ) cannot be correlated with another well marker described by a depositionally deeper facies at a more proximal position, or a depositionally shallower facies at a more distal position”. This approach produces consistent stratigraphic well correlations, and highlights the sensitivity of the solution to the order of wells in the correlation process. Therefore, the proposed rule offers a way to coherently consider chronostratigraphic correlation and the associated uncertainties at the parasequence scale, i.e., at a smaller scale than generally considered in deterministic correlation.*

## **Introduction**

Ideally, a quantification of correlation uncertainties would call for generating every topologically possible scenario and evaluating their likelihood. However, the very large number of topologically possible scenarios (number of Delannoy; [Dellano \(1886\)](#)) makes their manual validation almost impossible (e.g., [Lallier et al., 2016](#)). To overcome this limitation, numerical methods to provide automatically multiple stratigraphic scenarios have been proposed (e.g., [Edwards et al., 2018](#); [Lallier et al., 2016](#); [Pels et al., 1996](#)). These scenarios are consistent with the input data and with some explicitly defined correlation rules which allow to discern the most likely solutions. Therefore, correlation rules must be carefully chosen to produce solutions which are geologically acceptable.

As discussed in Chapter 1, the following chapters consider well correlations based on relative chronostratigraphic principles (Section 3.1), as they are considered as the most predictive to model the subsurface. Among chronostratigraphic approaches, sequence stratigraphy describes the stratigraphic structure of sedimentary basins based on depositional sequences (e.g., [Catuneanu, 2006](#); [Catuneanu](#)

et al., 2011; Galloway, 1989a; Mitchum, 1977). Depending on the relative well distality (relative well position along a proximal-to-distal transect), depositional processes vary and lead to different isochronous sedimentary facies and vertical stacking patterns (e.g., Bhattacharya, 2011; Borgomano et al., 2008; Knaust and Hoth, 2021; Lallier et al., 2016).

The Dynamic Time Warping algorithm (Sakoe and Chiba, 1978) is used to retrieve such isochronous surfaces from the stratigraphy sections. As described in Chapter 2, this algorithm computes the likelihood of a correlation set among all possible correlation sets and returns the best correlation set, *i.e.*, the most likely correlation set (e.g., Hale, 2013; Sakoe and Chiba, 1978; Waterman and Raymond, 1987; Wheeler and Hale, 2014) or the  $n$ -best correlation sets (e.g., Edwards et al., 2018; Pels et al., 1996) among all the computed realizations. Lallier et al. (2016) proposed a stochastic version of the Dynamic Time Warping algorithm to assess the uncertainties on the well correlations. The likelihood of one correlation set is computed by minimizing the sum of elementary correlation costs and transition costs between correlations.

In this chapter, the proposed significant methodological contribution is the explicit integration of distality in the elementary correlation cost of the Dynamic Time Warping algorithm (Section 3.2). This new rule enables to compute global correlation set likelihood and to rule out impossible lateral facies variations along the generated isochronous layers, assuming a prior sediment direction.

In this correlation cost function, all input data (well logs and core samples of the interval of interest) must be given within unfaulted stratigraphic parasequence successions. This condition can be ensured by using a few regional seismic markers corresponding to lower order cycles or by using dip analysis (see Chapters 5 and 6). The focus is set on relative chronostratigraphic well marker correlation based on (1) the sedimentary facies that correspond to the depositional environment interpreted as zones along the well paths, and (2) the relative distality of the well along the sediment transport direction. The proposed method is illustrated and validated with three simple synthetic data sets (Section 3.3). It will then be applied to real data in Chapters 5 and 6.

## 3.1 Principle of correlation

In this PhD work, relative chronostratigraphy is used to associate well markers. The objective of this PhD work is to propose correlation rule to correlate time-windows. Assuming that over a given area, some deposition events are quasi-synchronous depending on basin geometry, subsidence, distribution and depositional system. Therefore, along a given isochronous surface, all deposits

have (approximately) the same geological age (Figure 3.1). In this case, correlating these isochronous deposits is the same as correlating time windows and *vice versa*.

A sedimentary domain can be characterized by two main directions: proximal-to-distal direction (dip), given by the regional sediment transport direction, and the direction perpendicular to it (depositional strike). In practice, these two directions may change laterally (e.g., in fan-shaped deltas), but, for simplicity the case of a Cartesian geometry is considered here to schematize the internal structure of a sedimentary basin margin (Figure 3.1). In the direction of sediment transport ( $BB'$ ), there is a superposition of sigmoidal bodies whereas along the depositional strike direction ( $AA'$ ), a superposition of monoclinical bodies occurs.

These sedimentary bodies are defined as clinoforms (Driscoll and Karner, 1999; Hampson, 2000; Patruno and Helland-Hansen, 2018; Patruno et al., 2015; Rich, 1951) and are characterized by a lateral transition of facies (from the most proximal to the most distal region) during the same depositional event. Depending on the context (distance to fluvial sediment source, dominance of waves / tides in the depositional process), clinoforms are observed in every direction, even though they have different shapes along depositional dip and strike.

Figure 3.1 illustrates two successive clinoforms formed during a regressive system tract and bounded by isochronous surfaces (black bold lines). These two clinoforms may be divided into four sedimentary facies classified by their relative depositional depth. These clinoforms may be defined at a large time interval

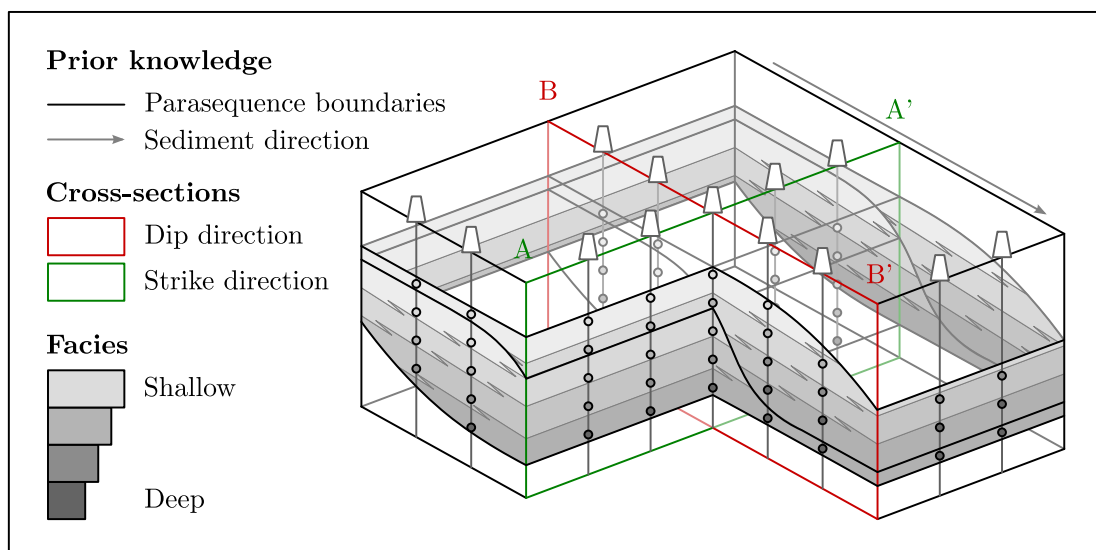


*Figure 3.1: Three-dimensional illustration of a simplified sedimentary basin margin geometry along the depositional strike direction ( $AA'$ ) and the principal sediment transport direction ( $BB'$ ). Parasequence boundaries (black bold lines) are isochronous lines separating clinoforms. Modified from [Baville et al. \(2022\)](#).*

(fourth order - parasequences), being in the range of 150,000 to 200,000 years (Knaust and Hoth, 2021), and at a lower temporal scale, clinoforms can be subdivided in several stratigraphic system tracts.

A clinoform may be subdivided into several sequences and the purpose of this work is to correlate well markers in order to reproduce these subdivisions and to generate a chronostratigraphic model of the subsurface.

Figure 3.2 illustrates that along the two principal directions, well marker correlation likelihood may be qualitatively evaluated using the clinoform internal geometry as the reference.

This leads to several configurations which are not geologically plausible if it is assumed that the depositional depth increases with the distality:

- A sedimentary facies in a well cannot be associated with a depositionally shallower facies in a more distal well.
- A sedimentary facies in a well cannot be associated with a depositionally deeper facies in a more proximal well.

Considering these two configurations of exclusion, it is possible to postulate a principle of correlation stating that “a well marker (described by facies and distality taken at the center of an interval having a constant facies and a constant

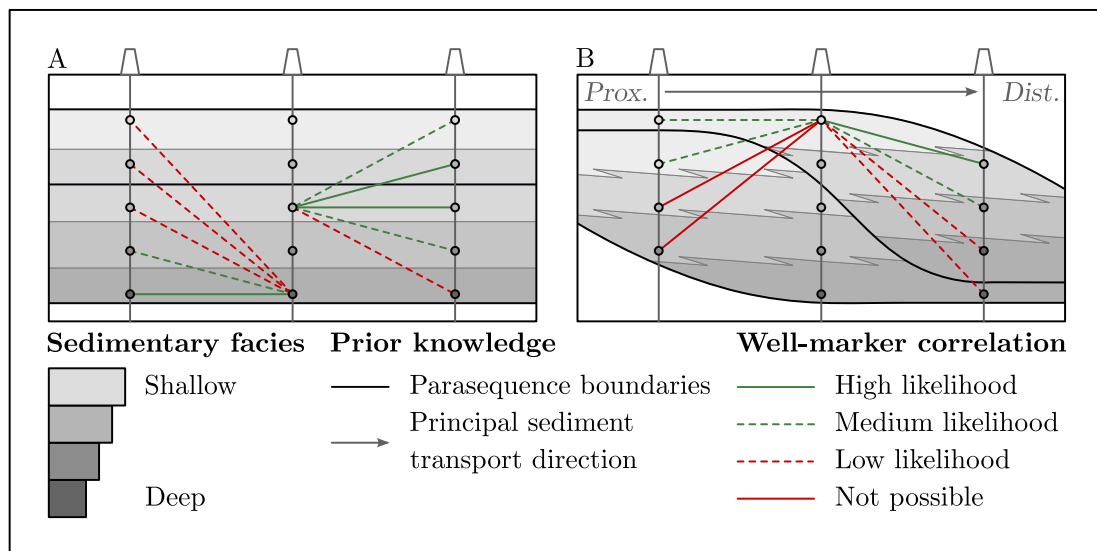


Figure 3.2: Well-marker correlation likelihood based on facies association within a sedimentary basin along (A) the depositional strike direction and (B) the principal sediment transport direction. Facies association likelihood is represented by a dashed or full green or red line. Modified from Baviile et al. (2022).

*distality) cannot be correlated with another well marker described by a depositionally deeper facies at a more proximal position, or a depositionally shallower facies at a more distal position”.*

This principle allows us to evaluate every single well marker correlation line independently and not the entire correlation set. Therefore, the next section focuses on the computation of likely correlation sets.

## 3.2 Correlation likelihood computation

For relative chronostratigraphy, the main difficulty is to define appropriate correlation costs. For example, [Lallier et al. \(2016\)](#) used paleobathymetry and depositional slope constraints to define carbonate facies correlation rules. [Edwards et al. \(2018\)](#) derived correlation and transition costs by scanning three-dimensional models obtained by process-based stratigraphic simulation. These approaches can incorporate depositional concepts into automatic correlation, but they call for determining quantitative parameters which may be difficult to infer in some depositional environments. In the next subsection, the more qualitative notion of distality discussed in Section 3.1 is used to define new correlation costs  $c_{ab}[i, j]$  and transition costs  $t_{ab}[i, j][k, l]$ .

### 3.2.1 Correlation cost computation

If Figure 3.1 is considered as a simple approximation for a sedimentary basin margin geometry along the depositional strike direction (AA') and depositional dip direction (BB'), it is possible to qualitatively estimate the well marker correlation likelihood as illustrated in Figure 3.2.

The proposed method may be applied on two wells, referred to as wells  $a$  and  $b$ . Input data are (1) sedimentary facies interpretation  $f$  defined along the entire well by their top and bottom depths, and (2) well distality  $d$  defined by a piecewise constant function of the depth according to the depositional context.

These two parameters must be preprocessed as follows:

- Well markers are taken at the center of each sedimentary facies, and assigned to  $f$  directly given by the sedimentary facies encoding (facies codes increase from the deepest, *i.e.*,  $f = 1$ , to the shallowest sedimentary facies).
- Well distality may vary along a vertical well, but is assumed to be constant within a clinoform (distality is increasingly defined from the most distal well

position within the basin, *i.e.*,  $d = 1$ , to the most proximal well position within the basin), *i.e.*, a parasequence.

Note that this ordering can be reversed as long as facies depositional depth and distality are encoded consistently.

Considering that well  $a$  is composed of  $I$  markers  $m_a(i)$ ,  $i \in \mathbb{I} = \llbracket 1, I \rrbracket$  and well  $b$  is composed of  $J$  markers  $m_b(j)$ ,  $j \in \mathbb{J} = \llbracket 1, J \rrbracket$ , each marker  $m_a(i)$  and  $m_b(j)$  can be expressed as:

$$m_a(i) = \left( f_a(i), d_a(i) \right) \text{ and } m_b(j) = \left( f_b(j), d_b(j) \right). \quad (3.1)$$

### 3.2.1.1 Contribution of the sedimentary facies

Sedimentary facies are interpreted along a paleogeographic depositional profile (*i.e.*, deep-to-shallow paleogeographic depositional conditions), and are encoded according to their relative position along this profile as illustrated for example in Figure 3.3.A.

The sedimentary facies normalization term  $f_0$  is computed from the entire data set ( $N$  wells) and corresponds to the maximal variation between two interpreted sedimentary facies (*i.e.*, the variation between the deepest facies and the shallowest facies):

$$f_0 = \left| \max_{i,n} \left( f_n(i) \right) - \min_{i,n} \left( f_n(i) \right) \right|, \quad (3.2)$$

with  $1 \leq n \leq N$ .

Between wells  $a$  and  $b$ , considering the facies normalization term  $f_0$ , an adimensional term  $\Delta f_{ab}(i, j)$  can be computed for each pair of sedimentary facies  $f_a(i)$  and  $f_b(j)$  by

$$\Delta f_{ab}(i, j) = \frac{|f_a(i) - f_b(j)|}{f_0}. \quad (3.3)$$

By construction,  $0 \leq \Delta f_{ab}(i, j) \leq 1$  and the number of values that  $\Delta f_{ab}(i, j)$  may take is finite and values are not necessarily regularly sampled (*e.g.*, Figure 3.3). The finite number of values may be plotted along an axis representing the sedimentary facies variation  $\Delta f_{ab}(i, j)$ .

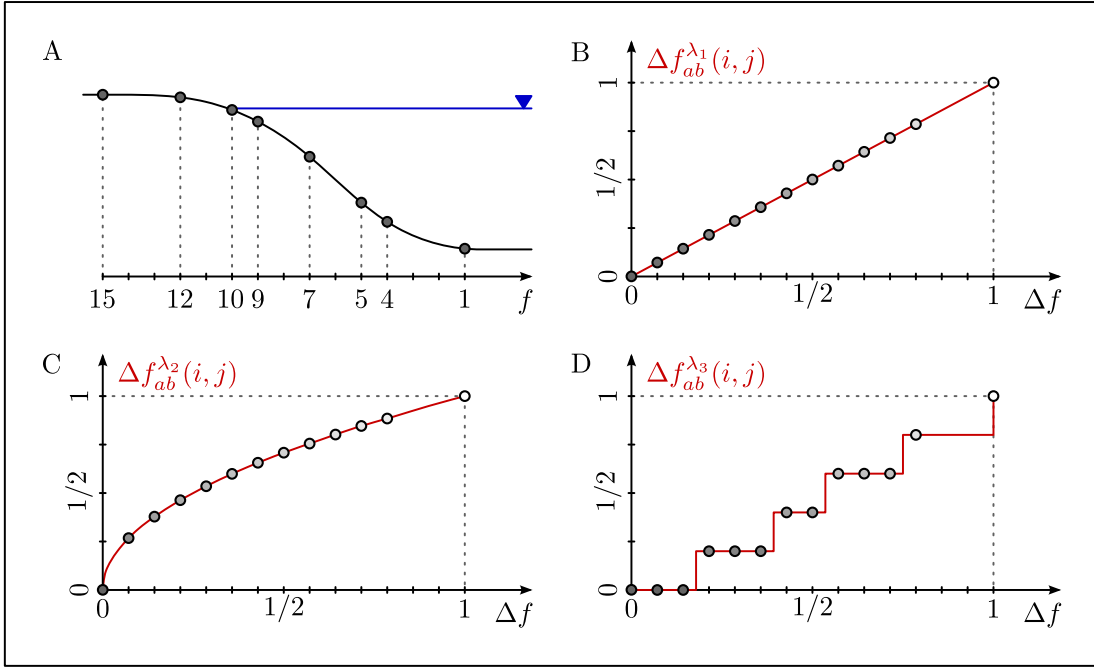


**Figure 3.3:** (A) Sedimentary facies  $f$  interpreted along a typical paleogeographic depositional profile and encoded from the most deep ( $f = 1$ ) to the most shallow ( $f = 15$ ). (B-C-D)  $\Delta f_{ab}^\lambda(i, j)$  is the relative facies variation  $\Delta f_{ab}(i, j)$  composed by the discretization function  $\lambda$  which characterizes possible relationship between several values of facies variations (Equation (3.4)).

The first assumption that may be made, is to consider each facies variation value independently (Figure 3.3.B-C). The second assumption that may be made, is to consider that some facies variation values are equivalent and that their values should be the same (Figure 3.3.D).

In both cases,  $\Delta f_{ab}^\lambda(i, j)$  is the facies variation  $\Delta f_{ab}(i, j)$  composed by a monotonic normalized function function  $\lambda$  such as

$$\begin{aligned} \Delta f_{ab}^\lambda : \mathbb{I} \times \mathbb{J} &\rightarrow [0, 1] \\ (i, j) &\mapsto \lambda\left(\Delta f_{ab}(i, j)\right) = \lambda\left(\frac{|f_a(i) - f_b(j)|}{f_0}\right), \end{aligned} \quad (3.4)$$

Figure 3.3 illustrates three examples of functions  $\lambda$  with the facies normalization term  $f_0 = 14$ :

- $\lambda_1$  is the identity function (Figure 3.3.B), and the corresponding facies variation  $\Delta f_{ab}^{\lambda_1}(i, j)$  is given by

$$\Delta f_{ab}^{\lambda_1}(i, j) = \frac{|f_a(i) - f_b(j)|}{f_0}. \quad (3.5)$$

- $\lambda_2$  is the  $p$ -root function (Figure 3.3.C), and the corresponding facies variation  $\Delta f_{ab}^{\lambda_2}(i, j)$  is given by

$$\Delta f_{ab}^{\lambda_2}(i, j) = \left( \frac{|f_a(i) - f_b(j)|}{f_0} \right)^p, \quad p \geq 0. \quad (3.6)$$

- $\lambda_3$  is a disjoint normalized membership function (Figure 3.3.D), and the corresponding facies variation  $\Delta f_{ab}^{\lambda_3}(i, j)$  is given by

$$\Delta f_{ab}^{\lambda_3}(i, j) = \bigcup_{p=0}^P \left[ c_p \times \mathbb{1}_{[f_p^-, f_p^+]} \left( \frac{|f_a(i) - f_b(j)|}{f_0} \right) \right], \quad (3.7)$$

where  $\mathbb{1}_{[f_p^-, f_p^+]}$  is the indicator function which returns 1 within the interval  $[f_p^-, f_p^+]$  and 0 outside,  $P$  is the number of disjoint intervals,  $f_p^-$  and  $f_p^+$  are the lower and upper bounds of the  $p$ th interval, and  $c_p$  is the value that takes  $\Delta f_{ab}^{\lambda_3}(i, j)$  in the  $p$ th interval, with  $0 = c_0 \leq c_p \leq c_P = 1$ , or  $1 = c_0 \geq c_p \geq c_P = 0$ .

Geologically, the function  $\lambda$  is difficult to validate or to justify because the facies variation  $\Delta f_{ab}(i, j)$  does not have a strict geological meaning. However, it may be used to assess the impact of the sedimentary facies digitalization on the stratigraphic well correlation, which are computed from the facies variation  $\Delta f_{ab}(i, j)$ .

In this PhD work,  $\lambda$  is always considered as the identity function (Equation (3.5)), *i.e.*, there is no equivalence between two different values of facies variations, and the sampling is regular. However, there is a possibility to infer on this discretization function in order to evaluate its impact on well correlation simulations.

### 3.2.1.2 Contribution of the relative well distality

Well distality may also be interpreted along a depositional profile (*i.e.*, distal-to-proximal depositional conditions), and is encoded according to the position of wells within the depositional system (*e.g.*, Figure 3.4.A).

The well distality normalization term  $d_0$  is computed from the entire data set ( $N$  wells) and corresponds to the maximal distality variation between two wells (*i.e.*, the variation between the most distal well and the most proximal well):

$$d_0 = \left| \max_{i,n} (d_n(i)) - \min_{i,n} (d_n(i)) \right|, \quad (3.8)$$

with  $1 \leq n \leq N$ .

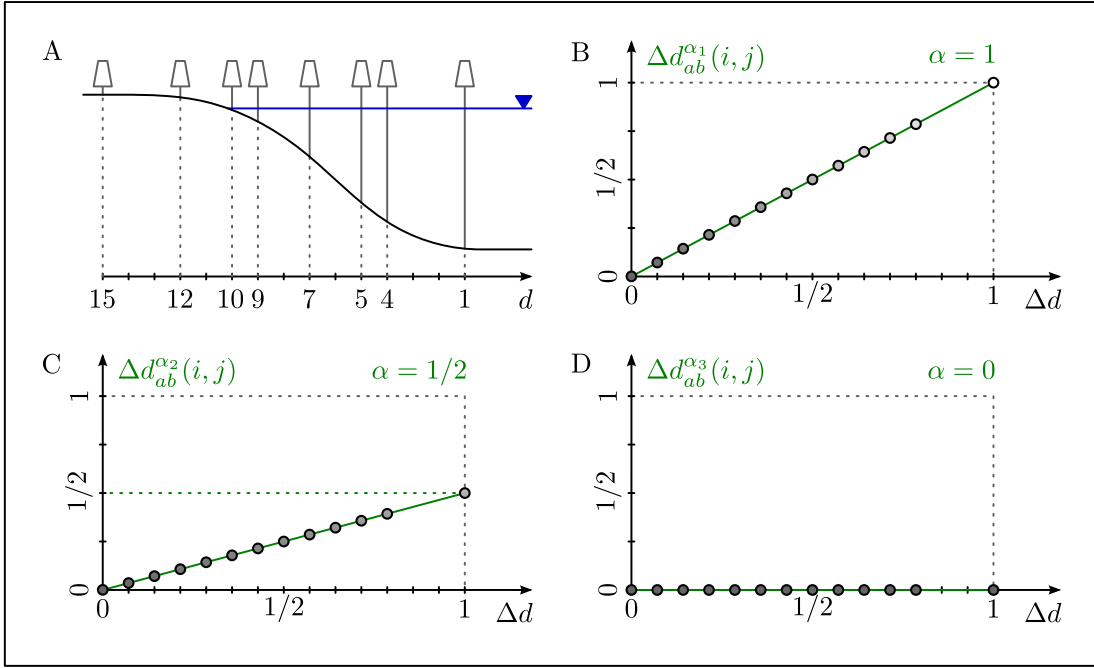


*Figure 3.4: (A) Well distality  $d$  interpreted along a typical paleogeographic depositional profile and encoded from the most distal ( $d = 1$ ) to the most proximal ( $d = 15$ ). (B-C-D)  $\Delta d_{ab}^{\alpha}(i, j)$  is the distality variation  $\Delta d_{ab}(i, j)$  weighted by the scaling coefficient  $\alpha$  which represents how the lateral size of the depositional system is deemed to scale with the inter-well distance (Equation (3.10)).*

Between wells  $a$  and  $b$ , considering the distality normalization term  $d_0$ , an adimensional term  $\Delta d_{ab}(i, j)$  can be computed for each pair of well distality  $d_a(i)$  and  $d_b(j)$  by

$$\Delta d_{ab}(i, j) = \frac{|d_a(i) - d_b(j)|}{d_0}. \quad (3.9)$$

By construction,  $0 \leq \Delta d_{ab}(i, j) \leq 1$  and the number of values that  $\Delta d_{ab}(i, j)$  may take is finite and values are not necessarily regularly sampled (e.g., Figure 3.4). The finite number of values may be plotted along an axis representing the distality variation  $\Delta d_{ab}(i, j)$ .

The first case that may be observed, is to consider that the position of the most distal (and, proximal) well of the data set corresponds to the most distal (and, proximal) depositional condition observed within the depositional system, i.e., the maximal distality variation corresponds to the global distality variation within the depositional system (Figure 3.4.B).

The second case that may be observed, is to consider that the position of the most distal (and, proximal) well of the data set does not correspond to the most distal (and, proximal) depositional condition observed within the depositional system,

*i.e.*, the maximal distality variation does not correspond to the global distality variation within the depositional system (Figure 3.4.C-D).

In both cases,  $\Delta d_{ab}^\alpha(i, j)$  is the distality variation  $\Delta d_{ab}(i, j)$  weighted by a scaling coefficient  $0 \leq \alpha \leq 1$  such as

$$\begin{aligned} \Delta d_{ab}^\alpha : \mathbb{I} \times \mathbb{J} &\rightarrow [0, 1] \\ (i, j) &\mapsto \alpha \times \Delta d_{ab}(i, j) = \alpha \times \frac{|d_a(i) - d_b(j)|}{d_0}, \end{aligned} \quad (3.10)$$

Figure 3.4 illustrates three examples of scaling coefficients  $\alpha$ :

- The maximal distality variation corresponds to the global distality variation observed within the depositional system, *i.e.*,  $\alpha_1 = 1$  (Figure 3.3.B), and the corresponding facies variation  $\Delta d_{ab}^{\alpha_1}(i, j)$  is given by

$$\Delta d_{ab}^{\alpha_1}(i, j) = \frac{|d_a(i) - d_b(j)|}{d_0}. \quad (3.11)$$

- The maximal distality variation is lower than the global distality variation observed within the depositional system, and corresponds to 50% of the global distality variation, *i.e.*,  $\alpha_2 = 1/2$  (Figure 3.3.C), and the corresponding facies variation  $\Delta d_{ab}^{\alpha_2}(i, j)$  is given by

$$\Delta d_{ab}^{\alpha_2}(i, j) = \frac{1}{2} \times \frac{|d_a(i) - d_b(j)|}{d_0}. \quad (3.12)$$

- The maximal distality variation correspond to no distality variation observed within the depositional system, *i.e.*,  $\alpha_3 = 0$  (Figure 3.3.D), and the corresponding facies variation  $\Delta d_{ab}^{\alpha_3}(i, j)$  is given by

$$\Delta d_{ab}^{\alpha_3}(i, j) = 0. \quad (3.13)$$

### 3.2.1.3 Correlation cost

In order to make every marker correlation  $[i, j]$  comparable, each correlation cost  $c_{ab}[i, j]$  is based on the adimensional terms  $\Delta f_{ab}^\lambda(i, j)$  and  $\Delta d_{ab}^\alpha(i, j)$  (Equations (3.4) and (3.10)) computed from normalization terms  $f_0$  and  $d_0$  (Equations (3.2) and (3.4)), the discretization function  $\lambda$ , and the scaling coefficient  $\alpha$ .

Based on a conceptual sedimentary basin geometry illustrated in Figure 3.1 and on the principle of correlation considering that *a facies cannot be associated with a*

*depositionally shallower (respectively, deeper) facies in a more distal (respectively, proximal) well*, it is finally possible to define two possible cases:

1. Facies and distality interpretations are inconsistent with the principle of correlation, this way the correlation cost is given by

$$c_{ab}[i, j] = +\infty. \quad (3.14)$$

2. Facies and distality interpretations are consistent with the principle of correlation, then the correlation cost is given by

$$c_{ab}[i, j] = \left( \Delta d_{ab}^\alpha(i, j) - \Delta f_{ab}^\lambda(i, j) \right)^2 = \left( \alpha \times \Delta d_{ab}(i, j) - \lambda \left( \Delta f_{ab}(i, j) \right) \right)^2, \quad (3.15)$$

Figure 3.5 illustrates the correlation cost function (3.15), with 8 sedimentary facies interpreted along a depositional profile, where the discretization function  $\lambda$  is a discretized identity function and the scaling coefficient  $\alpha = 1$ , *i.e.*, the maximal distality variation corresponds to the global distality variation of the depositional system.

The two-dimensional proposed cost function illustrated in Figure 3.5 may be geologically interpreted in three cases:

- $\Delta d_{ab}^\alpha(i, j) = 0$  (wells are orthogonal to the transport direction). In this case, facies are preferentially associated if their depositional depths are similar, *i.e.*, lithostratigraphic well correlation, and the cost function is assimilated to the normalized facies variation given by:

$$c_{ab}[i, j] = \Delta f_{ab}^\lambda(i, j)^2 = \lambda \left( \frac{|f_a(i) - f_b(j)|}{f_0} \right)^2. \quad (3.16)$$

- $\Delta d_{ab}^\alpha(i, j) = 1$  (wells are parallel to the transport direction and have extreme distality values). In this case, facies are preferentially associated if their depositional depths are different, and the cost function is assimilated to the opposite of the normalized facies variation:

$$c_{ab}[i, j] = (1 - \Delta f_{ab}^\lambda(i, j))^2 = \left( 1 - \lambda \left( \frac{|f_a(i) - f_b(j)|}{f_0} \right) \right)^2. \quad (3.17)$$

- In all the other cases, the cost function (3.6) entails that the closer the distality, the higher the correlation likelihood between facies having similar depositional depths (Figure 3.5).

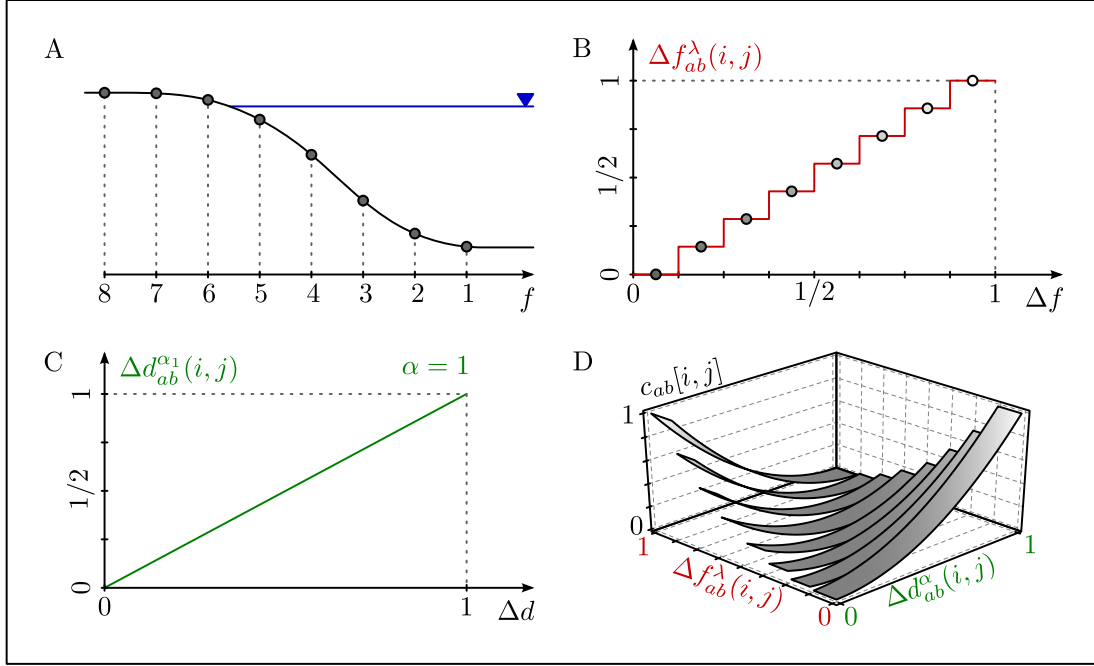


Figure 3.5: (A) Sedimentary facies interpretations given (B) facies variations (Equation (3.7)) and (C) distality variation ( $\alpha = 1$ , Equation (3.11)) used to compute (D) the correlation cost  $c[i, j]$  (Equation (3.15)) of each possible marker correlation  $[i, j]$ .  $f^\lambda(i, j)$  and  $d^\alpha(i, j)$  are normalized parameters given by Equations (3.4) and (3.10). The gray level corresponds to the correlation cost value  $c[i, j]$ . Modified from [Baville et al. \(2022\)](#).

### 3.2.2 Transition cost computation

According to the cost matrix illustrated in Figure 2.1, each well marker correlation is preceded by one well marker correlation among three possible correlations (red arrows) and their transitions are more or less likely. Transition costs are included within the Dynamic Time Warping algorithm to constrain the result as expressed in Equation (2.1).

Currently, the proposed method does not compute transition costs from input data. These vertical and horizontal transitions within the cost matrix correspond to gaps in correlation sets. In the Dynamic Time Warping algorithm, gaps are naturally penalized as the diagonal path in the cost matrix minimizes the number of transitions.

However, to further penalize stratigraphic gaps, a non-zero constant gap cost has been introduced, given by

$$t_{ab}[i - 1, j][i, j] = t_{ab}[i, j - 1][i, j] = 0.1 \text{ and } t_{ab}[i - 1, j - 1][i, j] = 0, \quad (3.18)$$

and, in this case,  $0 \leq c_{ab}[i, j] + t_{ab}[i - 1, j - 1][i, j] \leq 1.1$ , and the current cost is no more normalized.

A new version of the correlation cost is therefore given by

$$c_{ab}[i, j] = 0.9 \times (\Delta d_{ab}^{\alpha}(i, j) - \Delta f_{ab}^{\lambda}(i, j))^2, \quad (3.19)$$

and,  $0 \leq c_{ab}[i, j] + t_{ab}[i - 1, j - 1][i, j] \leq 1$  is attributed to admissible correlations.

### 3.3 First results: Synthetic data set

The proposed correlation cost function is tested on synthetic data sets. Each scenario is composed of five wells (1,2,3,4 and 5), so the Dynamic Time Warping algorithm is incrementally applied by defining a correlation path and computing the costs between each added well and the closest well already processed as discussed in Section 2.2.1 (Lallier et al., 2016).

The synthetic data set is composed of three particular depositional configurations:

1. Transverse cross-section in a sedimentary basin margin (Figure 3.6).
2. Longitudinal cross-section in a sedimentary basin margin (Figure 3.7).
3. Transverse cross-section in a sedimentary bay-head delta (Figure 3.8).

Configurations 1 and 2 correspond to the two principal well sections of the block diagram in Figure 3.1 illustrated in Figure 3.2.

In this three configurations, the five hundred best realizations (*i.e.*, the five hundred realizations having the lowest costs) are selected at each step of the Dynamic Time Warping algorithm in order to propagate the uncertainties during the process.

#### 3.3.1 Sedimentary margin transverse cross-section

Along a sedimentary basin margin transverse cross-section (Figure 3.6), all the considered wells have the same distality ( $\Delta d_{ab}^{\alpha}(i, j) = 0$ ), so every possible correlation cost  $c_{ab}[i, j]$  have been computed by the correlation costs (3.14) and (3.16).

In this example (Figure 3.6), note that independently from the correlation path, the best correlation set having the lowest cumulative cost ( $cost = 0.00$ ) is the same (green correlation lines) and corresponds to lithostratigraphic well correlation in the strike direction (Figure 3.6).

These outcomes are both consistent, because all facies are similar along correlation lines in the strike direction, the stratigraphic cost function (3.16) generates lithostratigraphic correlations. The layer cake structure of the best stratigraphic model explains the null value of the cumulative correlation cost and validates the proposed method in this configuration:

- There is no gap generated by the Dynamic Time Warping algorithm during the process, so all the transition costs  $t$  equal 0 (Equation (3.18)).
- The correlation cost  $c$  between two identical facies equals 0 in the strike direction (Equation (3.16)).

Moreover, hypothetical parasequence boundaries may be manually interpreted as horizontal lines and should reproduce the simple geometry and connectivity of the depositional model.

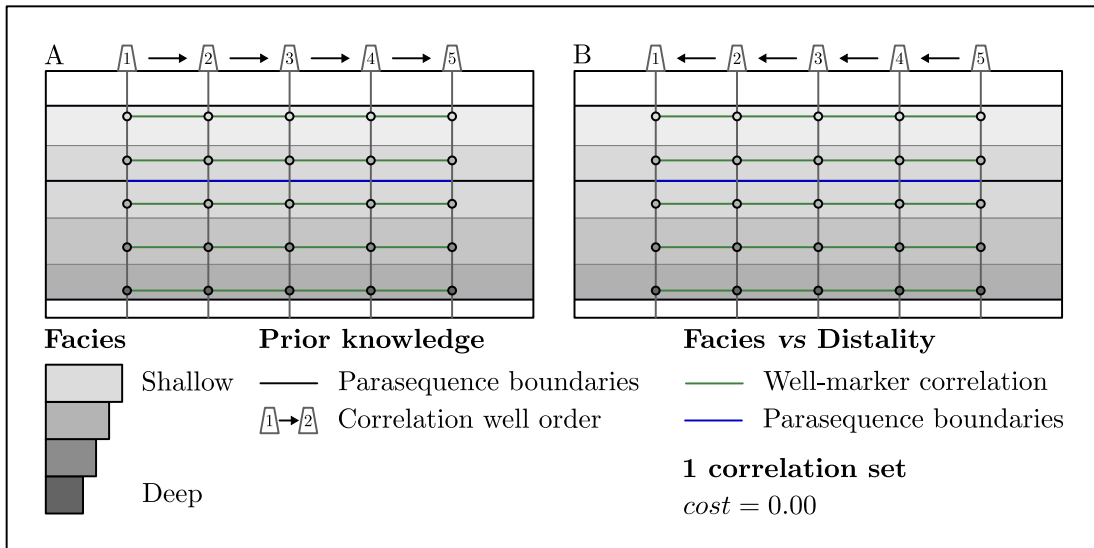


Figure 3.6: Best scenarios generated by applying the proposed cost function on a sedimentary basin margin transversal cross-section. (A) Wells are added to the correlation process from the left to the right, and (B) from the right to the left. Green lines are correlation lines, and the cost correspond to the cumulative correlation cost (combination of both correlation costs  $c$  and transition costs  $t$ ). Blue lines are manual interpretations of lower-order parasequence boundaries. Modified from (Baville et al., 2022).

### 3.3.2 Sedimentary margin longitudinal cross-section

Along a sedimentary basin margin or deltaic longitudinal cross-section (Figure 3.7), the well distality increases along a distal-to-proximal transect ( $1 \leq d_n(i) \leq 5$ ) and samples the entirety of the depositional system ( $\alpha = 1$ ). The correlation cost  $c_{ab}[i, j]$  is computed using the correlation costs (3.14) and (3.15).

In this example (Figure 3.7), note that independently from the correlation path, there are the same two correlation sets which reach the lowest cumulative cost ( $cost = 0.79$ ). In order to plot simultaneously several correlation sets in the same correlation panel, the correlation lines are colored according to their occurrence: green correlation lines are correlation lines which occur in the two scenarios, and red correlation lines are correlation lines that highlight well marker correlation which differ from one realization to the other (Figure 3.7).

These outcomes are both consistent, because along a correlation line in the sediment transport direction, depositionally deep facies in distal wells are correlated with depositionally shallower facies in less distal wells. Moreover, the cumulative cost cannot be null because of the simulation of, at least, one gap between wells 2 and 3, and one gap between wells 3 and 4, due to the different number of well markers in these wells.

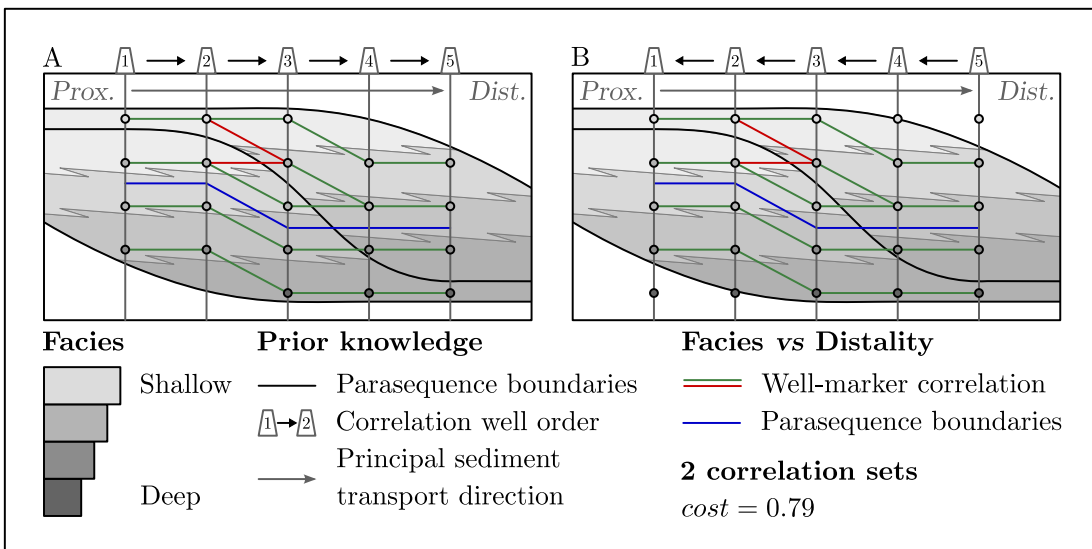


Figure 3.7: Best scenarios generated by applying the proposed cost function on a sedimentary basin margin or deltaic longitudinal cross-section. (A) Wells are added to the correlation process from the left to the right, and (B) from the right to the left. Green lines are correlation lines that occur in the both scenarios, whereas red lines are correlation lines which occur in only one of the two scenarios. The cost corresponds to the cumulative correlation cost (combination of both correlation costs  $c$  and transition costs  $t$ ). Blue lines are manual interpretations of the lower-order parasequence boundaries. Modified from (Baville et al., 2022).

In both cases, these two realizations return three distinct correlation groups (connected correlation lines), and hypothetical parasequence boundaries may be interpreted as lines separating two successive chronostratigraphic layers. Moreover, these parasequence boundaries have an overall geometry similar to the geometry of the depositional model.

### 3.3.3 Sedimentary bay-head delta transverse cross-section

Along a sedimentary deltaic lobe transverse cross-section (Figure 3.8), the well distality increases from the center to the borders ( $1 \leq d_n(i) \leq 3$ ) and samples the entirety of the depositional system ( $\alpha = 1$ ). The correlation cost  $c_{ab}[i, j]$  is computed using the correlation costs (3.14) and (3.15).

In this example (Figure 3.8), in both cases, there are eighteen correlation sets which reach the lowest cumulative cost ( $cost = 2.58$ ). It is important to note that in this example, the realizations are not the same depending on the correlation path. Green correlation lines are correlation lines which occur in all the scenarios, and red correlation lines are correlation lines that highlight well marker correlation which differ from one realization to the others.

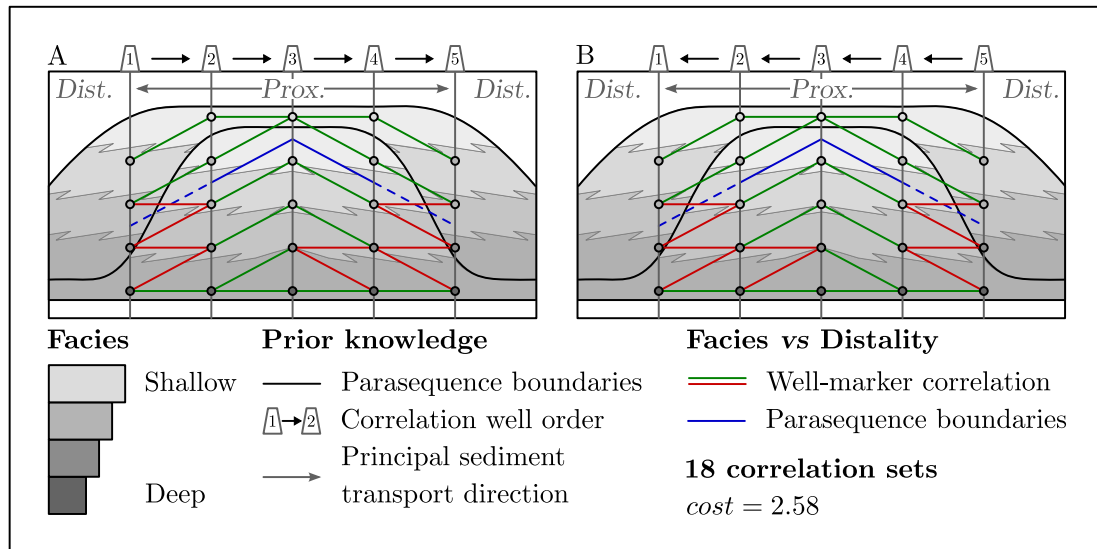


Figure 3.8: Best scenarios generated by applying the proposed cost function on a sedimentary deltaic transversal cross-section. (A) Wells are added to the correlation process from the left to the right, and (B) from the right to the left. Green lines are correlation lines that occur in all the scenarios, whereas red lines are correlation lines which do not occur in all the scenarios. The cost correspond to the cumulative correlation cost (combination of both correlation costs  $c$  and transition costs  $t$ ). Blue lines are manual interpretations of the lower-order parasequence boundaries. Modified from (Baville et al., 2022).

According to the correlation path, the simulated correlation sets are not identical but they are symmetric with respect to the most proximal well, so they can be interpreted in the same way. These outcomes are consistent, because along a correlation line, depositionally deep facies in distal wells are correlated with depositionally shallower facies in less distal wells. As in Section 3.3.2, the cumulative correlation costs cannot be null because of the simulation of, at least, one gap between wells 1 and 2, and one gap between wells 4 and 5, due to the different number of well markers in these wells.

## 3.4 Discussion

The proposed correlation cost function has been tested and validated on three simple configurations (Sections 3.3.1 to 3.3.3). In the two first cases, the reference correlation set is entirely (Figure 3.6) or partially (Figure 3.7) recovered. However, the more complex the model, the more difficult the recovery (Figure 3.8), and two correlations that have the same correlation cost may generate different connectivities, e.g., by crossing or not the interpreted parasequence boundary. This illustrates the indeterminacy of the interpretation based solely on incomplete data and on the proposed correlation cost.

### 3.4.1 Order of wells and correlation path

Figure 3.8 illustrates the importance of the correlation path, *i.e.*, by only inverting the correlation path and fixing all other parameters, the simulated correlation sets having the same correlation cost are different:

- The correlation starts between wells 1 and 2 and finishes with the integration of well 5. In this case, the highest variability occurs between wells 1 and 2 and wells 3, 4 and 5.
- The correlation starts between wells 4 and 5 and finishes with the integration of well 1. In this case, the highest variability occurs between wells 1, 2 and 3 and wells 4 and 5.

The variation on the correlation path enables to observe changes of the correlation line variability location from one model to another, because “only” five hundred correlations are propagated at once. It means that some models are not kept in memory and cannot be simulated at the end of the process, which leads to different stratigraphic well correlations according to the correlation path (Chapter 2).

In both cases, the variability is high between the wells integrated at the last steps of the process. It is easy to state that alternative correlations could be obtained by randomizing the correlation order.

### 3.4.2 Number of propagated realizations

In configurations 2 and 3, and as discussed in Chapter 2, it is important to note that the number of realizations having the lowest cost may be smaller than expected because of the sequential nature of the correlation. Indeed, five hundred realizations are kept at each step of the correlation process.

The proposed correlation cost function is applied on the configuration 3 (Figure 3.9). The only setting which vary between the two cases, is the number of realizations kept at each step of the simulation:

- At each step, the fifty best correlation sets are kept (Figure 3.9.A).
- At each step, the five hundred best correlation sets are kept (Figure 3.9.B).

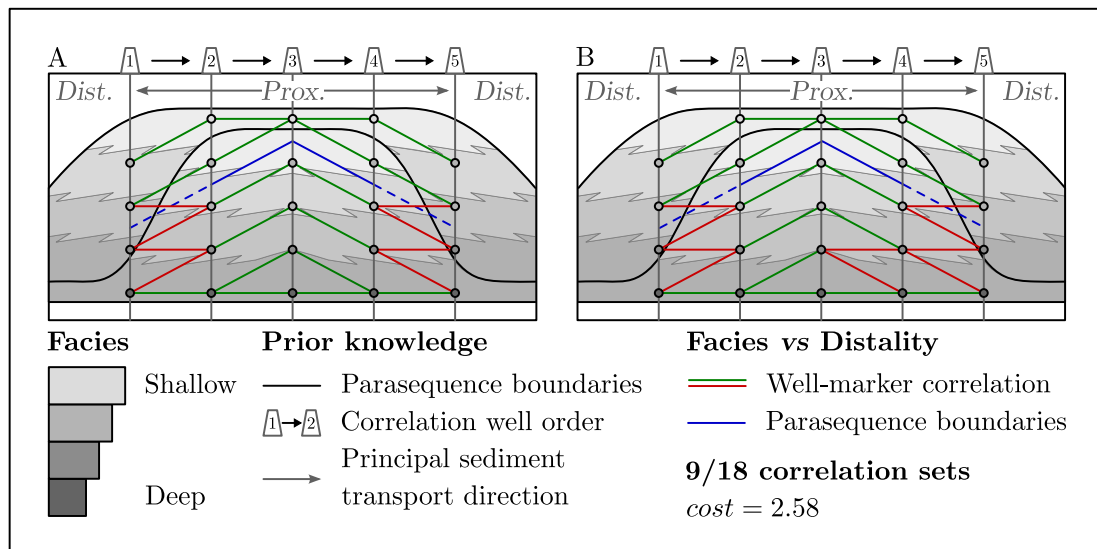


Figure 3.9: Best scenarios generated by applying the proposed cost function on a sedimentary deltaic transversal cross-section. (A) the fifty best correlation sets, and (B) the five hundred best correlation sets, are kept at each step of the process to propagate the uncertainties. Green lines are correlation lines that occur in all the scenarios, whereas red lines are correlation lines which do not occur in all the scenarios. The cost correspond to the cumulative correlation cost (combination of both correlation costs  $c$  and transition costs  $t$ ). Blue lines are manual interpretations of the lower-order parasequence boundaries.

In the case where five hundred realizations are kept at each step of the simulation, a variability, which is not recorded in the other case, is observed between wells 3-4. As described in Section 3.4.1, the variability is higher between the wells integrated at the last steps of the process (wells 3-4-5). It is possible that alternative correlations could be obtained by propagating more solutions at each step of the multi-well correlation.

### 3.4.3 Principal sediment transport direction

In sedimentary basins, the principal sediment transport direction may vary between two successive deltaic lobes, and the shift to several local sediment sources may lead to a variation of the principal sediment transport direction in the depositional system (e.g., [Bhattacharya, 2006](#)).

The proposed correlation cost function is applied on two pairs of identical wells whose only difference is their orientation:

- Figure 3.10.A shows the most likely correlation set considering that wells have the same distality, *i.e.*, they are located along the strike direction. The associated correlation cost to every marker correlations is always computed by Equation (3.16) - *i.e.*, lithostratigraphic correlation - because no well marker correlation is excluded. Indeed, the cost matrix corresponding to these two wells is entirely populated with correlation costs  $c$  (no transition costs  $t$  shown in Figure 3.10), and not excluding any correlation.
- Figure 3.10.B shows one of the two most likely correlation sets simulated from the same data set but considering that wells have different distalities, in this case, well 3 is more proximal than well 4. The corresponding correlation cost matrix illustrates that several well marker correlations are excluded thanks to the principle of correlation (black cells).

One may want to use this rule to test the impact of different transport direction scenarios. Indeed, considering two possible principal sediment transport directions in a circle of 360 degrees, a high number of correlation sets which are geologically possible with one principal transport direction may become geologically not possible with another transport direction. For example, if the relative well position along the distality axis switches, the outcomes will significantly change because of well marker association exclusion changes thanks the principle of correlation.

In both cases, the variation of the principal sediment transport direction may be captured with reasonable accuracy with dip data.

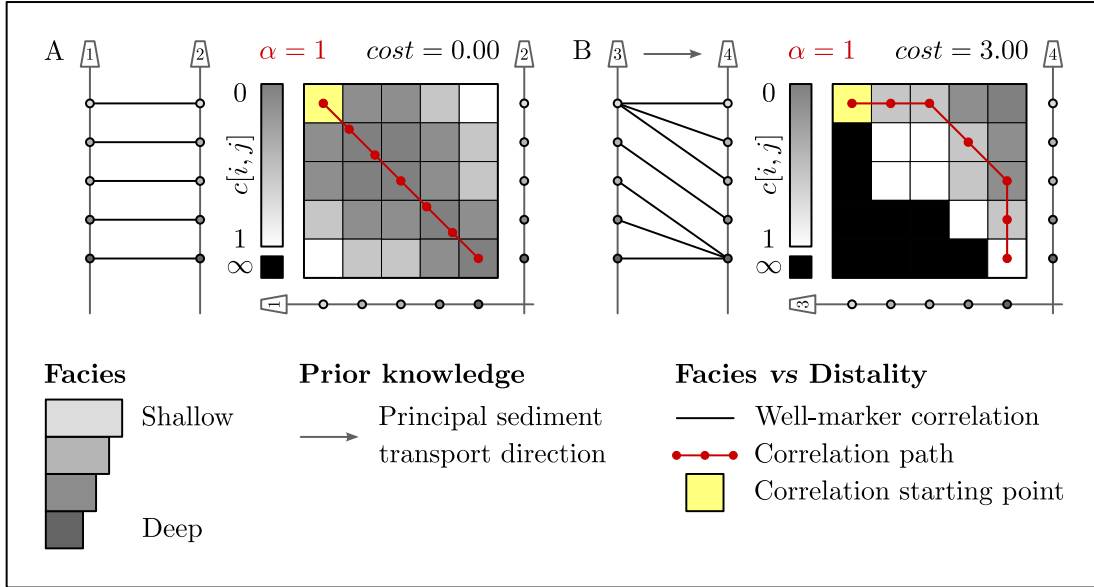


Figure 3.10: Best scenarios generated by applying the proposed cost function on the same data set but but modifying the principal sediment transport direction. (A) Wells are located along the depositional strike direction (i.e., the distality is the same), and (B) wells are located along the depositional dip direction (i.e., the distality is different).

### 3.4.4 Well position within the depositional system

Results are also sensitive to the distality variation along a proximal-to-distal transect, which cannot be determined with certainty. To visualize the effects of changing the relative well distality, two correlation cost matrices are computed: (1) a cost matrix associated to one depositional system (Figure 3.11.A) and (2) a cost matrix associated to the same depositional system, assuming that its lateral size is two times larger (corresponding to a scaling parameter  $\alpha = 1/2$ ) using the same input data set (Figure 3.11.B).

Comparing the two correlation costs ( $cost = 3.00$  with  $\alpha = 1$ , and  $cost = 0.73$  with  $\alpha = 1/2$ ), the distality rule of correlation is less discriminant and tends to generate correlation paths closer to the diagonal when the system is larger ( $0 \leq \alpha \leq 1$ ), i.e., corresponding to a more steady preservation rate in each well in the considered interval.

Both uncertainties about the variation of the principal sediment transport direction and the relative depositional system size can be addressed by changing the scaling coefficient  $\alpha$  in Equation (3.10):

- For a given orientation, a variation of the principal sediment transport direction may be modeled by a scaling coefficient varying between  $\alpha = -1$  and  $\alpha = 1$ . A scaling coefficient  $\alpha = -1$  corresponds to the inversion of the

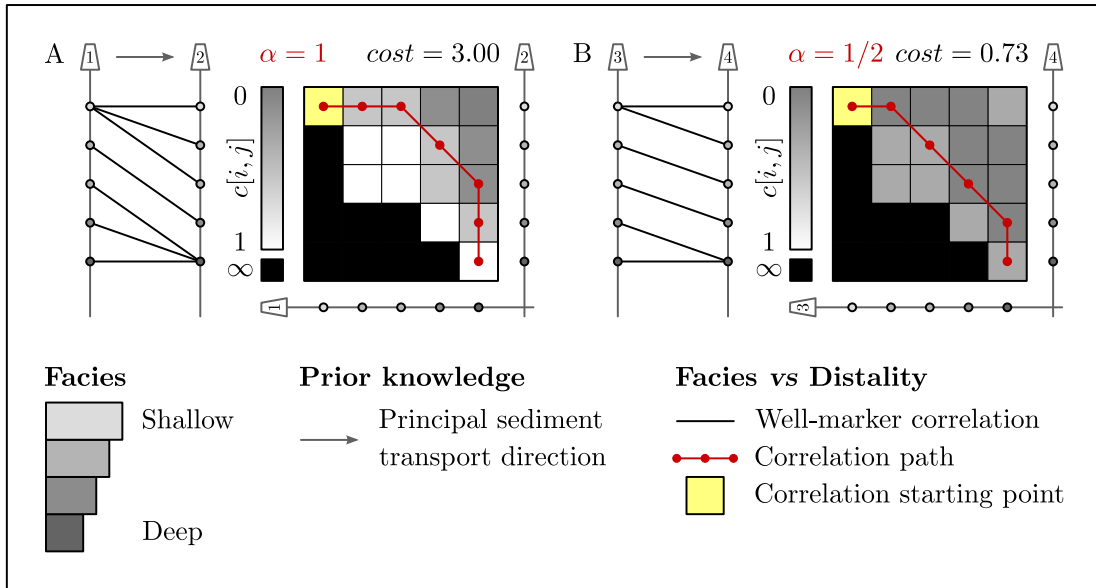


Figure 3.11: Best scenarios generated by applying the proposed cost function on the same data set but but modifying the scaling coefficient: (A)  $\alpha = 1$  and (B)  $\alpha = 1/2$ .

principal sediment transport direction and a scaling coefficient  $\alpha = 0$  corresponds to the principal sediment transport direction being perpendicular to the wells (Section 3.4.3).

- A variation of the depositional system size with respect to well spacing may be modeled by a scaling coefficient varying between  $\alpha = 0$  and  $\alpha = 1$ . A scaling coefficient  $\alpha = 1$  corresponds to the extreme position of wells within the positional system and a scaling coefficient  $\alpha = 0$  corresponds to two wells having the same depositional position within the system (Section 3.4.3).

### 3.4.5 Laterally equivalent sedimentary facies

Considering groups of lateral equivalent facies, the correlation cost matrix will be modified because two well markers interpreted as lateral equivalent sedimentary facies are allowed to be correlated. The correlation cost function takes as input parameters the sedimentary facies variation  $\Delta f_{ab}^\lambda(i, j)$  and the well distality variation  $\Delta d_{ab}^\alpha(i, j)$ . In the case that two sedimentary facies are laterally equivalent, the variation  $\Delta f_{ab}^\lambda(i, j)$  is null and the correlation cost function will always compute a correlation cost between the two given well markers.

Facies clustering allows facies belonging to the same group to be correlated even though some individual facies correlations are originally impossible according to the principle of correlation (Figure 3.12). The comparison between simulations

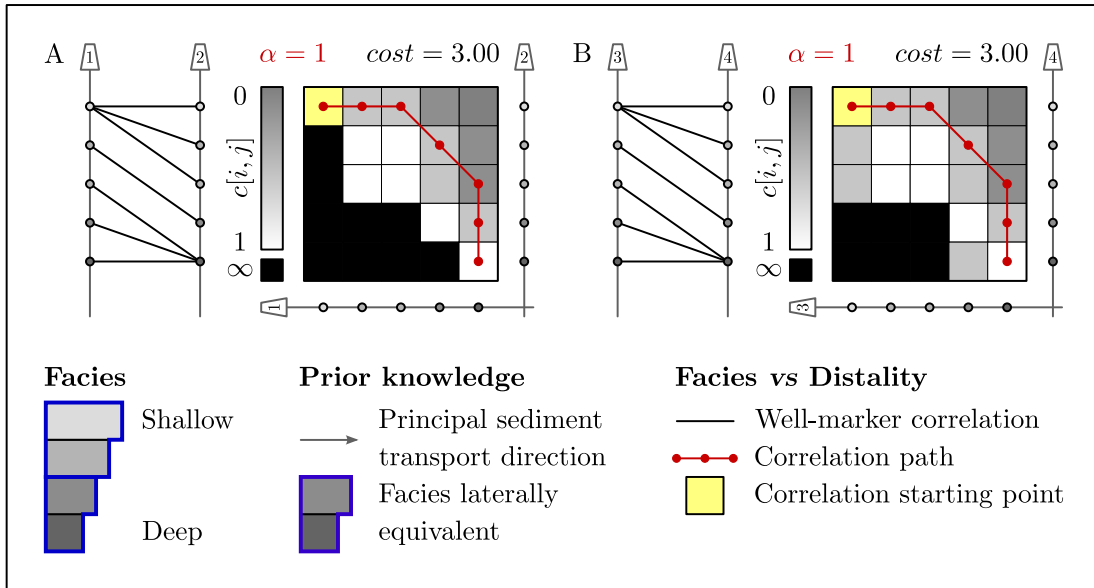


Figure 3.12: Best scenarios generated by applying the proposed cost function on the same data (A) without considering different laterally equivalent facies and (B) considering two groups of laterally equivalent facies.

without facies associations (Figure 3.12.A) and simulations with facies associations (Figure 3.12.B) may lead to the identification of the best facies association regarding the number of gaps, the cumulative correlation cost as compared to the reference without facies association or other auxiliary considerations such as the analysis of the sediment preservation rate.

## Conclusion

The purpose of the proposed correlation cost function is to generate several plausible higher-order chronostratigraphic scenarios between lower-order interpreted time lines (e.g., from seismic imaging and biostratigraphic analysis). The obtained correlation results are simulated based on sedimentary facies and well distality interpretations in several wells, and have implications in terms of detailed paleogeography in the considered interval.

The proposed correlation rule is based on the principle of correlation: *a facies cannot be associated with a depositionally deeper (respectively shallower) facies in a more distal (proximal) well*. This method requires sedimentary facies interpretations along well paths and the distality of all wells computed from the well position along a proximal-to-distal transect, to compute a correlation cost for each possible well marker correlation given by Equations (3.14) and (3.15).

The overall goal of the method is to generate time lines which reflect both allo

cycles and auto cycles (Chapter 1). Given the incomplete information available to recover such time lines, ambiguity is expected and it should not be hidden, as it may affect the understanding and the way applied geoscientists model facies, flow units and thin horizontal permeability barriers in subsurface reservoirs. The approach proposed in this work makes it possible to include the concept of distality in such uncertainty quantification and to generate alternative layer connectivities between linear stratigraphic sections.





# Chapter 4

## Depositional profile vs Dip data

### Contents

---

<b>4.1</b>	<b>From well markers to depositional surfaces . . . . .</b>	<b>88</b>
4.1.1	Sedimentary facies and vertical/lateral extension . . . . .	88
4.1.2	Depositional strike orientation and dip angle . . . . .	90
4.1.3	Depositional profile interpolation . . . . .	91
4.1.3.1	Depositional curve interpolation . . . . .	91
4.1.3.2	Depositional surface interpolation . . . . .	93
4.1.3.3	From well marker to correlation lines . . . . .	94
<b>4.2</b>	<b>From sediment source to depositional surfaces . . . . .</b>	<b>95</b>
4.2.1	Two-dimensional analytical model . . . . .	96
4.2.2	Three-dimensional analytical model . . . . .	97
<b>4.3</b>	<b>Correlation likelihood computation . . . . .</b>	<b>101</b>
4.3.1	Theoretical depositional profile translation . . . . .	101
4.3.2	Absolute integral computation . . . . .	104
4.3.3	Correlation cost computation . . . . .	107
<b>4.4</b>	<b>First results: Synthetic data set . . . . .</b>	<b>109</b>
<b>4.5</b>	<b>Discussion . . . . .</b>	<b>110</b>
4.5.1	Impact of the theoretical depositional profile. . . . .	110
4.5.2	Impact of the correlation cost computation. . . . .	111
4.5.3	Impact of the order of correlation. . . . .	112

---

This chapter presents the dip data rule of correlation. It defines the principle of correlation (Sections 4.1 and 4.2), describes the computation of the correlation likelihood (Section 4.3), presents the first results obtained on a synthetic data set (Section 4.4), and discusses the impact of each parameter (Section 4.5).

## **Abstract**

*Assisted well correlation aims at complementing sedimentological expertise with computational rigor to increase automation, improve reproducibility and assess uncertainties during stratigraphic correlation. In this work, a computer-assisted method is proposed to automatically generate possible well correlations based on facies interpretation, dipmeter data and prior knowledge about depositional environments. Facies interpretation and dipmeter data may be used to interpolate three-dimensional surfaces using the three-dimensional Bézier cubic curves between pairs of well markers and triangular Bézier cubic patches between triplets of well markers. These curves and surfaces are compared to a theoretical depositional profile generated from depositional environment knowledge by computing the area between the curves and the profile, or the volume between the patches and the profile. The main principle of correlation used in this method assumes that these areas and volumes may be linked to the likelihood of each possible correlation: the higher the area or the volume, the lower the correlation likelihood. Well correlations are computed using correlation costs between all possible marker combinations aggregated by the Dynamic Time Warping algorithm. The proposed method produces consistent stratigraphic well correlation with respect to the data set. However, this approach is highly sensitive to the well order of correlation because of the Dynamic Time Warping algorithm (Section 2.2.2).*

## **Introduction**

Stratigraphy is usually used to predict the subsurface geometry by correlating sparse well data (e.g., [Ainsworth et al., 1999](#); [Baville et al., 2022](#); [Bourquin et al., 1998](#); [Lallier et al., 2016](#)). In subsurface studies, these well correlations are generated at a vertical meter-scale and at a horizontal kilometer-scale from well logs and core samples. The main objective of the stratigraphic correlation is to determine the surfaces bounding the stratigraphic units and to reconstruct sedimentary body geometries, which can then be predicted away from observations (e.g. [Mallet, 2002, 2014](#); [Pyrzcz and Deutsch, 2014](#); [Ringrose and Bentley, 2015](#)).

The stratigraphic correlation of sedimentary series observed in boreholes or outcrops is a common procedure in basin studies. Correlations affect the understanding of sedimentary deposits, the quantitative analysis of subsurface resources and source-to-sink models. The reservoir geometry is used to generate a reservoir grid to simulate petrophysical properties using geostatistical methods to finally aid economic decisions ([Dubrule and Damsleth, 2001](#); [Larue and Legarre, 2004](#); [Mallet, 2004](#); [Pyrzcz and Deutsch, 2014](#)). Therefore, uncertainty in correlation has an impact on the connectivity, the petrographical model and the simulated

---

physical behavior of subsurface models (Baville et al., 2019; Lallier et al., 2012).

The purpose of this work is to develop methods that help geoscientists to provide multiple chronostratigraphic scenarios that are consistent with both data and some explicitly defined stratigraphic concepts. The ability to generate multiple scenarios makes it possible to consider smaller time-windows than in classical deterministic stratigraphic interpretation practice. These stratigraphic intervals, called clinofolds by Rich (1951), are delimited by chronostratigraphic surfaces at their base and their top (Patruno and Helland-Hansen, 2018). These chronostratigraphic surfaces may represent the buried paleo-topography or paleo-bathymetry if no deformation has occurred since deposition and by considering an uniform compaction rate along the depositional profile.

Lallier et al. (2016) propose an automatic method to compute stratigraphic correlations using prior knowledge such as theoretical chronostratigraphic profile geometries. As suggested by Borgomano et al. (2008), the likelihood of each possible correlation is computed from integrated paleobathymetric information. Lallier et al. (2016) generate stochastic well correlations, which provide reproducible results. Simulating and testing every possible well correlation provides a way to assess subsurface geometry uncertainties (e.g., Lallier et al., 2016; Pels et al., 1996).

The method proposed by Lallier et al. (2016) is based on paleo-bathymetry and facies interpretation to correlate wells but dipmeter data (structural dips and dip directions) are not taken into account. However, in marine and shallow marine deposits, structural dip and dip direction measurements provide very important information about the sediment routing. As facies do not vary along the depositional strike direction, as much as along the dip direction, determining distality from dipmeter data is important to constrain well correlations.

In this work, only sedimentary depositional events are considered. Every tectonic event observed after the sedimentation is supposed to be corrected (e.g., by computing dip differences with respect to major regional stratigraphic markers, or by flattening a major basal surface from seismic interpretation). In this case, structural dip and dip directions correspond to depositional conditions such as the basin slope and the sediment transport direction. Therefore, considering dipmeter data which correspond to structural dip and dip direction, and not the internal bedding dip, dipmeter data sample the depositional subsurface geometry at markers.

The purpose of the proposed method is to generate depositional surfaces from well data. The first step is to interpolate depositional surfaces from well data (Section 4.1) using Bézier three-dimensional cubic interpolation (Section 4.1.3) between well markers. These interpolations are constrained by facies interpre-

tations (Section 4.1.1) and structural dip and dip direction (Section 4.1.2). A paleogeographic depositional profile (Section 4.2) is also used to reflect regional and local knowledge. This profile is either represented by surfaces interpreted by experts (e.g., seismic analysis, manual well correlations) or by analytic equations (Adams and Schlager, 2000; Driscoll and Karner, 1999; Lallier et al., 2016).

Each possible marker association leads to an interpolated depositional surface, whose likelihood is computed comparing its geometry with a paleogeographic depositional profile (Section 4.3). Each correlation is therefore associated with a correlation cost which is used by the Dynamic Time Warping algorithm to compute the most likely set of correlations (Fang et al., 1992; Hale, 2013; Waterman and Raymond, 1987; Wheeler, 2015) or the  $n$ -best DTW which produces sets of correlations (Baville et al., 2022; Caumon and Antoine, 2019; Edwards, 2017; Edwards et al., 2018; Lallier et al., 2016; Pels et al., 1996).

## 4.1 From well markers to depositional surfaces

In most sedimentary basins, vertical wells provide a good vertical sampling of sedimentary strata since petrographic and biostratigraphic measurements can be taken at regular intervals ( $< 1$  m). However, the lateral distance between two wells, and therefore between two well markers, is generally very large compared to the vertical distance between two well markers within a well.

The objective of the proposed method is to correlate well markers interpreted along the wells as the interface between two sedimentary units by taking into account (1) the sedimentary facies interpretation along the well, and (2) the measurement of dipmeter data at the well marker position. Therefore, a well marker corresponds to the interface between two different units and is defined by two parameters: (1) the sedimentary facies of the unit below the interface and (2) the dipmeter data measured at the interface.

### 4.1.1 Sedimentary facies and vertical/lateral extension

Sedimentary facies characterize the paleo-environment and depositional event successions along the well path. While the proposed method is in general applicable to various sedimentary environments, it has been applied so far to the three-dimensional modeling of deltaic deposits dominated by waves or tides.

As discussed in Chapter 1, well markers are correlated according to chronostratigraphic principles. As mentioned before, the objective is to correlate time-lines.

It is assumed that some depositional events are quasi-synchronous over a characteristic area, which depends on basin geometry, subsidence distribution and depositional process.

Therefore, along a certain isochronous surface, all rocks have approximately the same depositional age. Correlating these isochronous rocks is, in this case, the same as correlating time-lines and *vice versa*.

Figure 4.1 roughly illustrates the internal structure of a fluvial-dominated delta. In the direction of sediment transport, there is a superposition of sigmoidal bodies, and along the depositional strike direction a superposition of bell-shaped bodies. These sedimentary bodies are referred to as clinoforms by Rich (1951) and are composed of various facies (from the most proximal to the most distal region) along the same depositional profile.

The figure illustrates three successive clinoforms corresponding to three successive regression events. These three clinoforms are divided into three sedimentary facies: (1) delta plain deposits (sand and mud) corresponding to the most proximal depositional conditions, (2) delta front deposits (mostly sand) corresponding to deposits in the delta slope, and (3) prodelta deposits (mostly silty mud) corresponding to the most distal depositional conditions (Gani and Bhattacharya, 2005).

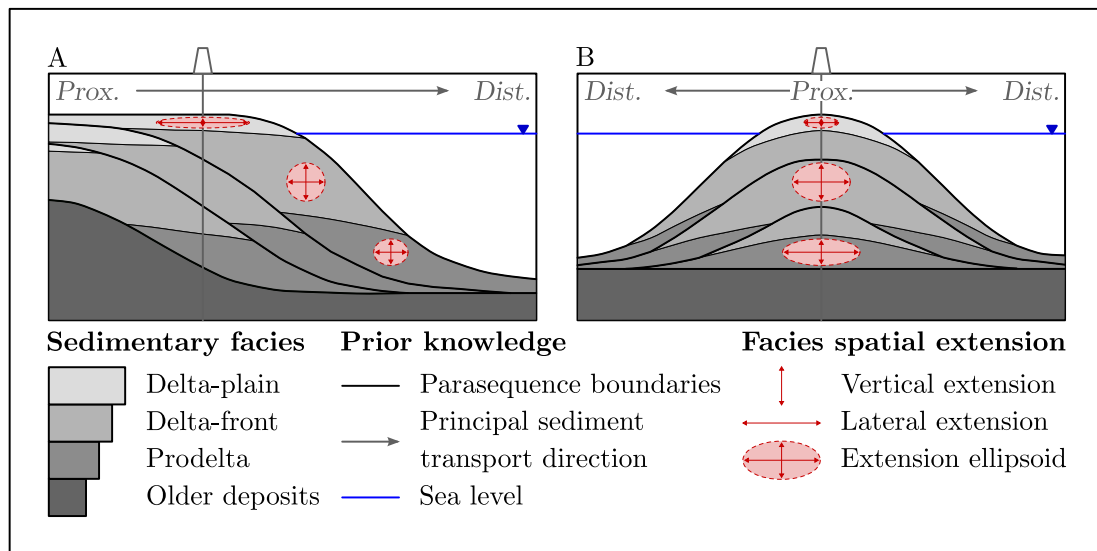


Figure 4.1: Generalized intra-parasequence bedding geometry and facies architecture of a prograding delta. (A) Dip section shows the seaward-dipping bedset boundaries (clinoforms), which follow time lines and are bidirectional in (B) strike section. Vertical and horizontal red arrows represent the vertical and lateral facies extension. Note that the drawings are not to scale. Inspired by Gani and Bhattacharya (2005).

Using the facies illustrated in Figure 4.1, it is easy to observe that very proximal and very distal parts of the depositional system (*i.e.*, delta-plain and prodelta) have a relatively large lateral extension as compared to their thickness. Delta-front deposits have a smaller lateral extension and a larger thickness (and preservation rate) than delta-plain and prodelta (*e.g.*, [Bhattacharya, 2006](#); [Shiers et al., 2014](#)). Figure 4.1 shows vertically exaggerated profiles, that make lateral extension observations easier.

Given this type of information, it is possible to build an anisotropy ellipsoid for each facies whose horizontal radius corresponds to its lateral extension and whose height corresponds to its thickness (Figure 4.1). In this method, these ellipsoids will be used to constrain the stiffness of the interpolated potential isochronous surfaces during the assisted correlation.

### 4.1.2 Depositional strike orientation and dip angle

The second property measured along the well path that is used in the well correlation process is the structural dip and dip direction of horizons crossed by the well. These structural dips and dip directions provide essential information on the geometry of the strata.

In this work, the geometry of the chronostratigraphic surfaces interpolated from these well data is therefore directly constrained by structural dip and dip direction since they must honor the well data. As dipmeter data can be representative of sedimentary structures, several cases are distinguished depending on the facies overlying the dip measurement:

- Within shale facies, the dipmeter data measurements correspond to structural dipmeter data (assuming a flat sedimentation, *i.e.*, horizontal bedding).
- For sand beds, however, the shale-to-sand interface dipmeter data is assigned to the entire bed.

Assuming that the shale-to-sand interface dipmeter data does not vary within the corresponding sand bed, the geometry of the depositional surface at the marker neighborhood is directly constrained by the dipmeter data. This uniformity can be achieved by forcing the dip at the marker within ellipsoids, whose height corresponds to the vertical facies thickness and width corresponds to the lateral extension.

However, wells are generally not aligned to the depositional dip direction. In these cases, an apparent structural dipmeter data ( $dir_{app}, dip_{app}$ ) must be calculated

along each well correlation direction ( $dir_{cor}$ ) to honor true structural dip ( $dip_{true}$ ) and strike direction ( $dir_{true}$ ) at each well marker position by

$$dip_{app} = \arctan(\tan(dip_{true}) \times \sin(dir_{cor} - dir_{true})), \quad (4.1)$$

and

$$dir_{app} = dir_{cor} - \pi/2. \quad (4.2)$$

### 4.1.3 Depositional profile interpolation

As described in previous sections, paleogeographic depositional surfaces may punctually record along wells: (1) sedimentary facies, and (2) dipmeter data, which give information about the depositional profile geometry. Indeed, in this approach, sedimentary facies is considered as a proxy of the stiffness, and dipmeter data is considered as a proxy of the inclination of the three-dimensional surface.

Note that this preliminary work does not yet take into account changes in the depositional profile at transgressive surfaces or erosion related to lowstand system tracts.

#### 4.1.3.1 Depositional curve interpolation

These two parameters can be integrated within the three-dimensional Bézier cubic curve interpolation computation between two points  $\mathbf{p}_{30}$  and  $\mathbf{p}_{03}$  (well markers) to constrain the depositional depth  $z_b$  (Bézier, 1977) defined by

$$z_b : [0, 1]^2 \rightarrow \mathbb{R} \quad (4.3)$$

$$(u, v) \mapsto \sum_{\substack{0 \leq i, j \leq 3 \\ i+j=3}} \left[ \binom{3}{ij} \times \mathbf{p}_{ij} \times u^i v^j \right],$$

with  $u + v = 1$  and is designed to honor inclination and stiffness at corner points positions as illustrated in Figure 4.2.

Equation (4.3) is computed using the barycentric coordinates  $(u, v)$  defined along the segment between the two well markers:  $(1, 0)$  corresponds to the first well

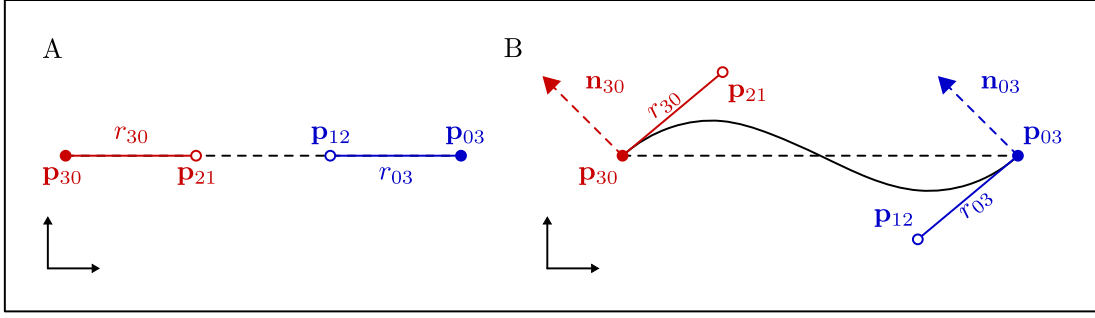


Figure 4.2: Three-dimensional Bézier cubic curve interpolations.  $\mathbf{p}_{30}$  and  $\mathbf{p}_{03}$  are corner points, defined by spatial extensions  $r_{30}$  and  $r_{03}$ , and normal vectors  $\mathbf{n}_{30}$  and  $\mathbf{n}_{03}$ .  $\mathbf{p}_{21}$  and  $\mathbf{p}_{12}$  are the control points constraining the inclination and the stiffness of the interpolation computed from corner points. (A) Initial position of corner and control points, and (B) final position of control points.

marker  $\mathbf{p}_{30}$  position and  $(0, 1)$  corresponds to the other well marker  $\mathbf{p}_{03}$  position. Equation (4.3) can be developed as

$$\begin{aligned} z_b(u, v) = & \mathbf{p}_{30} \times u^3 + 3 \times \mathbf{p}_{21} \times u^2v \\ & + \mathbf{p}_{03} \times v^3 + 3 \times \mathbf{p}_{12} \times v^2u, \end{aligned} \quad (4.4)$$

and finally separated into two members:

- $\mathbf{p}_{30} \times u^3 + 3 \times \mathbf{p}_{21} \times u^2v$  corresponds to the contribution of the first well marker  $\mathbf{p}_{30}$  and its associated control point  $\mathbf{p}_{21}$ .
- $\mathbf{p}_{03} \times v^3 + 3 \times \mathbf{p}_{12} \times v^2u$  corresponds to the contribution of the other well marker  $\mathbf{p}_{03}$  and its associated control point  $\mathbf{p}_{12}$ .

The control point positions are calculated from sedimentary facies interpretations, and apparent strike directions and apparent dip angle measurements by

$$\mathbf{p}_{ij} = \mathbf{p}_i + r_i \times \frac{\mathbf{n}_i \wedge (\mathbf{p}_j - \mathbf{p}_i) \wedge \mathbf{n}_i}{\|\mathbf{n}_i \wedge (\mathbf{p}_j - \mathbf{p}_i) \wedge \mathbf{n}_i\|}, \quad (4.5)$$

and

$$\mathbf{p}_{ji} = \mathbf{p}_j - r_j \times \frac{\mathbf{n}_j \wedge (\mathbf{p}_i - \mathbf{p}_j) \wedge \mathbf{n}_j}{\|\mathbf{n}_j \wedge (\mathbf{p}_i - \mathbf{p}_j) \wedge \mathbf{n}_j\|}, \quad (4.6)$$

where  $\times$  is the scalar product and  $\wedge$  is the cross products.

### 4.1.3.2 Depositional surface interpolation

This system of equations can be generalized to a triangular Bézier cubic patch (Bézier, 1977) interpolating the depositional depth  $z_b$  between three points  $\mathbf{p}_{300}$ ,  $\mathbf{p}_{030}$  and  $\mathbf{p}_{003}$  (well markers) by

$$z_b : [0, 1]^3 \rightarrow \mathbb{R} \quad (4.7)$$

$$(u, v, w) \mapsto \sum_{\substack{0 \leq i, j, k \leq 3 \\ i+j+k=3}} \left[ \binom{3}{ijk} \times \mathbf{p}_{ijk} \times u^i v^j w^k \right],$$

with  $u + v + w = 1$  and is designed to honor the inclination and the stiffness at corner points positions as illustrated in Figure 4.3.

As the three-dimensional Bézier cubic curve interpolation, Equation (4.7) is computed using the barycentric coordinates  $(u, v, w)$  between the three markers:  $(1, 0, 0)$  corresponds to the first well marker  $\mathbf{p}_{300}$  position,  $(0, 1, 0)$  corresponds to the second well marker  $\mathbf{p}_{030}$  position, and  $(0, 0, 1)$  corresponds to the last well marker  $\mathbf{p}_{003}$  position. Equation (4.7) may be developed in

$$\begin{aligned} z_b(u, v, w) = & \mathbf{p}_{300} \times u^3 + 3 \times (\mathbf{p}_{210} \times u^2 v + \mathbf{p}_{201} \times u^2 w) \\ & + \mathbf{p}_{030} \times v^3 + 3 \times (\mathbf{p}_{120} \times v^2 u + \mathbf{p}_{021} \times v^2 w) \\ & + \mathbf{p}_{003} \times w^3 + 3 \times (\mathbf{p}_{102} \times w^2 u + \mathbf{p}_{012} \times w^2 v) \\ & + 6 \times \mathbf{p}_{111} \times uvw, \end{aligned} \quad (4.8)$$

and finally separated into four members:

- $\mathbf{p}_{300} \times u^3 + 3 \times (\mathbf{p}_{210} \times u^2 v + \mathbf{p}_{201} \times u^2 w)$  corresponds to the corner point  $\mathbf{p}_{300}$  and its two associated control points  $\mathbf{p}_{210}$  and  $\mathbf{p}_{201}$ .
- $\mathbf{p}_{030} \times v^3 + 3 \times (\mathbf{p}_{120} \times v^2 u + \mathbf{p}_{021} \times v^2 w)$  corresponds to the corner point  $\mathbf{p}_{030}$  and its two associated control points  $\mathbf{p}_{021}$  and  $\mathbf{p}_{120}$ .
- $\mathbf{p}_{003} \times w^3 + 3 \times (\mathbf{p}_{102} \times w^2 u + \mathbf{p}_{012} \times w^2 v)$  corresponds to the corner point  $\mathbf{p}_{003}$  and its two associated control points  $\mathbf{p}_{012}$  and  $\mathbf{p}_{102}$ .

The spatial position of these six first control points is computed from the spatial position of the corner points using Equations (4.5) and (4.6).

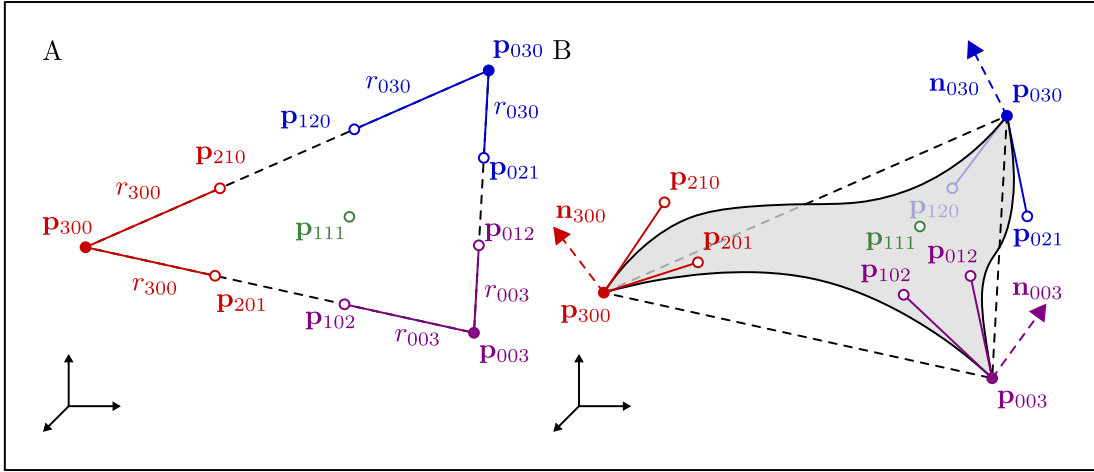


Figure 4.3: Three-dimensional Bézier cubic curve interpolations.  $\mathbf{p}_{300}$ ,  $\mathbf{p}_{030}$  and  $\mathbf{p}_{003}$  are corner points, defined by spatial extensions  $r_{300}$ ,  $r_{030}$  and  $r_{003}$ , and normal vectors  $\mathbf{n}_{300}$ ,  $\mathbf{n}_{030}$  and  $\mathbf{n}_{003}$ . All other  $\mathbf{p}_{ijk}$  are the control points constraining the inclination and the stiffness of the interpolation computed from corner points. (A) Initial position of corner and control points, and (B) final position of control points.

- $6 \times \mathbf{p}_{111} \times uvw$  corresponds to the last control point, whose spatial position is given by

$$\begin{aligned} \mathbf{p}_{111} &= \frac{1}{4} \times (\mathbf{p}_{210} + \mathbf{p}_{201} + \mathbf{p}_{021} + \mathbf{p}_{120} + \mathbf{p}_{012} + \mathbf{p}_{102}) \\ &- \frac{1}{6} \times (\mathbf{p}_{300} + \mathbf{p}_{030} + \mathbf{p}_{003}). \end{aligned} \quad (4.9)$$

#### 4.1.3.3 From well marker to correlation lines

Figure 4.4 illustrates several examples of chronostratigraphic line geometries interpolated from well markers using Equation (4.3). These interpolations are directly constrained by the lateral extensions of each sedimentary facies and apparent dips. The range of influence linked to the lateral extension relates directly to the surface stiffness: the higher the lateral extension, the stiffer the surface at the marker. The value of the apparent dip angle relates directly to the surface inclination as it imposes the tangential vector at the markers.

Without prior knowledge of facies lateral extension or apparent dip, control points are regularly placed between well markers along the well-to-well direction and interpolations are straight lines as illustrated by blue control points and dashed black lines in Figure 4.4. In this case, a correlation likelihood may be computed using the distality cost function proposed in Chapter 3, which excludes correlations if facies are not consistent with paleo-topography (Baville et al., 2022).

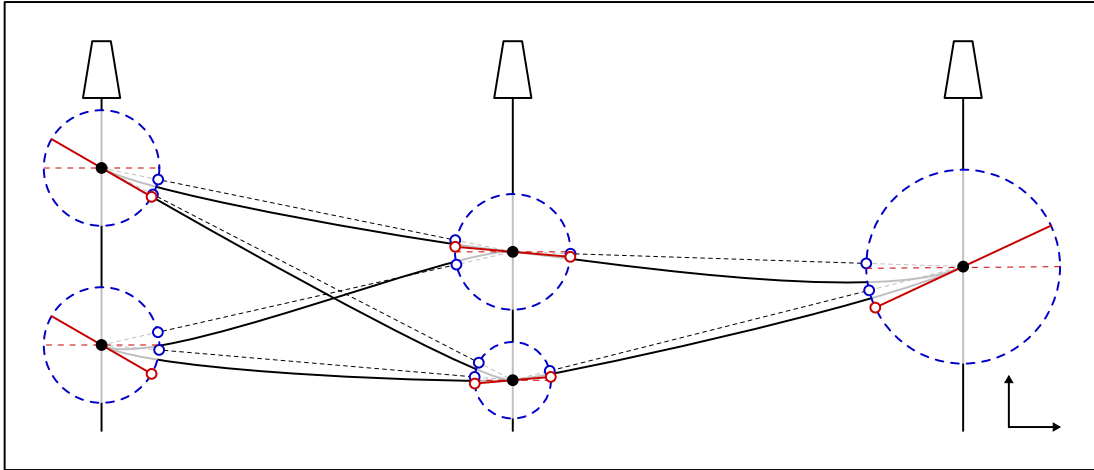


Figure 4.4: several examples of marker-to-marker Bézier cubic correlation line interpolation. Black dots are well markers. Dashed blue circles represent the lateral and vertical extension range around well markers (depending on the facies) and blue dots are the Bézier control point positions (for each pair of well markers) constrained by facies lateral extension. Red lines are dipmeter data at each well marker (apparent dip angle) and red dots are control point positions updated using apparent dip measurements at well markers. Black lines are Bézier cubic curve interpolations between well markers constrained by facies interpretations and dipmeter data.

## 4.2 From sediment source to depositional surfaces

As illustrated in Figure 4.1, clinoforms may be defined at a coarse (third order - system tract) time scale. Each clinoform corresponds to a depositional sequence which can be categorized following the sequence stratigraphic nomenclature proposed by [Catuneanu et al. \(2011\)](#), e.g., transgressive or regressive system tracks.

The proposed method correlates markers within a single system tract (fourth to fifth order - parasequences) trying to honor the geometry of chronostratigraphic surfaces at that scale based on:

1. Surfaces generated following prior knowledge of the local geology, such as surfaces interpreted from seismic data or regional geological knowledge. However, this requires a three-dimensional model of the sedimentary basin, or at least a simplified model of a clinoform within the basin as illustrated in Figure 4.1 ([Holbrook and Miall, 2020](#); [Kirschbaum and Hettinger, 2004](#); [Patruno et al., 2015](#); [Steel and Olsen, 2002](#)).
2. A theoretical clinoform geometry defined by analytic equations according to several parameters based on prior knowledge such as regional sediment sources ([Adams and Schlager, 2000](#); [Driscoll and Karner, 1999](#); [Lallier et al., 2016](#)). This allows to assess uncertainties using several possible geometries.

### 4.2.1 Two-dimensional analytical model

Adams and Schlager (2000) proposed to combine three types of two-dimensional analytical equations to describe a sedimentary depositional profile slope (Figure 4.5).

Considering  $z$  as the depositional depth along the direction  $x$ , the three analytical equations used by Adams and Schlager (2000) are:

- A linear equation representing a regular depositional slope given by

$$z = ax + b, \quad (4.10)$$

where  $a$  is the inclination of slope, and  $b$  is the intercept (Figure 4.5.C).

- An exponential equation representing a curved depositional slope given by

$$z = ae^{-bx} + c, \quad (4.11)$$

where  $a$  defines the position of coordinates system with respect to the curvature,  $b$  is a measure of the curvature, and  $c$  defines the horizontal asymptotic value of  $z$  (Figure 4.5.D).

- A Gaussian equation representing an inflected depositional slope given by

$$z = a + be^{\left(-\frac{(x-c)^2}{2d^2}\right)}, \quad (4.12)$$

where  $a$  defines the horizontal asymptotic value of  $z$ ,  $b$  is the height of the slope,  $c$  is the position at the  $x$  axis where the top of the distribution is horizontal, and  $d$  is the width from the center to the inflection point of the distribution (Figure 4.5.E).

Figure 4.5.A plots drawing lines from seismic profile of a siliciclastic continental submarine slope of the Antarctic Peninsula Pacific margin (Rebesco and Camerlenghi, 1997). The slope is measured from these lines, and the slope can be interpreted as: (1) a planar upper slope and (2) a concave lower slope, together with curve fits of the linear Equation (4.10) and the exponential Equation (4.11) as illustrated in Figure 4.5.A by Adams and Schlager (2000).

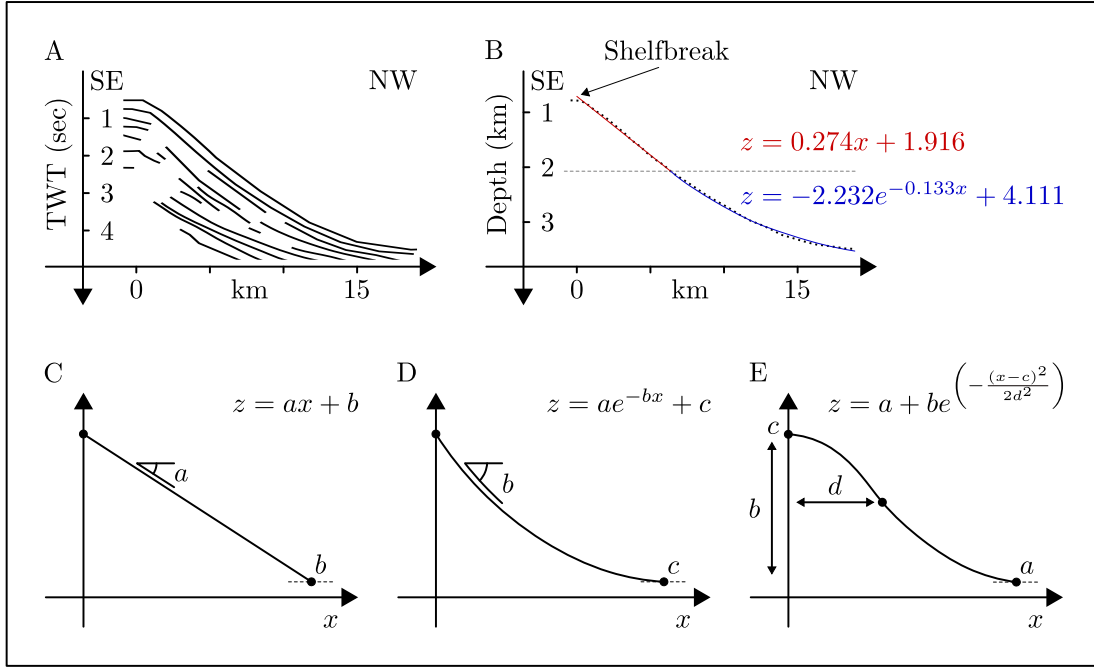


Figure 4.5: (A) Line drawings from seismic profiles, (B) seismic line interpolations, of a siliciclastic continental submarine slope of the Antarctic Peninsula Pacific margin (Rebesco and Camerlenghi, 1997). (C) Planar morphology described by a linear function (Equation (4.10)). (D) Concave curvature described by an exponential function (Equation (4.11)). (E) Sigmoidal morphology described by a Gaussian distribution (Equation (4.12)). See text for description of parameters. Modified from Adams and Schlager (2000).

## 4.2.2 Three-dimensional analytical model

Considering a sediment transport direction  $\theta$  (e.g., N045), the local coordinate system  $(x_p, y_p, z_p)$  corresponds to the translation and the rotation of the global coordinate system  $(x, y, z)$  defined by

$$\begin{pmatrix} x_p \\ y_p \\ z_p \end{pmatrix} = \begin{pmatrix} \sin \theta & \cos \theta & 0 \\ -\cos \theta & \sin \theta & 0 \\ 0 & 0 & 1 \end{pmatrix} \begin{pmatrix} x - x_s \\ y - y_s \\ z - z_s \end{pmatrix}, \quad (4.13)$$

in order to be centered on the principal sediment source location  $(x_s, y_s, z_s)$ .

The two main axes of this new coordinate system correspond to the principal sediment transport direction  $x_p$  and the strike direction  $y_p$ . Along these new directions, the lateral extension and the height of the delta are given by  $(\delta_{x_p}, \delta_{y_p}, \delta_{z_p})$ .

In this local coordinate system, and considering that the shape of the sedimentary slope is a sigmoidal slope along the depositional direction  $x_p$ , and is a bell-shaped

slope along the strike direction  $y_p$  (Figure 4.1). The two-dimensional analytical equations of the theoretical depositional depth  $z_p$  proposed by Adams and Schlager (2000) may be adapted to describe the paleogeographic depositional profile in three dimensions, and this new analytical equation is divided in three parts, corresponding each to a specific depositional zone (Figure 4.6):

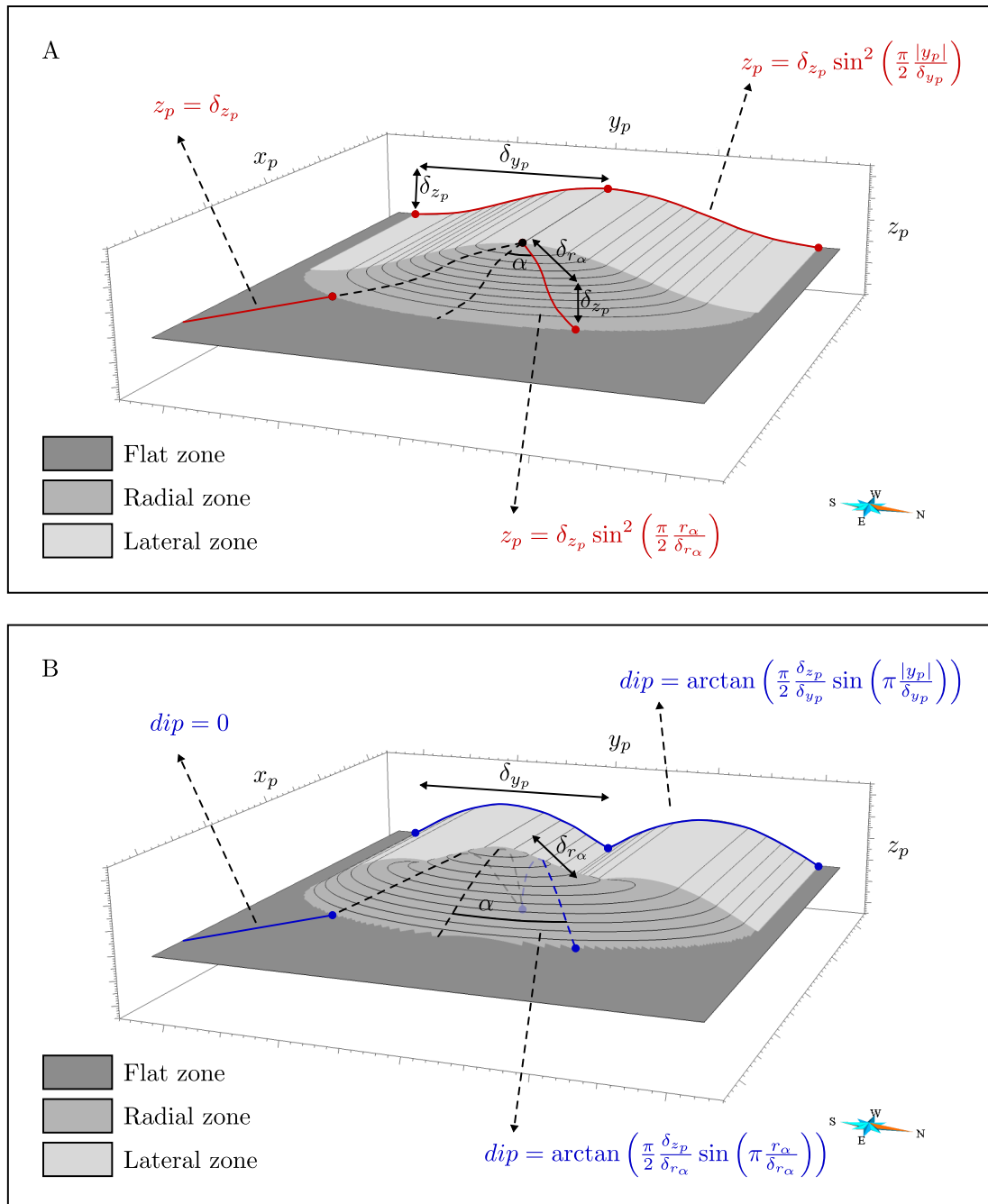


Figure 4.6: (A) Depositional depth  $z_p$  and (B) depositional dip divided in three zones: (1) the lateral zone described by Equations (4.14) and (4.15), (2) the radial zone described by Equations (4.17) and (4.19), and (3) the flat zone described by Equation (4.20).

- The lateral zone. The sediments are transported along a rectilinear direction  $x_p$  from the continent until the radial part ( $x_p < 0$ ). The paleogeographic depositional profile in this part is a bell-shaped slope in the lateral direction  $y_p$  until the slope toe ( $|y_p| < \delta_{y_p}$ ). The theoretical depositional depth  $z_p$  is given by

$$z_p(x_p, y_p) = \delta_{z_p} \sin^2 \left( \frac{\pi |y_p|}{2 \delta_{y_p}} \right), \quad (4.14)$$

and the depositional *dip* is given by the arctangent of the depositional depth derived from the lateral direction  $y_p$

$$dip = \arctan \left( \frac{dz_p}{dy_p}(x_p, y_p) \right) = \arctan \left( \frac{\pi \delta_{z_p}}{2 \delta_{y_p}} \sin \left( \pi \frac{|y_p|}{\delta_{y_p}} \right) \right). \quad (4.15)$$

- The radial zone. The transport of sediments is radial from the source of sediments ( $x_p > 0$ ) along a direction  $\alpha$  within an elliptical area corresponding to the deltaic lateral extension of the system ( $\delta_{x_p}, \delta_{y_p}$ ). The position of the point within this area is given by

$$r_\alpha(x_p, y_p) = \sqrt{x_p^2 + y_p^2}, \quad (4.16)$$

and the theoretical depositional depth  $z_p$  is given by

$$z_p(r_\alpha) = \delta_{z_p} \sin^2 \left( \frac{\pi r_\alpha}{2 \delta_{r_\alpha}} \right), \quad (4.17)$$

where

$$\delta_{r_\alpha} = \sqrt{\frac{\delta_{x_p}^2 \delta_{y_p}^2}{\delta_{y_p}^2 \cos^2 \alpha + \delta_{x_p}^2 \sin^2 \alpha}} \quad (4.18)$$

is the length of the segment between the source of sediments and the bottom of the deltaic slope in the direction  $\alpha$ .

The depositional *dip* is given by the arctangent of the depositional depth derived from the radial direction  $r_\alpha$

$$dip = \arctan \left( \frac{dz_p}{dr_\alpha}(r_\alpha) \right) = \arctan \left( \frac{\pi \delta_{z_p}}{2 \delta_{r_\alpha}} \sin \left( \pi \frac{r_\alpha}{\delta_{r_\alpha}} \right) \right). \quad (4.19)$$

- The flat zone. Sediments are not transported with the same energy in the flat prodelta area ( $|y_p| > \delta_{y_p}$  and  $r_\alpha > \delta_{r_\alpha}$ ). The theoretical depositional depth  $z_p$  and the depositional *dip* are given by

$$z_p = \delta_{z_p} \text{ and } dip = 0. \quad (4.20)$$

Figure 4.7 illustrates an example of a paleogeographic depositional profile in the depositional coordinate system  $(x_p, y_p, z_p)$  computed from a sediment source location  $(x_s, y_s, z_s)$  and a principal sediment transport direction  $\theta = N090$ .

The depositional coordinate system is defined by two directions  $x_p = N090$  and  $y_p = N000$ , and at the origin, there is the sediment source.

The deltaic shape of the depositional system is described by the spatial extension of the delta ( $\delta_{x_p} = 50$  m,  $\delta_{y_p} = 100$  m,  $\delta_{z_p} = 20$  m).

This parametrization allows to compute four parameters, which are directly given by the sediment source location and the delta spatial extension:

- The depositional depth  $z_p$  can be analytically computed within all the depositional coordinate system using Equations (4.14), (4.17) and (4.20) according to the position within the depositional system (Figure 4.7.A).
- The depositional *dip* can be analytically derived from the depositional depth within all the depositional system using Equations (4.15), (4.19) and (4.20) (Figure 4.7.B).

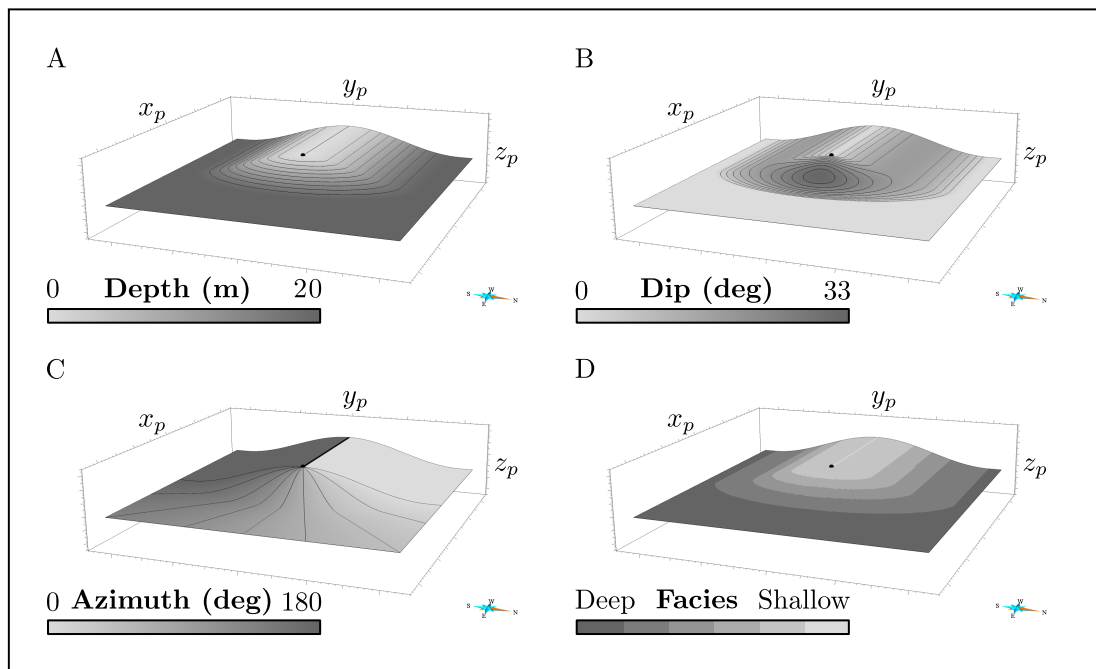


Figure 4.7: A theoretical depositional profile generated from a sediment source (black point) being described by a deltaic extension ( $\delta_{x_p} = 50$  m,  $\delta_{y_p} = 100$  m,  $\delta_{z_p} = 20$  m). (A) The depositional depth (Equations (4.14), (4.17) and (4.20)). (B) The depositional dip (Equations (4.15), (4.19) and (4.20)). (C) The azimuth (degree) computed from the position of the sediment source. (D) The facies repartition on the depositional profile depending on the depositional depth.

- The azimuth, that corresponds to the orientation of the line between every possible position within the depositional system and the sediment source, can be analytically computed (Figure 4.7.C).
- The sedimentary facies corresponding to the depositional condition can be interpreted using membership functions linking the depositional depth and the sedimentary facies (e.g., [Lallier et al., 2016](#)) (Figure 4.7.D).

## 4.3 Correlation likelihood computation

The purpose of this method is to evaluate the likelihood of a well marker correlation by comparing the depositional surface interpolated between these markers and a theoretical profile defined by a principal sediment source and the lateral and vertical extension of the delta.

The comparison process is divided in three steps:

1. The depositional profile is translated at each well marker position to fit the dipmeter data and the sedimentary facies (Section 4.3.1).
2. The absolute integral is computed between the Bézier interpolation and the depositional profile (Section 4.3.2).
3. Absolute integrals corresponding to each well marker are summed (two areas between two wells, and three volumes between three wells) to return a correlation cost (Section 4.3.3).

Once all the correlation costs have been computed, the Dynamic Time Warping algorithm generates all the possible sets of marker correlations and may return the  $n$ -most likely scenarios corresponding to the  $n$ -correlation sets having the  $n$ -lowest cumulated correlation cost (e.g., [Baville et al., 2022](#); [Edwards, 2017](#); [Lallier, 2012](#); [Waterman and Raymond, 1987](#)).

### 4.3.1 Theoretical depositional profile translation

The purpose of this step is to compute, for each well marker  $n$ , the source of sediments  $s_n$  corresponding to the depositional profile (Section 4.2.2) which honors the well marker data (facies, dip and azimuth) as best as possible.

The position  $\mathbf{m}_n$  of the well marker  $n$  in the spatial coordinate system  $(x, y, z)$  and the position  $\mathbf{m}_{p_{s_n}}$  of the source of sediments  $s_n$  in the depositional coordinate

system  $(x_p, y_p, z_p)$  are known. In the other side, the position  $\mathbf{m}_{p_n}$  of the well marker  $n$  in the depositional coordinate system  $(x_p, y_p, z_p)$  and the position  $\mathbf{m}_{s_n}$  of the source of sediments  $s_n$  in the spatial coordinate system  $(x, y, z)$  are unknown.

The two vectors  $\mathbf{v}_n$  and  $\mathbf{v}_{p_n}$  represent the spatial distance between the well marker  $n$  and the source of sediment  $s_n$  respectively in the spatial and the depositional coordinate systems  $(x, y, z)$  and  $(x_p, y_p, z_p)$ :

$$\mathbf{v}_n = \begin{pmatrix} x_n - x_{s_n} \\ y_n - y_{s_n} \\ z_n - z_{s_n} \end{pmatrix} \text{ and } \mathbf{v}_{p_n} = \begin{pmatrix} x_{p_n} - x_{p_{s_n}} \\ y_{p_n} - y_{p_{s_n}} \\ z_{p_n} - z_{p_{s_n}} \end{pmatrix} = \begin{pmatrix} x_{p_n} \\ y_{p_n} \\ z_{p_n} \end{pmatrix} \quad (4.21)$$

These two vectors are linked by the coordinate system transformation matrix defined in Equation (4.13) as follows:

$$\begin{pmatrix} x_{p_n} \\ y_{p_n} \\ z_{p_n} \end{pmatrix} = \begin{pmatrix} \sin \theta & \cos \theta & 0 \\ -\cos \theta & \sin \theta & 0 \\ 0 & 0 & 1 \end{pmatrix} \begin{pmatrix} x_n - x_{s_n} \\ y_n - y_{s_n} \\ z_n - z_{s_n} \end{pmatrix}. \quad (4.22)$$

The purpose of this step is to determine the position  $\mathbf{m}_{s_n}$  of the source of sediments  $s_n$  in the spatial coordinate system  $(x, y, z)$  corresponding to the well marker  $n$ . In order to solve Equation (4.22), the position  $\mathbf{m}_{p_n}$  of the well marker  $n$  in the depositional coordinate system  $(x_p, y_p, z_p)$  can be computed by using dipmeter data and sedimentary facies interpretation:

1. The dipmeter data (azimuth  $\theta$  and dip angle  $\phi$ ) gives the orientation and the inclination of the depositional surface at the well marker position (Figure 4.8.B).
2. A radial segment starting from the sediment source position returns all the possible positions  $(x_p, y_p)$  of the well marker along the axis  $r_p$  corresponding to the slope in the dip direction  $\theta^*$  (Figure 4.8.A). This segment is sampled by  $N + 1$  points  $(x_{p_n}, y_{p_n})$  is given by

$$\forall n \in \llbracket 0, N \rrbracket, \begin{pmatrix} x_{p_n} \\ y_{p_n} \end{pmatrix} = \begin{pmatrix} r_{p_n} \cos\left(\frac{\pi}{2} - \theta^*\right) \\ r_{p_n} \sin\left(\frac{\pi}{2} - \theta^*\right) \end{pmatrix}, \quad (4.23)$$

where  $r_{p_n}$  is the radius length given by

$$\forall n \in \llbracket 0, N \rrbracket, r_{p_n} = \frac{n}{N} \sqrt{\frac{\delta_{x_p}^2 \delta_{y_p}^2}{\delta_{y_p}^2 \cos^2\left(\frac{\pi}{2} - \theta^*\right) + \delta_{x_p}^2 \sin^2\left(\frac{\pi}{2} - \theta^*\right)}}, \quad (4.24)$$

where

$$\delta_{r_{\theta^*}} = \sqrt{\frac{\delta_{x_p}^2 \delta_{y_p}^2}{\delta_{y_p}^2 \cos^2(\frac{\pi}{2} - \theta^*) + \delta_{x_p}^2 \sin^2(\frac{\pi}{2} - \theta^*)}} \quad (4.25)$$

is the length of the segment between the source of sediments and the bottom of the deltaic slope in the direction  $\theta^*$ .

3. For each point, the facies of the well marker is then compared with the facies of the considered point  $(x_{p_n}, y_{p_n})$  computing the depositional depth  $z_p(x_{p_n}, y_{p_n})$  (Equations (4.14), (4.17) and (4.20) and Figures 4.6 and 4.7.A) and the corresponding facies defined by a membership function given as input parameter (Figure 4.7.D) (e.g., [Lallier et al., 2016](#)).
4. In the case that the facies is identical, the most likely position

$$\mathbf{m}_{p_n} = \begin{pmatrix} x_{p_n} \\ y_{p_n} \\ z_{p_n} \end{pmatrix} = \begin{pmatrix} r_{p_n} \cos\left(\frac{\pi}{2} - \theta^*\right) \\ r_{p_n} \sin\left(\frac{\pi}{2} - \theta^*\right) \\ z_p(r_{p_n}) \end{pmatrix} \quad (4.26)$$

is the one which minimizes the absolute difference between the dip angle  $\phi$  and the depositional *dip* (Equations (4.15), (4.19) and (4.20) and Figure 4.8) given by

$$\underset{0 \leq n \leq N}{\operatorname{argmin}} \left| \phi - \arctan\left(\frac{\pi}{2} \frac{\delta_{z_p}}{\delta_{r_{\theta^*}}} \sin\left(\pi \frac{r_{p_n}}{\delta_{r_{\theta^*}}}\right)\right) \right|. \quad (4.27)$$

This difference can be simplified as follows, and the best position  $\mathbf{m}_{p_n}$  is the one which minimizes the dip difference:

$$\underset{0 \leq n \leq N}{\operatorname{argmin}} \left| \phi - \arctan\left(\frac{\pi}{2} \frac{\delta_{z_p}}{\delta_{r_{\theta^*}}} \sin\left(\pi \frac{n}{N}\right)\right) \right|. \quad (4.28)$$

Once the best position  $\mathbf{m}_{p_n}$  of the well marker  $n$  is determined in the depositional coordinate system  $(x_p, y_p, z_p)$ , the position  $\mathbf{m}_{s_n}$  of the source of sediment  $s_o$  in the spatial coordinate system  $(x, y, z)$  is given by

$$\begin{pmatrix} x_{s_n} \\ y_{s_n} \\ z_{s_n} \end{pmatrix} = \begin{pmatrix} x_n \\ y_n \\ z_n \end{pmatrix} + \begin{pmatrix} \sin \theta & -\cos \theta & 0 \\ \cos \theta & \sin \theta & 0 \\ 0 & 0 & 1 \end{pmatrix} \begin{pmatrix} x_{p_n} \\ y_{p_n} \\ z_{p_n} \end{pmatrix}. \quad (4.29)$$

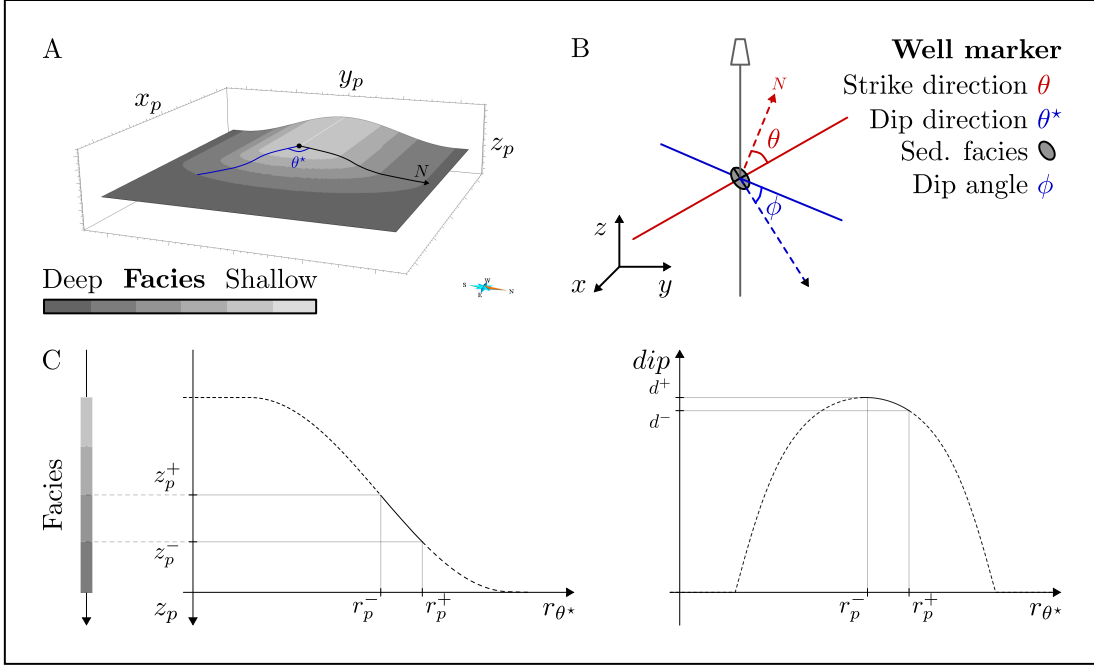


Figure 4.8: (A) A theoretical depositional profile generated from a sediment source (black point) being described by a delta spatial extension ( $\delta_{x_p} = 50$  m,  $\delta_{y_p} = 100$  m,  $\delta_{z_p} = 20$  m). (B) A well marker interpreted along a well, described by a strike direction  $\theta$ , a dip angle  $\phi$  (dip direction  $\theta^*$ ), and a sedimentary facies. (C) Depositional depth  $z_p$  and depositional dip ranges corresponding to the sedimentary facies interpreted at the marker position.

### 4.3.2 Absolute integral computation

The three-dimensional Bézier cubic interpolation is only defined in the barycentric space  $(u, v)$  or  $(u, v, w)$  defined by the well markers for which the correlation is computed. As the depositional profile is defined in the depositional coordinate system  $(x_p, y_p, z_p)$ , the barycentric coordinates between two well markers  $i$  and  $j$  can be parametrized in this coordinate system using the following transformation

$$\forall (u, v) \in [0, 1]^2, \begin{pmatrix} x_p(u, v) \\ y_p(u, v) \end{pmatrix} = \begin{pmatrix} x_{p_i} & x_{p_j} \\ y_{p_i} & y_{p_j} \end{pmatrix} \begin{pmatrix} u \\ v \end{pmatrix}, \quad (4.30)$$

with  $u + v = 1$ . Similarly the barycentric coordinates defined by three well markers  $i, j$  and  $k$  (with  $u + v + w = 1$ ) can be parametrized using the following transformation

$$\forall (u, v, w) \in [0, 1]^3, \begin{pmatrix} x_p(u, v, w) \\ y_p(u, v, w) \end{pmatrix} = \begin{pmatrix} x_{p_i} & x_{p_j} & x_{p_k} \\ y_{p_i} & y_{p_j} & y_{p_k} \end{pmatrix} \begin{pmatrix} u \\ v \\ w \end{pmatrix}. \quad (4.31)$$

The depositional depth  $z_p^b$  can be computed from barycentric coordinates using

$$\begin{aligned} z_p^b : [0, 1]^2 &\rightarrow \mathbb{R} \\ (u, v) &\mapsto z_p(x(u, v), y(u, v)), \end{aligned} \quad (4.32)$$

between two wells, with  $u + v = 1$ , and

$$\begin{aligned} z_p^b : [0, 1]^3 &\rightarrow \mathbb{R} \\ (u, v, w) &\mapsto z_p(x(u, v, w), y(u, v, w)), \end{aligned} \quad (4.33)$$

between three wells, with  $u + v + w = 1$ .

In the following part,  $z_{p_i}^b$  is the depositional profile translated to fit the marker  $i$ ,  $z_{b_{i,j}}$  is the depositional curve interpolation between markers  $i$  and  $j$ , and  $z_{b_{i,j,k}}$  is the depositional surface interpolation between markers  $i$ ,  $j$  and  $k$ . The absolute integral between the three-dimensional Bézier interpolation (Equations (4.3) and (4.7)) and the translated depositional profile is computed in two cases:

- The interpolation computed between two well markers  $i$  and  $j$  using Equation (4.3) is a three-dimensional Bézier cubic curve between the two well markers. The part of the depositional profile translated to fit marker  $i$  used to compute the absolute integral is a straight line between the two well markers. The two parametric curves are discretized in  $n$  segments, and  $n + 1$  nodes having the same barycentric coordinates  $(u, v)$  in both curves (Figure 4.9.A-B).

The absolute integral between the two discretized parametric curves is calculated by computing the vertical distance between two nodes having the same barycentric coordinates  $(u, v)$  using

$$\mathcal{A}_i(i, j) = \frac{D_{i,j}}{n} \sum_{\substack{0 < u, v < 1 \\ u+v=1}} \lambda(u, v) |z_{b_{i,j}}(u, v) - z_{p_i}^b(u, v)|, \quad (4.34)$$

where  $D_{i,j}$  is the vertical projected distance computed between well markers  $i$  and  $j$ .  $(u, v)$  are the barycentric coordinates defined by well markers  $i$  and  $j$  (Section 4.1.3.1 and Equation (4.3)).  $\lambda(u, v)$  are weights corresponding to the occurrence of the node in the integral computation (Figure 4.9.B) given by

$$\lambda(1, 0) = \lambda(0, 1) = 1/2 \text{ and } \forall (u, v) \in ]0, 1[^2, u + v = 1, \lambda(u, v) = 1. \quad (4.35)$$

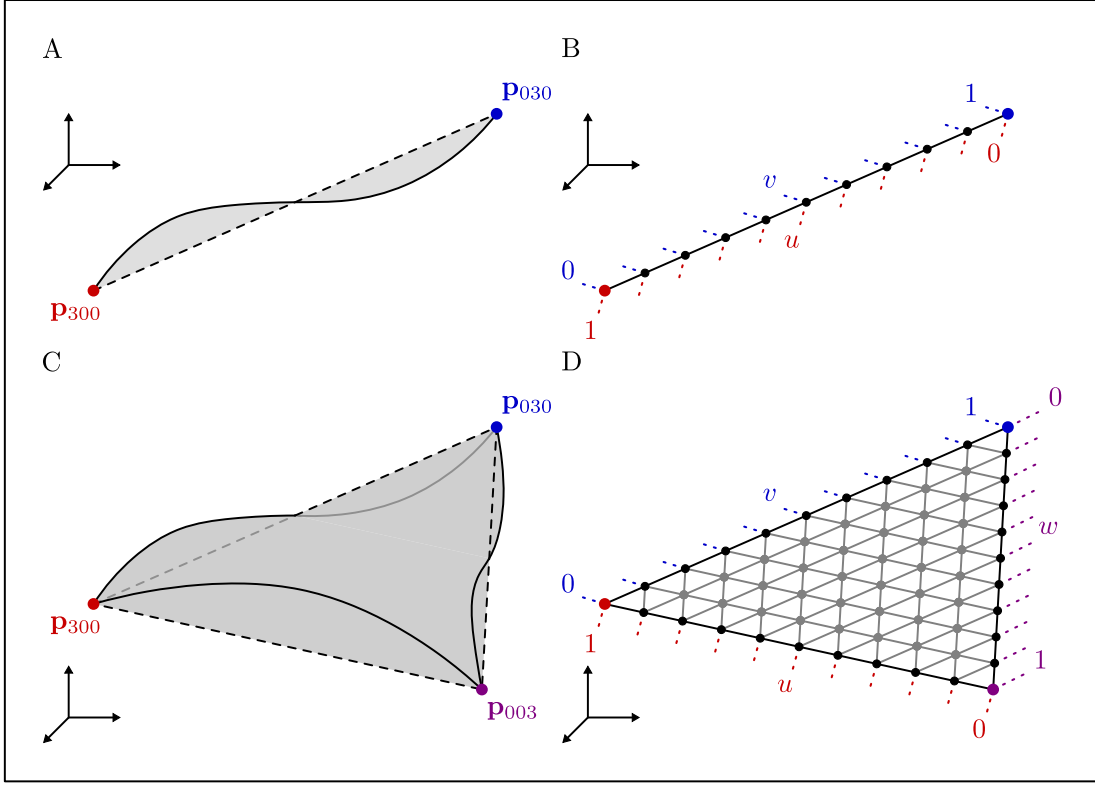


Figure 4.9: Correlation lines and correlation surfaces discretization for the absolute integral computation. (A) Absolute area between two lines (gray surface) and (B) the line discretization based on the vertical projected barycentric coordinates. (C) Absolute volume between two surfaces (gray volume) and (D) the surface discretization based on the vertical projected barycentric coordinates.

- The interpolation computed between three well markers  $i$ ,  $j$  and  $k$  using Equation (4.7) is a three-dimensional triangular Bézier cubic patch cornered by the three well markers. The part of the depositional profile translated to fit marker  $i$  used to compute the absolute integral is a triangular surface between the three well markers. The two surfaces are discretized in  $n^2$  triangles, and  $(n+1)(n+2)/2$  nodes having the same barycentric coordinates  $(u, v, w)$  in both triangular surfaces (Figure 4.9.C-D).

The absolute integral between the two discretized triangular surfaces is calculated by computing the vertical distance between two nodes having the same barycentric coordinates  $(u, v, w)$  using

$$\mathcal{V}_i(i, j, k) = \frac{S_{i,j,k}}{n^2} \sum_{\substack{0 < u, v, w < 1 \\ u+v+w=1}} \lambda(u, v, w) |z_{b_{i,j,k}}(u, v, w) - z_{p_i}^b(u, v, w)| \quad (4.36)$$

where  $S_{i,j,k}$  is the vertical projected surface computed between well markers  $i$ ,  $j$ ,  $k$ .  $u$ ,  $v$  and  $w$  are the barycentric coordinates defined by well markers

$i$ ,  $j$  and  $k$  (Equation (4.7)).  $\lambda(u, v, w)$  are weights corresponding to the occurrence of the node in the integral computation (Figure 4.9.D) given by

$$\lambda(1, 0, 0) = \lambda(0, 1, 0) = \lambda(0, 0, 1) = 1/3, \quad (4.37)$$

and

$$\forall (u, v) \in ]0, 1[{}^2, u + v = 1, \lambda(u, v, 0) = \lambda(u, 0, v) = \lambda(0, u, v) = 1, \quad (4.38)$$

and the weight of the nodes within the triangle is given by

$$\forall (u, v, w) \in ]0, 1[{}^3, u + v + w = 1, \lambda(u, v, w) = 2. \quad (4.39)$$

### 4.3.3 Correlation cost computation

As illustrated in Figure 4.10, the correlation cost  $c_{ab}[i, j]$  between two well markers  $i$  and  $j$  corresponds to the cumulative absolute areas between the translated depositional profile (three-dimensional line) and the Bézier interpolation computed between the two markers (three-dimensional line). This correlation cost is given by

$$c_{ab}[i, j] = \frac{\mathcal{A}_i(i, j) + \mathcal{A}_j(i, j)}{2}, \quad (4.40)$$

and the correlation cost  $c_{ab}[i, j, k]$  between three well markers  $i$ ,  $j$  and  $k$  corresponds to the cumulative absolute areas between the translated depositional profile (three-dimensional surface) and the Bézier interpolation computed between the three markers (three-dimensional surface). This correlation cost is given by

$$c_{abc}[i, j, k] = \frac{\mathcal{V}_i(i, j, k) + \mathcal{V}_j(i, j, k) + \mathcal{V}_k(i, j, k)}{3}. \quad (4.41)$$

The cost can be integrated by the Dynamic Time Warping algorithm which is, as discussed in Chapter 2, commonly used for automatic stratigraphic correlation and uncertainty assessment (e.g. [Baville et al., 2022](#); [Edwards et al., 2018](#); [Fang et al., 1992](#); [Hale, 2013](#); [Lallier et al., 2016](#); [Pels et al., 1996](#); [Smith and Waterman, 1980](#); [Waterman and Raymond, 1987](#); [Wheeler and Hale, 2014](#)).

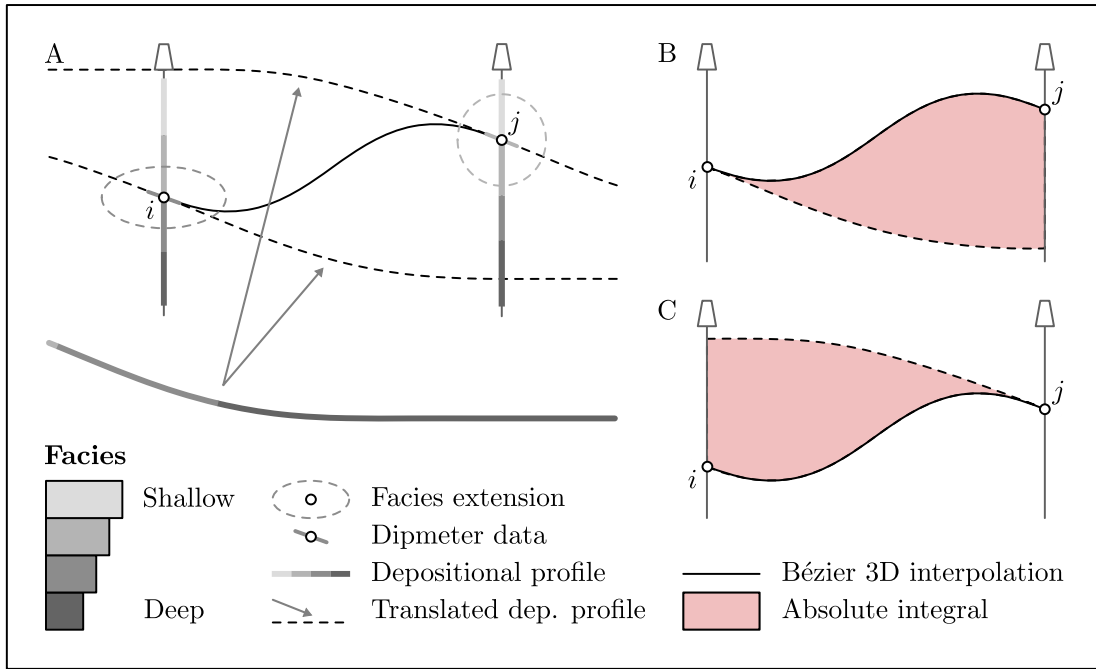


*Figure 4.10: Likelihood computation of candidate isochronous lines obtained by Bézier interpolation. (A) A paleogeographic depositional profile on which the facies are drawn is translated within the model to define the paleogeographic depositional profile for each well marker  $i$  and  $j$  to be compared to Bézier cubic interpolations. (B-C) The two markers are located on two different theoretical depositional profiles, the likelihood is the sum of the absolute integral between the Bézier cubic interpolation and the two paleogeographic depositional profiles.*

The proposed method takes as input parameters two wells composed of  $I$  and  $J$  well markers and computes a correlation cost  $c_{ab}[i, j]$  for each pair of well markers  $[i, j]$  (Equation (4.40)), and a transition cost  $t_{ab}[i, j][k, l]$  between two correlations  $[i, j]$  and  $[k, l]$  as illustrated in Figure 2.1.

The three-dimensional version of the Dynamic Time Warping algorithm uses a similar principle with a three-dimensional cost matrix (Figure 2.3). It is used to compare sets of three wells, whose correlation costs  $c_{abc}[i, j, k]$  are given by Equation (2.6).

If the number of wells is larger than three, the  $n$ -dimensional version of the Dynamic Time Warping algorithm exists but is computationally challenging (Section 2.2.2). Therefore, the correlation is successively applied on wells forming a Delaunay triangulation (Figure 4.11). However, as the triangulation traversal may generate loops, multi-well correlations may lead to inconsistent outcomes (e.g., Lallier et al., 2016; Wheeler and Hale, 2014).

Currently, the issue generated by correlation loops is not taken into account, the piecewise triangular surface generated by the wells stays hold.

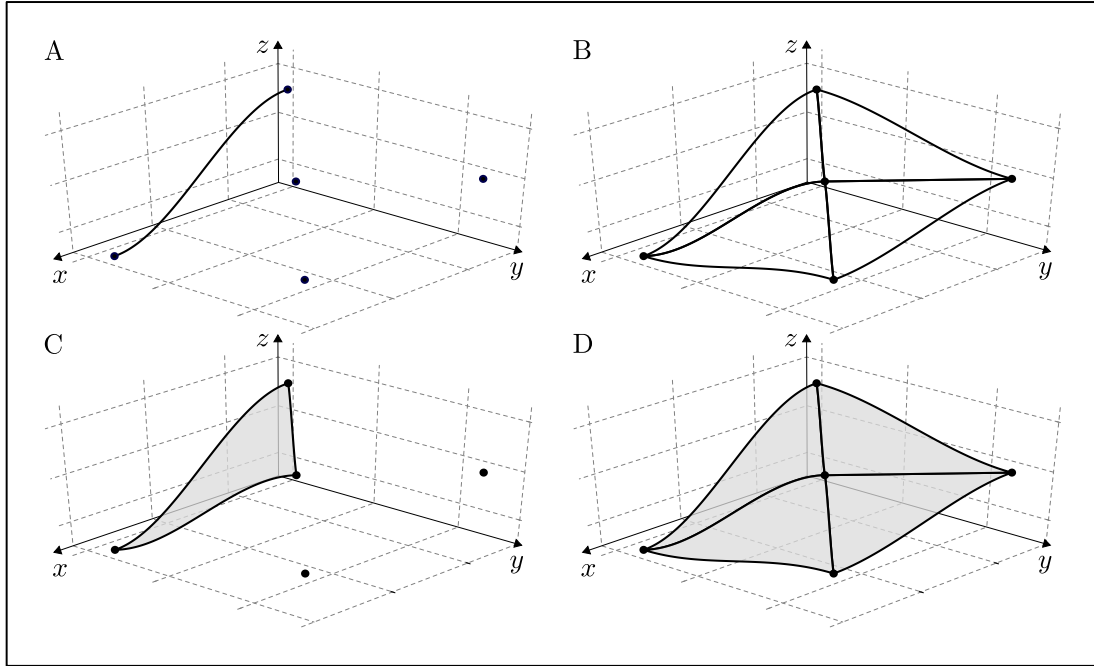


Figure 4.11: Multi-well correlation using (A) triangular surface interpolated between three markers, and (B) piece-wise triangular surface interpolated between five markers.

## 4.4 First results: Synthetic data set

The proposed correlation cost function is tested on a synthetic data set (Figure 4.12.A-B) composed of nine wells located along the principal transport sediment direction  $\theta = N135$  crossing six successive chronostratigraphic horizons generated by Equations (4.14), (4.17) and (4.20) with a displacement of the sediment source from the North-West to the South-East with an increasing depth (the oldest source is located in  $(-90 \text{ m}, 90 \text{ m}, 30 \text{ m})$  and the youngest source is located in  $(60 \text{ m}, -60 \text{ m}, 0 \text{ m})$  with a deltaic extension  $(100 \text{ m}, 500 \text{ m}, 20 \text{ m})$ .

Every possible correlation between pairs of well markers belonging to two successive wells is computed using Equation (4.3) (Figure 4.12.C). All these chronostratigraphic line interpolations are compared to paleogeographic depositional profiles fitting well markers in order to compute a correlation cost (Equation (4.38)). The most likely well correlation set is illustrated in Figure 4.12.D and corresponds to the synthetic model used to generate the well markers. Moreover, the geometry of the chronostratigraphic lines corresponding to three-dimensional Bézier cubic curves are very close to the synthetic model used as reference.

Finally the cost of the most likely correlation set equals  $152706.88 \text{ m}^2$  whereas the second most likely correlation set have a larger cost which reaches  $154730.97 \text{ m}^2$ . This large difference means that the most likely correlation set is much more

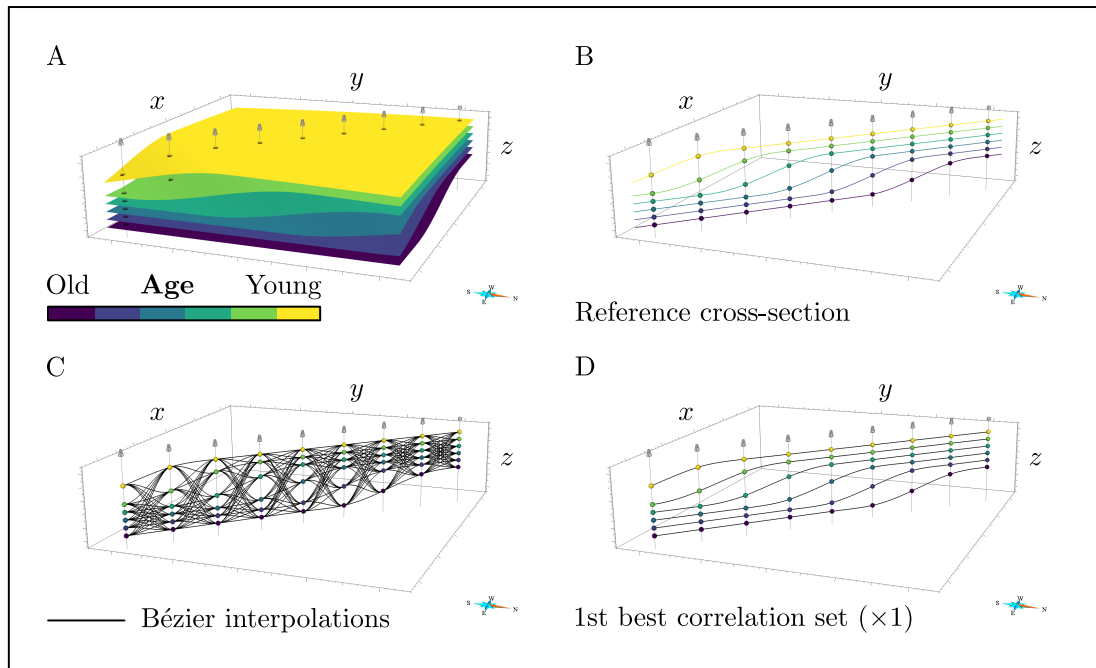


**Figure 4.12:** (A) Nine wells drilling six successive paleogeographic depositional profiles generated using Equations (4.14), (4.17) and (4.20) with a deltaic extension (100 m, 500 m, 20 m) and a principal sediment transport direction  $\theta = N135$ . (B) Paleogeographic depositional lines along the principal sediment transport direction and well markers corresponding to each paleogeographic depositional profile. (C) Every possible well marker correlation corresponding to a three-dimensional Bézier cubic interpolation. (D) The most likely correlation set ( $cost = 152706.88 \text{ m}^2$ ) generated using the proposed correlation cost function.

likely than the second.

## 4.5 Discussion

### 4.5.1 Impact of the theoretical depositional profile.

In this synthetic data set, the principal sediment transport direction is constant but may vary from one lobe to another (e.g., [Bhattacharya, 2006](#); [Knaust and Hoth, 2021](#)). Moreover, the successive sediment sources are located along the same direction (the principal sediment transport direction) but should be not aligned in order to generate successive overlapping deltaic lobes (e.g., [Bhattacharya, 2006](#); [Knaust and Hoth, 2021](#)).

As illustrated in Figure 4.7.A, the flat zone of the theoretical depositional profile corresponds to a null dipmeter data, *i.e.*, there is no true strike direction in this area. However, the translation of the profile to fit well markers is done minimizing

the difference between the true dip angle and the theoretical depositional dip (Equations (4.15), (4.19) and (4.20)) along the dip direction. If the dip angle is null, the strike direction (*i.e.*, the dip direction) may be all the directions and the translation of the depositional profile to fit well markers is not constrained.

The depositional profile translation presents an other limit if the dip angle is null because all the flat zone corresponds to a null dip angle. Well markers, having a null dip angle, give only information about the chronostratigraphic model in the close neighborhood of the well. In this case, the position of the well marker on the depositional profile is put on the interface between the flat zone and the radial zone according to the dip direction randomly simulated.

#### 4.5.2 Impact of the correlation cost computation.

As described in Section 4.3.3, the correlation cost corresponds to the sum of the absolute area (respectively volume) between the three-dimensional Bézier curve (respectively Bézier triangular patch) and the theoretical depositional profile at each well marker. However, this correlation cost is not normalized, then the cumulated correlation cost computed by the Dynamic Time Warping algorithm (Equation (4.38)) vary a lot from one realization to an other. In this example, the three lowest correlation set costs equal to 152706.88 m<sup>2</sup> (one realization), 154730.97 m<sup>2</sup> (five realizations) and 154808.684 m<sup>2</sup> (one realization) and the differences between the most likely scenario and the scenarios having the two closest costs are between the two last wells (Figure 4.13). Moreover, the cost difference is very large and the likelihood decreases a lot between the best outcome and the following.

The main limit of these non normalized correlation costs is the combination of several correlation cost functions within the correlation cost computation, because the very large cost generated by the proposed correlation cost function may blind the other correlation cost functions (e.g. [Baville et al., 2022](#)).

The correlation cost computed by the proposed correlation cost function may be normalized by a characteristic area  $\mathcal{A}_0$  (respectively characteristic volume  $\mathcal{V}_0$ ) computed by multiplying the vertical projected distance (respectively vertical projected surface) between wells and the delta height, *i.e.*,  $\mathcal{A}_0 = D_{wells} \times \delta_{z_p}$  (respectively  $\mathcal{V}_0 = S_{wells} \times \delta_{z_p}$ ).

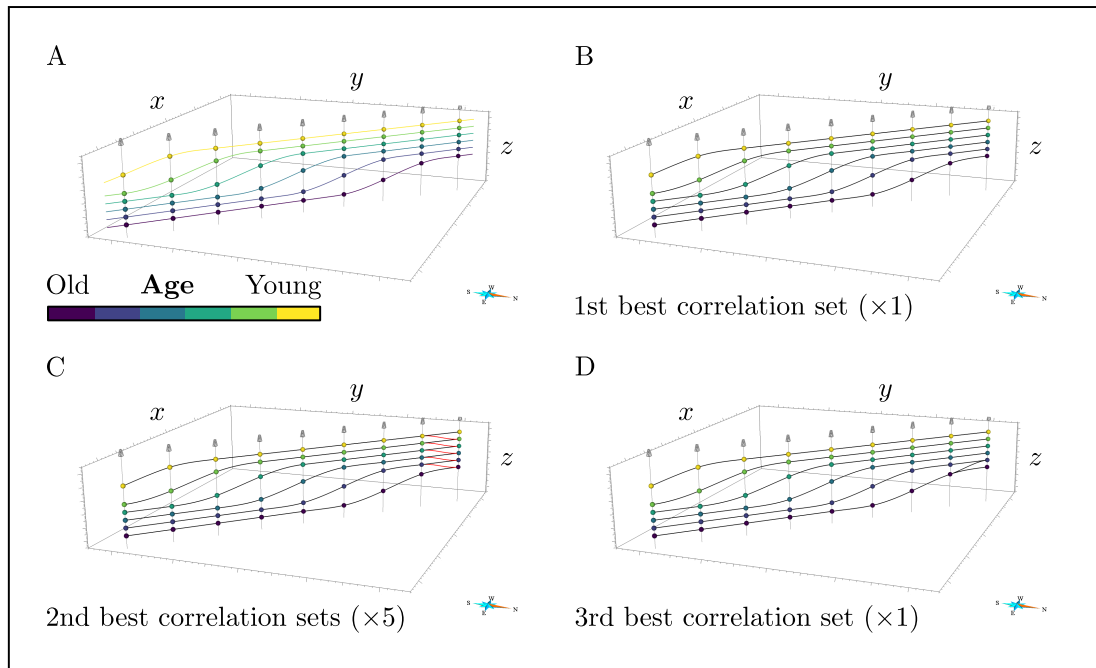


*Figure 4.13: (A) Paleogeographic depositional lines along the principal sediment transport direction  $\theta = N135$  and well markers corresponding to each paleogeographic depositional profile generated with a deltaic extension (100 m, 500 m, 20 m). (B) The most likely correlation set. (C) Five realizations having the second highest likelihood (red lines highlight the difference between the five realizations). (D) The correlation having the third highest likelihood.*

### 4.5.3 Impact of the order of correlation.

In multi-well correlation, the higher the number of correlated wells, the higher the number of computable correlation sets (Figure 4.12.C). This high number of correlation sets makes the computation longer. In order to reduce this time of computation, the number of correlation sets generated at one step of the process is truncated before being propagated to the next step (Antoine and Caumon, 2018; Caumon and Antoine, 2019). This truncation is observed in the final outcomes where the differences between the most likely correlation sets are concentrated between the last wells added to the correlation process.

Figure 4.14.C illustrates the well marker correlations belonging to the hundred most likely correlation set computed using the proposed method correlating wells from Northwest to Southeast. The differences between those hundred correlation sets are focused between the three last wells added to the correlation process. At the opposite, Figure 4.14.D illustrates the well marker correlations belonging to the hundred most likely correlation sets computed using the proposed method correlating wells from the Southeast to the Northwest, and in this case, the differences are focused between the last wells added to the correlation process.

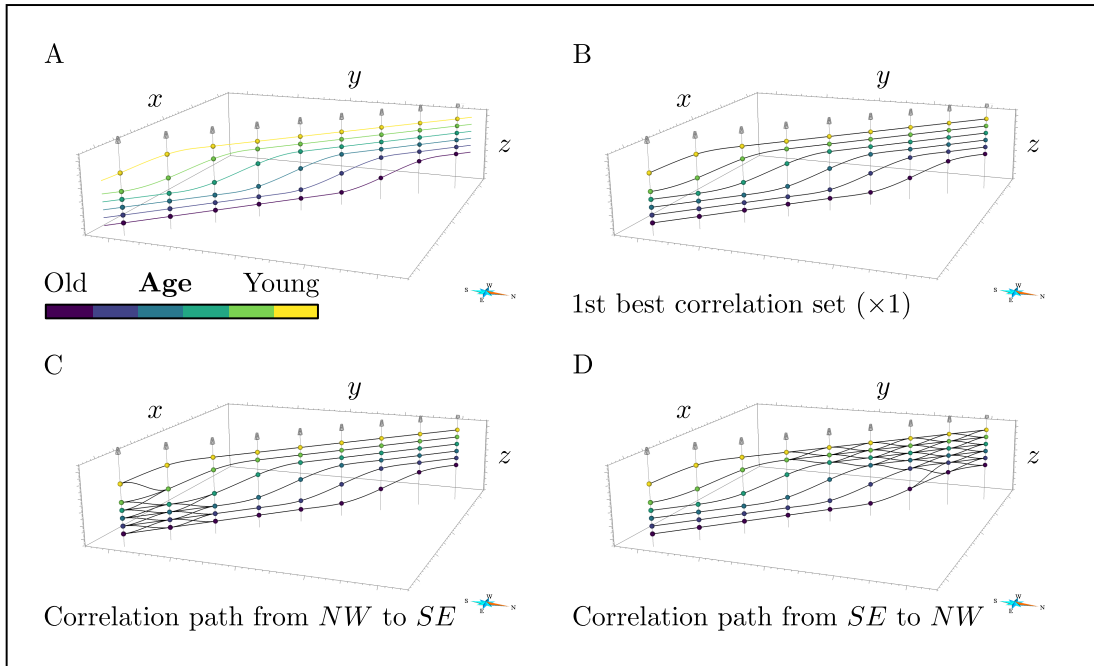


**Figure 4.14:** (A) Paleogeographic depositional lines along the principal sediment transport direction  $\theta = N135$  and well markers corresponding to each paleogeographic depositional profile generated with a deltaic extension (100 m, 500 m, 20 m). (B) The most likely correlation set and its cost according to the path of correlation. (C) Well marker correlations belonging to the hundred most likely correlation sets computed using the proposed method correlating wells from Northwest to Southeast. (D) Well marker correlations belonging to the hundred most likely correlation sets computed using the proposed method correlating wells from Southeast to Northwest.

Moreover, the correlation cost is propagated during the correlation process, and the final correlation cost is impacted by the order of wells, *i.e.*, two opposite order of correlation return two different lowest correlation costs  $152706.88 \text{ m}^2$  and  $131196.80 \text{ m}^2$  even if the outcomes is identical (Figure 4.14.A-B).

## Conclusion

The purpose of the proposed method is to correlate well markers with respect to a theoretical depositional profile in order to generate likely chronostratigraphic well correlation sets. The correlation likelihood is computed for every possible well marker correlation by minimizing the mismatch between chronostratigraphic Bézier interpolation constructed from dipmeter data and depositional facies (Section 4.1.3) and a theoretical depositional profile defined by a principal sediment transport direction and a deltaic vertical and lateral extension (Section 4.2.2).

The proposed method has only been tested on a synthetic data set, and the first results are promising but may be biased by the construction of the synthetic data set. Indeed, the analytical depositional profile to compute the likelihood of the well correlation is the same as the depositional profile used to construct the reference model.

This method must be improved by being applied on more complex synthetic data set and the main goal of this method is to be applied on a real data set to generate a chronostratigraphic models from sparse well data and evaluate the uncertainties on these models.





## Part III

# APPLICATIONS



# Chapter 5

## Middle Jurassic Hugin Formation: Paleogeographic context

### Contents

---

<b>5.1</b>	<b>Zone of interest: Gudrun-Sigrun Field area . . . . .</b>	<b>123</b>
5.1.1	Sedimentary facies interpretation . . . . .	123
5.1.2	Biostratigraphic interpretation . . . . .	125
5.1.3	Relative well distality interpretation . . . . .	126
<b>5.2</b>	<b>Application of the distality rule of correlation . . . . .</b>	<b>130</b>
5.2.1	Scenario A: One single bay-head delta . . . . .	131
5.2.2	Scenario B: Several independent bay-head deltas . . . . .	131
5.2.2.1	Southeast bay-head delta . . . . .	132
5.2.2.2	Northwest bay-head delta . . . . .	133
5.2.2.3	Bay-head deltas and lagoonal environments . . . . .	135

---

The purpose of this chapter is to apply the distality rule of correlation proposed in Chapter 3 on the Middle Jurassic Hugin Formation in the Gudrun-Sigrun Field area (Section 5.1) based on two different paleogeographic contexts. The first paleogeographic context proposed by [Knaust et al. \(2019\)](#) consists of one bay-head delta (Section 5.2.1). The second paleogeographic context proposed by [Knaust and Hoth \(2021\)](#) consists of several independent bay-head deltas (Section 5.2.2). The distality rule of correlation proposed in Chapter 3 is based on sedimentary facies interpretations (identical in the two configurations) and on the well relative distality (depending on the paleogeography) and leads to different outcomes (Section 5.2). This outcomes are compared to biostratigraphic interpretations to evaluate their consistency, and therefore the consistency of the paleogeographic context.

## **Abstract**

*Two different paleogeographic depositional contexts of the Middle Jurassic Hugin Formation in the Gudrun-Sigrun Field area have been interpreted from well logs and core samples (1) by [Knaust et al. \(2019\)](#) as one bay-head delta supplied from Southeast prograding into a lagoonal depositional environment and (2) by [Knaust and Hoth \(2021\)](#) as several independent bay-head deltas supplied from two different directions prograding into a lagoonal depositional environment. The purpose of this chapter is, for each paleogeographic depositional environment interpretation, to generate stochastic chronostratigraphic well correlations at the parasequence scale within the zone of interest using the distality rule of correlation (Chapter 3), and to compare them to biostratigraphic data in order to qualitatively evaluate their consistency with respect to the biostratigraphy. The application of the distality rule of distality does not support the paleogeographic interpretation proposed by [Knaust et al. \(2019\)](#) and does not discard and support the alternative interpretation of [Knaust and Hoth \(2021\)](#) which is consistent with respect to biostratigraphic data.*

## **Introduction**

As discussed in Chapter 1, stratigraphic well correlation consists of associating well markers on one well with well markers on other wells. It may be manually performed by geologists guided by their prior knowledge of the zone of interest (e.g., [Bourquin et al., 1998](#); [Knaust and Hoth, 2021](#); [Shiers et al., 2014](#)) or, as discussed in Chapter 2, it may be automatically generated using computer-assisted approaches (e.g., [Edwards, 2017](#); [Lallier, 2012](#); [Smith and Waterman, 1980](#)).

Both, manual and computer-assisted stratigraphic well correlations can be constrained by the prior definition of the regional paleogeographic depositional context of the zone of interest. However, a robust knowledge of a type of depositional environment and the habit of performing well correlations may have an impact on the result of a well correlation performed from a random data set (e.g., [Baville et al., 2019](#); [Borgomano et al., 2008](#); [Koehrer et al., 2011](#)). As discussed in previous chapters, increasing the number of interpreters may increase significantly the number of outcomes because of the field of expertise of each interpreter ([Bond et al., 2007](#); [Dewan, 1983](#); [Hsieh et al., 2005](#); [Serra and Serra, 2003](#)).

Stratigraphic well correlation may be used to generate subsurface models based on interpreted regional depositional systems, and the comparison of these outcomes to additional data such as biostratigraphic interpretations may qualitatively support or discard the prior hypothesis on the regional depositional system. Indeed,

---

stratigraphic well correlations, constrained by a hypothetical depositional context, may lead to consistent or inconsistent outcomes with respect to additional subsurface data (e.g., biozones):

- If the computer-assisted stratigraphic well correlations are not consistent with additional subsurface data, the hypothetical depositional context may be wrong, and the stratigraphic well correlations are invalidated.
- In contrast, if the stratigraphic well correlations are consistent with additional subsurface data, the hypothetical depositional context is not contradicted given the principles of correlation used to compute the well correlation. It can be one of the possible hypotheses given the geological rules but cannot be completely validated.

The purpose of this chapter is to confront the distality rule of correlation to two hypothetical paleogeographic depositional interpretations of the Middle Jurassic Hugin Formation in the Gudrun-Sigrun Field area using additional data such as revised biostratigraphic interpretations to discuss their consistency (Figure 5.1):

- [Knaust et al. \(2019\)](#) interpreted it as one bay-head delta supplied from Southeast prograding into a lagoonal depositional environment.
- Based on two additional wells and revised biostratigraphic interpretations, [Knaust and Hoth \(2021\)](#) interpreted it as several independent bay-head deltas supplied from two different directions prograding into a lagoonal depositional environment.

These two possible paleogeographic depositional systems can be used to constrain the stratigraphic well correlations generated using the principle of correlation proposed in Chapter 3. The generation of stratigraphic well correlations is based on sedimentary facies and relative well distality interpretations.

In this application, the sedimentary facies interpretation is the same in the two configurations (Figure 5.1) and is based on the sedimentary facies described in Appendix A. However, the principal sediment transport direction, which may be derived from dipmeter logs and borehole image data (e.g., [Knaust and Hoth, 2021](#)), is different in the two paleogeographic depositional interpretation. It means that the relative well distality, which is interpreted from the principal sediment transport direction is different in the two configurations.

Additionally, biozones were interpreted along several wells (Figure 5.1) and are compared to the outcomes to discuss the consistency of the two hypothetical paleogeographic depositional contexts.

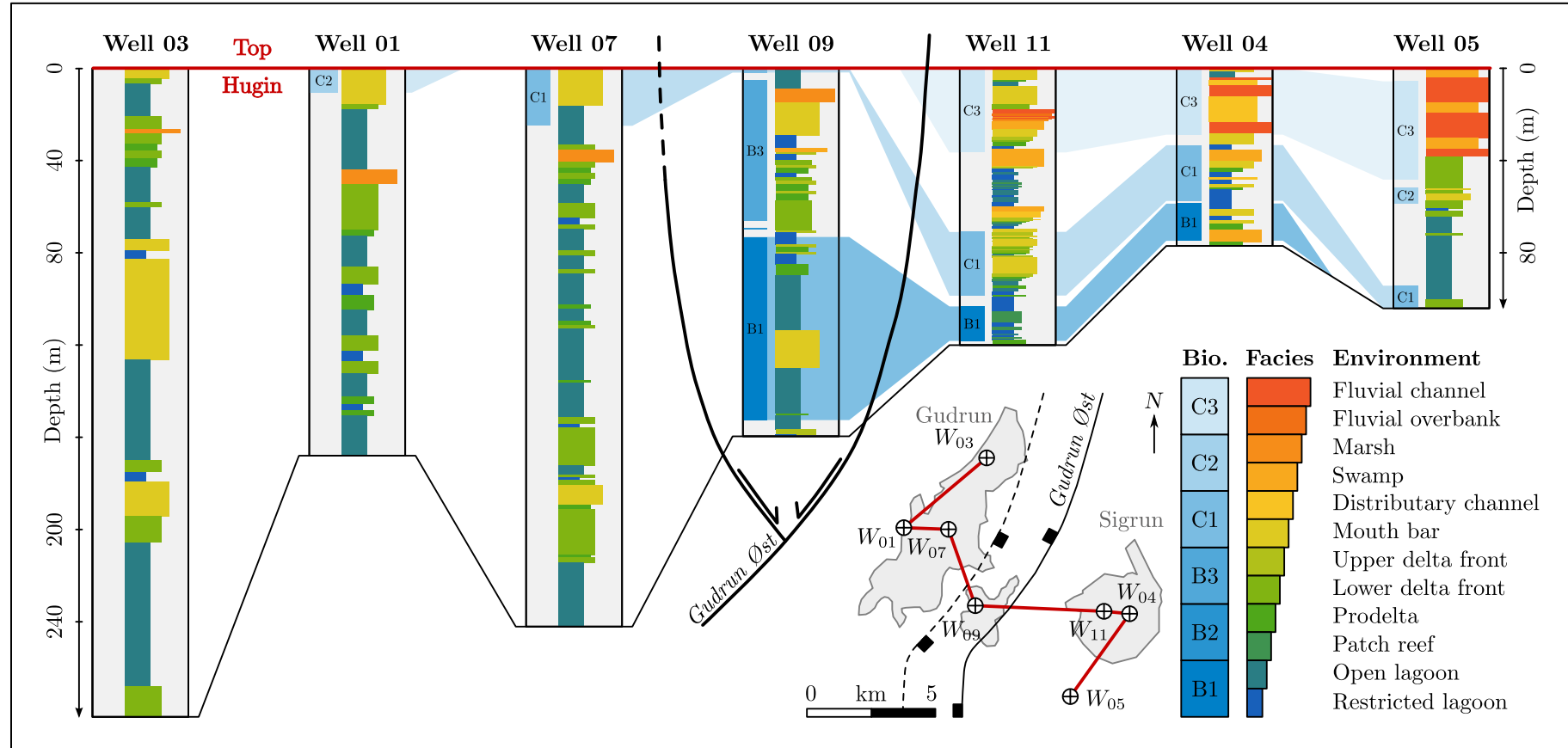


Figure 5.1: Well section: the Middle Jurassic Hugrin Formation in the Gudrun-Sigrun Field area (map based on <http://www.npd.no>). Facies correspond to twelve depositional environments interpreted along wells and described in Section 5.1.1 and Appendix A. Biozones correspond to the six depositional time-periods interpreted from Early Bathonian to Late Callovian along the wells (Section 5.1.2). Note the poor chronostratigraphic resolution and lack of interpreted biozones in the three western wells due to lack of data.

It is important to note that the Middle Jurassic Hugin Formation in the Gudrun-Sigrun Field area has been studied for decades. Moreover, additional wells have been drilled since the first interpretation (e.g., wells 09 and 11) enabling the acquisition of additional subsurface data (e.g., core samples and biostratigraphic data) to update and improve the database of the zone of interest.

## 5.1 Zone of interest: Gudrun-Sigrun Field area

As discussed in Appendix A, the Middle Jurassic Hugin Formation in the Gudrun-Sigrun Field area is mainly interpreted as a bay-head deltaic system (Figure 5.2.B) (e.g., Hoth et al., 2018; Kieft et al., 2010; Knaust and Hoth, 2021; Sneider et al., 1995). This interpretation of the regional depositional system is based on analysis of well logs and core samples acquired along seven nearly vertical wells, which reveal the stratigraphic situation in the zone of interest (Figure 5.2.A).

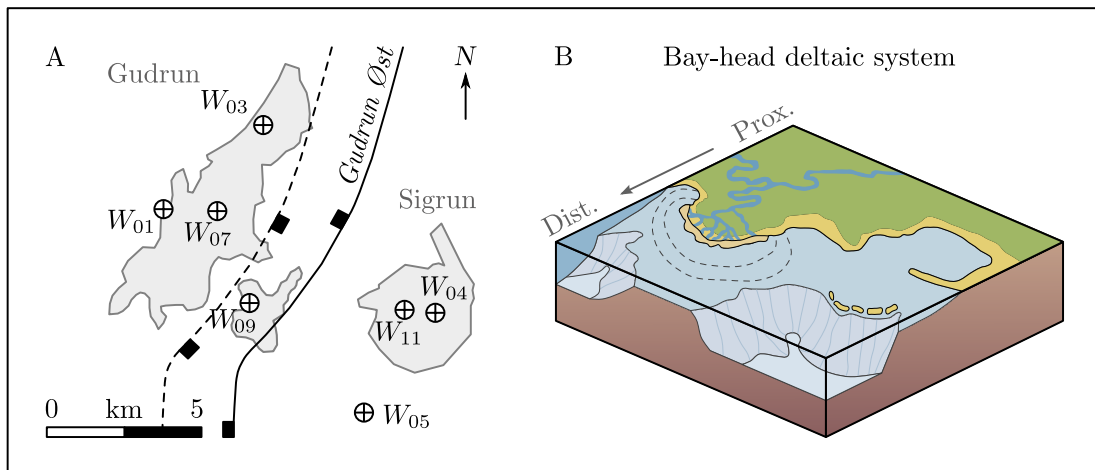


Figure 5.2: (A) Map view of the Gudrun-Sigrun Field area (Block 15/3), and spatial location of the seven wells drilled into the Middle Jurassic Hugin Formation. Gray areas are oil, gas and condensate reservoirs. Map based on <http://www.npd.no>. (B) Middle Jurassic Hugin Formation regional depositional system, a siliciclastic bay-head delta within a lagoonal environment. Modified from (Baville et al., 2022).

### 5.1.1 Sedimentary facies interpretation

Lithofacies have been described by Knaust and Hoth (2021) and interpreted as deposited in various depositional environments corresponding to a regional bay-head deltaic system (Figure 5.2.B). Figure 5.3 illustrates and Table 5.1 lists the twelve sedimentary facies (see the full description and interpretation in Appendix A) which have been interpreted along the seven wells (Figure 5.1).

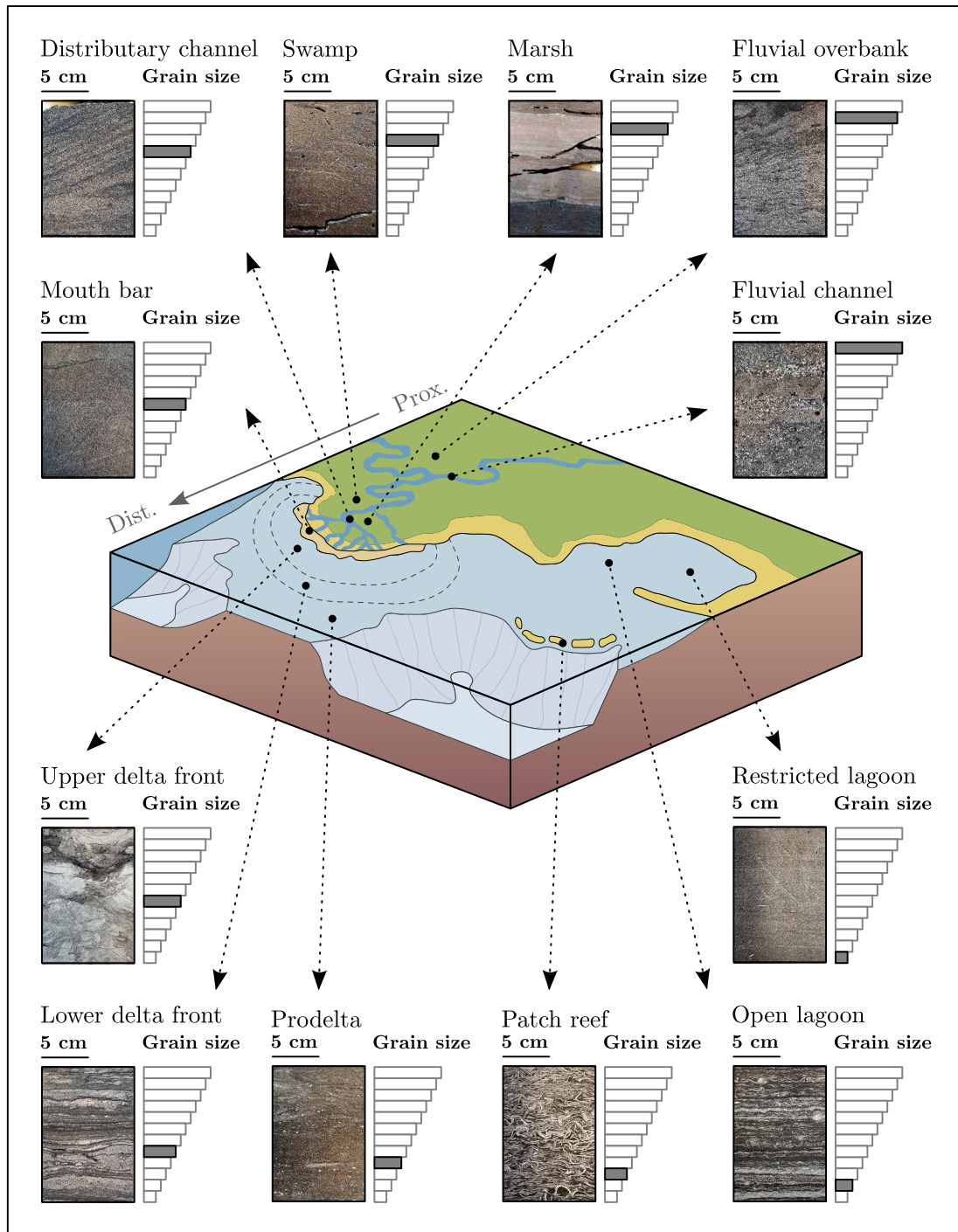


Figure 5.3: Twelve sedimentary facies interpreted by [Knaust and Hoth \(2021\)](#) from core samples of the Middle Jurassic Hugin Formation in the Gudrun-Sigrun Field area. Sedimentary facies are described in Appendix A. Redrawn from ([Baville et al., 2022](#)).

The indexing of these twelve sedimentary facies is based on their inferred paleogeographic position of deposition (Figure 3.3.A), *i.e.*, the lowest sedimentary facies index  $f$  corresponds to the deepest paleogeographic depositional conditions. It enables the computation of well marker correlation cost using Equation (3.15).

*Table 5.1: Sedimentary facies indexing for correlation cost computation and coloring for correlation panel interpretation.*

Depositional environment	Sedimentary facies	Index	Color
Fluvial depositional environment	Fluvial channel	$f = 12$	
	Fluvial overbank	$f = 11$	
	Marsh	$f = 10$	
Deltaic depositional environment	Swamp	$f = 09$	
	Distributary channel	$f = 08$	
	Mouth bar	$f = 07$	
	Upper delta front	$f = 06$	
	Lower delta front	$f = 05$	
	Prodelta	$f = 04$	
Lagoonal depositional environment	Patch reef	$f = 03$	
	Open lagoon	$f = 02$	
	Restricted lagoon	$f = 01$	

The coloring of these twelve sedimentary facies enables the interpretation of well-marker associations in correlation panels by displaying colored rectangles along the well paths (Figure 5.1). The facies corresponding to the depositionally deepest condition (restricted lagoon,  $f = 01$ ) is coloured in blue, and the facies corresponding to the depositionally shallowest condition (fluvial channel,  $f = 12$ ) is coloured in red. In between, the facies are coloured using a blue to red through yellow shading, depending on their deposition condition.

## 5.1.2 Biostratigraphic interpretation

The Hugin Formation has been deposited during the Middle Jurassic (e.g., Kieft et al., 2010; Sneider et al., 1995). Biostratigraphic analyses have been performed on core samples and cuttings, and biozones have been interpreted along the seven wells (Figure 5.1). The biozones are intervals in which the depositional age has been confidently determined. Table 5.2 lists the six different biozones corresponding to Middle Jurassic deposition periods (from Early Bathonian to Late Callovian) which have been identified along the seven wells.

The coloring of these six biozones enables the comparison of well correlations with biostratigraphic interpretations in correlation panels by displaying bands between wells (Figure 5.1). The oldest interpreted biozone (Early Bathonian, B1) is coloured in dark blue, and the youngest interpreted biozone (Late Callovian, C3) is coloured in light blue. In between, the biozones are coloured using a blue shading, depending on their depositional age.

Table 5.2: Biozone indexing and coloring for correlation panel interpretation (ages based on the *International Chronostratigraphic Chart - May 2021*).

Numerical age (Ma)	Depositional age (Biozone)	Index	Color
$166.1 \pm 1.2$ to $163.5 \pm 1.0$	Late Callovian	C3	
	Middle Callovian	C2	
	Early Callovian	C1	
$168.3 \pm 1.3$ to $166.1 \pm 1.2$	Late Bathonian	B3	
	Middle Bathonian	B2	
	Early Bathonian	B1	

As discussed in Section 1.3.2, the biozones correspond to confident biostratigraphic interpretations. However, intervals between biozones are interpreted as uncertain biostratigraphic intervals. Sediment deposited within these intervals cannot have a depositional age which is younger (respectively older) than the youngest (respectively oldest) adjacent biozone, *i.e.*, these unassigned biostratigraphic intervals must not be crossed by correlation lines.

### 5.1.3 Relative well distality interpretation

Based on seismic imaging and sparse sediment transport directions measured in wells (*e.g.*, [Knaust et al., 2019](#)), the Middle Jurassic Hugin Formation in the Gudrun-Sigrun Field area appears as a faulted and highly diachronous unit ([Kieft et al., 2010](#); [Knaust and Hoth, 2021](#); [Sneider et al., 1995](#)). The top and bottom of the Middle Jurassic Hugin Formation are highlighted in seismic images by coal bed reflectors ([Hoth et al., 2018](#)). However, the three-dimensional internal geometry of the Hugin Formation cannot be interpreted from seismic data because of the low seismic resolution, and can only be determined from well data ([Knaust and Hoth, 2021](#)).

#### Scenario A: One single bay-head delta

*N.B.: The paleogeographic depositional context interpreted by [Knaust et al. \(2019\)](#) has been made before the drilling of wells 09 and 11. Therefore, it has been made without taking into consideration sedimentary facies, sediment transport direction and biostratigraphic interpretations along these two wells, and the interpretation of the normal fault in between.*

[Knaust et al. \(2019\)](#) propose a first interpretation of the paleogeographic Middle Jurassic Hugin Formation depositional context in the Gudrun-Sigrun Field area,

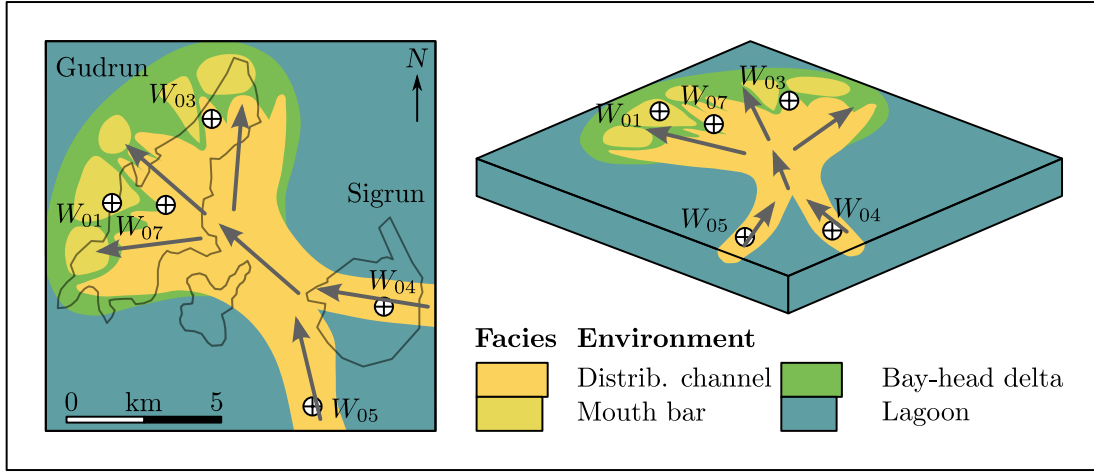


Figure 5.4: Middle Jurassic Hugin Formation paleogeographic depositional system interpretation of [Knaust et al. \(2019\)](#): a single bay-head delta prograding into a lagoonal depositional environment. (left) Plan view and (right) block diagram of the five wells in the Gudrun-Sigrun Field area (<http://www.npd.no>). Gray arrows represent the sediment transport directions, derived from dipmeter logs and borehole images, corresponding to the depositional system.

which corresponds to one single bay-head delta supplied from Southeast and prograding into a lagoonal environment (Figure 5.4).

In this first configuration, the relative distality of the five wells may be interpreted from the regional deltaic system. The sediment transport direction is defined along the distributary channel axis, *i.e.*, linearly in the fluvial zone, and radially in the deltaic zone (gray arrows in Figure 5.4). The relative distality of the five wells is given by

$$NW \quad \Leftarrow \quad \left( \begin{array}{ccccc} W_{01} & & & & W_{04} & \Leftarrow \\ & \Leftarrow & W_{07} & \Leftarrow & & \\ W_{03} & & & & W_{05} & \Leftarrow \end{array} \right) \quad SE, \quad (5.1)$$

where double arrows represent the hypothetical sediment transport direction from one well to another, and parentheses represent the different deltaic systems.

Wells 04 and 05 are assumed to belong to different distributary channels, making them having the same relative distality but disconnected from each other. The relative well distalities within this paleogeographic depositional system interpretation are given by

$$NW \quad \Leftarrow \quad \left( \begin{array}{ccccc} d_{01} = 1 & & & & d_{04} = 5 & \Leftarrow \\ & \Leftarrow & d_{07} = 2 & \Leftarrow & & \\ d_{03} = 1 & & & & d_{05} = 5 & \Leftarrow \end{array} \right) \quad SE, \quad (5.2)$$

where distality are integer values between  $d = 1$  and  $d = 5$ . Well 07 is geographically closer to wells 01 and 03 ( $d_{01} = d_{03} = 1$ ) than to wells 04 and 05 ( $d_{04} = d_{05} = 5$ ), therefore its distality is closer to wells 01's and 03's than to wells 04's and 05's, *i.e.*,  $d_{07} = 2$ .

### Scenario B: Several independent bay-head deltas

Based on the additional cored wells 09 and 11, along which additional data such as dipmeter data and revised biostratigraphic interpretation are acquired, [Knaust and Hoth \(2021\)](#) propose a new interpretation of the zone of interest. This new paleogeographic depositional environment interpretation is composed of two time-equivalent bay-head deltas supplied from two different directions on both sides of well 09 (Figure 5.5).

This interpretation is supported by regional seismic cross sections, which show a pronounced westward thickening of the Hugin Formation (*e.g.*, [Hoth et al., 2018](#); [Knaust and Hoth, 2021](#)). Moreover, additional biostratigraphic interpretations along wells 09 and 11 (Figure 5.1) highlight the diachronous behavior of the paralic Hugin Formation with decreasing age towards the East ([Knaust and Hoth, 2021](#)). According to biostratigraphic data, the Hugin Formation have been deposited in two different time-periods: Bathonian East and Callovian West of the Gudrun Øst fault Figure 5.1.

In this second configuration, the relative distality of the seven wells may be interpreted for each depositional time in the zone of interest considering that the sediment transport direction is defined within each deltaic system along the distributary channel axis. However, there is no biostratigraphic interpretation along well 03, and only the tops of wells 01 and 07 are biostratigraphically interpreted and correspond to Callovian deposits (Figure 5.1).

**Bathonian Hugin Formation paleogeography interpretation** (Figure 5.5). The depositional position of well 09 in the Bathonian Hugin Formation is interpreted as a bay-head delta, whereas the other wells along which the Bathonian biozone is interpreted (*i.e.*, wells 04 and 11) correspond to lagoonal depositional environment in the Hugin Formation (Figure 5.1). In this configuration, the relative distality of the seven wells is given by

$$NW \quad \begin{matrix} W_{03} \\ W_{07} \\ W_{01} \end{matrix} \quad \Leftarrow \quad \left( W_{09} \right) \quad \Rightarrow \quad \begin{matrix} W_{11} \\ W_{04} \\ W_{05} \end{matrix} \quad SE, \quad (5.3)$$

where the double arrows represent the sediment transport direction from one well

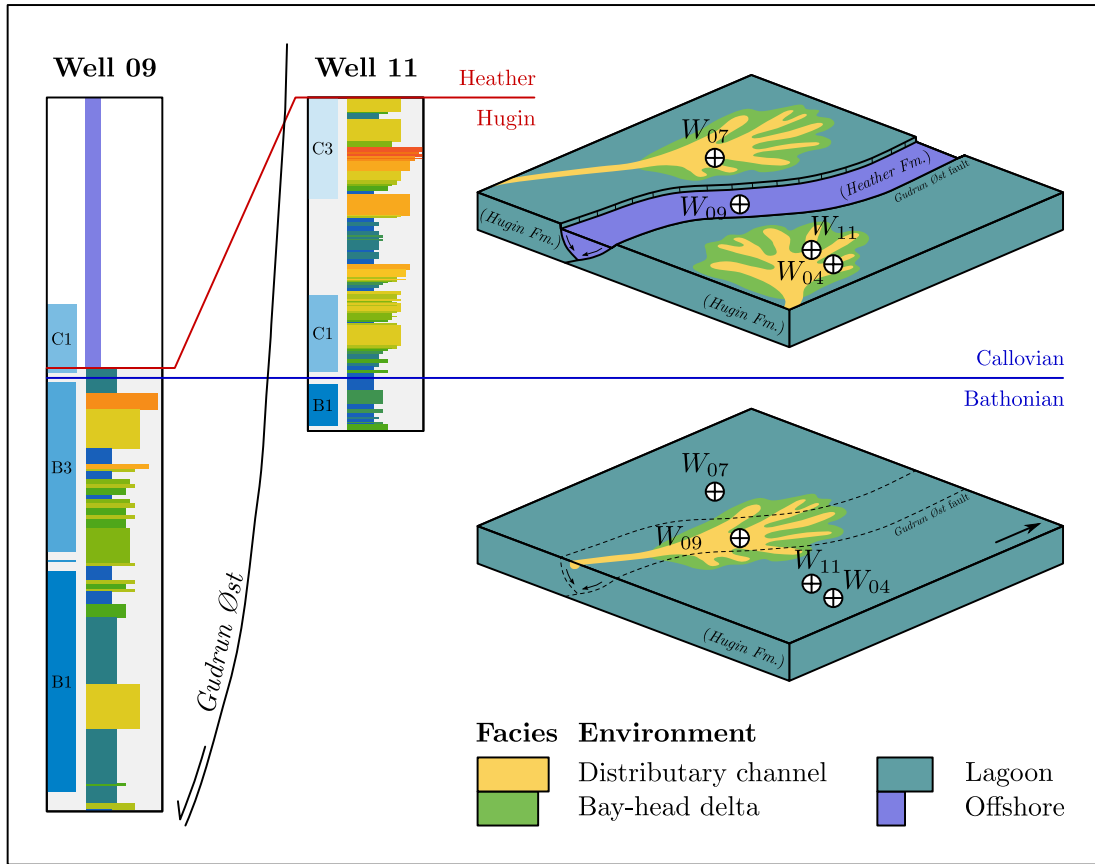


Figure 5.5: Middle Jurassic Hugin Formation paleogeographic depositional system interpretation of *Knaust and Hoth (2021)*: (Bathonian) a bay-head delta interpreted in well 09 prograding into a lagoonal depositional environment interpreted in wells 04 and 11, and (Callovian) several independent bay-head deltas in both sides of well 09. (left) wells 09 and 11 along which are interpreted the Bathonian and Callovian paleogeographic depositional systems, and (right) block diagrams of wells in the Gudrun-Sigrun Field area.

to an other, and parentheses represent the different deltaic systems. The relative well distalities within this paleogeographic depositional system interpretation are given by

$$\begin{array}{c}
 \text{NW} \\
 d_{03} = ? \\
 d_{07} = ? \\
 d_{01} = ?
 \end{array}
 \leftarrow
 \left(
 \begin{array}{c}
 d_{09} = 5
 \end{array}
 \right)
 \Rightarrow
 \begin{array}{c}
 d_{11} = 1 \\
 d_{04} = 1 \\
 d_{05} = ?
 \end{array}
 \text{SE}, \quad (5.4)$$

where gray well distalities are not very confident because of the lack of Bathonian biostratigraphic interpretations. Indeed, there is no biostratigraphic information about well 03 and well 05 does not penetrate the Bathonian Hugin Formation (only Callovian deposits). Finally, the upper part of wells 01 and 07 are interpreted as Callovian deposits. In this configuration, the relative distality of these gray wells in the Bathonian Hugin Formation is not defined.

**Callovian Hugin Formation paleogeography interpretation** (Figure 5.5). Sedimentary facies interpreted along well 09 in the Callovian Hugin Formation correspond to offshore deposits, whereas the other wells along which the Callovian biozone is interpreted correspond to deltaic environment in the Hugin Formation Figures 5.1 and 5.5. In this configuration, the relative distality of the seven wells is given by

$$NW \left( \begin{array}{c} W_{03} \\ W_{07} \\ W_{01} \end{array} \right) \Rightarrow W_{09} \Leftarrow \left( \begin{array}{c} W_{11} \Leftarrow \\ W_{04} \\ W_{05} \end{array} \right) SE, \quad (5.5)$$

where the double arrows represent the sediment transport direction from one well to an other, and parentheses represent the different deltaic systems.

Wells 04 and 07 have a similar position within the two separated deltas making them having the same relative distality but they should not be connected. The relative distalities within this depositional system are given by

$$NW \left( \begin{array}{c} d_{03} = 3 \\ d_{07} = 3 \\ d_{01} = 3 \end{array} \right) \Rightarrow d_{09} = 1 \Leftarrow \left( \begin{array}{c} d_{11} = 4 \Leftarrow \\ d_{04} = 5 \\ d_{05} = 5 \end{array} \right) SE, \quad (5.6)$$

where gray well position are not very confident because of the lack of Callovian biostratigraphic interpretations. Indeed, there is no biostratigraphic information about well 03. However, wells 01, 03 and 07 have similar sedimentary facies, which mainly correspond to deltas prograding into lagoonal environments (Figure 5.1). Moreover, the upper part of wells 01 and 07 corresponds to Callovian deposits. In this configuration, deposits recorded along these three wells may belong to the same Callovian depositional system and their distality ( $d = 3$ ) is approximately chosen between a lagoonal depositional environment ( $d = 1$ ) and a proximal depositional environment ( $d = 5$ ).

## 5.2 Application of the distality rule of correlation

The correlation rule based on the sedimentary facies and relative well distality defined in Chapter 3 follows the principle of correlation stating that “a well marker (described by facies and distality taken at the center of an interval having a constant facies and a constant distality) cannot be correlated with another well marker described by a positionally deeper facies at a more proximal position, or a positionally shallower facies at a more distal position” (i.e., Walther’s law of

the correlation of facies, in a broader sense). This principle is applied to evaluate the likelihood of the proposed depositional systems according to the consistency of the generated well correlations.

### 5.2.1 Scenario A: One single bay-head delta

[Knaust et al. \(2019\)](#) interpret the depositional system of the Hugin Formation in the Gudrun-Sigrun Field area as a single bay-head delta supplied from the Southeast. Sedimentary facies are displayed along the seven wells in [Figure 5.1](#) and [Equation \(5.3\)](#) describes the relative well distalities of the seven wells.

However, the integration of wells 09 and 11 in the database makes the scenario A not conformable with the principle of correlation. Indeed, facies at the top of well 09 (open lagoon in the Hugin Formation and offshore facies in the Heather Formation; see [Figure 5.5](#)), cannot be correlated with the facies at the top of well 07 (mouth bar) according to their relative distality within the depositional system ([Equations \(5.1\) and \(5.2\)](#)). The same problem is observed between facies at the bottom of wells 07 and 09 ([Figure 5.1](#)).

In this scenario, the correlation cost function proposed in [Chapter 3](#) cannot compute a correlation cost and returns no correlation set. This rule is very strict and excludes impossible well-marker correlations according to their sedimentary facies and their relative well distality ([Equation \(3.14\)](#)). The relative distality assigned to the wells in scenario A leads to non-conformable well chronostratigraphic correlation.

### 5.2.2 Scenario B: Several independent bay-head deltas

[Knaust and Hoth \(2021\)](#) interpret the depositional system of the Middle Jurassic Hugin Formation in the Gudrun-Sigrun Field area as several independent bay-head deltas supplied from two different directions and separated by a lagoonal depositional environment. Sedimentary facies are displayed along the seven wells in [Figure 5.1](#), and [Equations \(5.4\) and \(5.6\)](#) describe the relative well distalities of the seven wells in the Bathonian and the Callovian Hugin Formation.

Unlike the scenario A, scenario B proposed by [Knaust and Hoth \(2021\)](#) is conformable with the principle of correlation defined in [Chapter 3](#). In this case, the correlation cost function may be applied on the entire data set. However, as illustrated in [Figure 5.5](#), the Middle Jurassic Hugin Formation is diachronous in the Gudrun-Sigrun Field area:

- The Bathonian Hugin Formation paleogeography corresponds to a delta (interpreted in well 09) prograding into a lagoonal depositional environment (interpreted in wells 04 and 11).
- The Callovian Hugin Formation paleogeography corresponds to two independent deltas (wells 01, 03 and 07 to the Northwest, and wells 04, 05 and 11 to the Southeast) prograding into a lagoonal depositional environments in both sides of the Heather Formation interpreted as offshore deposits in well 09.

In both depositional periods, there are two independent groups of wells in both sides of well 09: (1) the correlation cost function is first applied to the southeast group of wells (wells 04, 05 and 11; see Figure 5.6), (2) the correlation cost function is then applied to the northwest group of wells (wells 01, 03 and 07; see Figure 5.7), and (3) the correlation cost function is finally applied to wells 07, 09 and 11 in order to evaluate the correlations between these three wells belonging to different depositional systems (Figure 5.8).

#### 5.2.2.1 Southeast bay-head delta

Wells 04 and 11 are very close (approximately 1 km) and the well correlation between these two wells can be computed thanks to the consistency of the sedimentary facies interpretations with respect to the relative well distalities. Additionally, the outcome is very consistent with respect to the biostratigraphic interpretations. Indeed there no correlation line which crosses a biostratigraphic interval (Figure 5.6). This outcome supports the hypothesis stating that these two wells belong to a lagoonal depositional environment during the Bathonian, and to the same delta during, in which well 11 is a bit more distal than well 04, during the Callovian.

However, wells 05 and 11 are more distant than wells 04 and 11 (approximately 4 km), and between the latter two wells, the outcome returns more gaps (one facies correlated with a group of facies). Moreover, well marker correlations (between wells 05 and 11) are consistent with respect to the biostratigraphic interpretations, *i.e.*, few correlation lines which correlate Middle Callovian deposits (C2) with Early Callovian deposits (C1) (Figure 5.6).

Consequently, the application of the correlation cost function on these three wells supports the hypothesis stating that they belong to the same depositional system, even if the correlation between wells 05 and 11 is less consistent than between wells 04 and 11.

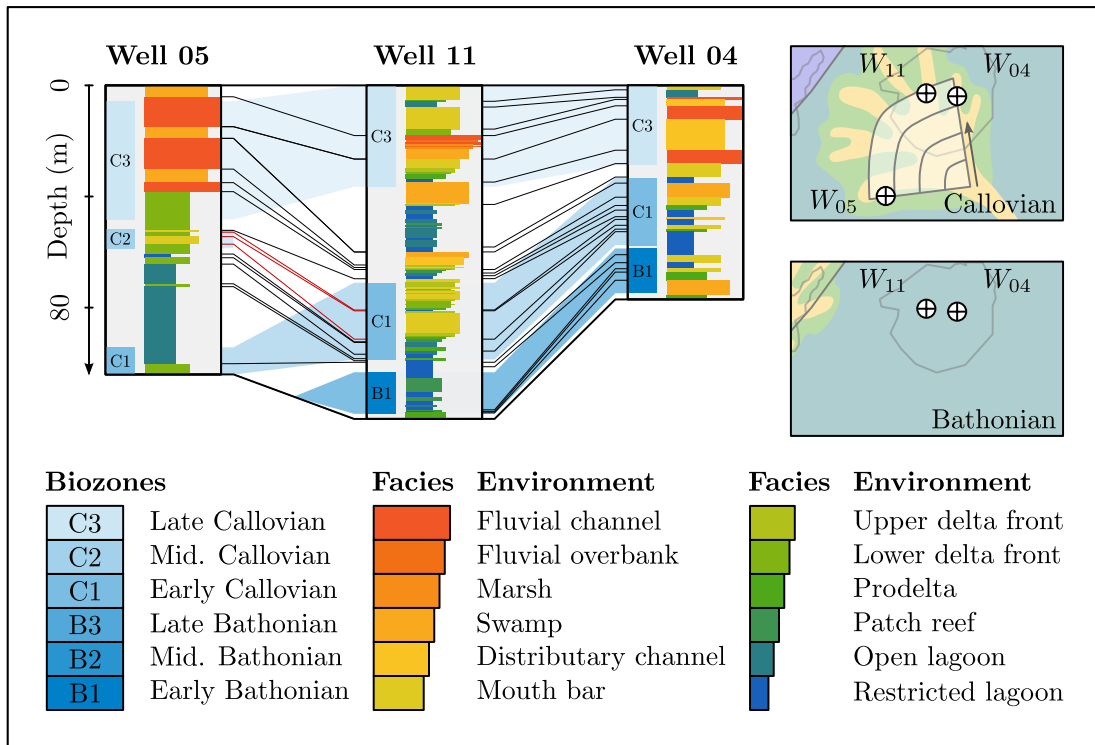


Figure 5.6: Computer-assisted chronostratigraphic correlation computed between wells 04, 05 and 11 using the distality rule of correlation defined in Chapter 3. The relative well distalities correspond to the scenario B (Figure 5.5 and Equations (5.4) and (5.6)). Bathonian: wells 04 and 11 are distal ( $d_{04} = d_{11} = 1$ ). Callovian: well 04 (and  $d = 5$  Callovian) is more proximal than well 11 ( $d = 3$ ), and well 05 ( $d = 5$ ) is a bit more off-axis of the system. Red correlation lines are inconsistent with respect to the biozones.

### 5.2.2.2 Northwest bay-head delta

The relative well distality of the three wells belonging to the Northwest bay-head delta is constant and the same in the three wells ( $d = 3$ ). In this configuration, the distality rule of correlation returns lithostratigraphic well correlations. However, the similarity of the facies interpretations along wells 01 and 07, whose distance is approximately 2 km, is not inconsistent with the use of lithostratigraphic well correlation. Moreover, the application of the distality rule of correlation is not inconsistent with respect to the biostratigraphic interpretations, i.e., even without that much biostratigraphic interpretations, there is no biostratigraphic interval crossed by correlation lines and well markers belonging to a biozone are not correlated with well markers belonging to an other biozone (Figure 5.7).

This outcome does not discard the hypothesis stating that these two wells belong to the same delta and that wells have approximately the same distality. There is no biostratigraphic interpretations along well 03, so the correlation lines between wells 03 and 07 cannot be discussed with respect to the biostratigraphy.

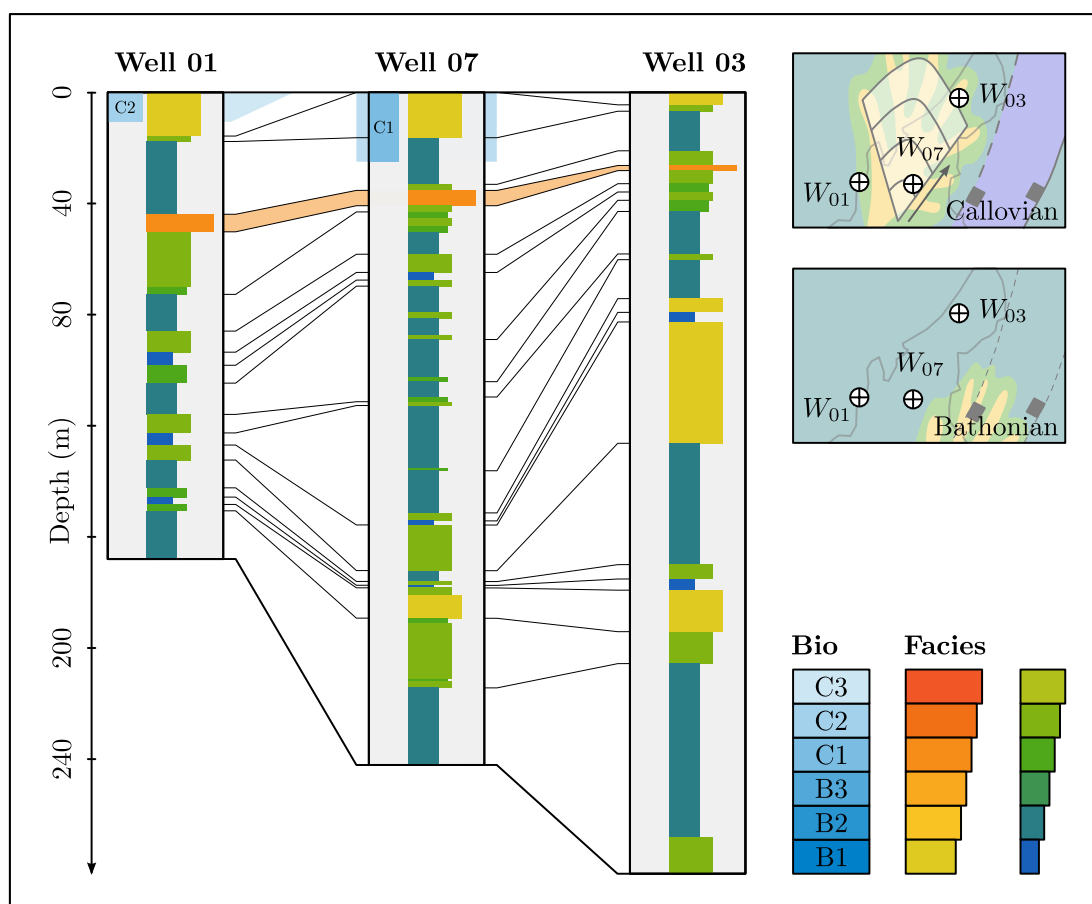


Figure 5.7: Computer-assisted chronostratigraphic correlation computed between wells 01, 03 and 07 using the distality rule of correlation defined in Chapter 3. The relative well distalities correspond to the scenario B (Figure 5.5 and Equations (5.4) and (5.6)). Bathonian: No information given by biostratigraphic interpretation. Callovian: Wells 01 and 07 correspond to delta and have approximately the same relative distality ( $d_{01} = d_{07} = 3$ ) and there is no biostratigraphic interpretation along the well 03, but it mainly corresponds to deltaic depositional environments ( $d_0 =$ ).

Moreover, thin coal beds are interpreted in the three wells and the correlation cost function highlights this coal bed by correlating three coal beds together (orange correlation band in Figure 5.7). This correlation band between the three wells is consistent with the seismic interpretation, because the top of the Middle Jurassic Hugin Formation in the Gudrun-Sigrun Field area is characterized by continuous thin coal beds (Hoth et al., 2018; Knaust and Hoth, 2021; Styán and Bustin, 1983). However, there is no certainty about the time-equivalence of these coal beds (e.g., Knaust and Hoth, 2021).

Consequently, the application of the correlation cost function on these three wells does not disprove the hypothesis stating that they belong to the same delta, even if these correlations are not as confident as possible because of the lack of

biostratigraphic interpretations in these three wells.

*N.B.: If the relative well distality variation between wells 01 and 07 was the same in this configuration than in the scenario A, i.e.,  $d_{01} < d_{07}$ , the stratigraphic well correlation generated by the distality rule of correlation would have been very similar to Figure 5.7 because of the presence of one mouth bar and one coal bed in the two wells. Indeed, in order to satisfy the principle of correlation proposed in Chapter 3, the mouth bar in well 01 would have been correlated to the mouth bar in well 07, the coal bed in well 01 would have been correlated to the coal bed in well 07, and restricted lagoons in well 07 would have been correlated to restricted lagoons in well 01.*

### 5.2.2.3 Bay-head deltas and lagoonal environments

The scenario B is based on the hypothesis stating that well 09 corresponds to deltaic depositional conditions in the Bathonian ( $d_{09} = 5$ ), and to offshore depositional conditions in the Callovian ( $d_{09} = 1$ ). In both depositional periods, it does not belong to the same depositional systems as the other wells in the Gudrun-Sigrun Field area (Figure 5.5). In this scenario, wells 04, 05 and 11 belong to one Callovian delta on the Southeast of well 09, and wells 01, 03 and 07 belong to another Callovian delta on the West of well 09. In order to evaluate the consistency of this scenario, well 09 is correlated with the two closest wells from the two other deltas, i.e., well 11 in the Southeast and well 07 in the Northwest (Figure 5.8).

Biostratigraphic interpretations are poor in well 07, and biozones are not similar in wells 09 and 11. Indeed, the main part of the well 09 correspond to Bathonian deposits, whereas the main part of the well 11 corresponds to Callovian deposits, and only the bottom of well 11 corresponds to Early Bathonian deposits. Moreover, the Middle to Late Bathonian depositional period is missing in well 11.

The diachronous behavior of the Hugin Formation is highlighted in wells 09 and 11 (Figure 5.5). However, the definition of various well distalities in the Bathonian and Callovian and the application of the distality rule of correlation returns promising outcomes which honor Early Bathonian interpretation (B1) (Figure 5.8).

The correlation between wells 07, 09 and 11 generates few gaps, and the correlation lines are not entirely inconsistent with respect to the biostratigraphic interpretations. Indeed, only the upper part of well 09 (Middle to Late Bathonian) is correlated with the upper part of well 11 (Callovian).

Finally, the global consistency of results with respect to biostratigraphic interpre-

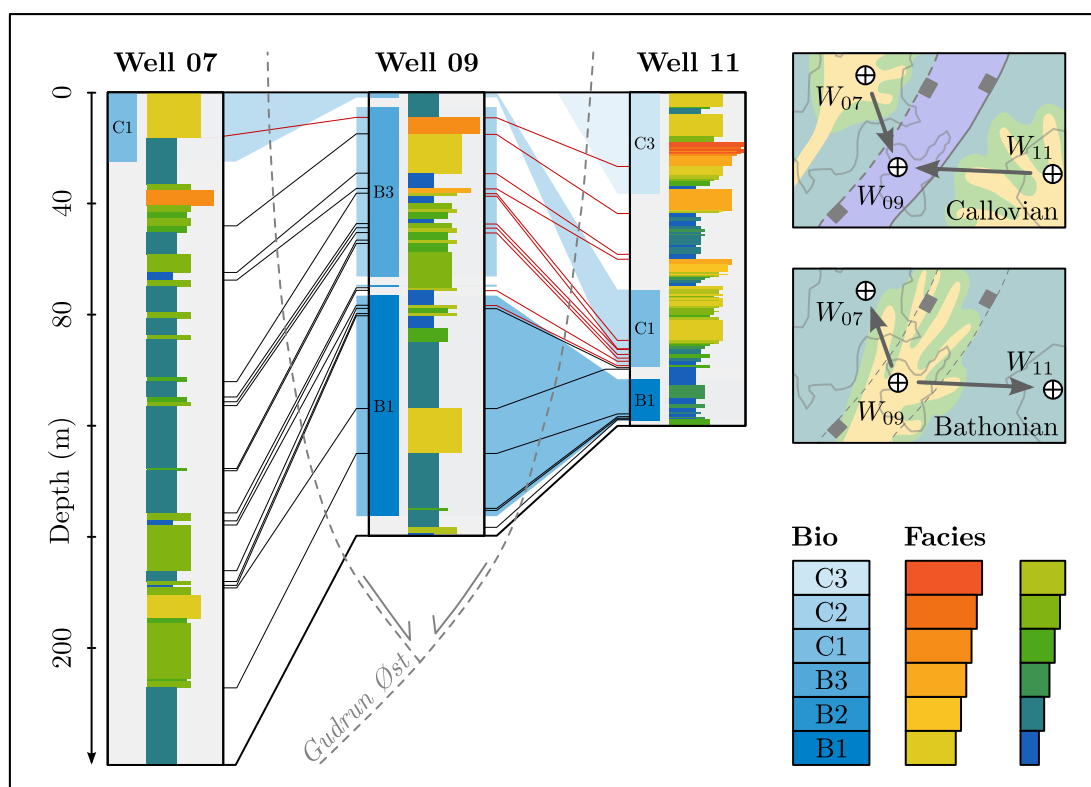


*Figure 5.8: Computer-assisted chronostratigraphic correlation computed between wells 07, 09 and 11 using the distality rule of correlation defined in Chapter 3. The relative well distalities correspond to the scenario B (Figure 5.5 and Equations (5.4) and (5.6)). Bathonian: well 11 ( $d_{11} = 1$ ) is more distal than well 09 ( $d_{09} = 5$ ). Callovian: wells 07 and 11 have approximately the same distality ( $d_{07} = 3$  and  $d_{11} = 4$ ) and are more proximal than well 09 ( $d_{09} = 1$ ). Red correlation lines are inconsistent with respect to the biozones.*

tations is consistent with the hypothesis stating that the three wells do not belong to the same chronostratigraphic depositional system and that the correlation cost function proposed in Chapter 3 can be applied to generate a chronostratigraphic model of the subsurface between these three wells (Chapter 6).

## Conclusion

The correlation cost function proposed in Chapter 3 has been applied to the Middle Jurassic Hugin Formation in the Gudrun-Sigrun Field area in order to evaluate the consistency of two possible paleogeographic depositional system interpretations:

- A. A single bay-head delta supplied from the Southeast prograding into a lagoonal depositional environment (Figure 5.4) (Knaust et al., 2019). In this

configuration, all the wells belong to the same delta.

- B. Several independent bay-head deltas supplied from different directions prograding into a lagoonal depositional environment (Knaust and Hoth, 2021). In this latter scenario, during the Bathonian, the well 09 corresponds to a bay-head delta prograding into a lagoonal depositional environment interpreted in wells 04 and 11, and during the Callovian, wells 01, 03 and 07 belong to one delta, wells 04, 05 and 11 belong to another delta, and in between well 09 represents the most marine depositional system being deposited at the same period (Knaust and Hoth, 2021) (Figure 5.5).

The application of the correlation cost function proposed in Chapter 3 does not support and rejects the scenario A because of the unconformity of the sedimentary facies at the top of the wells with respect to their relative distalities. On the other hand, it does not discard the scenario B and supports it thanks to the consistency of the well correlation with respect to the biostratigraphic interpretations (Figures 5.6 to 5.8).



# Chapter 6

## Middle Jurassic Hugin Formation: Subsurface modeling

### Contents

---

<b>6.1</b>	<b>Zone of interest: Sigrun Field area . . . . .</b>	<b>141</b>
<b>6.2</b>	<b>Application of the distality rule of correlation . . . . .</b>	<b>142</b>
6.2.1	Lithostratigraphic subsurface model simulation . . . . .	144
6.2.2	Chronostratigraphic subsurface model simulation . . . . .	146
6.2.3	Impact of the sedimentary facies clustering . . . . .	150
<b>6.3</b>	<b>Discussion . . . . .</b>	<b>156</b>
6.3.1	Principal sediment transport direction . . . . .	156
6.3.2	Size of the system with respect to well spacing . . . . .	157
6.3.3	Sedimentary facies clustering . . . . .	158
6.3.4	Minor changes in the correlation cost . . . . .	159
6.3.5	Additional principles of correlation . . . . .	159

---

The purpose of this chapter is to apply the distality rule of correlation proposed in Chapter 3 to Wells 04 and 11 in the Early Callovian Hugin Formation in the Sigrun Field area (Section 6.1). This approach produces consistent stratigraphic well correlations, and highlights the sensitivity of the solution to the facies zonation and to the relative well distality.

*N.B.: This chapter contains paragraphs which are modified or partially/entirely taken from [Baville et al. \(2022\)](#).*

## **Abstract**

*The distality rule of correlation reflects prior knowledge about sediment transport directions (Chapter 3), and it is tested on Wells 04 and 11 penetrating the Middle Jurassic Hugin Formation in the Sigrun Field area. Well markers are described by two parameters: (1) the sedimentary facies corresponding to a depositional environment, and (2) the relative distality of the well computed from its position along the sediment transport direction. The main principle of correlation used in this chapter assumes that a well marker (described by a facies and a distality) cannot be correlated with another well marker described by a positionally deeper facies at a more proximal position, or a positionally shallower facies at a more distal position. This approach produces promising stratigraphic well correlations, and highlights the sensitivity of the solution to the facies zonation and to the relative well distality. Therefore, the proposed rule offers a way to coherently consider chronostratigraphic correlation and the associated uncertainties at the parasequence scale, i.e., at a smaller scale than generally considered in deterministic correlation.*

## **Introduction**

The distality rule of correlation defined in Chapter 3 for computing the likelihood of a well-marker correlation from sedimentary facies and well distality yields promising results on simple synthetic data sets. It has also been applied to a large data set composed of seven wells drilled in the Middle Jurassic Hugin Formation in the Gudrun-Sigrun Field area (Block 15/3) (Hoth et al., 2018; Kieft et al., 2010; Knaust and Hoth, 2021; Sneider et al., 1995) to compare two regional depositional contexts interpretations proposed by Knaust et al. (2019) and Knaust and Hoth (2021) with biostratigraphic data (Chapter 5).

The application of the distality rule of correlation has supported the paleogeographic interpretation of the Middle Jurassic Hugin Formation in the Gudrun-Sigrun Field area proposed by Knaust and Hoth (2021) as two independent bay-head deltas supplied from two different directions prograding into a lagoonal depositional environment (Figure 5.4).

Considering this paleogeographic interpretation (Section 5.2.2), the purpose of this chapter is to use the distality rule of correlation to simulate likely subsurface stratigraphic models from well data and to assess the stratigraphic uncertainties. The area of interest is the Early Callovian section of two wells from the Middle Jurassic Hugin Formation in the Sigrun Field area, i.e., Wells 04 and 11 (Figure 6.1).

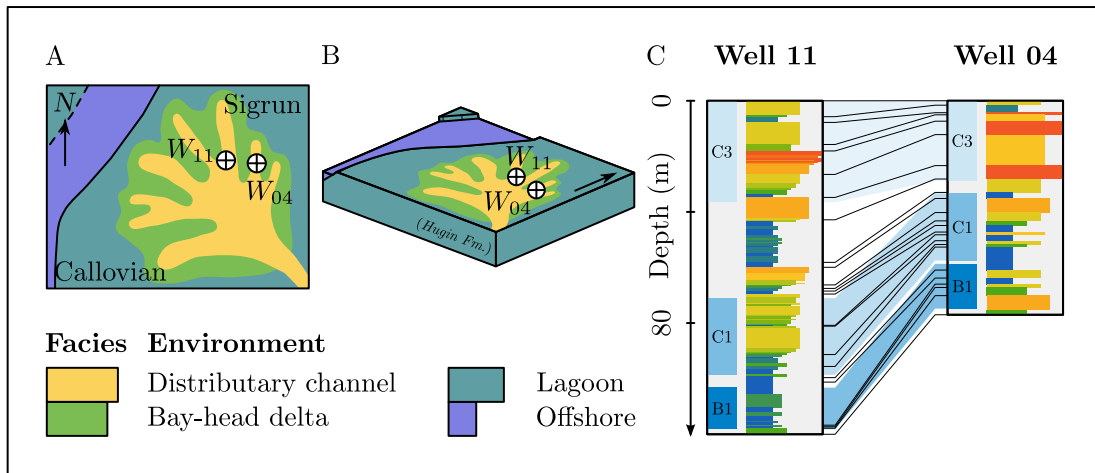


Figure 6.1: (A) Map view and (B) block diagram of the Sigrun Field area (Block 15/3), and spatial location of wells 04 and 11 in the Callovian Hugoin Formation (Maps based on <http://www.npd.no>). (C) Stratigraphic correlation between wells 04 and 11 generated by the distality rule of correlation defined in Chapter 3 (Section 5.2.2.3).

The first objective of the distality rule of correlation is to simulate stratigraphic subsurface models from sedimentary facies and well distalities (Sections 6.2.1 and 6.2.2). The second objective of this application is to evaluate the impact of the sedimentary facies and well distality interpretation on the subsurface stratigraphic models by using different groups of sedimentary facies (Section 6.2.3).

## 6.1 Zone of interest: Sigrun Field area

Based on dipmeter data analysis and biostratigraphic interpretation, the Hugoin Formation in the Gudrun-Sigrun Field area appears as a faulted and a highly diachronous unit (Kieft et al., 2010; Knaust and Hoth, 2021; Sneider et al., 1995). However, Wells 04 and 11 are about one kilometer apart one from another, no major fault occurs in between and the well data belong to an interval of roughly the same age based on biostratigraphic interpretations (Knaust and Hoth, 2021).

The top and bottom of the Hugoin Formation are marked in seismic images by coal bed reflectors (Hoth et al., 2018). However, the three-dimensional internal geometry of the Hugoin Formation cannot be interpreted from seismic data because of the limited seismic resolution, and can only be determined from well data (Knaust and Hoth, 2021).

As described in Appendix A, sedimentary facies have been interpreted from partly cored wells in the Gudrun-Sigrun Field area. The two wells of Early Callovian age contain eight sedimentary facies (Figure 6.2), as interpreted by Knaust and

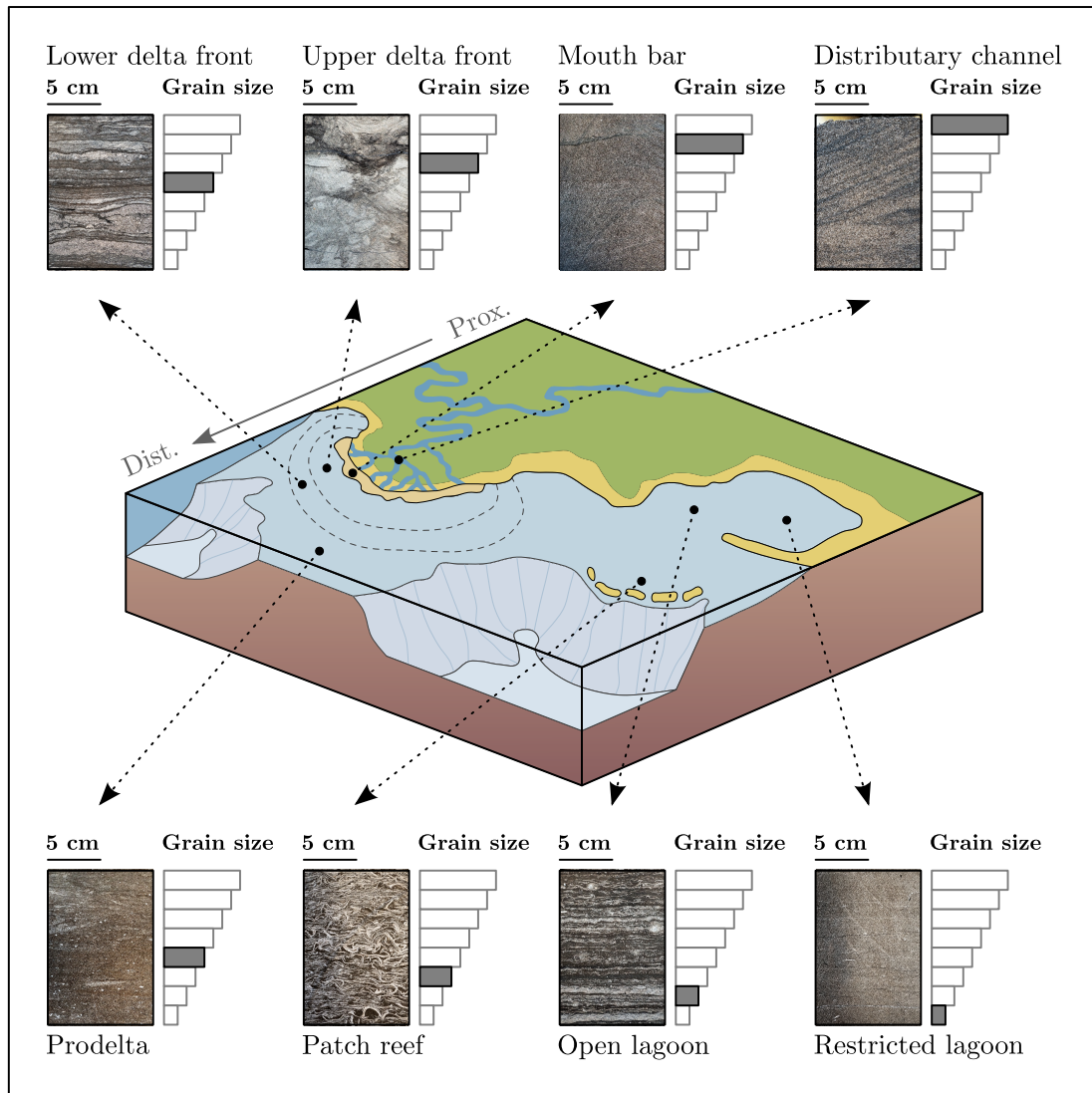


Figure 6.2: Eight sedimentary facies interpreted by [Knaust and Hoth \(2021\)](#) from core samples of the Early Callovian Hugin Formation in the Sigrun Field area. Sedimentary facies are described in Appendix A. Redrawn from ([Baville et al., 2022](#)).

[Hoth \(2021\)](#) (Appendix A) and digitalized to compute well-marker correlation costs using Equations (3.3) and (3.15) (Table 5.1).

## 6.2 Application of the distality rule of correlation

Wells 04 and 11 (Gudrun-Sigrun Field area) are fully cored in the base of the Hugin Formation. Biostratigraphic analyses have been performed and have confirmed that the lower part of the Hugin Formation in both wells belong to the same biozone, *i.e.*, Early Callovian (Figure 6.3).

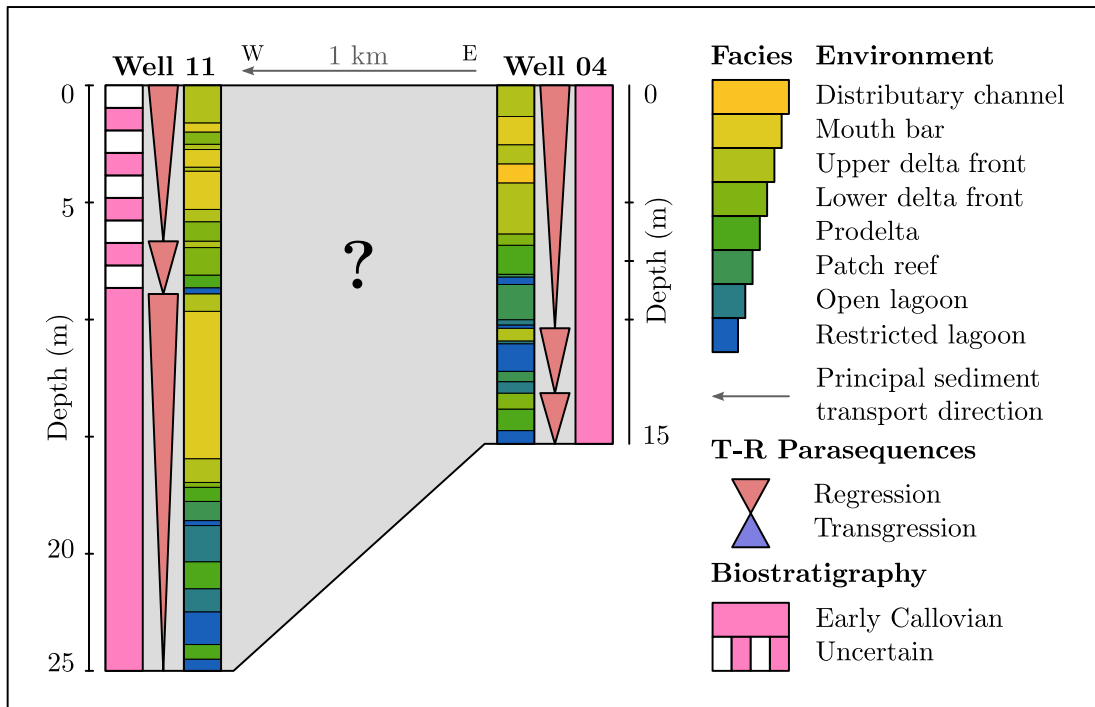


Figure 6.3: Sedimentary facies, parasequence and biostratigraphic interpretation of Wells 04 and 11 in the lower part of the Hugin Formation in the Sigrun Field area. Redrawn from [Baville et al. \(2022\)](#).

[Knaust and Hoth \(2021\)](#) propose that deposits in Wells 04 and 11 were part of the same bay-head delta supplied with Early Callovian sediments from East to Southeast. The application of the distality rule of correlation on a large data set supports this hypothesis (Chapter 5). Well 11 is referred to as the distal well because of its western position and well 04 is referred to as the proximal well because of its eastern position, in relation to an assumed direction of deposition from roughly East to West (Figure 6.2).

In both wells, the relative distality is considered constant along the entire well path, *i.e.*,  $d_{W11}(i) = 1$  and  $d_{W04}(j) = 2$  in Equation (3.9). This assumption is based on a stable direction of sediment transport during the considered time interval, which is supported by dipmeter data ([Knaust and Hoth, 2021](#)).

Additionally, transgressive and regressive parasequences (T-R parasequences) were interpreted along these two wells. These parasequences are supported by biostratigraphic interpretation and by the identification of major marine flooding events characterized by reworked sediments and scattered pebbles above these ravinement surfaces ([Knaust and Hoth, 2021](#)).

However, it is important to note that no absolute evidence exists about how these regressive sequences are correlated between both wells, essentially because they are interpreted below the biostratigraphic resolution (*cf.* the difference be-

tween absolute and relative chronostratigraphy in Section 1.2.3). The deepest parasequence identified in well 11 and the shallowest parasequence identified in well 04 (Figure 6.3) were analyzed by Knaust and Hoth (2021) and dipmeter data acquired in these parasequences suggest a sediment transport direction towards West-Southwest.

Applying computer-assisted correlations on this data set involves computing a correlation cost  $c$  for each possible well-marker correlation. First, a correlation cost minimizing the facies variation is computed from the interpreted well markers using Equation (3.16), corresponding to lithostratigraphic correlation (Section 6.2.1). Then, the distality correlation cost function is applied on the data using Equation (3.17) (Section 6.2.2), and on three different facies associations defined in Section 6.2.3.

### 6.2.1 Lithostratigraphic subsurface model simulation

The first scenario considers the principle of lithostratigraphy (Section 1.2.3) to generate stratigraphic well correlations, *i.e.*, well markers are preferentially correlated if sedimentary facies are similar. In order to minimize the sedimentary facies variation (e.g., Hale, 2013), the well distality  $\Delta d$  is not taken into account, *i.e.*, the correlation cost function is given by Equation (3.16). In this configuration, the outcomes correspond to lithostratigraphic well correlation sets (Figure 6.4).

Figure 6.4.A plots the best correlation set computed with Equation (3.16), *i.e.*, the correlation set having the lowest cumulative correlation cost ( $cost = 2.39$ ). These outcomes are computed considering that both wells have the same distality, and corresponds to a lithostratigraphic well correlation. Figure 6.4.B plots the correlation path of the best correlation set within the correlation cost matrix (black line). As expected, the correlation path goes through cells with the lowest costs (*i.e.*, the most likely well-marker correlations) and generally avoid cells having the largest costs (*i.e.*, the less likely well-marker correlations).

Following lithostratigraphic principle of correlation, the simulation outcome highlights inconsistent well-marker correlations which are inconsistent with the distality rule of correlation (red correlation bands on Figure 6.4.A). For example, a well marker interpreted as a patch reef sedimentary facies in well 11 (between 17.7 m and 18.59 m) is correlated with a well marker interpreted as an open lagoon in well 04 (between 10.91 m and 11.03 m). These inconsistent well-marker correlations contradict the principle of correlation formulated in Chapter 3.

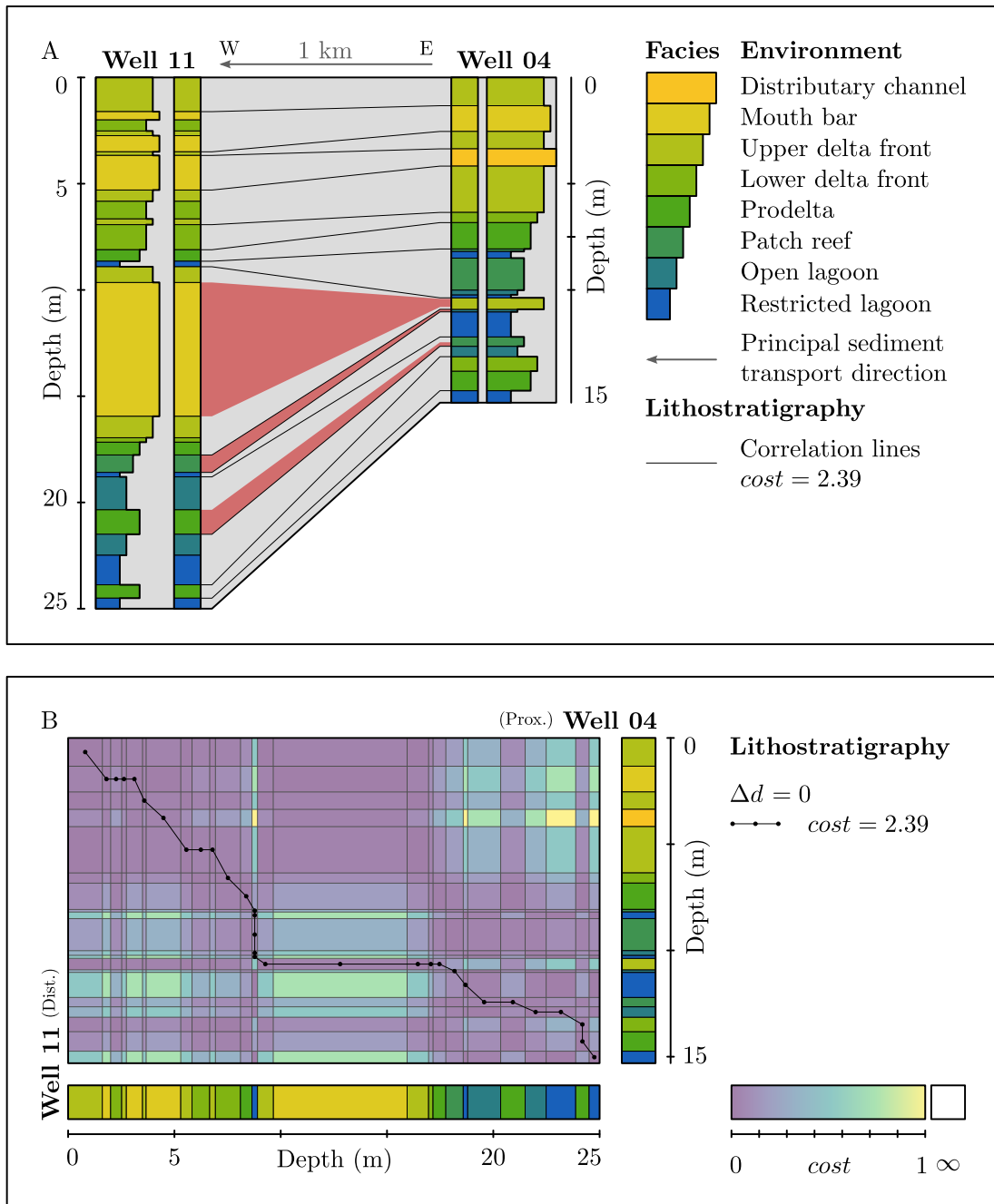


Figure 6.4: (A) Correlation panel. Black lines correspond to the best correlation set computed by Equation (3.16) (i.e., lithostratigraphic well correlation). Red bands highlight well-marker correlations which are inconsistent with the distality interpreted in both wells. (B) Correlation cost matrix. The black line corresponds to the correlation path of the best correlation set minimizing the facies variation  $\Delta f$ . Cells are colored by the correlation cost computed by Equation (3.16). Modified from (Baville et al., 2022).

## 6.2.2 Chronostratigraphic subsurface model simulation

As discussed in Section 6.2.1, well correlations computed by minimizing the sedimentary facies variation did not return convincing outcomes according to the principle of correlation (Chapter 3). Indeed, lithostratigraphic concepts do not, in general, yield isochronous stratigraphic surfaces (Section 1.2.3). Using Equations (3.14) and (3.15) to account for distality significantly changes the correlation outcomes as illustrated in Figure 6.5.A.

The correlation panel illustrated in Figure 6.5.A eases the comparison between the result of the two most likely correlation sets among the  $n$ -most likely scenarios computed by the lithostratigraphic cost function given by Equation (3.16) (dashed red lines) and the distality correlation rule given by Equations (3.14) and (3.15) (full black lines).

Green correlation bands highlight that well markers which were inconsistently correlated using the sedimentary facies variation minimization (red correlation bands in Figure 6.4) are now consistently correlated using the proposed correlation cost function. This consistency is ensured by the cost function given by Equation (3.14), which excludes impossible well-marker correlations.

Moreover, several facies in one well are correlated with only one facies in the other well: the computer-assisted correlation process generates a gap due to erosion or non-deposition. The depths of these gaps are not defined *a priori* by the algorithm which only considers a gap cost penalty for each transition, so they emerge from the method in order to maximize the correlation set likelihood. However, if the number of well markers in the wells are different, multiple correlations to one single marker must occur, and gaps must be simulated.

Figure 6.5.B plots the correlation path of the best correlation set within the correlation cost matrix (black line). This matrix highlights that a high number of well-marker correlations are excluded thanks to the principle of correlation implemented by Equation (3.14). Indeed, an infinite correlation cost means that the well-marker correlation is not consistent with respect to the principle of correlation.

For example, the large mouth bar observed in well 11 (between 9.75 m and 15.95 m) can only be associated with mouth bars (between 1.33 m and 2.54 m) and distributary channels (between 3.36 m and 4.17 m) in the more proximal well 04. The principle of correlation constrains the computer-assisted well-correlation process and generates only admissible scenarios.

Additionally, the correlation cost matrix enables the comparison between two principles of correlation. Indeed, Figure 6.5.B plots the best correlation simulated

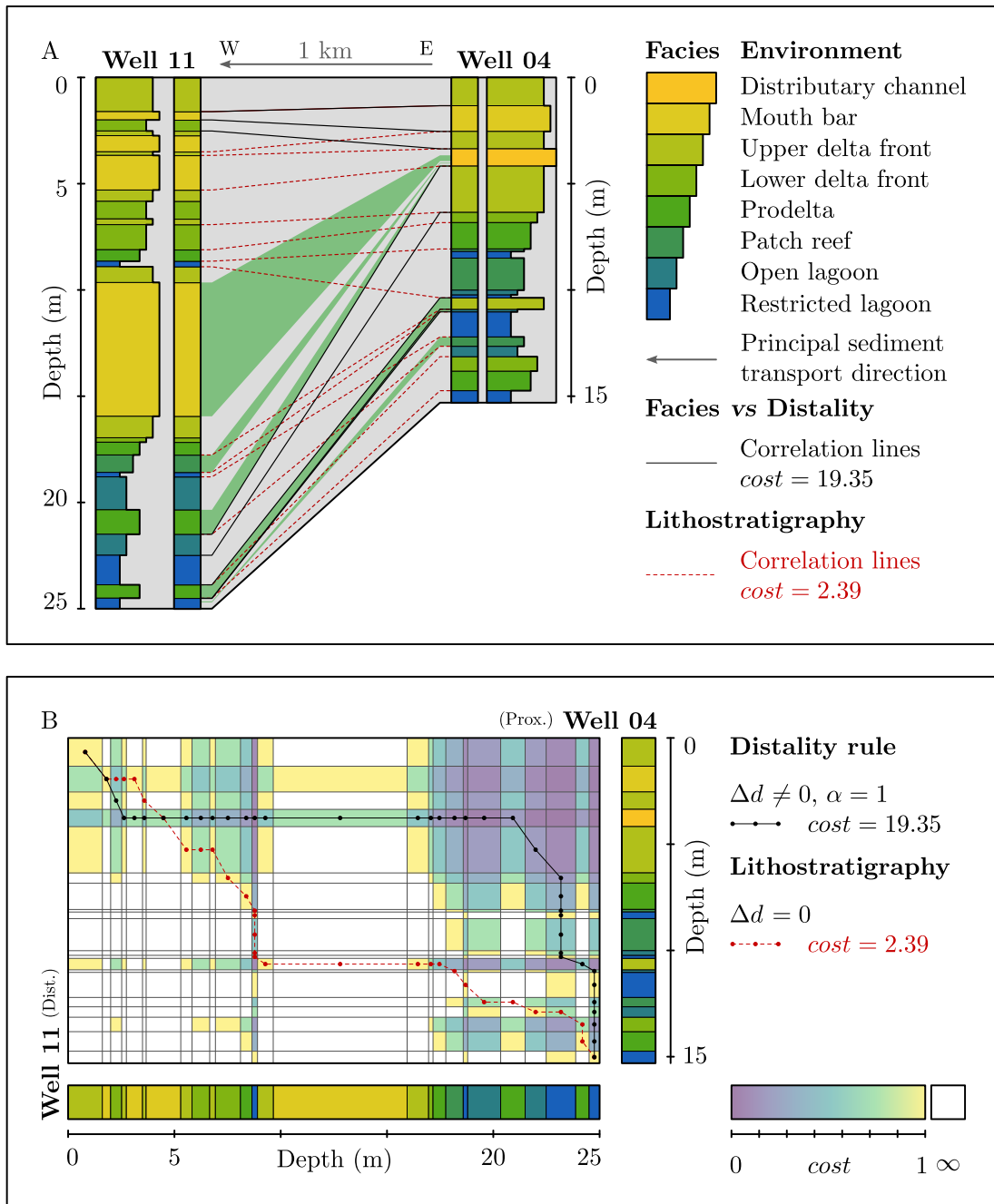


Figure 6.5: (A) Correlation panel. Black lines (respectively dashed red lines) correspond to the best correlation set computed by Equation (3.17) (respectively using Equation (3.16)). Green bands highlight well-marker correlations which were inconsistent using the variation minimization and which are consistent using the distality rule of correlation. (B) Correlation cost matrix. Black line (respectively dashed red line) corresponds to the correlation path of the best correlation computed by the distality rule of correlation (respectively the variation minimization). Cells are colored by the correlation cost computed by Equation (3.17). Modified from (Baville et al., 2022).

using lithostratigraphic well correlation (dashed red correlation path) overlaid on the correlation cost matrix corresponding to the distality correlation cost. The lithostratigraphic correlation path passes three times through white cells (impossible well-marker correlation) which correspond to the three red correlation bands in Figure 6.4.A.

In the correlation cost matrix, correlation sets are represented by their correlation paths, and each bullet corresponds to each well-marker correlation belonging to these correlation sets. It is possible to display several scenarios, for example the four scenarios having the lowest cost in Figure 6.6. Unlike the correlation panel (Figure 6.6.A), the cost matrix view (Figure 6.6.B) eases the analysis of differences between correlation sets because well-marker correlations which are never, seldom or often simulated could be directly identified.

However, the correlation panel eases the observation of layering connectivity variation between several correlation sets, which may lead to models which differ in terms of fluid flow behavior. Figure 6.6.A, for example, highlights the difference between the four most likely well correlation sets using the distality rule of correlation (Chapter 3). The green correlation band corresponds to the main difference between the third most likely scenario (green correlation lines and correlation path) and the three other displayed scenarios (bold well-marker correlation cell in Figure 6.6.B): an additional layer is simulated corresponding to laminated mudstones (restricted lagoon) in well 11. This additional layer may have an impact on dynamic reservoir modeling because of its potential low permeability (e.g., [Baville et al., 2019](#)).

Moreover, the two-dimensional cost matrix highlights simulated gaps (vertical and horizontal lines) by applying the proposed correlation cost function on the North Sea data set returns two specific types of gaps in the most likely chronostratigraphic scenario (Figure 6.5.B):

1. One well marker interpreted as a distributary channel in well 04 (between 3.36 m and 4.17 m) is correlated with a group of well markers in well 11 (between 2.52 m and 21.50 m). This significant gap stems from the lack of a proximal facies (distributary channel or mouth bar) below 4.5 m in well 04.
2. Two well markers interpreted as a restricted lagoon in well 04 (between 22.49 m and 23.88 m and between 24.51 m and 25.00 m) are correlated with two groups of well markers in well 11 (between 6.35 m and 10.37 m and between 10.91 m and 15.30 m).

These observations are consistent with the interpretation of regressive parasequences during which sediments are preferentially deposited along the basin margin rather than in the proximal or distal positions ([Borgomano et al., 2008](#);

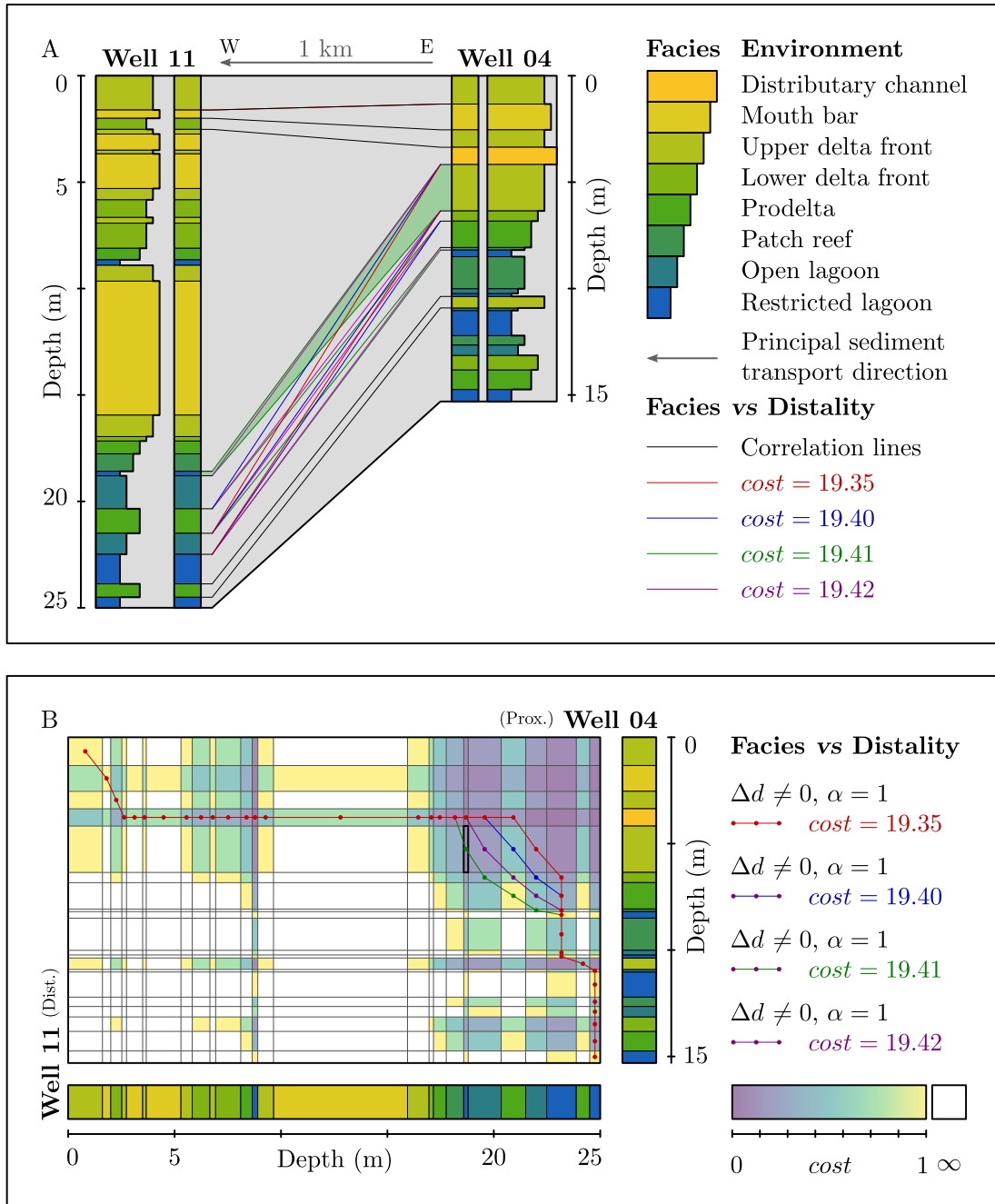


Figure 6.6: (A) Correlation panel. Black lines correspond to identical well-marker correlations among the four best correlation sets computed by Equation (3.17) i.e., the four correlation sets with the four lowest cumulative costs computed by Equation (2.1). Colored correlation lines are the different well-marker correlations in the four best correlation sets. (B) Correlation cost matrix. The four lines correspond to the four most likely scenarios. Note that the transition costs  $t$  associated to the edges or corners of the cost matrix are not visible in this display. Modified from (Baville et al., 2022).

Catuneanu et al., 2010; Galloway, 1989a; Homewood et al., 1992). Hence, this realization, which is defined by the highest likelihood and based on the principle of correlation, yields consistent results for the sedimentary facies correlation that is constrained by the well distality.

However, these results are not consistent with the stratigraphic parasequence interpretation (red triangles in Figure 6.3). Therefore, this method can help to target zones of uncertainty in order to make alternative interpretations of core samples and well logs. Alternatively, some method parameters such as the relative well distality ( $\alpha$  in Equations (3.10) and (3.15)) could be tuned to match ancillary constraints, before using the approach to explore uncertainties.

### 6.2.3 Impact of the sedimentary facies clustering

The correlation cost function Equation (3.14) is very strict and excludes well-marker correlations according to their distality and sedimentary facies interpretations. However, some depositional environments may be laterally equivalent and this equivalence may not be captured by the rules.

Facies codes defined in Section 6.1 are globally ordered by decreasing distality from 1 to 8, so they can be used directly in Equations (3.14) and (3.15). Moreover, facies can also be grouped before correlation to reduce complexity, reflect the laterally equivalence of some facies along a distal-to-proximal transect, and assess the impact of the level of interpretation detail on the correlation outcomes.

To this end, the eight initial facies are grouped in three possible facies associations according to their depositional positions along a distal-to-proximal transect (Table 6.1):

*Table 6.1: Sedimentary indexing and coloring corresponding to the three sedimentary facies clusters.*

Sedimentary facies	No Cluster	Cluster A	Cluster B	Cluster C
Distributary channel	$f = 08$	$f = 03$	$f = 03$	$f = 02$
Mouth bar	$f = 07$	$f = 03$	$f = 03$	$f = 02$
Upper delta front	$f = 06$	$f = 02$	$f = 03$	$f = 02$
Lower delta front	$f = 05$	$f = 02$	$f = 03$	$f = 02$
Prodelta	$f = 04$	$f = 02$	$f = 02$	$f = 01$
Patch reef	$f = 03$	$f = 01$	$f = 01$	$f = 01$
Open lagoon	$f = 02$	$f = 01$	$f = 01$	$f = 01$
Restricted lagoon	$f = 01$	$f = 01$	$f = 01$	$f = 01$

- A. Sedimentary facies are divided into three groups. (1) Distal sedimentary facies 1-3 correspond to depositional environments from restricted lagoons to patch reefs. (2) Intermediate sedimentary facies 4-6 correspond to deltaic environments from the prodelta to the upper delta front. (3) Proximal sedimentary facies 7-8 correspond to mouth bars and distributary channels.
- B. Sedimentary facies are divided into three groups. (1) Distal sedimentary facies 1-3 correspond to depositional environments from restricted lagoons to patch reefs. (2) Intermediate sedimentary facies 4 correspond the prodelta. (3) Proximal sedimentary facies 5-8 correspond to depositional environments from the lower delta front to distributary channels.
- C. Sedimentary facies are divided into two groups. (1) Distal sedimentary facies 1-4 correspond to depositional environments from restricted lagoons to the prodelta. (2) Intermediate sedimentary facies 5-8 correspond to depositional environments from the lower delta front to distributary channels.

This three different sedimentary facies associations are tested in order to evaluate the impact of sedimentary facies lateral equivalence:

- A. Figure 6.7.A plots one of the most likely computed correlation sets using the facies association A (black correlation lines) as input against the most likely computed correlation set without facies associations (dashed red correlation lines). Figure 6.7.B illustrates the correlation cost matrix, the best correlation set computed from the facies association A (black correlation path), and the best correlation set computed from no facies association (dashed red correlation path).
- B. Figure 6.8.A plots one of the most likely computed correlation sets using the facies association B (black correlation lines) as input against the most likely computed correlation set without facies associations (dashed red correlation lines). Figure 6.8.B illustrates the correlation cost matrix, the best correlation set computed from the facies association B (black correlation path), and the best correlation set computed from no facies association (dashed red correlation path).
- C. Figure 6.9.A plots one of the most likely computed correlation sets using the facies association C (black correlation lines) as input against the most likely computed correlation set without facies associations (dashed red correlation lines). Figure 6.9.B illustrates the correlation cost matrix, the best correlation set computed from the facies association C (black correlation path), and the best correlation set computed from no facies association (dashed red correlation path).



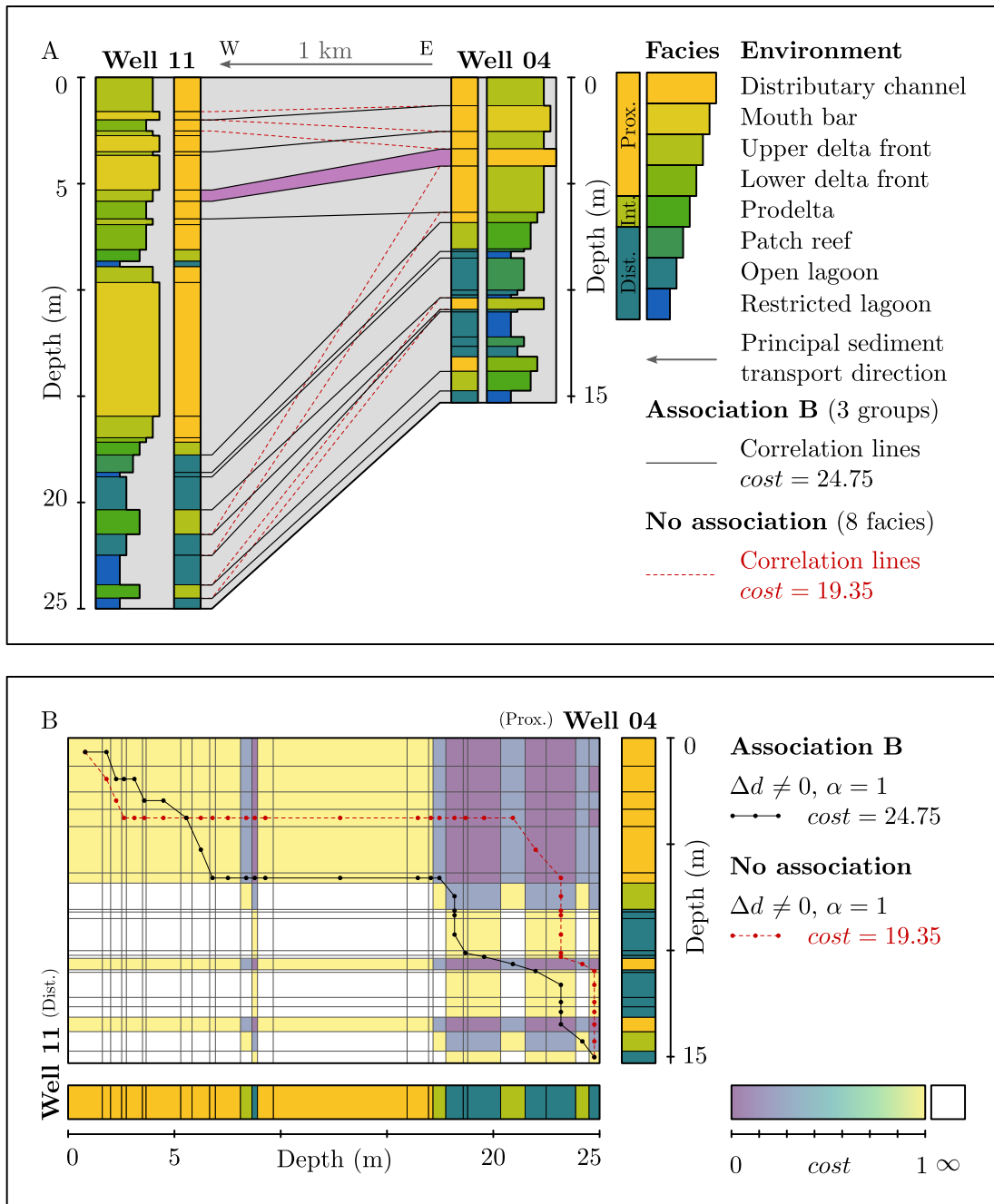


Figure 6.8: (A) Correlation panel. Black lines (respectively dashed red lines) correspond to the best correlation set computed by Equation (3.17) with the facies association B (respectively without facies association). Purple bands highlight the main difference between the correlation sets generated with the facies association B, and without the facies association. (B) Correlation cost matrix. Black line (respectively dashed red line) corresponds to the correlation path of the best correlation set computed with the facies association B (respectively without facies association). Modified from (Baville et al., 2022).

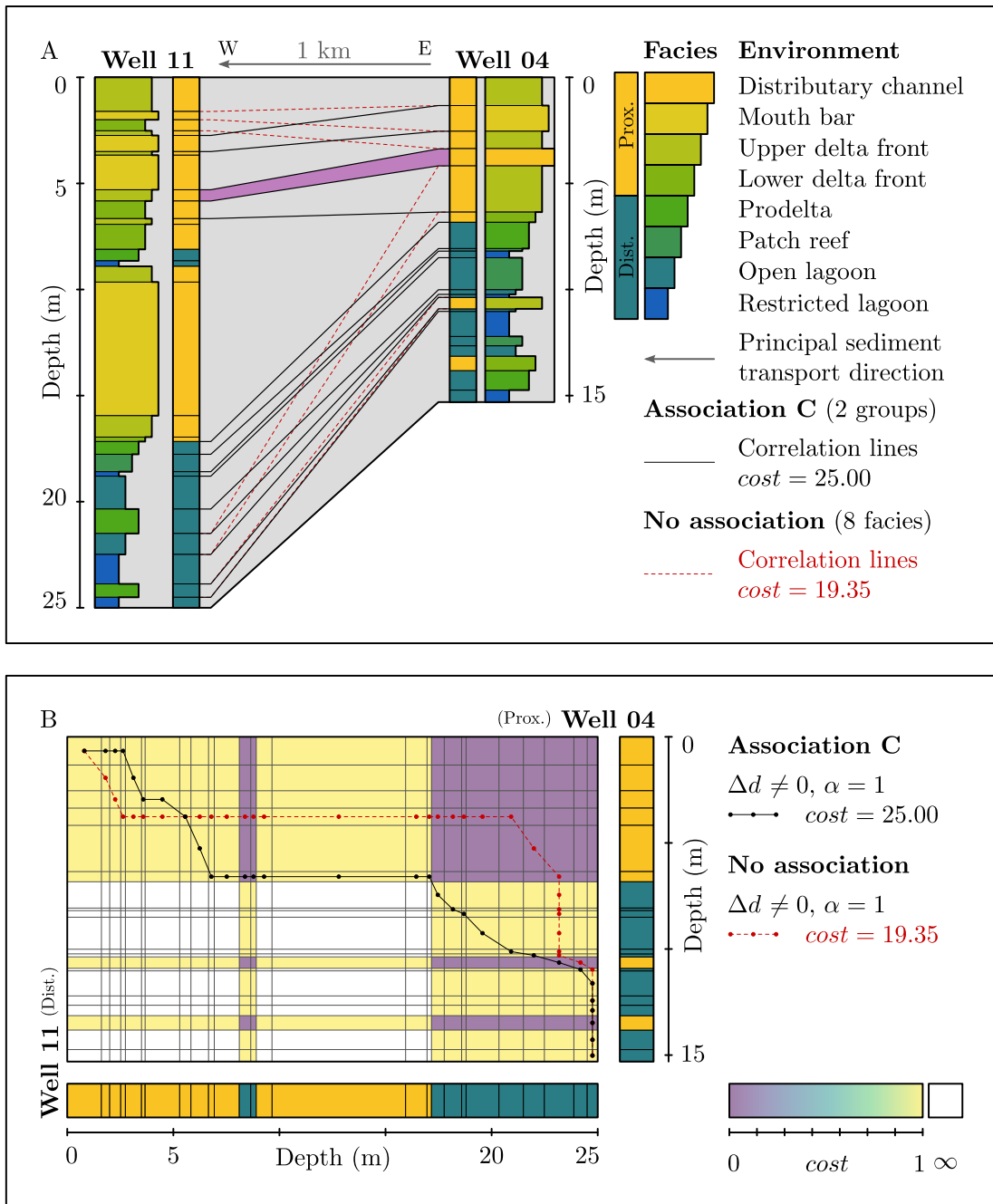


Figure 6.9: (A) Correlation panel. Black lines (respectively dashed red lines) correspond to the best correlation set computed by Equation (3.17) with the facies association C (respectively without facies association). Purple bands highlight the main difference between the correlation sets generated with the facies association C, and without the facies association. (B) Correlation cost matrix. Black line (respectively dashed red line) corresponds to the correlation path of the best correlation set computed with the facies association C (respectively without facies association). Modified from (Baville et al., 2022).

The main difference between these correlation sets (associations A, B and C) and the most likely correlation set based on the eight sedimentary facies (dashed red correlation lines) are highlighted by the purple correlation bands in correlation panels (Figures 6.7 to 6.9). Without facies groups, the well marker interpreted as a restricted lagoon in well 11 (between 8.65 m and 8.91 m) seems to pinch out between the wells (outcome is a gap), but with the facies association A, this well marker is correlated with a well marker interpreted as an upper delta front in well 04 (between 2.54 m and 3.36 m). Considering facies associations B and facies association C, the well marker interpreted as an open lagoon in well 11 (between 8.65 m and 8.91 m) is correlated with a well marker interpreted as a lower delta front in well 04 (between 6.35 m and 6.83 m).

The main difference between the outcome computed with eight facies and outcomes based on facies associations A, B and C is the number of simulated gaps (Figure 6.10). Assigning the same value to several facies presenting very close depositional conditions (lateral equivalence) leads to a smaller number of gaps and amounts to a more relaxed interpretation of the principle of correlation. Indeed, two facies belonging to the same group have the same code value even if their association goes against the principle of correlation.

For example, considering the facies association A, a well marker interpreted as patch reef (distal facies) in well 11 can be associated to a well marker interpreted as restricted lagoon (distal facies) in the proximal well (Figure 6.7.). The number of plausible well-marker correlations (*i.e.*, the number of colored cells within the cost matrix) should increase directly by associating facies according to their depositional conditions (*e.g.*, Figure 6.7.B). Increasing the number of plausible correlations may increase the number of diagonal correlation transitions (no gap) and should lead to outcomes with less gaps because of their cost penalty (Section 3.2.2).

The well correlation sets computed from the three facies groups have been graphically compared to the well correlation set computed with eight facies (Figures 6.7 and 6.9). However, they have not been compared on correlation panels with each other, but only on the correlation cost matrix (Figure 6.10). As illustrated in Figures 6.7 and 6.9, the three outcomes present a correlation band, highlighted in purple, which splits the main gap simulated by the proposed correlation cost function without facies association. There are also minor differences between outcomes generated using facies associations B and C but not really in term of stratigraphic unit connectivity, *i.e.*, these two facies associations do generate similar stratigraphic models which are very different from the model obtained without facies clustering. Finally, the well correlation generated with the facies association A seems to be an intermediate between the outcome generated without facies groups and the outcomes generated with facies associations B and C.

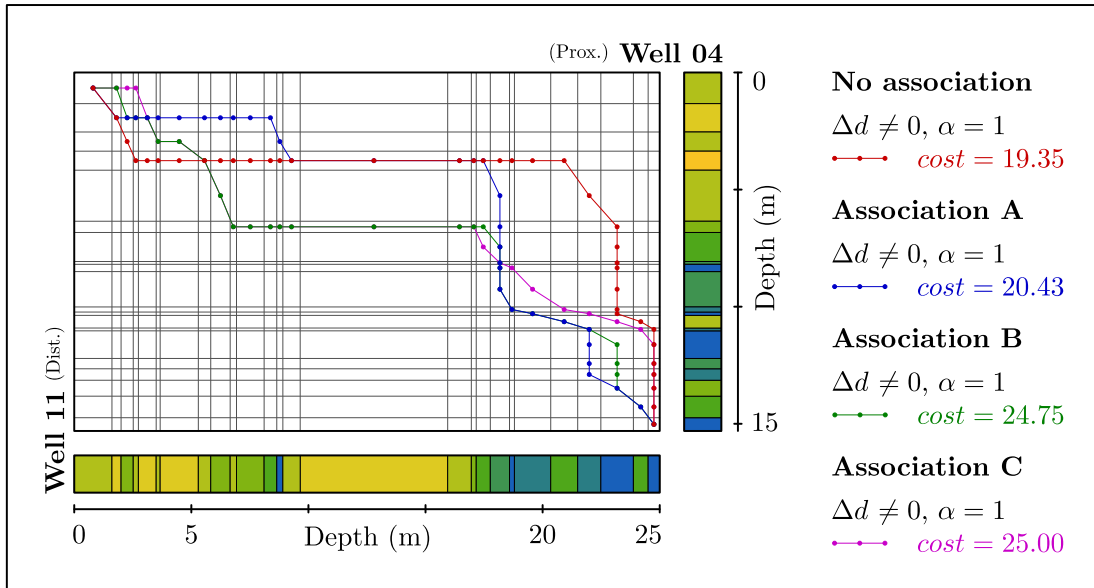


Figure 6.10: Correlation cost matrix summarizing the best correlation sets generated by the distality rule of correlation using the eight initial facies and the three facies associations A, B and C. Modified from (Baville et al., 2022).

## 6.3 Discussion

The distality correlation rule has been applied on two wells of the Gudrun-Sigrun Field area, but it can be extended to  $n$  wells as described in Chapter 3. In this case, wells must be classified by their relative positions. Normalization terms defined in Equations (3.2) and (3.8) are computed on the entire data set to ensure the consistency of the results. However, the order of well correlation may have a strong impact on the outcomes because only a limited set of scenarios can be propagated through the multi-well correlation process (Edwards et al., 2018; Wu et al., 2018).

Independent of the well order, the application of the proposed correlation rule on two wells of the Hugin Formation in the Sigrun Field area shows that the definition of well distality and sedimentary facies values have a strong impact on the results.

### 6.3.1 Principal sediment transport direction

In sedimentary basins, the principal sediment transport direction may vary between two overlapping deltaic lobes, and the shift to several sediment local sources may lead to a variation of the principal sediment transport direction in the system. In both cases, the variation of the principal sediment transport direction may be captured with reasonable accuracy with dipmeter data.

Figure 6.4.A shows the most likely correlation set considering that both Wells 04 and 11 have the same relative distality, *i.e.*, they are located along the sediment strike direction. The associated correlation cost matrix given by Equation (3.16) - *i.e.*, lithostratigraphic correlation - enables the simulation of every well-marker correlation (no cells with infinite correlation cost in Figure 6.4.B).

Figure 6.5.A shows the most likely correlation set considering that well 04 is drilled in the most proximal position of the basin, and that well 11 is drilled in the most distal position of the basin, *i.e.*, wells are located along the principal sediment transport direction. The corresponding correlation cost matrix (Figure 6.5.B) illustrates that several well-marker correlations are impossible (white cells) and cannot be simulated thanks to the principle of correlation.

### 6.3.2 Size of the system with respect to well spacing

Results are also sensitive to the distality variation along a distal-to-proximal transect, which cannot be determined with certainty. To visualize the effects of changing the relative well distality, the correlation cost matrix is computed assuming a depositional system of lateral size equal to 3.5 km, corresponding to a scaling parameter  $\alpha = 2/7$  (Figure 6.11).

Comparing the correlation costs of Figures 6.6 and 6.11, the distality rule of correlation is less discriminant and tends to generate correlation paths closer to the diagonal, *i.e.*, corresponding to a more steady preservation rate in each well in the considered interval.

Both uncertainties about the variation of the principal sediment transport direction and the relative depositional system size can be addressed by changing the scaling coefficient  $\alpha$  in Equation (3.15):

- For a given direction between two wells, a variation of the principal sediment transport direction may be modeled by a scaling coefficient varying between  $\alpha = -1$  and  $\alpha = 1$ . A scaling coefficient  $\alpha = -1$  corresponds to the inversion of the principal sediment transport direction and a scaling coefficient  $\alpha = 0$  corresponds to the principal sediment transport direction being perpendicular to the wells.
- A variation of the depositional system size with respect to well spacing may be modeled by a scaling coefficient varying between  $\alpha = 0$  and  $\alpha = 1$ . A scaling coefficient  $\alpha = 1$  corresponds to the extreme position of wells within the positional system and a scaling coefficient  $\alpha = 0$  corresponds to two wells having the same depositional position within the system.

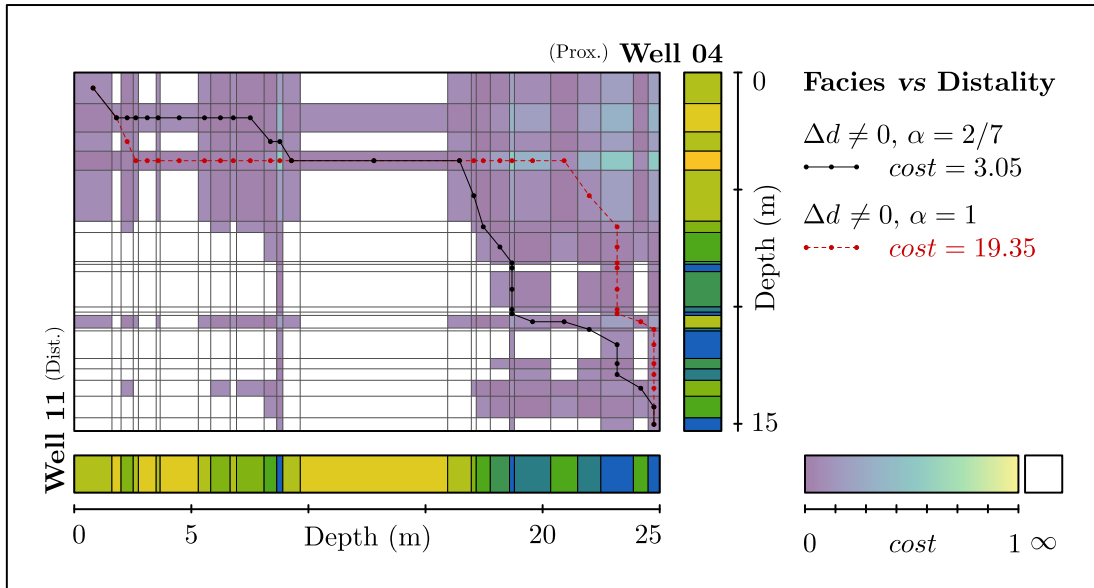


Figure 6.11: Correlation cost matrix corresponding to chronostratigraphic correlation given by Equation (3.15) (facies versus distality). This case is intermediate between Equations (3.11) and (3.13) with  $\alpha = 2/7$ . The black line corresponds to the most likely correlation set and the dashed red line corresponds to the most likely correlation set computed with  $\alpha = 1$  (Figure 6.6). Modified from (Baville et al., 2022).

### 6.3.3 Sedimentary facies clustering

Figures 6.5 and 6.7 to 6.9 show chronostratigraphic correlation outcomes computed with Equation (3.17) using three different facies associations and no facies association. Considering groups of lateral equivalent facies, the correlation cost matrix will be modified because two well markers interpreted as lateral equivalent sedimentary facies are allowed to be correlated. The correlation cost function takes as input parameters the sedimentary facies variation  $\Delta f$  and the well distality variation  $\Delta d$ .

In the case that two sedimentary facies are laterally equivalent, the facies variation  $\Delta f$  is null and the correlation cost function will always compute a correlation cost between the two given well markers. Figure 6.7.A shows the correlation cost matrix associated to the facies association A. This highlights that more plausible well-marker correlations exist than when considering the initial 8 facies (Figure 6.5.B). For instance, well markers interpreted as prodeltas in the proximal well can be correlated to well markers interpreted as upper or lower delta fronts in the distal well (Figure 6.7).

In this application, three facies groups are proposed to make the correlation cost function smoother, *i.e.*, the clustering allows facies belonging to the same group to be correlated even though some individual facies correlations are originally

impossible. The comparison between simulations without facies association (Figure 6.5) and simulations with facies associations (Figures 6.7 to 6.9) may lead to the identification of the best facies association regarding the number of gaps, the cumulative correlation cost as compared to the reference outcome without facies association or other auxiliary considerations such as the analysis of the sediment preservation rate.

Finally, two different well correlations can be graphically compared as illustrated in Figures 6.5 and 6.7 to 6.9. However, increasing the number of realizations in one graph makes the comparison and the interpretation challenging.

### 6.3.4 Minor changes in the correlation cost

Figures 6.6 and 6.11 illustrate that small changes in the correlation cost leads to different well correlations. These differences can be the number of gaps, or the size of the gap itself, *i.e.*, the connectivity of stratigraphic units may be strongly different from one correlation to another because of a minor change in the correlation cost.

The paleogeography is directly linked to the connectivity of stratigraphic units and a small variation in the correlation cost may have an impact in the stratigraphic unit connectivity, so a minor change in the correlation cost may have an impact on the paleogeographic model. Moreover, a change in the correlation cost which makes a correlation possible rather than not possible (a white cell in the cost matrix in Figure 6.6.B may become colored as illustrated in Figure 6.9.B) may lead to significant changes in the correlation and may have a strong impact on the corresponding stratigraphic model and fluid flow (*e.g.*, [Baville et al., 2019](#)).

### 6.3.5 Additional principles of correlation

In addition to distality and facies, additional sedimentological rules could be integrated in the proposed method. Especially, very thin distal facies or proximal facies may be associated with a thicker succession of intermediate facies during marine regression ([Homewood et al., 1992](#)). Considering the consistency of the correlation cost function applied on sedimentary coastal deltaic data set, it may be used to confront manual parasequence interpretations from well-logs and core-samples, and highlight where uncertainties exist.

Because the correlation set simulation is solely based on correlation cost functions used by the Dynamic Time Warping, the results are only as good as the input rules, and in this application, the likelihood of the principle of correlation (Chap-

ter 3). For example, the correlation process does not take into consideration the erosion surfaces observed at the top of regressive parasequences.

Therefore, additional rules could be integrated in the method. Based on sequence stratigraphy, and considering that during a regressive period sediments are mainly deposited in the intermediate area of the basin, and that during a transgressive period sediments are eroded in the distal part and mainly deposited in the proximal part of the basin as qualitatively illustrated in Figures 1.7 and 1.8, a transition cost  $t$  may be implemented based on the facies vertical transitions (e.g., Homewood et al., 1992). The thickness of facies intervals could also be considered to further constrain the preservation rate emerging from the correlations (Hagen et al., 2020; Lallier et al., 2013).

More generally, the proposed correlation cost normalization,  $0 \leq c \leq 1$ , makes it possible to define multi-criteria correlation costs. Indeed, several independent normalized costs may be combined in the Dynamic Time Warping algorithm by an averaging process. As another example, detailed biostratigraphic interpretations are available in the South Viking Graben data set and may be used to constrain the correlation by adding a binary cost function, which allows or excludes a correlation considering the biostratigraphy (Caumon and Antoine, 2019).

Additional data or concepts could also be integrated in the method, as an ancillary geological likelihood to evaluate the results (e.g., de la Varga and Wellmann, 2016). Other posterior analysis on the generated stratigraphic model may be achieved to evaluate the physical likelihood of the correlation outcomes (layer connectivities) like hydraulic or tracer simulation tests (e.g., Baviile et al., 2019; Lallier et al., 2012). Another way to scrutinize and improve the results could be to analyze the geometry of the chronostratigraphic units and their consistency with dip data and subsidence analysis (Chapter 4).

Finally, the well correlation process generally involves iterations between the identification of intervals or markers in each well, and the correlation of these across wells. The distality correlation rule allows loops between the well data interpretation and their correlations according to the likelihood of simulations. The likelihood of simulations is first defined by the algorithm but may be evaluated *a posteriori* by an expert who may decide to modify the interpretation in order to improve the well correlation, so the proposed method defers human bias.

## Conclusion

In this chapter, the purpose of the proposed correlation cost function is to generate several plausible higher-order chronostratigraphic scenarios between lower-order

interpreted time lines (e.g., from seismic imaging and biostratigraphic analysis). The obtained correlation results are simulated based on sedimentary facies and well distality interpretations in several wells, and have implications in terms of detailed paleogeography in the considered interval.

The correlation rule defined in Chapter 3 is based on the principle of correlation: “a facies cannot be associated with a *depositionally shallower (respectively depositionally deeper) facies in a more distal (respectively proximal) well*”. This method requires sedimentary facies interpretations along well paths and the distality of all wells computed from the well position along a distal-to-proximal transect, to compute a correlation cost for each possible well-marker correlation given by Equations (3.14) and (3.15).

Given the incomplete information available to recover such time lines, ambiguity is clearly expected and it should not be hidden, as it may affect the understanding and the way that applied geoscientists model facies, flow units and thin horizontal permeability barriers in subsurface reservoirs. The approach proposed in this application makes it possible to include the concept of distality in such uncertainty quantification and to generate alternative layer connectivities between linear stratigraphic sections.



# Conclusion

As discussed at the very beginning of this PhD thesis, it is impossible to see what lies underground, or to get a full view at a fine scale of the subsurface. For this, the subsurface may be numerically represented using geological principles of subsurface modeling constrained by conditioning data (e.g., Mallet, 2002).

This PhD thesis has addressed the question of the consistency between interpretative stratigraphic concepts and well correlation. Indeed, as reviewed in Chapters 1 and 2, lithostratigraphy, although it has been easily implemented (e.g., Hale, 2013; Smith and Waterman, 1980; Waterman and Raymond, 1987), is unable to reproduce paleogeographic depositional environments. Therefore, several adaptations of automatic and expert-based correlation methods enable to take into consideration some depositional interpretations such as paleobathymetric information (e.g., Borgomano et al., 2008), theoretical chronostratigraphic profile geometries (e.g., Lallier et al., 2016), or the integration of a stratigraphic column into the multi-well correlation process (e.g., Edwards et al., 2018).

In the continuity of the previous methods which attempt to reproduce the paleogeography by generating computer-assisted multi-well correlations, this PhD work proposes two principles of correlation by integrating the sediment transport direction as a constraint.

**The distality rule of correlation** (Chapter 3). The purpose of this first proposed correlation cost function is to generate stratigraphic well correlations based on the principle stating that “*a facies cannot be associated with a depositionally deeper (respectively shallower) facies in a more distal (proximal) well*”. This method requires sedimentary facies interpretations along well paths, and the distality of all wells computed from the well position along a distal-to-proximal transect, to compute a correlation cost for each possible well-marker correlation. This method has been applied on the Middle Jurassic Hugin Formation in the Gudrun-Sigrun Field area in order to evaluate the consistency of the paleogeographic interpretation with respect to biostratigraphic data (Chapter 5). It has also been applied to model the stratigraphic layering of the Early Callovian Hugin Formation in the Sigrun Field area (Chapter 6). In both applications, the dis-

tality rule of correlation leads to promising outcomes which are consistent with respect to biostratigraphic interpretations.

**The dipmeter rule of correlation** (Chapter 4). The purpose of this second proposed correlation cost function method is to generate stratigraphic well correlation based on the principle stating that “*the lower the difference between a chronostratigraphic interpolation (in between well markers) and a conceptual depositional profile, the higher the likelihood of the well marker association*”. This method requires dipmeter data and depositional facies interpretations along wells to interpolate stratigraphic horizons, and a theoretical depositional profile defined by a principal sediment transport direction and a deltaic vertical and lateral extension, to compute a correlation cost for each possible well-marker correlation. The proposed method has only been tested on a synthetic data set, and the first results are promising but may be biased by the construction of the synthetic data set. This method must be improved by being applied on more complex synthetic data set and the main goal of this method is to be applied on a real data set to generate a chronostratigraphic models from sparse well data and evaluate the uncertainties on these models.

These two principles of correlation can then be used to evaluate the consistency of a paleogeographic interpretation with respect to additional subsurface data, and to model subsurface at the parasequence scale. These two principles of correlation may be used to test several paleogeographic depositional system and to evaluate their consistency with respect to additional subsurface data.

However, the combination of these two principles which is enabled by the Dynamic Time Warping algorithm (Chapter 2), is currently not efficient because the dipmeter correlation cost is not normalized (Chapter 4) and should blind the impact of the normalized distality correlation cost (Chapter 3). Furthermore, the combination of additional normalized correlation costs enables to take into consideration more prior information about the zone of interest and to compute correlation costs from other input parameters such as vertical / horizontal facies transitions or paleobathymetry (e.g., [Kedzierski et al., 2005](#)).

As discussed in Chapter 5, the distality rule of correlation may be used to test several interpretations or simulations of distalities along wells by evaluating the outcomes consistency. The dipmeter rule of correlation may be used to test several dipmeter data interpretations or simulations along wells by interpolating stratigraphic horizon between well markers. In both cases, the differences between stratigraphic well correlation may lead to different stratigraphic layering which could differ in term of connectivity and fluid flow behavior (e.g., [Baville et al., 2019](#)). Indeed, the stratigraphic well correlation is a preliminary step of the geomodel building, and a different outcomes may lead to different interpolated geometries and to different reservoir property simulations (Figure 1).

However, as discussed in this manuscript, loops between well data stratigraphic interpretations and well correlation are necessary to build the most consistent stratigraphic well correlation with respect to every possible subsurface data. To conclude this PhD thesis, these two principles, and generally all the principles of correlation can be used to automatically generate stratigraphic well correlations but should always be considered as a tool to help geologists to understand the subsurface structure and to target uncertain subsurface areas, but the generated models must not be considered as the truth.



# Bibliography

- E. W. Adams and W. Schlager. Basic types of submarine slope curvature. *Journal of Sedimentary Research*, 70(4): 814–828, 2000. ISSN 1527-1404. doi:[10.1306/2DC4093A-0E47-11D7-8643000102C1865D](https://doi.org/10.1306/2DC4093A-0E47-11D7-8643000102C1865D).
- D. V. Ager. *The nature of the stratigraphical record*. John Wiley, New York, 1981.
- D. V. Ager. *The new catastrophism*. Cambridge University Press, 1993.
- R. B. Ainsworth, M. Sanlung, and S. T. C. Duivenvoorden. Correlation techniques, perforation strategies, and recovery factors: An integrated 3-D reservoir modeling study, Sirikit field, Thailand. *AAPG Bulletin*, 83(10): 1535–1551, 1999. ISSN 0149-1423. doi:[10.1306/E4FD420B-1732-11D7-8645000102C1865D](https://doi.org/10.1306/E4FD420B-1732-11D7-8645000102C1865D).
- J. R. L. Allen. The classification of cross-stratified units. With notes on their origin. *Sedimentology*, 2(2): 93–114, 1963. ISSN 1365-3091. doi:[10.1111/j.1365-3091.1963.tb01204.x](https://doi.org/10.1111/j.1365-3091.1963.tb01204.x).
- A. Amosu and Y. Sun. WheelerLab: An interactive program for sequence stratigraphic analysis of seismic sections, outcrops and well sections and the generation of chronostratigraphic sections and dynamic chronostratigraphic sections. *SoftwareX*, 6: 19–24, 2017. ISSN 2352-7110. doi:[10.1016/j.softx.2016.12.003](https://doi.org/10.1016/j.softx.2016.12.003).
- J. E. Andrews and W. Walton. Depositional environments within Middle Jurassic oyster-dominated lagoons: an integrated litho-, bio- and palynofacies study of the Duntulm Formation (Great Estuarine Group, Inner Hebrides). *Earth and Environmental Science Transactions of The Royal Society of Edinburgh*, 81(1): 1–22, 1990. ISSN 1473-7116, 0263-5933. doi:[10.1017/S0263593300005095](https://doi.org/10.1017/S0263593300005095).
- C. Antoine and G. Caumon. HM-WELLSTOC: A hierarchical graph-based method for multiple well stochastic stratigraphic correlation. In *RING Meeting*, vol. 29, p. 55–61, 2018.
- C. Antoine and G. Caumon. Advances on the hierarchical and stochastic multiple well stratigraphic correlation in WeCo. In *RING Meeting*, vol. 31, p. 68–76, 2020.

## BIBLIOGRAPHY

---

- P. Baviile, J. Peisker, and G. Caumon. From well logs to stratigraphic layering: Automation, uncertainties and impact on reservoir behavior. In *81st EAGE Conference and Exhibition 2019*, vol. 2019, p. 1–5, 2019. doi:[10.3997/2214-4609.201901293](https://doi.org/10.3997/2214-4609.201901293).
- P. Baviile, M. Apel, S. Hoth, D. Knaust, C. Antoine, C. Carpentier, and G. Caumon. Computer-assisted stochastic multi-well correlation: Surface simulation versus depositional profile. In *RING Meeting*, vol. 32, p. 338–361, 2021a.
- P. Baviile, M. Apel, S. Hoth, D. Knaust, and G. Caumon. Application of the Distality rule of WeCo on the Gudrun-Sigrun Middle Jurassic data set, North Sea. In *RING Meeting*, vol. 32, p. 162–174, 2021b.
- P. Baviile, M. Apel, S. Hoth, D. Knaust, C. Antoine, C. Carpentier, and G. Caumon. Computer-assisted stochastic multi-well correlation: Sedimentary facies versus well distality. *Marine and Petroleum Geology*, 135: 105371, 2022. ISSN 0264-8172. doi:[10.1016/j.marpetgeo.2021.105371](https://doi.org/10.1016/j.marpetgeo.2021.105371).
- D. F. Belknap. *Encyclopedia of sediments and sedimentary rocks*. Springer, Dordrecht, 2003.
- R. Bellman and R. Kalaba. On the role of dynamic programming in statistical communication theory. *IRE Transactions on Information Theory*, 3(3): 197–203, 1957. ISSN 2168-2712. doi:[10.1109/TIT.1957.1057416](https://doi.org/10.1109/TIT.1957.1057416).
- J. P. Bhattacharya. Deltas. In *Facies model revisited*, p. 237–292. Sepm special pblication edition, 2006.
- J. P. Bhattacharya. Practical problems in the application of the sequence stratigraphic method and key surfaces: Integrating observations from ancient fluvial–deltaic wedges with Quaternary and modelling studies. *Sedimentology*, 58(1): 120–169, 2011. ISSN 1365-3091. doi:[10.1111/j.1365-3091.2010.01205.x](https://doi.org/10.1111/j.1365-3091.2010.01205.x).
- C. E. Bond, A. D. Gibbs, Z. K. Shipton, and S. Jones. What do you think this is? "Conceptual uncertainty" in geoscience interpretation. *GSA Today*, 17(11): 4–10, 2007. ISSN 1052-5173. doi:[10.1130/GSAT01711A.1](https://doi.org/10.1130/GSAT01711A.1).
- J. R. F. Borgomano, F. Fournier, S. Viseur, and L. Rijkels. Stratigraphic well correlations for 3-D static modeling of carbonate reservoirs. *AAPG Bulletin*, 92(6): 789–824, 2008. ISSN 0149-1423. doi:[10.1306/02210807078](https://doi.org/10.1306/02210807078).
- J. R. F. Borgomano, C. Lanteaume, P. Léonide, F. Fournier, L. F. Montaggioni, and J. Masse. Quantitative carbonate sequence stratigraphy: Insights from stratigraphic forward models. *AAPG Bulletin*, p. 1 – 28, 2020. doi:[10.1306/11111917396](https://doi.org/10.1306/11111917396).

- S. Bourquin, C. Rigollet, and P. Bourges. High-resolution sequence stratigraphy of an alluvial fan–fan delta environment: Stratigraphic and geodynamic implications – An example from the Keuper Chaunoy Sandstones, Paris Basin. *Sedimentary Geology*, 121(3): 207–237, 1998. ISSN 0037-0738. doi:[10.1016/S0037-0738\(98\)00081-5](https://doi.org/10.1016/S0037-0738(98)00081-5).
- I. M. Brown. A new method for correlation of multiple stratigraphic sequences. *Computers & Geosciences*, 23(6): 697–700, 1997. ISSN 0098-3004. doi:[10.1016/S0098-3004\(97\)00046-0](https://doi.org/10.1016/S0098-3004(97)00046-0).
- L. A. Buatois, N. Santiago, M. Herrera, P. Plink-Björklund, R. Steel, M. Espin, and K. Parra. Sedimentological and ichnological signatures of changes in wave, river and tidal influence along a Neogene tropical deltaic shoreline. *Sedimentology*, 59(5): 1568–1612, 2012. ISSN 1365-3091. doi:[10.1111/j.1365-3091.2011.01317.x](https://doi.org/10.1111/j.1365-3091.2011.01317.x).
- P. M. Burgess, D. G. Roberts, and A. Bally. A brief review of developments in stratigraphic forward modelling, 2000-2009. In *Regional geology and tectonics: Principles of geologic analysis*, vol. 1, p. 379–404. 2012.
- J. R. Bushman. Hutton’s Uniformitarianism. *Brigham Young University Studies*, 23(1): 41–48, 1983. ISSN 0007-0106.
- P. Bézier. *Essai de définition numérique des courbes et des surfaces expérimentales. Contribution à l’étude des propriétés des courbes et des surfaces paramétriques polynomiales à coefficients vectoriels*. phdthesis, Université Paris VIII - Pierre et Marie Curie, 1977.
- O. Catuneanu. Sequence stratigraphy of clastic systems: Concepts, merits, and pitfalls. *Journal of African Earth Sciences*, 35(1): 1–43, 2002. ISSN 1464-343X. doi:[10.1016/S0899-5362\(02\)00004-0](https://doi.org/10.1016/S0899-5362(02)00004-0).
- O. Catuneanu. *Principles of sequence stratigraphy*. Elsevier, 2006. ISBN 978-0-08-047398-7.
- O. Catuneanu, J. P. Bhattacharya, M. D. Blum, R. W. Dalrymple, P. G. Eriksson, C. R. Fielding, W. L. Fisher, W. E. Galloway, P. Gianolla, M. R. Gibling, K. A. Giles, J. M. Holbrook, R. Jordan, H. W. Posamentier, B. R. Pratt, K. W. Shanley, R. J. Steel, A. Strasser, and M. E. Tucker. Sequence stratigraphy: Common ground after three decades of development. *Fisrt Break*, 28: 21–34, 2010.
- O. Catuneanu, W. E. Galloway, C. G. S. C. Kendall, A. D. Miall, H. W. Posamentier, A. Strasser, and M. E. Tucker. Sequence stratigraphy: Methodology and nomenclature. *Newsletters on Stratigraphy*, 44(3): 173–245, 2011. ISSN ., doi:[10.1127/0078-0421/2011/0011](https://doi.org/10.1127/0078-0421/2011/0011).

- G. Caumon. Towards stochastic time-varying geological modeling. *Mathematical Geosciences*, 42(5): 555–569, 2010. ISSN 1874-8953. doi:[10.1007/s11004-010-9280-y](https://doi.org/10.1007/s11004-010-9280-y).
- G. Caumon and C. Antoine. Stochastic stratigraphic correlation of multiple wells seen as a directed acyclic graph creation problem. In *IAMG 2019*, 2019.
- J. Cavero, N. H. Orellana, I. Yemez, V. Singh, and E. Izaguirre. Importance of conceptual geological models in 3D reservoir modelling. *First Break*, 34(7), 2016. ISSN 0263-5046, 1365-2397. doi:[10.3997/1365-2397.2016010](https://doi.org/10.3997/1365-2397.2016010).
- N. Christie-Blick. Onlap, offlap, and the origin of unconformity-bounded depositional sequences. *Marine Geology*, 97(1): 35–56, 1991. ISSN 0025-3227. doi:[10.1016/0025-3227\(91\)90018-Y](https://doi.org/10.1016/0025-3227(91)90018-Y).
- C.-J. F. Chung and A. G. Fabbri. Probabilistic prediction models for landslide hazard mapping. *Photogrammetric engineering and remote sensing*, 65(12): 1389–1399, 1999.
- P. Chéneau and V. Risser. Cartographie en temps réel et système de pré-alerte pour les glissements de terrain dans les Alpes Suisses: La méthode OLPAC. *Swiss Bulletin für angewandte Geologie*, 24(2): 55–66, 2019.
- R. M. Clark and R. Thompson. A new statistical approach to the alignment of time series. *Geophysical Journal International*, 58(3): 593–607, 1979. ISSN 0956-540X. doi:[10.1111/j.1365-246X.1979.tb04796.x](https://doi.org/10.1111/j.1365-246X.1979.tb04796.x).
- D. R. Collins and J. H. Doveton. Automated correlation based on Markov analysis of vertical successions and Walther’s Law. In *Automated Correlation Based on Markov Analysis of Vertical Successions and Walther’s Law*, Computer in Geology - 25 years of progress. Oxford University Press, 1993. doi: [10.1093/oso/9780195085938.003.0015](https://doi.org/10.1093/oso/9780195085938.003.0015).
- L. Colombera, F. Felletti, N. P. Mountney, and W. D. McCaffrey. A database approach for constraining stochastic simulations of the sedimentary heterogeneity of fluvial reservoirs. *AAPG Bulletin*, 96(11): 2143–2166, 2012. ISSN 0149-1423. doi:[10.1306/04211211179](https://doi.org/10.1306/04211211179).
- T. A. Cross and P. W. Homewood. Amanz Gressly’s role in founding modern stratigraphy. *GSA Bulletin*, 109(12): 1617–1630, 1997. ISSN 0016-7606. doi:[10.1130/0016-7606\(1997\)109<1617:AGSRIF>2.3.CO;2](https://doi.org/10.1130/0016-7606(1997)109<1617:AGSRIF>2.3.CO;2).
- W. B. Dade, J. R. Lister, and H. E. Huppert. Fine-sediment deposition from gravity surges on uniform slopes. *Journal of Sedimentary Research*, 64 (3a): 423–432, 1994. ISSN 1527-1404. doi:[10.1306/D4267DD4-2B26-11D7-8648000102C1865D](https://doi.org/10.1306/D4267DD4-2B26-11D7-8648000102C1865D).

- J. C. Davis. *Statistic and data analysis in geology*. John Wiley, New York, 1973. ISBN 0-471-19895-1.
- M. de la Varga and J. F. Wellmann. Structural geologic modeling as an inference problem: A Bayesian perspective. *Interpretation*, 4(3): SM1–SM16, 2016. ISSN 2324-8858. doi:[10.1190/INT-2015-0188.1](https://doi.org/10.1190/INT-2015-0188.1).
- W. E. Dean and R. Y. Anderson. Application of some correlation coefficient techniques to time-series analysis. *Journal of the International Association for Mathematical Geology*, 6(4): 363–372, 1974. ISSN 1573-8868. doi:[10.1007/BF02082357](https://doi.org/10.1007/BF02082357).
- A. Delcoigne and P. Hansen. Sequence comparison by dynamic programming. *Biometrika*, 62(3): 661–664, 1975. ISSN 0006-3444. doi:[10.2307/2335525](https://doi.org/10.2307/2335525).
- H. A. Dellanoy. Emploi de l'échiquier pour la solution de problèmes arithmétiques. *Association française pour l'avancement des sciences*, 1886.
- J. Dewan. Essentials of modern open-hole log interpretation. 1983.
- J. H. Doveton. *Geologic log analysis using computer methods*. Number 2 in AAPG Computer Applications in Geology. American Association of Petroleum Geologists, 1994. ISBN 978-0-89181-701-7.
- S. Dreyfus. Richard Bellman on the birth of dynamic programming. *Operations Research*, 50(1): 48–51, 2002. ISSN 0030-364X, 1526-5463. doi:[10.1287/opre.50.1.48.17791](https://doi.org/10.1287/opre.50.1.48.17791).
- N. W. Driscoll and G. D. Karner. Three-dimensional quantitative modeling of clinof orm development. *Marine Geology*, 154(1): 383–398, 1999. ISSN 0025-3227. doi:[10.1016/S0025-3227\(98\)00125-X](https://doi.org/10.1016/S0025-3227(98)00125-X).
- O. Dubrule and E. Damsleth. Achievements and challenges in petroleum geostatistics. *Petroleum Geoscience*, 7(S): S1–S7, 2001. ISSN 1354-0793. doi:[10.1144/petgeo.7.S.S1](https://doi.org/10.1144/petgeo.7.S.S1).
- L. J. Durlofsky. Upscaling and gridding of fine scale geological models for flow simulation. In *8th International forum on reservoir simulation Iles Borromees*, vol. 2024, p. 1–59, 2005.
- T. T. Eaton. On the importance of geological heterogeneity for flow simulation. *Sedimentary Geology*, 184(3): 187–201, 2006. ISSN 0037-0738. doi:[10.1016/j.sedgeo.2005.11.002](https://doi.org/10.1016/j.sedgeo.2005.11.002).
- J. Edwards. *Construction de modèles stratigraphiques à partir de données éparses*. phdthesis, Université de Lorraine, 2017. NNT : 2017LORR0367. tel-01836225.

- J. Edwards, F. Lallier, G. Caumon, and C. Carpentier. Uncertainty management in stratigraphic well correlation and stratigraphic architectures: A training-based method. *Computers & Geosciences*, 111: 1–17, 2018. ISSN 0098-3004. doi:[10.1016/j.cageo.2017.10.008](https://doi.org/10.1016/j.cageo.2017.10.008).
- A. L. Eide, H. Omre, and B. Ursin. Stochastic reservoir characterization conditioned on seismic data. In *Scho (eds), Geostatistics Wollongong '96*, p. 442–453, 1996.
- A. F. Embry and E. P. Johannessen. T–R sequence stratigraphy, facies analysis and reservoir distribution in the uppermost Triassic–Lower Jurassic succession, western Sverdrup Basin, Arctic Canada. In *Arctic geology and petroleum potential*, number 2 in NPF Special Publications, p. 121–146. Norwegian Petroleum Society (NPF), elsevier edition, 1992. doi: [10.1016/B978-0-444-88943-0.50013-7](https://doi.org/10.1016/B978-0-444-88943-0.50013-7).
- J. H. Fang, H. C. Chen, A. W. Shultz, and W. Mahmoud. Computer-Aided Well Log Correlation. *AAPG Bulletin*, 76(3): 307–317, 1992. ISSN 0149-1423. doi:[10.1306/BDFE87E0-1718-11D7-8645000102C1865D](https://doi.org/10.1306/BDFE87E0-1718-11D7-8645000102C1865D).
- J. B. J. Fourier. *Théorie analytique de la chaleur*. Chez Firmin Didot, père et fils, 1822.
- F. Fournier and J. Borgomano. Geological significance of seismic reflections and imaging of the reservoir architecture in the Malampaya gas field (Philippines). *AAPG Bulletin*, 91(2): 235–258, 2007. ISSN 0149-1423. doi:[10.1306/10160606043](https://doi.org/10.1306/10160606043).
- T. Frank, A.-L. Tertois, and J.-L. Mallet. 3D-reconstruction of complex geological interfaces from irregularly distributed and noisy point data. *Computers & Geosciences*, 33(7): 932–943, 2007. ISSN 0098-3004. doi:[10.1016/j.cageo.2006.11.014](https://doi.org/10.1016/j.cageo.2006.11.014).
- D. E. Frazier. Depositional episodes : Their relationship to the Quaternary stratigraphic framework in the northwestern portion of the Gulf Basin. *University of Texas at Austin, Bureau of Economic Geology*, 4(1): 28, 1974.
- N. Fredman, J. Tveranger, S. Semshaug, A. Braathen, and E. Sverdrup. Sensitivity of fluid flow to fault core architecture and petrophysical properties of fault rocks in siliciclastic reservoirs: a synthetic fault model study. *Petroleum Geoscience*, 13(4): 305–320, 2007. ISSN 1354-0793. doi:[10.1144/1354-079306-721](https://doi.org/10.1144/1354-079306-721).
- G. Fuellen. A gentle guide to multiple alignment. *Complexity International*, 4: 1–56, 1997.
- F. T. Fürsich, W. Werner, and S. Schneider. Autochthonous to parautochthonous bivalve concentrations within transgressive marginal marine strata of the Upper

- Jurassic of Portugal. *Palaeobiodiversity and Palaeoenvironments*, 89(3-4): 161–190, 2009. ISSN 1867-1594, 1867-1608. doi:[10.1007/s12549-009-0008-2](https://doi.org/10.1007/s12549-009-0008-2).
- W. E. Galloway. Genetic stratigraphic sequences in basin analysis II: Application to Northwest Gulf of Mexico Cenozoic Basin. *AAPG Bulletin*, 73(2): 143–154, 1989a. ISSN 0149-1423. doi:[10.1306/703C9AFA-1707-11D7-8645000102C1865D](https://doi.org/10.1306/703C9AFA-1707-11D7-8645000102C1865D).
- W. E. Galloway. Genetic stratigraphic sequences in basin analysis I: Architecture and genesis of flooding-surface bounded depositional units. *AAPG Bulletin*, 73(2): 125–142, 1989b. ISSN 0149-1423. doi:[10.1306/703C9AF5-1707-11D7-8645000102C1865D](https://doi.org/10.1306/703C9AF5-1707-11D7-8645000102C1865D).
- M. R. Gani and J. P. Bhattacharya. Lithostratigraphy versus chronostratigraphy in facies correlations of quaternary deltas: Application of bedding correlation. In *River Deltas - Concepts, models, and examples*, vol. 83, p. 31–48. Sepm special pblication edition, 2005. ISBN 1-56576-113-8.
- A. D. Gordon. SLOTSEQ: A Fortran IV program for comparing two sequences of observations. *Computers & Geosciences*, 6(1): 7–20, 1980. ISSN 0098-3004. doi:[10.1016/0098-3004\(80\)90003-5](https://doi.org/10.1016/0098-3004(80)90003-5).
- A. D. Gordon and R. A. Reyment. Slotting of borehole sequences. *Journal of the International Association for Mathematical Geology*, 11(3): 309–327, 1979. ISSN 1573-8868. doi:[10.1007/BF01034996](https://doi.org/10.1007/BF01034996).
- D. Granjeon. *Modélisation stratigraphique déterministe : conception et applications d'un modèle diffusif 3D multilithologique*. phdthesis, Université Rennes 1, 1997.
- A. Gressly. Observations géologiques sur le Jura soleurois. *Neuchâtel: Nouveaux mémoires de la Société Helvétique des Sciences Naturelles*, 2, 1838.
- J. Grötsch and C. Mercadier. Integrated 3D reservoir modeling based on 3D seismic: The Tertiary Malampaya and Camago Buildups, Offshore Palawan, Philippines. *AAPG Bulletin*, 83(11): 1703–1728, 1999. ISSN 0149-1423. doi:[10.1306/E4FD4247-1732-11D7-8645000102C1865D](https://doi.org/10.1306/E4FD4247-1732-11D7-8645000102C1865D).
- F. Guillocheau. Modalité d'empilement des séquences génétiques dans un bassin de plate-forme (Dévonien armoricain) : nature et distorsion des différents ordres de séquences de dépôts emboîtés. *Bulletin des centres de recherches exploration - Production Elf-Aquitaine*, 15(2): 383–410, 1991. ISSN 0396-2687.
- C. J. Hagen, B. T. Reilly, J. S. Stoner, and J. R. Creveling. Dynamic time warping of palaeomagnetic secular variation data. *Geophysical Journal International*, 221(1): 706–721, 2020. ISSN 0956-540X. doi:[10.1093/gji/ggaa004](https://doi.org/10.1093/gji/ggaa004).

## BIBLIOGRAPHY

---

- H. H. Haldorsen and E. Damsleth. Stochastic Modeling (includes associated papers 21255 and 21299 ). *Journal of Petroleum Technology*, 42(4): 404–412, 1990. ISSN 0149-2136. doi:[10.2118/20321-PA](https://doi.org/10.2118/20321-PA).
- D. Hale. Dynamic warping of seismic images. *GEOPHYSICS*, 78(2): S105–S115, 2013. ISSN 0016-8033. doi:[10.1190/geo2012-0327.1](https://doi.org/10.1190/geo2012-0327.1).
- G. J. Hampson. Discontinuity Surfaces, Clinoforms, and Facies Architecture in a Wave-Dominated, Shoreface-Shelf Parasequence. *Journal of Sedimentary Research*, 70(2): 325–340, 2000. ISSN 1527-1404. doi:[10.1306/2DC40914-0E47-11D7-8643000102C1865D](https://doi.org/10.1306/2DC40914-0E47-11D7-8643000102C1865D).
- B. U. Haq, J. Hardenbol, and P. R. Vail. Chronology of fluctuating sea levels since the Triassic. *Science*, 235(4793): 1156–1167, 1987. ISSN 0036-8075, 1095-9203. doi:[10.1126/science.235.4793.1156](https://doi.org/10.1126/science.235.4793.1156).
- B. U. Haq, J. Hardenbol, P. R. Vail, L. E. Stover, J. P. Colin, N. S. Ioannides, R. C. Wright, G. R. Baum, A. M. Gombos, C. E. Pflum, T. S. Loutit, R. J. du Chêne, K. K. Romine, J. F. Sarg, H. W. Posamentier, and B. E. Morgan. Mesozoic and Cenozoic Chronostratigraphy and Cycles of Sea-Level Change. In *Sea-level changes: An integrated approach*, vol. 42 of *SEPM Special Publication*, p. 71–108. The Society of Economic Paleontologists and Mineralogists, 1988. doi: 10.2110/pec.88.01.0071.
- J. W. Harbaugh and D. F. Merriam. *Computer applications in stratigraphic analysis*. John Wiley, 1968.
- W. W. Hay and J. R. Southam. Quantifying Biostratigraphic Correlation. *Annual Review of Earth and Planetary Sciences*, 6(1): 353–375, 1978. doi:[10.1146/annurev.ea.06.050178.002033](https://doi.org/10.1146/annurev.ea.06.050178.002033).
- W. Helland-Hansen and J. G. Gjelberg. Conceptual basis and variability in sequence stratigraphy: a different perspective. *Sedimentary Geology*, 92(1-2): 31–52, 1994. ISSN 0037-0738. doi:[10.1016/0037-0738\(94\)90053-1](https://doi.org/10.1016/0037-0738(94)90053-1).
- D. G. Higgins and P. M. Sharp. CLUSTAL: a package for performing multiple sequence alignment on a microcomputer. *Gene*, 73(1): 237–244, 1988. ISSN 0378-1119. doi:[10.1016/0378-1119\(88\)90330-7](https://doi.org/10.1016/0378-1119(88)90330-7).
- J. M. Holbrook and J. P. Bhattacharya. Reappraisal of the sequence boundary in time and space: Case and considerations for an SU (subaerial unconformity) that is not a sediment bypass surface, a time barrier, or an unconformity. *Earth-Science Reviews*, 113(3): 271–302, 2012. ISSN 0012-8252. doi:[10.1016/j.earscirev.2012.03.006](https://doi.org/10.1016/j.earscirev.2012.03.006).

- J. M. Holbrook and A. D. Miall. Time in the Rock: A field guide to interpreting past events and processes from siliciclastic stratigraphy. *Earth-Science Reviews*, 203: 103121, 2020. ISSN 0012-8252. doi:[10.1016/j.earscirev.2020.103121](https://doi.org/10.1016/j.earscirev.2020.103121).
- M. M. Holgate. The microlog as a porosity datum for the neutron log in the swan hills field, alberta. In *Trans., CIM*, p. 324–328, 1960.
- P. Homewood, F. Guillocheau, R. Eschard, and T. A. Cross. Corrélations haute résolution et stratigraphie génétique : une démarche intégrée. *Bulletin des centres de recherches exploration - Production Elf-Aquitaine*, 16(2): 357–381, 1992. ISSN 0396-2687.
- P. Homewood, P. Mauriaud, and F. Lafont. *Best practices in sequence stratigraphy: for explorationists and reservoir engineers*, vol. 25. Editions Technip, 2000.
- S. Hoth, D. Knaust, A. Sánchez-López, S. Kassold, and S. Sviland-Østre. The Gudrun Field: Gravity-Flow Deposition during Rifting and Inversion. Rift-Related Coarse-Grained Submarine Fan Reservoirs; the Brae Play, South Viking Graben, North Sea. *AAPG Memoir*, 115: 387–421, 2018. doi:[10.1306/13652188M1153814](https://doi.org/10.1306/13652188M1153814).
- J. A. Howell, A. W. Martinius, and T. R. Good. The application of outcrop analogues in geological modelling: a review, present status and future outlook. *Geological Society, London, Special Publications*, 387(1): 1–25, 2014. ISSN 0305-8719, 2041-4927. doi:[10.1144/SP387.12](https://doi.org/10.1144/SP387.12).
- B.-Z. Hsieh, C. Lewis, and Z.-S. Lin. Lithology identification of aquifers from geophysical well logs and fuzzy logic analysis: Shui-Lin Area, Taiwan. *Computers & Geosciences*, 31(3): 263–275, 2005. ISSN 00983004. doi:[10.1016/j.cageo.2004.07.004](https://doi.org/10.1016/j.cageo.2004.07.004).
- D. Hunt and M. E. Tucker. Stranded parasequences and the forced regressive wedge systems tract: Deposition during base-level fall. *Sedimentary Geology*, 81(1-2): 1–9, 1992. ISSN 00370738. doi:[10.1016/0037-0738\(92\)90052-S](https://doi.org/10.1016/0037-0738(92)90052-S).
- J. Hutton. X. Theory of the Earth; or an Investigation of the Laws observable in the Composition, Dissolution, and Restoration of Land upon the Globe. *Transactions of The Royal Society of Edinburgh*, 1(2): 209–304, 1788. ISSN 2053-5945, 0080-4568. doi:[10.1017/S0080456800029227](https://doi.org/10.1017/S0080456800029227).
- A. A. Ichaso and R. W. Dalrymple. Tide- and wave-generated fluid mud deposits in the Tilje Formation (Jurassic), offshore Norway. *Geology*, 37(6): 539–542, 2009. ISSN 1943-2682, 0091-7613. doi:[10.1130/G25481A.1](https://doi.org/10.1130/G25481A.1).
- M. D. Jackson, G. J. Hampson, and R. P. Sech. Three-dimensional modeling of a shoreface-shelf parasequence reservoir analog: Part 2. Geologic controls on

- fluid flow and hydrocarbon recovery. *AAPG Bulletin*, 93(9): 1183–1208, 2009. ISSN 0149-1423. doi:[10.1306/05110908145](https://doi.org/10.1306/05110908145).
- R. M. Jerrett, L. I. Bennie, S. S. Flint, and S. F. Greb. Extrinsic and intrinsic controls on mouth bar and mouth bar complex architecture: Examples from the Pennsylvanian (Upper Carboniferous) of the central Appalachian Basin, Kentucky, USA. *GSA Bulletin*, 128: 1696–1716, 2016. ISSN 0016-7606. doi:[10.1130/B31429.1](https://doi.org/10.1130/B31429.1).
- M. T. Jervey. Quantitative geological modeling of siliciclastic rock sequences and their seismic expression. In *Sea-level changes: An integrated approach*, vol. 42 of *SEPM Special Publication*. The Society of Economic Paleontologists and Mineralogists, 1988. ISBN 0-918985-74-9.
- J. G. Johnson and M. A. Murphy. Time-rock model for Siluro-Devonian continental shelf, Western United States. *GSA Bulletin*, 95(11): 1349–1359, 1984. ISSN 0016-7606. doi:[10.1130/0016-7606\(1984\)95<1349:TMFSCS>2.0.CO;2](https://doi.org/10.1130/0016-7606(1984)95<1349:TMFSCS>2.0.CO;2).
- A. G. Journel. Geostatistics for Conditional Simulation of Ore Bodies. *Economic Geology*, 69(5): 673–687, 1974. ISSN 0361-0128. doi:[10.2113/gsecongeo.69.5.673](https://doi.org/10.2113/gsecongeo.69.5.673).
- P. Kedzierski. *Intégration de connaissances sédimentologiques et stratigraphiques dans la caractérisation 3D des faciès sédimentaires marins*. phdthesis, Institut National Polytechnique de Lorraine, 2007.
- P. Kedzierski, A. Le Solleuz, J. L. Mallet, and J. J. Royer. Sedimentological and stratigraphic modeling combining membership functions and sequence stratigraphy principles. In *Gocad Meeting*, vol. 25, 2005.
- P. Kedzierski, J. L. Mallet, and G. Caumon. Combining stratigraphic and sedimentological information for realistic facies simulations. In *EAGE Conference on Petroleum Geostatistics*, p. cp-32, 2007. ISBN 978-90-73781-48-1. doi:[10.3997/2214-4609.201403080](https://doi.org/10.3997/2214-4609.201403080).
- P. Kedzierski, G. Caumon, J.-L. Mallet, J.-J. Royer, and P. Durand-Riard. 3D Marine Sedimentary Reservoir Stochastic Simulation Accounting for High Resolution Sequence Stratigraphy and Sedimentological Rules. In *Eighth Geostatistical Geostatistics Congress*, p. 657–666, 2008.
- F. Kemp. An algorithm for the stratigraphic correlation of well logs. *Journal of the International Association for Mathematical Geology*, 14(3): 271–285, 1982. ISSN 1573-8868. doi:[10.1007/BF01032889](https://doi.org/10.1007/BF01032889).
- C. G. S. C. Kendall, J. Strobel, R. Cannon, J. Bezdek, and G. Biswas. The simulation of the sedimentary fill of basins. *Journal of Geophysical Research: Solid Earth*, 96(B4): 6911–6929, 1991. ISSN 2156-2202. doi:[10.1029/90JB01406](https://doi.org/10.1029/90JB01406).

- R. L. Kieft, C. A.-L. Jackson, G. J. Hampson, and E. Larsen. Sedimentology and sequence stratigraphy of the Hugin Formation, Quadrant 15, Norwegian sector, South Viking Graben. *Geological Society, London, Petroleum Geology Conference series*, 7(1): 157–176, 2010. ISSN 2047-9921. doi:[10.1144/0070157](https://doi.org/10.1144/0070157).
- M. J. King and M. Mansfield. Flow Simulation of Geologic Models. *SPE Reservoir Evaluation & Engineering*, 2(04): 351–367, 1999. ISSN 1094-6470. doi:[10.2118/57469-PA](https://doi.org/10.2118/57469-PA).
- M. A. Kirschbaum and R. D. Hettinger. Facies analysis and sequence stratigraphic framework of upper Campanian strata (Neslen and Mount Garfield formations, Bluecastle Tongue of the Castlegate sandstone, and Mancos shale), Eastern Book cliffs, Colorado and Utah. Digital Data Series 69-G, U.S. Geological Survey, 2004.
- D. Knaust. Teichichnus zigzag Frey and Bromley, 1985: a probable echiuran or holothurian burrow from the Jurassic offshore Norway. *PalZ*, 92(4): 617–632, 2018. ISSN 1867-6812. doi:[10.1007/s12542-018-0413-9](https://doi.org/10.1007/s12542-018-0413-9).
- D. Knaust and S. Hoth. Bay-head deltas as hydrocarbon reservoirs: The Middle Jurassic Hugin Formation in Block 15/3 of the South Viking Graben, Norway. *Marine and Petroleum Geology*, 126: 104841, 2021. ISSN 0264-8172. doi:[10.1016/j.marpetgeo.2020.104841](https://doi.org/10.1016/j.marpetgeo.2020.104841).
- D. Knaust, M. Apel, S. Hoth, and P. Baviile. The Middle Jurassic Hugin Formation in Block 15/3 of the South Viking Graben, North Sea, Norway. In *Norwegian Petroleum Society*, 2019.
- B. Koehrer, T. Aigner, and M. Pöppelreiter. Field-scale geometries of Upper Khuff reservoir geobodies in an outcrop analogue (Oman Mountains, Sultanate of Oman). *Petroleum Geoscience*, 17(1): 3–16, 2011. ISSN 1354-0793. doi:[10.1144/1354-079310-009](https://doi.org/10.1144/1354-079310-009).
- J. Koppka. *Revision of the Bivalvia from the Upper Jurassic Reuchenette Formation, Northwest Switzerland: Ostreoidea*. 2015. ISBN 978-1-77557-652-5.
- F. Lallier. *Corrélation stratigraphique stochastique de puits*. phdthesis, Université de Lorraine, 2012. NNT : 2012LORR0414. tel-01750420.
- F. Lallier, G. Caumon, J. Borgomano, S. Viseur, F. Fournier, C. Antoine, and T. Gentilhomme. Relevance of the stochastic stratigraphic well correlation approach for the study of complex carbonate settings: application to the Malampaya buildup (Offshore Palawan, Philippines). *Geological Society, London, Special Publications*, 370(1): 265–275, 2012. ISSN 0305-8719, 2041-4927. doi:[10.1144/SP370.12](https://doi.org/10.1144/SP370.12).

- F. Lallier, C. Antoine, J. Charreau, G. Caumon, and J. Ruiu. Management of ambiguities in magnetostratigraphic correlation. *Earth and Planetary Science Letters*, 371-372: 26–36, 2013. ISSN 0012-821X. doi:[10.1016/j.epsl.2013.04.019](https://doi.org/10.1016/j.epsl.2013.04.019).
- F. Lallier, G. Caumon, J. Borgomano, S. Viseur, J.-J. Royer, and C. Antoine. Uncertainty assessment in the stratigraphic well correlation of a carbonate ramp: Method and application to the Beausset Basin, SE France. *Comptes Rendus Geoscience*, 348(7): 499–509, 2016. ISSN 1631-0713. doi:[10.1016/j.crte.2015.10.002](https://doi.org/10.1016/j.crte.2015.10.002).
- M. Larson. Coastal lagoons. In *Encyclopedia of lakes and reservoirs*, p. 171–174. Springer Netherlands, Dordrecht, 2012. ISBN 978-1-4020-4410-6. doi:[10.1007/978-1-4020-4410-6\\_236](https://doi.org/10.1007/978-1-4020-4410-6_236).
- D. K. Larue and H. Legarre. Flow units, connectivity, and reservoir characterization in a wave-dominated deltaic reservoir: Meren reservoir, Nigeria. *AAPG Bulletin*, 88(3): 303–324, 2004. ISSN 0149-1423. doi:[10.1306/10100303043](https://doi.org/10.1306/10100303043).
- D. T. Lawrence, M. Doyle, and T. Aigner. Stratigraphic Simulation of Sedimentary Basins: Concepts and Calibration. *AAPG Bulletin*, 74(3): 273–295, 1990. ISSN 0149-1423. doi:[10.1306/0C9B22C7-1710-11D7-8645000102C1865D](https://doi.org/10.1306/0C9B22C7-1710-11D7-8645000102C1865D).
- V. I. Levenshtein. Binary codes capable of correcting deletions, insertions, and reversals. *Soviet Physic Doklady*, 10(8): 707–710, 1966.
- Y. Li and J. P. Bhattacharya. Facies architecture of asymmetrical branching distributary channels: Cretaceous Ferron Sandstone, Utah, USA. *Sedimentology*, 61(5): 1452–1483, 2014. ISSN 1365-3091. doi:[10.1111/sed.12104](https://doi.org/10.1111/sed.12104).
- C. Lyell. *Principles of Geology*. London, 1830.
- M. Machalski. Oyster life positions and shell beds from the Upper Jurassic of Poland. *Acta Palaeontologica Polonica*, 43(4): 609–634, 1998.
- J. L. Mallet. GOCAD: A Computer Aided Design Program for Geological Applications. In *Three-Dimensional Modeling with Geoscientific Information Systems*, NATO ASI Series, p. 123–141. Springer Netherlands, Dordrecht, 1992. ISBN 978-94-011-2556-7. doi: [10.1007/978-94-011-2556-7\\_11](https://doi.org/10.1007/978-94-011-2556-7_11).
- J.-L. Mallet. *Geomodeling*. Oxford University Press, 2002. ISBN 978-0-19-803303-5.
- J.-L. Mallet. Space–Time Mathematical Framework for Sedimentary Geology. *Mathematical Geology*, 36(1): 1–32, 2004. ISSN 1573-8868. doi:[10.1023/B:MATG.0000016228.75495.7c](https://doi.org/10.1023/B:MATG.0000016228.75495.7c).
- J.-L. Mallet. *Elements of mathematical sedimentary geology: The GeoChron model*. EAGE Publications, 2014.

- O. Man. On the identification of magnetostratigraphic polarity zones. *Studia Geophysica et Geodaetica*, 52(2): 173–186, 2008. ISSN 1573-1626. doi:[10.1007/s11200-008-0012-4](https://doi.org/10.1007/s11200-008-0012-4).
- O. Man. The maximum likelihood dating of magnetostratigraphic sections. *Geophysical Journal International*, 185(1): 133–143, 2011. ISSN 0956-540X. doi:[10.1111/j.1365-246X.2010.04920.x](https://doi.org/10.1111/j.1365-246X.2010.04920.x).
- C. J. Mann and T. P. L. Dowell. Quantitative lithostratigraphic correlation of subsurface sequences. *Computers & Geosciences*, 4(3): 295–306, 1978. ISSN 0098-3004. doi:[10.1016/0098-3004\(78\)90064-X](https://doi.org/10.1016/0098-3004(78)90064-X).
- D. G. Martinson, W. Menke, and P. Stoffa. An inverse approach to signal correlation. *Journal of Geophysical Research: Solid Earth*, 87(B6): 4807–4818, 1982. ISSN 2156-2202. doi:[10.1029/JB087iB06p04807](https://doi.org/10.1029/JB087iB06p04807).
- G. J. Massonnat. Sampling space of uncertainty through stochastic modelling of geological facies. 1997. doi:[10.2118/38746-MS](https://doi.org/10.2118/38746-MS).
- G. Matheron. Principles of geostatistics. *Economic Geology*, 58(8): 1246–1266, 1963. ISSN 0361-0128. doi:[10.2113/gsecongeo.58.8.1246](https://doi.org/10.2113/gsecongeo.58.8.1246).
- G. Matheron. Universal kriging. In *Matheron's Theory of Regionalised Variables*, p. 123–180. Oxford University Press, 1969. ISBN 978-0-19-883566-0. doi: [10.1093/oso/9780198835660.003.0005](https://doi.org/10.1093/oso/9780198835660.003.0005).
- D. R. Matuszak. Stratigraphic correlation of subsurface geologic data by computer. *Journal of the International Association for Mathematical Geology*, 4(4): 331–343, 1972. ISSN 1573-8868. doi:[10.1007/BF02114094](https://doi.org/10.1007/BF02114094).
- J. H. G. Melo and S. Loboziak. Visan miospore biostratigraphy and correlation of the Poti Formation (Parnaba Basin, northern Brazil). *Review of Palaeobotany and Palynology*, 112(1): 147–165, 2000. ISSN 0034-6667. doi:[10.1016/S0034-6667\(00\)00043-9](https://doi.org/10.1016/S0034-6667(00)00043-9).
- D. F. Merriam. Computer applications in stratigraphic problem solving. *Decision-making in the mineral industry : Canadian Institut of Mining & Metallurgy*, Sepcial 12: 139–147, 1971.
- A. D. Miall. Stratigraphic sequences and their chronostratigraphic correlation. *Journal of Sedimentary Research*, 61(4): 497–505, 1991. ISSN 1527-1404. doi:[10.1306/D4267744-2B26-11D7-8648000102C1865D](https://doi.org/10.1306/D4267744-2B26-11D7-8648000102C1865D).
- A. D. Miall. Time in Sequence Stratigraphy. In *The Geology of Stratigraphic Sequences*, p. 273–279. Springer, Berlin, Heidelberg, 1997. ISBN 978-3-662-03380-7. doi: [10.1007/978-3-662-03380-7\\_12](https://doi.org/10.1007/978-3-662-03380-7_12).
- A. D. Miall. *Fluvial depositional systems*. Springer, 2014.

## BIBLIOGRAPHY

---

- A. D. Miall. The valuation of unconformities. *Earth-Science Reviews*, 163: 22–71, 2016. ISSN 0012-8252. doi:[10.1016/j.earscirev.2016.09.011](https://doi.org/10.1016/j.earscirev.2016.09.011).
- G. V. Middleton. Johannes Walther’s Law of the Correlation of Facies. *Geological Society of America Bulletin*, 84(3): 979–988, 1973. ISSN 0016-7606. doi:[10.1130/0016-7606\(1973\)84<979:JWLOTTC>2.0.CO;2](https://doi.org/10.1130/0016-7606(1973)84<979:JWLOTTC>2.0.CO;2).
- R. M. Mitchum. Seismic stratigraphy and global changes of sea level. Part 11: Glossary of terms used in seismic stratigraphy. In *Seismic stratigraphy — Applications to hydrocarbon exploration*, vol. 26 of *AAPG Memoir*, p. 205–212. American Association of Petroleum Geologists, 1977.
- R. M. Mitchum and J. C. Van Wagoner. High-frequency sequences and their stacking patterns: Sequence-stratigraphic evidence of high-frequency eustatic cycles. *Sedimentary Geology*, 70(2): 131–160, 1991. ISSN 0037-0738. doi:[10.1016/0037-0738\(91\)90139-5](https://doi.org/10.1016/0037-0738(91)90139-5).
- R. M. Mitchum, P. R. Vail, and J. B. Sangree. Seismic stratigraphy and global changes of sea level. Part 6: Stratigraphic interpretation of seismic reflection patterns in depositional sequences. In *Seismic stratigraphy — Applications to hydrocarbon exploration*, vol. 26 of *AAPG Memoir*, p. 117–133. American Association of Petroleum Geologists, 1977a.
- R. M. Mitchum, P. R. Vail, and S. Thompson III. Seismic stratigraphy and global changes of sea level. Part 2: The depositional sequence as a basic unit for stratigraphic analysis. In *Seismic stratigraphy — Applications to hydrocarbon exploration*, vol. 26 of *AAPG Memoir*, p. 53–62. American Association of Petroleum Geologists, 1977b.
- J. H. Moran, M. A. Couffleau, G. K. Miller, and J. P. Timmons. Automatic computation of dipmeter logs digitally recorded on magnetic tapes. *Journal of Petroleum Technology*, 14(7): 771–782, 1962. ISSN 0149-2136. doi:[10.2118/174-PA](https://doi.org/10.2118/174-PA).
- T. Muto and R. J. Steel. Principles of regression and transgression: The nature of the interplay between accommodation and sediment supply. *Journal of Sedimentary Research*, 67(6): 994–1000, 1997. ISSN 1527-1404. doi:[10.1306/D42686A8-2B26-11D7-8648000102C1865D](https://doi.org/10.1306/D42686A8-2B26-11D7-8648000102C1865D).
- C. Myers and L. Rabiner. A level building dynamic time warping algorithm for connected word recognition. *IEEE Transactions on Acoustics, Speech, and Signal Processing*, 29(2): 284–297, 1981. ISSN 0096-3518. doi:[10.1109/TASSP.1981.1163527](https://doi.org/10.1109/TASSP.1981.1163527).
- J. Nagy and K. Bjørlykke. Stratigraphy. In *Petroleum Geoscience: From Sedimentary Environments to Rock Physics*, p. 231–253. Springer, 2015. ISBN 978-3-642-34132-8. doi: [10.1007/978-3-642-34132-8\\_7](https://doi.org/10.1007/978-3-642-34132-8_7).

- S. B. Needleman and C. D. Wunsch. A general method applicable to the search for similarities in the amino acid sequence of two proteins. *Journal of molecular biology*, 48: 443–453, 1970.
- N. S. Neidell. Ambiguity functions and concept of geological correlation. *AAPG Bulletin*, 53(3): 734–734, 1969. ISSN 0149-1423.
- H. Nøhr-Hansen, G. L. Williams, and R. A. Fensome. Biostratigraphic correlation of the western and eastern margins of the Labrador-Baffin Seaway and implications for the regional geology. *GEUS Bulletin*, 37: 1–74, 2017. ISSN 2597-2154. doi:[10.34194/geusb.v37.4356](https://doi.org/10.34194/geusb.v37.4356).
- C. Olariu and J. P. Bhattacharya. Terminal distributary channels and delta front architecture of river-dominated delta systems. *Journal of Sedimentary Research*, 76(2): 212–233, 2006. ISSN 1527-1404. doi:[10.2110/jsr.2006.026](https://doi.org/10.2110/jsr.2006.026).
- S.-Y. Pan, B.-Z. Hsieh, M.-T. Lu, and Z.-S. Lin. Identification of stratigraphic formation interfaces using wavelet and Fourier transforms. *Computers & Geosciences*, 34(1): 77–92, 2008. ISSN 0098-3004. doi:[10.1016/j.cageo.2007.01.002](https://doi.org/10.1016/j.cageo.2007.01.002).
- S. Patruno and W. Helland-Hansen. Clinoforms and clinoform systems: Review and dynamic classification scheme for shorelines, subaqueous deltas, shelf edges and continental margins. *Earth-Science Reviews*, 185: 202–233, 2018. ISSN 0012-8252. doi:[10.1016/j.earscirev.2018.05.016](https://doi.org/10.1016/j.earscirev.2018.05.016).
- S. Patruno, G. J. Hampson, C. A.-L. Jackson, and T. Dreyer. Clinoform geometry, geomorphology, facies character and stratigraphic architecture of a sand-rich subaqueous delta: Jurassic Sognefjord Formation, offshore Norway. *Sedimentology*, 62(1): 350–388, 2015. ISSN 1365-3091. doi:[10.1111/sed.12153](https://doi.org/10.1111/sed.12153).
- T. J. Pearce, B. M. Besly, D. S. Wray, and D. K. Wright. Chemostratigraphy: a method to improve interwell correlation in barren sequences — a case study using onshore Duckmantian/Stephanian sequences (West Midlands, U.K.). *Sedimentary Geology*, 124(1-4): 197–220, 1999. ISSN 00370738. doi:[10.1016/S0037-0738\(98\)00128-6](https://doi.org/10.1016/S0037-0738(98)00128-6).
- B. Pels, J. J. Keizer, and R. Young. Automated biostratigraphic correlation of palynological records on the basis of shapes of pollen curves and evaluation of next-best solutions. *Palaeogeography, Palaeoclimatology, Palaeoecology*, 124(1): 17–37, 1996. ISSN 0031-0182. doi:[10.1016/0031-0182\(96\)00017-X](https://doi.org/10.1016/0031-0182(96)00017-X).
- Y. Perrier, P. Baviile, and G. Caumon. Stochastic simulation of stratigraphic sequences from well log data using continuous wavelet transforms. In *RING Meeting*, vol. 32, p. 317–337, 2021.
- H. W. Posamentier and P. R. Vail. Eustatic controls on clastic deposition II - Sequence and systems tract models. In *Sea-level changes - An integrated*

## BIBLIOGRAPHY

---

- approach*, vol. 42 of *SEPM Special Publication*, p. 125–154. 1988a. ISBN 0-918985-74-9.
- H. W. Posamentier and P. R. Vail. Sequence Stratigraphy: Sequences and Systems Tract Development. *AAPG Memoir*, 15: 571–572, 1988b.
- H. W. Posamentier, M. T. Jervey, and P. R. Vail. Eustatic controls on clastic deposition I - Conceptual framework. In *Sea-level changes - An integrated approach*, vol. 42 of *SEPM Special Publication*. 1988. ISBN 0-918985-74-9.
- H. W. Posamentier, G. P. Allen, and D. P. James. High resolution sequence stratigraphy; the East Coulee Delta, Alberta. *Journal of Sedimentary Research*, 62(2): 310–317, 1992. ISSN 1527-1404. doi:[10.1306/D42678ED-2B26-11D7-8648000102C1865D](https://doi.org/10.1306/D42678ED-2B26-11D7-8648000102C1865D).
- F. W. Preston and J. Henderson. Fourier Series Characterization of Cyclic Sediment for Stratigraphic Correlation. In *Symposium on Cyclic Sedimentation*, number 169 in Kansas Geological Survey Bulletin, p. 415–425. 1964.
- M. J. Pyrcz and C. V. Deutsch. *Geostatistical Reservoir Modeling*. OUP USA, 2014. ISBN 978-0-19-973144-2.
- F. Qayyum, C. Betzler, and O. Catuneanu. The Wheeler diagram, flattening theory, and time. *Marine and Petroleum Geology*, 86: 1417–1430, 2017. ISSN 0264-8172. doi:[10.1016/j.marpetgeo.2017.07.034](https://doi.org/10.1016/j.marpetgeo.2017.07.034).
- M. Ragueneil. *Modélisation des phénomènes thermo-hydrauliques dans des réservoirs fracturés sur des maillages non structurés : application au réservoir géothermique de Basse-Terre, Guadeloupe*. phdthesis, Université de Lorraine, 2019.
- M. Rebesco and A. Camerlenghi. Sediment Drifts on the Continental Rise of the Antarctic Peninsula. In *Glaciated Continental Margins: An Atlas of Acoustic Images*, p. 294–296. Springer Netherlands, Dordrecht, 1997. ISBN 978-94-011-5820-6. doi: [10.1007/978-94-011-5820-6\\_97](https://doi.org/10.1007/978-94-011-5820-6_97).
- H. E. Reineck and I. B. Singh. *Depositional sedimentary environments*. Springer, Berlin, 1980.
- J. Rey. *Biostratigraphie et lithostratigraphie : principes fondamentaux*. Méthodes et Applications, Editions Technip, 1983. ISBN 978-2-7108-0459-8.
- J. L. Rich. Three critical environments of deposition, and criteria for recognition of rocks deposited in each of them. *GSA Bulletin*, 62(1): 1–20, 1951. ISSN 0016-7606. doi:[10.1130/0016-7606\(1951\)62\[1:TCEODA\]2.0.CO;2](https://doi.org/10.1130/0016-7606(1951)62[1:TCEODA]2.0.CO;2).

- P. Ringrose and M. Bentley. Reservoir model types. In *Reservoir model design: A practitioner's guide*, p. 173–231. Springer Netherlands, Dordrecht, 2015. ISBN 978-94-007-5497-3. doi: [10.1007/978-94-007-5497-3\\_6](https://doi.org/10.1007/978-94-007-5497-3_6).
- P. Ringrose and M. Bentley. *Reservoir model design*. Springer, Berlin, 2016. ISBN 978-3-030-70163-5. doi: [10.1007/978-3-030-70163-5](https://doi.org/10.1007/978-3-030-70163-5).
- C. Robin. *Mesure stratigraphique de la deformation : application a l'evolution jurassique du bassin de paris*. phdthesis, Université Rennes 1, 1995.
- R. Rodrigues. Chemostratigraphy. In *Applied Stratigraphy*, p. 165–178. Springer, Dordrecht, 2005. ISBN 978-1-4020-2763-5. doi: [10.1007/1-4020-2763-X\\_8](https://doi.org/10.1007/1-4020-2763-X_8).
- G. Ruiz and I. Le Nir. Sequence stratigraphy and facies analysis - Computer aided interpretation and correlation. In *61st EAGE Conference and Exhibition*, p. cp-132–00448, 1999. ISBN 978-90-73781-10-8. doi:[10.3997/2214-4609.201408045](https://doi.org/10.3997/2214-4609.201408045).
- M. J. Sackin. ALGOL program for cross-association of nonnumeric sequences using a medium-size computer. Meriam P. H. A., State Geological Survey, University of Kansas, 1965.
- M. J. Sackin and D. F. Merriam. Autoassociation, a new geological tool. *Journal of the International Association for Mathematical Geology*, 1(1): 7–16, 1969. ISSN 1573-8868. doi:[10.1007/BF02047068](https://doi.org/10.1007/BF02047068).
- H. Sakoe and S. Chiba. Dynamic programming algorithm optimization for spoken word recognition. *IEEE Transactions on Acoustics, Speech, and Signal Processing*, 26(1): 43–49, 1978. ISSN 0096-3518. doi:[10.1109/TASSP.1978.1163055](https://doi.org/10.1109/TASSP.1978.1163055).
- A. E. Scheidegger. On the prediction of the reach and velocity of catastrophic landslides. *Rock mechanics*, 5(4): 231–236, 1973. ISSN 1434-453X. doi:[10.1007/BF01301796](https://doi.org/10.1007/BF01301796).
- C. H. Scholz, L. R. Sykes, and Y. P. Aggarwal. Earthquake Prediction: A Physical Basis. *Science*, 181(4102): 803–810, 1973. ISSN 0036-8075.
- O. Serra and L. Serra. *Well logging and geology*. 2003.
- M. N. Shiers, N. P. Mountney, D. M. Hodgson, and S. L. Cobain. Depositional controls on tidally influenced fluvial successions, Neslen Formation, Utah, USA. *Sedimentary Geology*, 311: 1–16, 2014. ISSN 0037-0738. doi:[10.1016/j.sedgeo.2014.06.005](https://doi.org/10.1016/j.sedgeo.2014.06.005).
- M. N. Shiers, D. M. Hodgson, and N. P. Mountney. Response of a coal-bearing coastal-plain succession to marine transgression: Campanian Neslen Formation, Utah, U.S.A. *Journal of Sedimentary Research*, 87(2): 168–187, 2017. ISSN 1527-1404. doi:[10.2110/jsr.2017.7](https://doi.org/10.2110/jsr.2017.7).

## BIBLIOGRAPHY

---

- L. L. Sloss. Forty years of sequence stratigraphy. *Geological Society of America Bulletin*, 100(11): 1661–1665, 1988. ISSN 0016-7606. doi:[10.1130/0016-7606\(1988\)100<1661:FYOSS>2.3.CO;2](https://doi.org/10.1130/0016-7606(1988)100<1661:FYOSS>2.3.CO;2).
- L. L. Sloss, W. C. Krumbein, and E. C. Dapples. Integrated facies analysis. In *Sedimentary facies in geologic history*, vol. 39, p. 91–124. Geological Society of America, 1949. ISBN 978-0-8137-1039-6.
- T. F. Smith and M. S. Waterman. New Stratigraphic Correlation Techniques. *The Journal of Geology*, 88(4): 451–457, 1980. ISSN 0022-1376. doi:[10.1086/628528](https://doi.org/10.1086/628528).
- J. S. Sneider, P. de Clarens, and P. R. Vail. Sequence stratigraphy of the middle to upper jurassic, viking graben, north sea. In *Sequence Stratigraphy on the Northwest European Margin*, vol. 5 of *Norwegian Petroleum Society Special Publications*, p. 167–197. Elsevier, 1995. doi: [10.1016/S0928-8937\(06\)80068-8](https://doi.org/10.1016/S0928-8937(06)80068-8).
- J. R. Southam and W. W. Hay. Correlation of stratigraphic sections by continuous variables. *Computers & Geosciences*, 4(3): 257–260, 1978. ISSN 00983004. doi:[10.1016/0098-3004\(78\)90058-4](https://doi.org/10.1016/0098-3004(78)90058-4).
- J. d. C. Sowerby. *The mineral conchology of Great Britain*, vol. 4. W. Arding, London, 1822.
- R. J. Steel and T. Olsen. Clinoforms, Clinoform Trajectories and Deepwater Sands. In *Sequence Stratigraphic Models for Exploration and Production: Evolving Methodology, Emerging Models, and Application Histories*, p. 367–380. 2002. ISBN 978-0-9836096-8-1. doi: [10.5724/gcs.02.22.0367](https://doi.org/10.5724/gcs.02.22.0367).
- N. Steno. *De solido intra solidum naturaliter contento dissertationis prodromus*. Florence, 1669.
- W. B. Styant and R. M. Bustin. Sedimentology of Fraser River delta peat deposits: A modern analogue for some deltaic coals. *International Journal of Coal Geology*, 3(2): 101–143, 1983. ISSN 0166-5162. doi:[10.1016/0166-5162\(83\)90006-X](https://doi.org/10.1016/0166-5162(83)90006-X).
- A.-L. Tertois. *Création et modification de modèles géologiques par champs de potentiel. Application au modèle GeoChron*. phdthesis, Institut National Polytechnique de Lorraine, 2007. NNT : 2007INPL032N. tel-01752878.
- J. D. Testerman. A statistical reservoir-zonation technique. *Journal of Petroleum Technology*, 14(8): 889–893, 1962. ISSN 0149-2136, 1944-978X. doi:[10.2118/286-PA](https://doi.org/10.2118/286-PA).
- D. M. Tetzlaff and J. W. Harbaugh. Simulating clastic sedimentation. 1989.
- R. Thompson and R. M. Clark. Sequence slotting for stratigraphic correlation between cores: theory and practice. In *Paleolimnology and the reconstruction*

- of ancient environments*, p. 229–240. Springer, Dordrecht, 1990. ISBN 978-94-009-2655-4. doi: 10.1007/978-94-009-2655-4\_15.
- P. R. Vail, R. M. M. Jr, and S. T. Iii. Seismic stratigraphy and global changes of sea level. Part 4: Global cycles of relative changes of sea level. In *Seismic stratigraphy — Applications to hydrocarbon exploration*, vol. 26 of *AAPG Memoir*, p. 83–97. American Association of Petroleum Geologists, 1977.
- P. R. Vail, J. P. Colin, R. J. du Chene, J. Kuchly, F. Mediavilla, and V. Trifilieff. La stratigraphie sequentielle et son application aux correlations chronostratigraphiques dans le Jurassique du bassin de Paris. *Bulletin de la Société Géologique de France*, III(7): 1301–1321, 1987. ISSN 0037-9409. doi:10.2113/gssgfbull.III.7.1301.
- J. T. van Gorsel. Biostratigraphy in Indonesia: methods, pitfalls and new directions. In *17th Annual Convention*, p. 275–300, 1988.
- J. C. van Wagoner, H. W. Posamentier, R. M. Mitchum, P. R. Vail, J. F. Sarg, T. S. Loutit, and J. Hardenbol. An overview of the fundamentals of sequence stratigraphy and key definitions. In *Sea-level changes: An integrated approach*, vol. 42 of *SEPM Special Publication*, p. 39–45. The Society of Economic Paleontologists and Mineralogists, 1988. ISBN 0-918985-74-9. doi: 10.2110/pec.88.01.0039.
- J. C. van Wagoner, R. M. Mitchum, K. M. Campion, and V. D. Rahmanian. Sili-ciclastic sequence stratigraphy in well logs, cores, and outcrops: Concepts for high-resolution correlation of time and facies. *AAPG Methods in Exploration*, 7: III–55, 1990.
- T. Vermaas, A. Forzoni, and J. E. A. Storms. Drawing the line, when do we need process-based models? p. cp–483, 2016. ISBN 978-94-6282-189-7. doi:10.3997/2214-4609.201600358.
- G. Vincent, B. Corre, and P. Thore. Managing Structural Uncertainty in a Mature Field for Optimal Well Placement. *SPE Reservoir Evaluation & Engineering*, 2(04): 377–384, 1999. ISSN 1094-6470. doi:10.2118/57468-PA.
- J. Walther. *Einleitung in die geologie als historische wissenschaft: Beobachtungen über die bildung der gesteine und ihrer organischen einschlüsse*, vol. 3. G. Fischer, 1894.
- M. S. Waterman and R. Raymond. The match game: New stratigraphic correlation algorithms. *Mathematical Geology*, 19(2): 109–127, 1987. ISSN 1573-8868. doi:10.1007/BF00898191.
- H. Weissert, M. Joachimski, and M. Sarnthein. Chemostratigraphy. *Newsletters on Stratigraphy*, p. 145–179, 2008. doi:10.1127/0078-0421/2008/0042-0145.

## BIBLIOGRAPHY

---

- F. Wellmann and G. Caumon. 3-D Structural geological models: Concepts, methods, and uncertainties. In *Advances in Geophysics*, vol. 59, p. 1–121. Elsevier, 2018. doi: [10.1016/bs.agph.2018.09.001](https://doi.org/10.1016/bs.agph.2018.09.001).
- H. E. Wheeler. Time-Stratigraphy. *AAPG Bulletin*, 42(5): 1047–1063, 1958. ISSN 0149-1423. doi:[10.1306/0BDA5AF2-16BD-11D7-8645000102C1865D](https://doi.org/10.1306/0BDA5AF2-16BD-11D7-8645000102C1865D).
- L. Wheeler. *Automatic and simultaneous correlation of multiple well logs*. MSc thesis, Colorado School of Mines, 2015.
- L. Wheeler and D. Hale. Simultaneous correlation of multiple well logs. In *SEG Technical Program Expanded Abstracts 2014*, p. 618–622. Society of Exploration Geophysicists, 2014. doi: [10.1190/segam2014-0227.1](https://doi.org/10.1190/segam2014-0227.1).
- W. Whewell. *History of the Inductive Sciences : From the Earliest Times to the Present*. 1837.
- X. Wu, Y. Shi, S. Fomel, and F. Li. Incremental correlation of multiple well logs following geologically optimal neighbors. *Interpretation*, 6(3): T713–T722, 2018. ISSN 2324-8858. doi:[10.1190/INT-2018-0020.1](https://doi.org/10.1190/INT-2018-0020.1).
- O. Yilmaz. *Seismic data analysis: Processing, inversion, and interpretation of seismic data. Volume II*, vol. 10 of *Investigations in Geophysics*. Society of Exploration Geophysicists, 2001. ISBN 978-1-56080-094-1. doi: [10.1190/1.9781560801580](https://doi.org/10.1190/1.9781560801580).





# APPENDIXES



# Appendix A

## Middle Jurassic Hugin Formation: Sedimentary facies

This chapter presents first three different facies which correspond to the lagoonal depositional environments in the background of the Middle Jurassic Hugin Formation (Appendix A.1). Second, it presents the succession of six facies corresponding to bay-head deltas prograding into the lagoon (Appendix A.2). Finally, it presents three different facies that correspond to fluvial depositional environments upstream of the delta (Appendix A.3).

## **Abstract**

*The South Viking Graben in the Norwegian North Sea is a mature hydrocarbon province that yields many producing oil and gas fields, particularly in the Middle Jurassic Hugin Formation. The depositional system of the Middle Jurassic Hugin Formation in the South Viking Graben has been interpreted as shallow-marine (e.g., Sneider et al., 1995). Based on well-data analyses from the Gudrun Field area, Kieft et al. (2010) have interpreted the Hugin Formation in that area as barred shorefaces, river-dominated deltas, and barred lagoons. Considering these depositional environments, Knaust and Hoth (2021) have proposed an interpretation of twelve sedimentary facies from well-log and core-sample analyses.*

## **Introduction**

The Middle Jurassic Hugin Formation is located in the South Viking Graben of the Norwegian North Sea (Figure A.1.A-B) (Knaust and Hoth, 2021). The Gudrun-Sigrun Field area in Block 15/3 has proven oil, gas and condensate in the Hugin Formation (Figure A.1.C) (Hoth et al., 2018).

The purpose of this chapter is not to describe the Hugin Formation in the Gudrun-Sigrun Field area in details, but to focus on the presentation of sedimentary facies interpreted from seven wells on which we tested the correlation rule defined in Chapter 3 (Figure A.1). From drilled and partially cored wells, well logs and core samples were analyzed to define twelve sedimentary facies (Figures A.2 to A.13) and described by Knaust and Hoth (2021) as “*part of idealized shallowing-upward successions that are bounded by marine flooding surfaces interpreted and therefore are interpreted as parasequences [...] and prograding delta lobes*”.

The Middle Jurassic Hugin Formation corresponds to a shallow-marine depositional system (e.g., Kieft et al., 2010; Knaust and Hoth, 2021; Sneider et al., 1995). The background correspond to a lagoonal depositional environment into which bay-head deltas prograde (Knaust and Hoth, 2021).

First, Appendix A.1 presents three different facies which correspond to the lagoonal depositional environments in the background of the Middle Jurassic Hugin Formation. Second, Appendix A.2 presents the succession of six facies corresponding to bay-head deltas prograding into the lagoon. Finally, Appendix A.3 presents three different facies that correspond to fluvial depositional environments upstream of the delta.

For a deeper understanding of the Hugin Formation in the Gudrun Field area, readers are highly encouraged to refer to the work of Knaust and Hoth (2021).

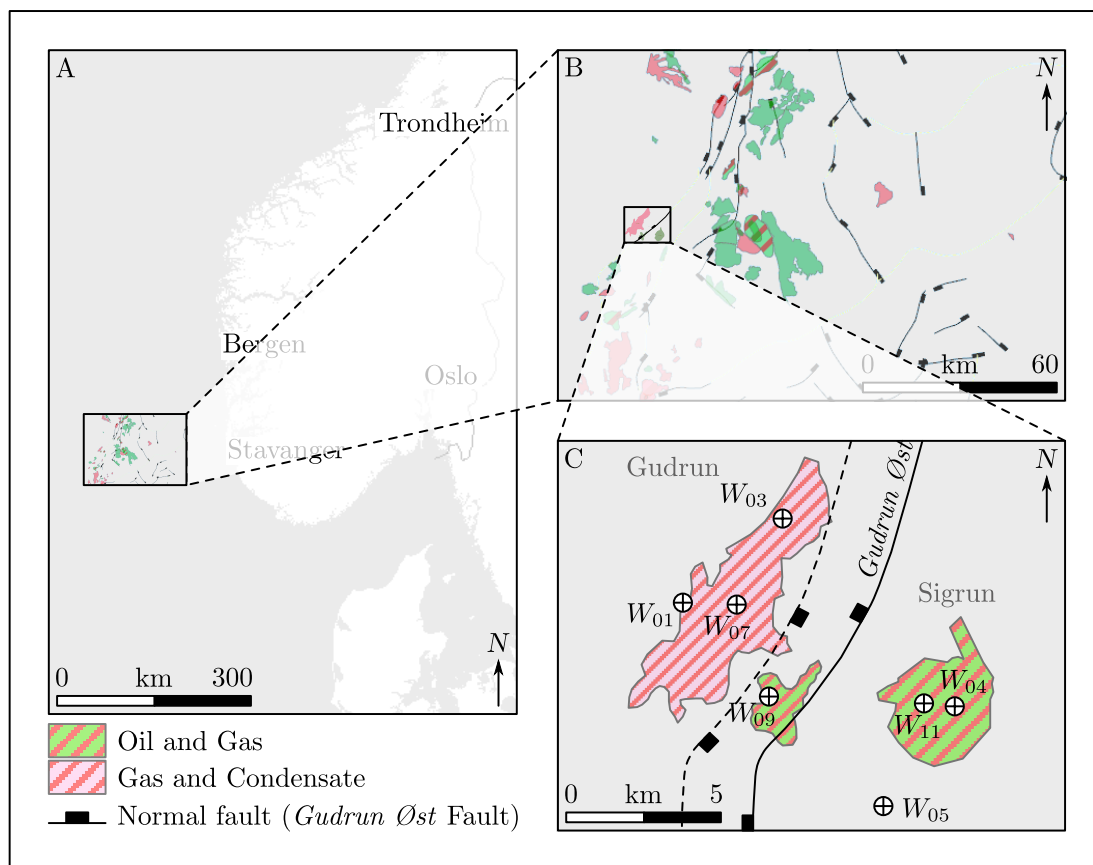


Figure A.1: Location of the area of interest and the seven studied wells (A) within the Norwegian North Sea, (B) within the South Viking Graben together with other fields, and (C) within the Gudrun Field area (Block 15/3). Map based on <http://www.npd.no>.

They have proposed a complete tectono-stratigraphic overview based on detailed core description and interpretation, calibration with wireline log data, facies classification, and reconstruction of depositional environments.

## A.1 Lagoonal depositional environments

Three lithofacies corresponding to mudstones, more or less bioturbated, are interpreted by [Knaust and Hoth \(2021\)](#) as lagoonal depositional environments in the Middle Jurassic Hugin Formation from well cores analyses.

### Mudstone, laminated (restricted lagoon)

**Description:** “Dark-grey mudstone with planar or low-angle lamination marks the first lithofacies type above the marine flooding surfaces, which in turn are

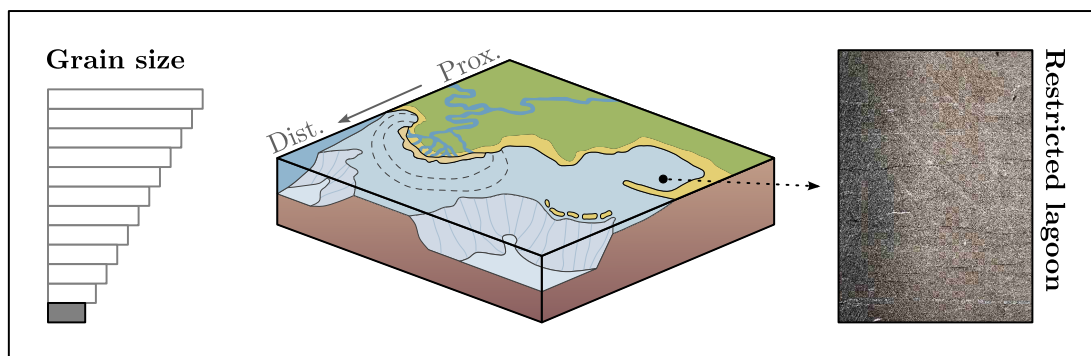


Figure A.2: Relative grain size of the laminated mudstone, depositional environment corresponding to restricted lagoon, and lithofacies core photograph. Modified from [Baville et al. \(2022\)](#).

characterized by a sharp break in lithofacies from the underlying parasequence (typically sandstone or coal) and concentration of granules and pebbles of foremost crystalline rocks (i.e., lag deposit). Towards the top, the mudstone may contain a few silt laminae and scattered bioclasts (mainly ostracod shells) and intergrades with sandy to bioclastic mudstone above. The laminated mudstone is free of bioturbation. Beds of laminated mudstone can be stacked on top of each other, in which case they are separated by erosional surfaces with thin lag deposits” ([Knaust and Hoth, 2021](#)).

**Interpretation:** “Laminated mudstone represents the deepest and most distal lithofacies, occurring just above the marine flooding surface and marking the initial transgression. It was deposited in a restricted coastal lagoon or central basin of an estuary within a low-energetic setting and relatively long-term background sedimentation (e.g., [Larson, 2012](#)), in contrast to the sandier lithofacies types higher up in the parasequences. Lack of bioturbation is due to restricted water circulation and depleted bottom-water oxygenation, subordinately due to brackish water conditions. The stacking of individual laminated mudstone beds probably results from stacked parasequences in a distal (basin-ward) position without significant clastic sediment input, where bounding surfaces are representing correlative surfaces of marine flooding surfaces” ([Knaust and Hoth, 2021](#)).

### Mudstone, sandy-bioclastic (open lagoon)

**Description:** “A dark-grey mudstone gradually develops from the underlying laminated mudstone and intergrades with oyster shell beds. It consists of crude, partly wavy lamination interlayering with fine-grained sandstone laminae as well as laminae with concentrations of bioclasts (mainly oyster shells). No bioturbation occurs” ([Knaust and Hoth, 2021](#)).

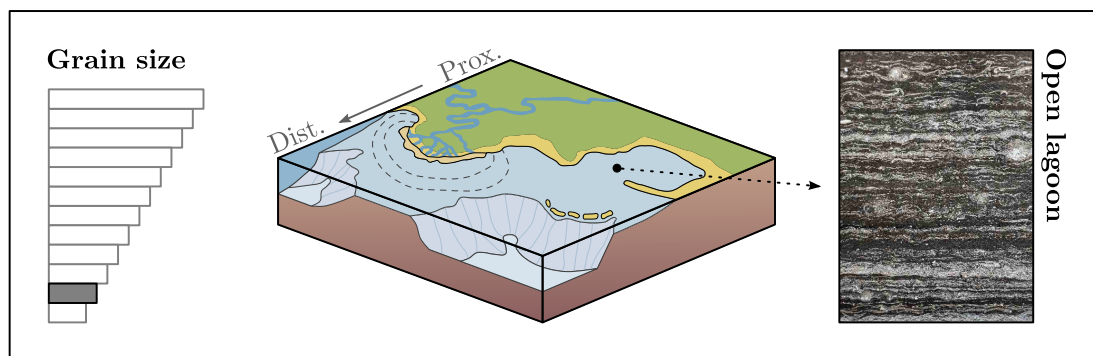


Figure A.3: Relative grain size of the sandy-bioclastic mudstone, depositional environment corresponding to open lagoon, and lithofacies core photograph. Modified from [Baville et al. \(2022\)](#).

**Interpretation:** “Sandy to bioclastic mudstone is genetically related to the laminated mudstone but increased sandy input and scattered oyster bioclasts indicate a more open lagoon nearby local oyster patch reefs or biostromes (comparable to the forereef facies) in the distal vicinity of a bay-head prodelta. Lack of bioturbation indicates depleted bottom-water oxygenation combined with brackish water. Oyster accumulations and the associated sandy-bioclastic mudstone facies are common in the Middle to Upper Jurassic (e.g., [Andrews and Walton, 1990](#))” ([Knaust and Hoth, 2021](#)).

### Oyster shell bed (biostrome, patch reef)

**Description:** “This lithofacies type occurs above the sandy to bioclastic mudstone, more rarely above the laminated mudstone, or interbedded with the mudstone facies with either gradual or sharp boundaries. It consists of a grey, oyster-supported fabric intercalated with dark-grey mudstone matrix. The oyster shells are monospecific accumulations of *Nanogyra (Nanogyra) nana* ([Sowerby, 1822](#)), commonly tightly packed valves stacked into each other either convex-up or convex-down. Intervals of more loosely distributed shells are transitional to the bioclastic mudstone facies. Internal bedding on decimeter- to meter-scale can occur, but internal sorting is lacking. No bioturbation or bioerosion has been observed” ([Knaust and Hoth, 2021](#)).

**Interpretation:** “The oyster shell beds are a common lithofacies type in the Gudrun-Sigrun area and represent oyster patch reefs on local highs within the low-energy open lagoon with a brackish environment ([Koppka, 2015](#)). Monospecific occurrence of the oyster species *Nanogyra nana* is related to opportunistic and quick colonization of the sea bottom. Although articulated oyster valves are rather uncommon, the dense accumulation of oyster shells and the lack of sorting indicate mainly autochthonous accumulations with only little reworking by

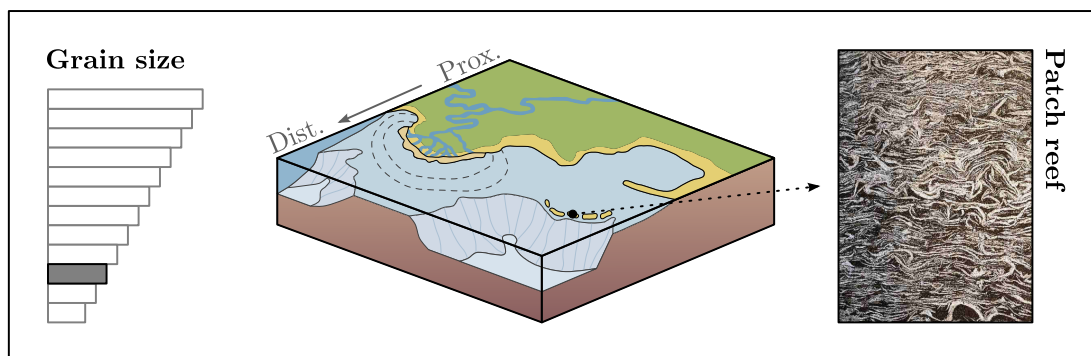


Figure A.4: (Relative grain size of the oyster shell bed, depositional environment corresponding to patch reef, and lithofacies core photograph. Modified from [Baville et al. \(2022\)](#)).

currents (e.g., [Fürsich et al., 2009](#)). *Nanogyra* species only have a weak hinge between their left and right valve, thus allowing for rapid disarticulation after the bivalve's dead. Different stacking patterns (e.g. convex-up or convex-down) reflect different life positions within unique substrates (e.g., soft versus hard; see [Machalski \(1998\)](#))” ([Knaust and Hoth, 2021](#)).

## A.2 Bay-head delta depositional environments

A succession of six lithofacies is interpreted by [Knaust and Hoth \(2021\)](#) as prograding deltas in the Middle Jurassic Hugin Formation from well cores analyses.

### Siltstone, muddy, disturbed (prodelta)

**Description:** “Brownish-grey, heterogeneous siltstone with admixtures of mud and sand is typically intercalated between mud-rich lithofacies types below and sand-dominated lithofacies above. It consists of weakly developed lamination with upwards increasing lamina thickness, weak to moderate bioturbation with low ichnodiversity and burrow size. Intervals of synsedimentary deformation in form of slide scars and folds are common” ([Knaust and Hoth, 2021](#)).

**Interpretation:** “Based on its position within the shallowing-upward succession, the heterogeneous siltstone facies is interpreted as prodelta facies belt in front of a bay-head delta (e.g., [Bhattacharya, 2006](#)). Synsedimentary deformation resulted from rapid deposition, sediment overpressure and a relative steep gradient. Limited bioturbation, low ichnodiversity and burrow size are best explained by fluctuating and reduced salinity due to freshwater influx” ([Knaust and Hoth, 2021](#)).

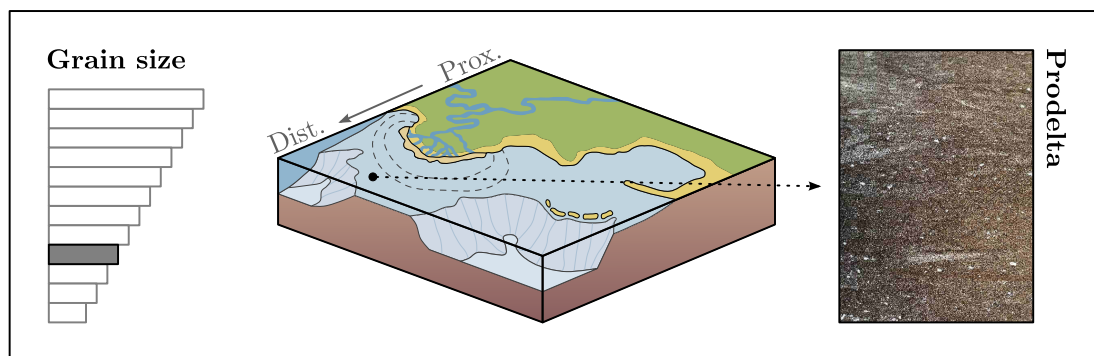


Figure A.5: Relative grain size of the muddy disturbed siltstone, depositional environment corresponding to prodelta, and lithofacies core photograph. Modified from [Baville et al. \(2022\)](#).

### Sandstone, heterolithic (lower delta front)

**Description:** “Brownish-grey sandstone and siltstone layers are intercalated with dark-brown mudstone drapes, thinly bedded but slightly thickening-upwards beds. Sandstone layers include medium-grained, poorly sorted sandstone with granules and scattered oyster shells (reworked), and fine-grained, well-sorted sandstone with current-ripple cross-lamination. Erosional structures are common at the base of the sandstone layers, as well as small-scale soft-sediment deformation structures (e.g., convolute bedding, load casts). The mud layers are either laminated or have a homogeneous texture with flame structures at the top and into the overlying sandstone layer. The heterolithic sandstone is moderately bioturbated and contains *Palaeophycus*, *Siphonichnus* and *Arenicolites* in the sandy fraction, as well as *Nereites* in the mud” ([Knaust and Hoth, 2021](#)).

**Interpretation:** “Heterolithic sandstone originated in the distal part of a prograding bay-head delta in the lower delta front (e.g., [Bhattacharya, 2006](#)), where medium-grained and poorly sorted sand was sourced from distributary channels,

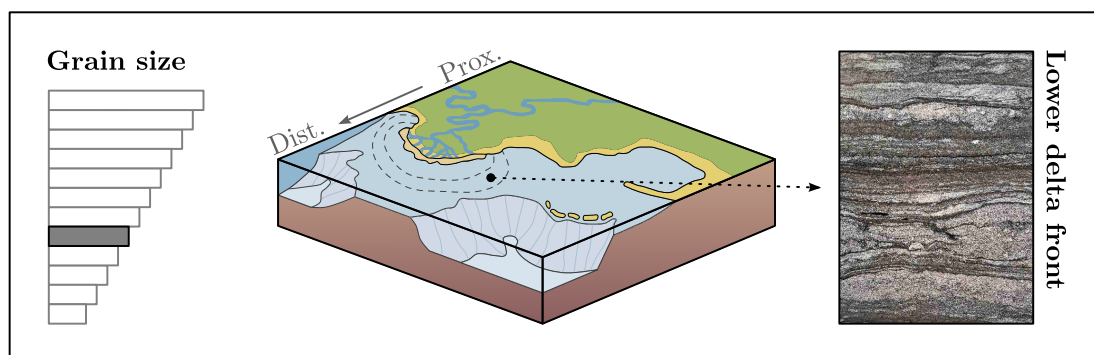


Figure A.6: Relative grain size of the heterolithic sandstone, depositional environment corresponding to lower delta front, and lithofacies core photograph. Modified from [Baville et al. \(2022\)](#).

and fine-grained and well-sorted sand contributed from the upper delta front. The laminated mud layers represent the background sediment of the receiving lagoon, whereas homogeneous mud layers are fluid-mud deposits from suspension in the fluvial-tidal transition zone (e.g., [Ichaso and Dalrymple, 2009](#))” ([Knaust and Hoth, 2021](#)).

### Sandstone, bioturbated (upper delta front)

**Description:** “This lithofacies type consists of light-grey, silty to muddy, fine-grained sandstone beds with a thickening and coarsening-upward trend. It contains reworked oyster shells and intense or total bioturbation, predominantly consisting of a *Teichichnus zigzag* ichnofabric with low diversity and high abundance” ([Knaust and Hoth, 2021](#)).

**Interpretation:** “Bioturbated sandstone is a part of the upper delta front of a bay-head delta, where it occurs in interdistributary bays with moderate current energy (e.g., [Buatois et al., 2012](#); [Reineck and Singh, 1980](#)). Patchy oyster accumulations growth during relative quite periods and the shells were grew during higher-energetic events. Low-diversity and high-density occurrences of *Teichichnus zigzag* indicates a marginal-marine (paralic) environment with reduced salinity (i.e., brackish water; [Knaust \(2018\)](#))” ([Knaust and Hoth, 2021](#)).

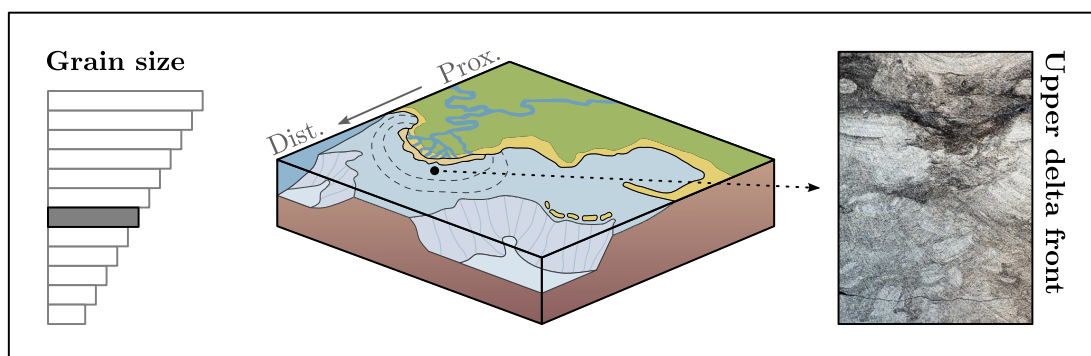


Figure A.7: Relative grain size of the bioturbated sandstone, depositional environment corresponding to upper delta front, and lithofacies core photograph. Modified from [Baville et al. \(2022\)](#).

### Sandstone, cross-bedded (mouth bar)

**Description:** “Thickly bedded, brownish-grey, fine- to medium-grained and moderately to well sorted sandstone occurs in close association with bioturbated and heterolithic sandstone. It shows weak cross bedding or a structureless appearance. Low amount of bioturbation occurs in form of diffuse burrows and

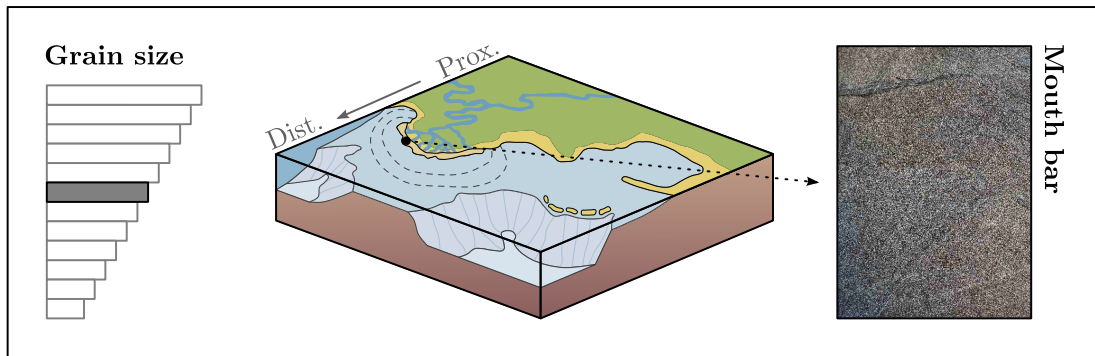


Figure A.8: Relative grain size of the cross-bedded sandstone, depositional environment corresponding to mouth bar, and lithofacies core photograph. Modified from [Baville et al. \(2022\)](#).

loosely winded subvertical burrows” ([Knaust and Hoth, 2021](#)).

**Interpretation:** “The facies association, grain size, sorting, sedimentary structures and bioturbation of this sandstone support an interpretation as mouth-bar deposits occurring at the termination of distributary channels and within the upper delta-front area (e.g., [Jerrett et al., 2016](#)). Bioturbation is limited due to high salinity fluctuation and freshwater influx” ([Knaust and Hoth, 2021](#)).

### Sandstone, cross-bedded (distributary channel)

**Description:** “Brownish-grey, medium- to coarse-grained sandstone occurs in thick beds with basal and internal erosion surfaces. It is moderately to poorly sorted, contains tabular and trough cross-stratification and faint dewatering structures. Burrows occur only sporadically (e.g., *Skolithos* isp.)” ([Knaust and Hoth, 2021](#)).

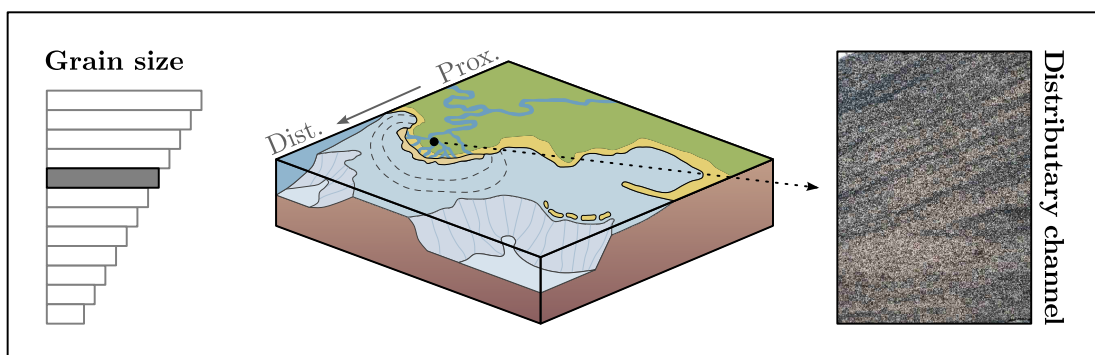


Figure A.9: Relative grain size of the cross-bedded sandstone, depositional environment corresponding to distributary channel, and lithofacies core photograph. Modified from [Baville et al. \(2022\)](#).

**Interpretation:** “Grain size, sorting, erosional features, cross bedding and de-watering structures indicate a higher energetic depositional regime with rapid deposition. This and the stratigraphic context suggest deposition in distributary channels on the lower delta plain of a bay-head delta (e.g., [Li and Bhattacharya, 2014](#); [Olariu and Bhattacharya, 2006](#)), dominated by fluvial processes but within the microtidal range” ([Knaust and Hoth, 2021](#)).

### Coal (peat, swamp)

**Description:** “This lithofacies comprises thin to thick beds of dark-brown to black lignite with a massive appearance, crude bedding and caverns” ([Knaust and Hoth, 2021](#)).

**Interpretation:** “The coal originated as peat-swamp deposits on top of a bay-head delta plain (e.g., [Styan and Bustin, 1983](#))” ([Knaust and Hoth, 2021](#)).

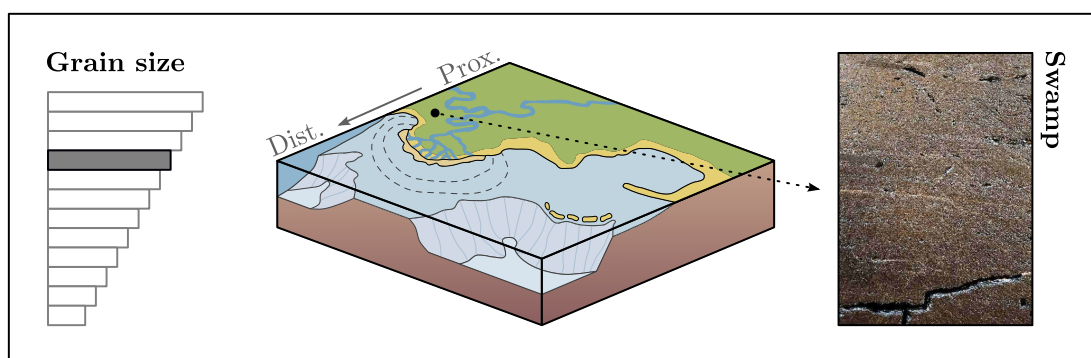


Figure A.10: Relative grain size of the coal, depositional environment corresponding to swamp, and lithofacies core photograph. Modified from [Baville et al. \(2022\)](#).

## A.3 Fluvial depositional environments

Three lithofacies corresponding to fluvial depositional environments are interpreted in the Middle Jurassic Hugin Formation from well cores analyses by [Knaust and Hoth \(2021\)](#).

### Mudstone, silty (marsh)

**Description:** “Some parasequences with coal contain in their upper parts a lithofacies consisting of brownish-grey, silty mudstone with horizontal and low-

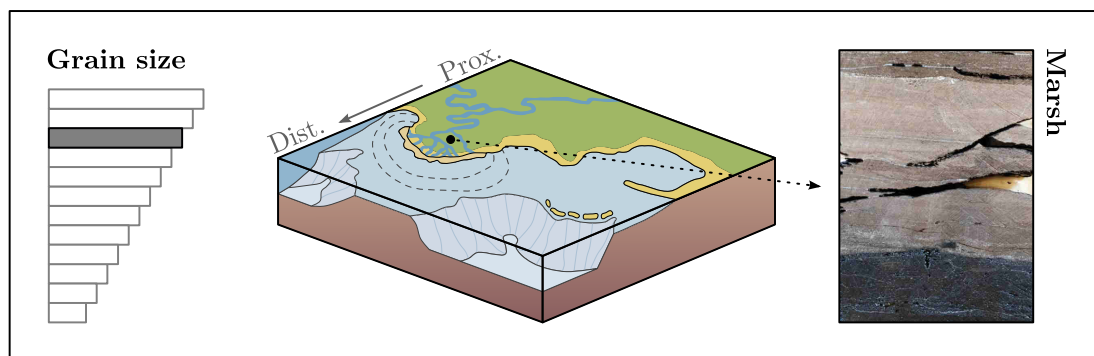


Figure A.11: Relative grain size of the silty mudstone, depositional environment corresponding to marsh, and lithofacies core photograph. Modified from [Baville et al. \(2022\)](#).

angle cross-lamination, coaly streaks and locally root traces” ([Knaust and Hoth, 2021](#)).

**Interpretation:** “The occurrence of this lithofacies type in the upper part of the parasequences between the coal and ripple-laminated sandstone indicates its relative proximal position within the lower delta plain adjacent to distributary channels and swamp areas. Sediment type, admixture of coal and the occurrence of root traces indicate deposition in a marsh land (e.g., [Belknap, 2003](#))” ([Knaust and Hoth, 2021](#)).

### Sandstone, cross-laminated (fluvial overbank)

**Description:** “Current-ripple cross-laminated sandstone occurs in some parasequences at the top of the Hugin Formation and in association with silty mudstone (below) and conglomeratic sandstone (above). The dark brownish-grey, fine-grained sandstone is moderately sorted and contains current-ripple cross-

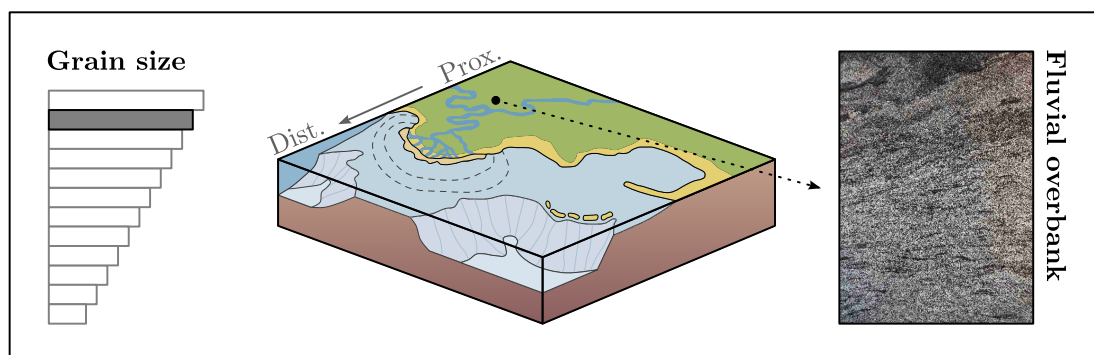


Figure A.12: Relative grain size of the current-ripple cross-laminated sandstone, depositional environment corresponding to fluvial overbank, and lithofacies core photograph. Modified from [Baville et al. \(2022\)](#).

*lamination and small-scale deformation structures. No bioturbation is observed” (Knaust and Hoth, 2021).*

**Interpretation:** *“Based on its facies association and lithological characteristics, the current-ripple cross-laminated sandstone is interpreted as fluvial-overbank, levee and crevasse splay deposits adjacent to distributary channels on the upper delta plain (e.g., Miall, 2014)” (Knaust and Hoth, 2021).*

## Sandstone, conglomeratic (fluvial channel)

**Description:** *“This lithofacies sporadically occurs on top of parasequences in the upper part of the Hugin Formation and gradationally develops from the underlying current-ripple cross-laminated sandstone. It comprises dark brownish-grey, coarse-grained sandstone with crude bedding, reworked lithoclasts (intraclasts) and granules. Sorting is poor and bioturbation is absent” (Knaust and Hoth, 2021).*

**Interpretation:** *“Conglomeratic sandstone was deposited in fluvial channels on the upper delta plain (e.g., Miall, 2014)” (Knaust and Hoth, 2021).*

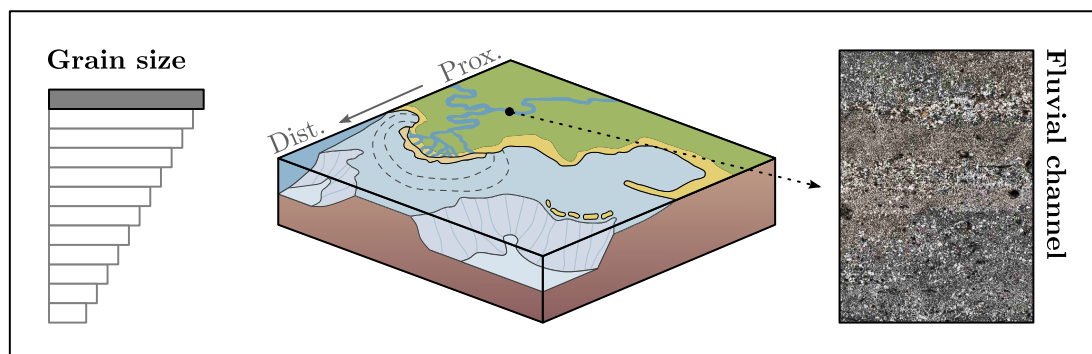


*Figure A.13: Relative grain size of the laminated mudstone, depositional environment corresponding to restricted lagoons, and lithofacies core photograph. Modified from Baille et al. (2022).*

## Conclusion

The study of the Middle Jurassic Hugin Formation in the Gudrun Field area by Knaust and Hoth (2021) has led to the interpretation of twelve sedimentary facies corresponding to depositional environments located along a distal-to-proximal transect from core sample or interpolated from well logs (e.g., gamma ray, neutron porosity, and density porosity) by Knaust and Hoth (2021). These twelve sedimentary facies interpreted along the seven wells of the Hugin Formation in

the Gudrun-Sigrun Field area can easily be used in the distality rule presented in Chapter 3 to be compared with relative well distality in order to compute stratigraphic well correlations of the zone of interest.

The sedimentary facies interpretation along the seven wells of the Hugin Formation in the Gudrun-Sigrun Field area is considered as accurate and constant in the next chapters:

- It is used in Chapter 5 to compute stratigraphic well correlations in order to evaluate the likelihood of several possible depositional systems by inferring the relative well distalities.
- It is used in Chapter 6 to compute stratigraphic well correlations in order to simulate stratigraphic subsurface models of the Hugin Formation in the Sigrun Field area.





## Stratigraphic correlation uncertainty: On the impact of the sediment transport direction in computer-assisted multi-well correlation

**Abstract:** Subsurface modeling is a way to predict the structure and the connectivity of stratigraphic units by honoring subsurface observations. These observations are commonly sampled along wells at a large and sparse horizontal scale (kilometer-scale) but at a fine vertical scale (meter-scale). There are two types of well data: (1) well logs, corresponding to quasi-continuous (regular sampling) geophysical measurements along the well path (e.g., gamma ray, sonic, neutron porosity), and (2) regions, corresponding to categorical reservoir properties and defined by their top and bottom depths along the well path (e.g., biozones, structural zones, sedimentary facies).

Markers are interpreted along the well path and can be associated to generate consistent sets of marker associations called well correlations. These well correlations may be generated manually (deterministic approach) by experts, but this may be prone to biases and does not ensure reproducibility. They may also be generated automatically (deterministic or probabilistic approach) by computing a large number of consistent well correlations with an algorithm, and by ranking these realizations according to their likelihood. The likelihood of these computer-assisted well correlations are directly linked to the principle of correlation used to associate markers.

This work introduces two principles of correlation, which tend to reproduce the chronostratigraphy and the depositional processes at the parasequence scale: (1) “a marker

(described by facies and distality taken at the center of an interval having a constant facies and a constant distality) cannot be associated with another marker described by a positionally deeper facies at a more proximal position, or a positionally shallower facies at a more distal position”, and (2) “the lower the mismatch between a chronostratigraphic interpolation (in between markers) and a conceptual depositional profile, the higher the likelihood of the marker association”.

These two principles of correlation are first benchmarked with analytical solutions and applied on synthetic cases. They have then been used (1) to compare the proposed depositional context with additional subsurface data such as biostratigraphic interpretations, or (2) to evaluate the likelihood of a hypothetical depositional environment by generating stochastic realizations and assessing the uncertainties.

These methods are applied on a siliciclastic coastal deltaic system targeting a Middle Jurassic reservoir in the South Viking Graben in the North Sea.

This work enables (1) to define two specific principles of correlation defined by a few parameters that can be used to generate stochastically well correlations within coastal deltaic systems, and (2) to open the path towards a simple combination of specific principles of correlation to obtain a better characterization of coastal deltaic systems by assessing the uncertainties.

**Keywords:** Multi-well correlations, Sequence stratigraphy, Sediment transport direction, Coastal sedimentary depositional environments, Uncertainty assessment, Dynamic Time Warping Algorithm.

---

## Incertitude des corrélations stratigraphiques : À propos de l'impact de la direction de transport des sédiments sur les corrélations multi-puits assistées par ordinateur

**Résumé :** La modélisation du sous-sol est un moyen de prédire la structure et la connectivité des unités stratigraphiques en honorant les observations de subsurface. Ces observations sont en général échantillonnées le long de puits à grande échelle horizontale (kilomètre) mais à petite échelle verticale (mètre). Il y a deux types de données de puits : (1) les diagraphies, qui correspondent à des acquisitions géophysiques quasi-continues (échantillonnage régulier) le long du puits (e.g., gamma ray, sonique, porosité neutron), et (2) les régions, qui correspondent à des propriétés réservoir discrètes définies par des profondeurs maximales et minimales le long du puits (e.g., biozones, zones structurales, faciès sédimentaires).

Des marqueurs sont interprétés le long des puits et peuvent être associés pour générer un ensemble d'associations de marqueurs conformes, appelé des corrélations de puits. Ces corrélations de puits peuvent être réalisées manuellement (approche déterministe) par des experts, mais cela peut être sujet à des biais et ne garantit pas la reproductibilité. Les corrélations de puits peuvent également être générées automatiquement (approche déterministe ou probabiliste) en calculant un grand nombre de corrélations de puits conformes à l'aide d'un algorithme et en classant ces réalisations en fonction de leurs vraisemblances. La vraisemblance de ces corrélations de puits assistées par ordinateur est directement liée au principe de corrélation utilisé pour associer les marqueurs.

Ces travaux de thèse introduisent deux principes de corrélation, qui tendent à reproduire la chronostratigraphie et les processus de dépôts à l'échelle de la paraséquence :

(1) “un marqueur (décrit par un faciès et une distalité pris au centre d'un intervalle ayant un faciès constant et une distalité constante) ne peut pas être associé avec un autre marqueur décrit par un faciès plus profond à une position plus proximale, ou un faciès moins profond à une position plus distale”, et (2) “plus la différence entre une interpolation chronostratigraphique (entre les marqueurs) et un profil de dépôt conceptuel est faible, plus la probabilité d'association des marqueurs est élevée”.

Ces deux principes de corrélation sont d'abord validés avec des solutions analytiques et appliqués sur des cas synthétiques. Ils ont ensuite été utilisés (1) pour prédire la connectivité des unités stratigraphiques à partir de données de puits sans connaissances solides sur les environnements de dépôt en inférant les paramètres de corrélation, ou (2) pour évaluer la probabilité d'un environnement de dépôt hypothétique en générant des réalisations stochastiques et en évaluant les incertitudes.

Les méthodes sont appliquées sur un système silicoclastique de dépôts deltaïques côtiers ciblant un réservoir du Jurassique Moyen dans le South Viking Graben en Mer du Nord.

Ces travaux de thèse permettent (1) de définir deux principes de corrélation spécifiques définis par quelques paramètres qui peuvent être utilisés pour générer des corrélations de puits stochastiques dans les systèmes deltaïques côtiers, et (2) d'ouvrir la voie vers une combinaison simple de principes de corrélation spécifiques pour obtenir une meilleure caractérisation des systèmes deltaïques côtiers en évaluant les incertitudes.

**Mots-clés :** Corrélations multi-puits, Stratigraphie séquentielle, Direction de transport de sédiments, Environnement de dépôts sédimentaires côtiers, Gestion d'incertitudes, Algorithme de Déformation Temporelle Dynamique.